Electrospun Fibers for HIV Prevention: Translational Design for *In Vivo* Efficacy

Anna K. Blakney

A dissertation

submitted in partial fulfillment of the

requirements for the degree of

Doctor of Philosophy

University of Washington

2016

Reading Committee:

Kim Woodrow, Chair

Buddy Ratner

Jeanne Marrazzo

Program Authorized to Offer Degree:

Bioengineering

University of Washington

Abstract

Electrospun Fibers for HIV Prevention: Translational Design for *In Vivo* Efficacy

Anna K. Blakney

Chair of the Supervisory Committee:
Kim Woodrow, Associate Professor
Bioengineering

Women are disproportionately affected by the HIV epidemic, especially in sub-Saharan Africa, where the majority of the world's HIV burden is located. The development of female-initiated protection methods is motivated by the gender power disparity between men and women, which often leads to inability for women to negotiate condom use and/or faithfulness, coupled with the greater risk of male-to-female than female-to-male transmission per sex act. The current prevention strategy, referred to as 'microbicides', is to incorporate one or more antiretroviral drugs into a delivery vehicle, such gels, intravaginal rings, tablets, films, and injectables, all of which are in varying stages of development. Recently, electrospun fibers have been explored in proof-of-concept studies as a novel microbicide delivery vehicle. Drug-eluting fibers offer a number of advantages including the possibility of discreet use by women, the potential for easy scale-up, the ability to incorporate multiple physicochemically diverse drugs, and the use of different polymers and microarchitecture to tailor release of active compounds.

Here, we investigate the role of formulation, including microarchitecture and the use of novel polyurethane polymers, on *in vitro* release of antiretroviral drug combinations with varying physicochemical properties. We have developed a pre-clinical *in vitro* hydrogel release model that allows for rapid, high throughput and anisotropic evaluation of microbicide formulations. Finally, we tested two formulations of electrospun fibers containing a triple-antiretroviral combination for safety and efficacy against RT-SHIV challenge in a nonhuman primate model.

TABLE OF CONTENTS

List of Figures vii

List of Tables x

Chapter 1. Executive Summary And Specific Aims 14

1.1 Aim 1 15

1.2 Aim 2 15

1.3 Aim 3 16

Chapter 2. Introduction 17

2.1 Abstract 17

2.2 Introduction 18

2.3 Electrospun fibers for drug delivery 20

2.3.1 Breadth of API delivery using electrospun fibers 22

2.3.2 Rapid and sustained release from drug-eluting fibers 24

2.3.3 Challenges in electrospun fibers for vaginal delivery 29

2.4 Scale-up of electrospun fibers 31

2.4.1 3.1 Materials and capital investments 31

2.4.2 3.2 Manufacturing capability 32

2.4.3 Scale-up equipment 33

2.5 Conclusion 35

Chapter 3. Delivery Of Multipurpose Prevention Drug Combinations From Electrospun Nanofibers Using Composite Microarchitectures 37

3.1 Abstract 37

3.2 Introduction 38
3.3 Materials and methods 39
3.3.1 Polymer Solution Preparation 39
3.3.2 Electrospinning 40
3.3.3 Solution, Fiber and Fabric Characterization 40
3.3.4 Drug Loading and Release 42
3.3.5 Cytotoxicity and HIV Inhibition Assays 42
3.3.6 Statistical Analysis 43
3.4 Results 43
3.4.1 Properties of Electrospun Fabrics 43
3.4.2 Differential Scanning Calorimetry Analysis of Electrospun Fibers 46
3.4.3 Mechanical Testing of Electrospun Fibers 48
3.4.4 Visualization of Composite Microarchitectures 49
3.4.5 In Vitro Release of TFV and LNG 52
3.4.6 In Vitro Cytotoxicity and Inhibition of HIV-1 BaL Infection 55
3.5 Discussion 56
3.6 Conclusions 58

Chapter 4. Rapidly Biodegrading PLGA-Polyurethane Fibers for Sustained Release of Physicochemically Diverse Drugs 59

4.1 Abstract 59
4.2 Introduction 60
4.3 Materials and methods 62
4.3.1 PLGA-based poly(urethane urea) (PUUr) synthesis 62
4.3.2 Bulk polymer characterization 63
4.3.3 Electrospinning and fabric characterization 65

4.3.4 In vitro release 65
4.3.5 Cytotoxicity of biodegradation products and cytocompatibility of electrospun fibers .. 66
4.4 Results 67
4.4.1 Characteristics of synthesized PLGA-PUs 67
4.4.2 Drug and polymer compatibility in electrospun fibers 72
4.4.3 Release of physicochemically diverse drugs from PLGA-PUs with higher hard to soft segment ratio 75
4.4.4 Release of physicochemically diverse drugs from PLGA-PUs with higher fluorobenzene pendant group content 77
4.4.5 Biodegradation and cytocompatibility of PLGA-PU fibers and degradation products . 78
4.5 Discussion 82
4.6 Conclusions 84
Chapter 5. In vitro-ex vivo correlations between a cell-laden hydrogel and mucosal tissue for screening composite delivery systems 86
5.1 Abstract 86
5.2 Introduction 87
5.3 Materials and Methods 89
5.3.1 Burst- and sustained-release fiber preparation 89
5.3.2 Hydrogel formulation and characterization 90
5.3.3 Hydrogel extraction validation 90
5.3.4 In vitro hydrogel release 91
5.3.5 Tissue extraction validation 91
5.3.6 Ex vivo tissue explant release 92
5.3.7 Statistical analysis 92
5.4 Results 92

5.4.1 Burst- and sustained-release fibers exhibit uniform fiber morphology and fiber mat properties 92
5.4.2 Validation of hydrogel and tissue extraction methods 95
5.4.3 DPV loading, but not stacking order or microarchitecture, enhances burst drug release in vitro and ex vivo 96
5.4.4 PLGA/PCL content does not alter release rate of TFV in vitro or ex vivo but incorporating cells into hydrogel improves hydrogel/tissue release correlation 99
5.5 Discussion 101
5.6 Conclusion 104

Chapter 6. Simultaneous Measurement of Etravirine, Maraviroc and Raltegravir in Pigtail Macaque Plasma, Vaginal Secretions and Vaginal Tissue using a LC-MS/MS Assay 105

6.1 Abstract 105
6.2 Introduction 106
6.3 Materials & Methods 107
6.3.1 Reagents and tissues 107
6.3.2 Instrumentation and equipment 108
6.3.3 Calibration standard, internal standard and quality control (QCs) solutions 108
6.3.4 LC-MS/MS conditions 109
6.3.5 Sample preparation 110
6.3.6 Quantification 111
6.3.7 Accuracy and precision 112
6.3.8 Limit of quantification and limit of detection 113
6.3.9 Stability of antiretroviral drugs in plasma, vaginal secretions and vaginal tissue 113
6.3.10 Matrix effect and recovery 114
6.4 Results and Discussion 115

6.4.1 Chromatograms 115
6.4.2 Calibration curve and internal standard 118
6.4.3 Precision, accuracy, LOQ and LOD 118
6.4.4 Stability of extracted antiretrovirals 120
6.4.5 Matrix effect and recovery 121
6.5 Conclusions 124
Chapter 7. In Vivo Pharmacokinetics and Ex Vivo Protection of Pigtail Macaque Vaginal Mucosal Tissue from RT-SHIV by Drug-Eluting Fibers Containing a Triple Antiretroviral Combination ... 125
7.1 Abstract 125
7.2 Introduction 126
7.3 Materials & Methods 128
7.3.1 Preparation of electrospun fiber dosage forms 128
7.3.2 Nonhuman primate dosing schedule 130
7.3.3 Safety observation 131
7.3.4 Pharmacokinetic sample collection 131
7.3.5 Pharmacokinetic sample processing and analysis 132
7.3.6 Ex vivo tissue biopsy challenge assay 133
7.3.7 Data analysis 133
7.4 Results 134
7.4.1 Dual layer and FIF formulations are safe despite high ARV concentrations in secretions 134
7.4.2 Dual layer formulation resulst in rapid and high ARV concentrations while FIF formulation results in more constant concentrations in secretions and plasma 135
7.4.3 ARV concentrations in secretions and plasma are positively correlated after 24h 140

7.4.4 A single dose of dual layer fibers results in high vaginal and cervical tissue concentrations of all three ARVs after just 1 hour and for up to 14 days 141

7.4.5 A single dose of dual layer fibers prevents RT-SHIV infection in tissue biopsies for 24 hours 142

7.5 Discussion 144

7.6 Conclusion 147

7.7 Future Work 148

References 150

Appendix A: Chapter 4 Supplementary Files 166

Appendix B: Chapter 5 Supplementary Files 169

Appendix C: Properties and Structures of Selected APIs 170

LIST OF FIGURES

Figure 2.1: Schematic by Huang *et al.* depicting a layer of vaginal epithelial cells covered by a web of electrospun fibers containing antiretroviral drug before (left) and after (right) contacting human semen contaminated with HIV.[5] 20
Figure 2.2: Potential manufacturing geometry as presented by Ball *et al*. 21
Figure 2.3: Comparison of multi-nozzle electrospinning and wire electrospinning. 35
Figure 3.1: Electrospun fabric microarchitectures for topical delivery of single and combination drugs. 45
Figure 3.2: Photographs of NS 1WS500U cartridges used to fabricate TFV and LNG medical fabrics. 45
Figure 3.3: Thermograms of electrospun fibers of varying microarchitectures as determined by differential scanning calorimetry. 48
Figure 3.4: Mechanical properties, including Young's Modulus and tensile strength, for electrospun fabrics. 49
Figure 3.5: Confocal images of fabric microarchitectures. LNG and TFV were fabricated alone (a and b, respectively) or combined in different composites (c-e). 51
Figure 3.6: Cross-sectional scanning electron micrographs of electrospun fabrics. 52
Figure 3.7: *In vitro* release profiles (a,b,e) and dosage profiles (c,d,f) of LNG and TFV delivered from different composite fibers. 53
Figure 3.8: Effect of LNG and TFV release from stacked composites of different thickness. 54
Figure 3.9: *C*ytotoxicity and HIV antiviral activity of drug-loaded fabrics of varying microarchitecture. 56
Figure 4.1: PLGA-based polyurethane urea synthesis. 68
Figure 4.2: Evolution of PLGA-PU compositions. 72
Figure 4.3: Scanning electron micrographs of electrospun polyurethane polymers. 73
Figure 4.4: Thermal properties of polymers in blank and drug-loaded electrospun fibers as determined by differential scanning calorimetry. 75
Figure 4.5: Release of LNG (a), MVC (b), NFL (c), and TFV (d) from electrospun fibers from polyurethanes PLGA-PU and PLGA-2PU (both sans fluorobenzene pendant) into 2% solutol in deionized water at sink conditions over 72 hours. 76
Figure 4.6: Release of LNG (a), MVC (b), NFL (c), and TFV (d) from electrospun fibers from polyurethanes PLGA-PU-FB and PLGA-PU-2FB (2 and 4 mol% fluorobenzene

pendant, respectively) into 2% solutol in deionized water at sink conditions over 72 hours. 77
Figure 4.7: Degradation characteristics of PLGA-PUs over 4 weeks. 79
Figure 4.8: TZM-bl cell cytocompatibility with electrospun PLGA-PU fibers. 81
Figure 5.1: Scanning electron micrographs of electrospun PVA fibers containing either a single drug (DPV, MVC or TFV) (a-d) or the triple-drug combination (DPV + MVC + TFV) (e-f), and treatment arms of triple-drug combinations (g-h) 94
Figure 5.2: Scanning electron micrographs of electrospun sustained release fibers containing 15 wt.% TFV, and schematic of single-drug sustained release microarchitecture. 95
Figure 5.3. Release profiles of burst fiber formulations of DPV (a,d), MVC (b,e) and TFV (c,f) in hydrogels (a-c) and tissue explants (d-f). 98
Figure 5.4: Correlation between hydrogel and tissue explant release profiles for burst release fiber formulations of a) DPV, b) MVC and c) TFV. 99
Figure 5.5: Release profiles of sustained release fiber formulations loaded with 15 wt.% TFV in a) hydrogel, b) hydrogels with encapsulated cells, and c) tissue explants. 100
Figure 5.6: Correlation between hydrogel and tissue explant release profiles for burst release fiber formulations. 101
Figure 6.1: Chemical structures of antiretroviral drugs. 109
Figure 6.2: Chromatograms for drugs (MVC, RAL, ETR) and internal standards (MVC-d_6, RAL-d_6, ETR-$^{13}C_6$) at high and low concentrations. 116
Figure 6.3: Chromatograms for (ETR, MVC, RAL) in each matrix. 117
Figure 7.1: Schematic of drug-eluting electrospun fiber formulations loaded with ETR, MVC and RAL. 130
Figure 7.2: Dosing and sampling schedule for safety and pharmacokinetic studies of dual layer and fiber-in-fiber formulations. 131
Figure 7.3: Concentrations of ETR, MVC and RAL in vaginal secretions (a) and blood plasma (b) after daily dosing for dual layer formulation. 134
Figure 7.4: Concentrations of ETR, MVC and RAL in vaginal secretions (a-c) and blood plasma (d-f) for 14 days after a single dose of dual layer or fiber-in-fiber formulations. 137
Figure 7.5: Tissue penetration ratio (TPR) of plasma concentration to vaginal secretion concentration for ETR, MVC and RAL after a single application of dual layer fibers. 140

Figure 7.6: Correlations between vaginal secretion and blood plasma concentrations for ETR (a), MVC (b) and RAL (c). 141
Figure 7.7: Concentration of ETR (a), MVC (b) and RAL (c) in cervical and vaginal tissue over 7 days after a single dose of dual layer fibers. 142
Figure 7.8: Infectivity of pigtail macaque cervical and vaginal biopsies after a single dose of dual layer fibers and subsequent challenge with RT-SHIV. 144

LIST OF TABLES

Table 2.1: Reported in vitro release kinetics of small molecule drugs from polymeric fibers. 26
Table 2.2: Common attributes of electrospun materials used for drug delivery *in vivo*.[60-78] 28
Table 2.3: Electrospinning platforms for scalable manufacturing.[47, 80, 82, 89-104] 33
Table 3.1: Composition and solution properties of fiber formulations.[a] 44
Table 3.2: Properties of drug-loaded electrospun fibers.[a] 46
Table 4.1: Polymer molecular weights and polydispersity index (PDI) as determined by gel permeation chromatography.* 69
Table 4.2: Fluorine content of PLGA-PU polymers containing a fluorobenzene pendant group. 70
Table 4.3: Composition of polymers as determined by x-ray photoelectron spectroscopy. 71
Table 4.4: Wettability and equilibrium water content of polymers. 72
Table 5.1: Validation of extraction of DPV, MVC and TFV from hydrogels and tissue explants alone and in the presence of the triple drug formulation. 96
Table 6.1: Concentrations of stock solutions, working solutions and QC controls. 109
Table 6.2: Instrument method for the LC-MS/MS analysis for ETR, MVC and RAL with ETR-$^{13}C_6$, MVC-d_6, and RAL-d_6 as internal controls. 110
Table 6.3: Precision and accuracy of the assay for the three antiretroviral drugs in pigtail macaque plasma, vaginal secretions and vaginal tissue at low, medium and high concentrations. 112
Table 6.4: Limit of detection and limit of quantification of antiretroviral drugs. 113
Table 6.5: Stability of ETR, MVC, RAL in plasma, vaginal secretions and vaginal tissue after storage at room temperature, 4°C and three freeze(-80°C)/thaw cycles. 120
Table 6.6: Matrix effect, extraction yield, process efficiency, and overall recovery of antiretroviral drugs. 123
Table 7.1: Pharmacokinetic parameters of ETR, MVC and RAL in blood plasma and vaginal secretions for dual layer and fiber-in-fiber formulations. 136
Table 7.2: Pharmacokinetic parameters comparing capacity of dual layer and fiber-in-fiber electrospun fiber formulations to sustain release of ETR, MVC and RAL. 139
Table 7.3: Pharmacokinetic parameters of ETR, MVC and RAL in vaginal and cervical tissue after a single dose of the dual layer formulation. 142
Table 7.4: Proposed challenge schedule for efficacy study of dual layer fibers. 149

ACKNOWLEDGEMENTS

I have been fortunate to work with my advisor, Kim Woodrow, over the course of my doctorate. I am grateful for her support and enthusiasm over the years. Kim is truly a brilliant, curious scientist, and her quest for a deeper scientific understanding of all of her work has been inspirational to me. I appreciate her willingness to let me pursue unique opportunities during my education and her encouragement to pursue new research paths. It has been a pleasure to work with such a dedicated and insightful mentor, who provides excellent feedback and challenges me to become a better scientist. I cannot thank her enough for her time and effort, and am grateful that I was given the opportunity to be a student in her lab.

I would like to thank the members of my supervisory committee, all of who added a fresh perspective to different aspects of my work. I would like to thank Buddy Ratner for his insight on biomaterials and the translational aspects of this project, Suzie Pun for her expertise on drug delivery systems, Jeanne Marrazzo for her invaluable knowledge on the field of microbicides as a whole, and David Fredericks for his clinically oriented outlook. I am grateful for the time, feedback and dedication to furthering my career as a scientist that each of my committee members has granted me.

A number of individuals have been integral to my scientific training. I am forever indebted to Stephanie Bryant, who believed in me from the time I was a freshman at the University of Colorado and encouraged me to go to graduate school. I will always feel like her little undergrad. I am grateful that I got to spend 6 months of my PhD with Heather Jaspan at the University of Cape Town, who served as a wonderful host and mentor while I was there, and is now a friend and trusted source of advice. I owe Dale Whittington many thanks for my LC-MS/MS training, and for always being available to troubleshoot the instrument, no matter the time of day. I also received excellent instrumentation training from Gerry Hammer and Scott Braswell of the Molecular Analysis Facility, Tuesday Kuykendall and Tatyana Galenko in the Materials Science Department. I was honored to be a part of the Molecular Medicine

Training Program, and am grateful to Nancy Maizels and Conrad Liles for running such a wonderful program.

I owe many thanks for my fellow lab members for their collaboration, support and experimental feedback. I am grateful that I got to work so closely with Yonghou Jiang (NK), who was an excellent collaborator on all of my projects, while providing encouragement and comedic relief. I am your number one fan. Arielle Steger was an excellent office mate and was always willing to let me bounce ideas off of her. Cameron Ball, Renuka Ramanathan, Emily Krogstad and Joe Phan served as role models during my early years in the lab, and I appreciate their continuous encouragement and advice. Thanks to the rest of the fiber team- Rick Edmark, Edward Roberts, Ryan Stoddard, Shih-Feng Chou, Huarong Nie, Daniel Carson, and Hannah Frizzell, for technical advice, support and intellectual discussion. I had the privilege of working with three talented undergraduates during my time as a graduate student, including Annie Wu, Christina Nhan, and Adam Little, who all contributed in significant ways to my research.

This work was funded in part by grants to Kim from the Gates Foundation (OPP1067729) and NIH/NIAID (AI098648, AI112002). I was supported by the National Science Foundation Graduate Research Fellowship, including a Graduate Opportunities Worldwide award, and the Molecular Medicine Training Grant (T32GM095421).

My friends and family provided endless support throughout my PhD. Special thanks to Amanda Sudduth and Marvin Mecwan for always being up for coffee breaks, Hanna Kern and Natalie Miller for companionship at Palermo, and David Younger, Blake Bluestein and Andrew Wang for climbing mornings. I am thankful that Allison Beller is always willing to help me remember to ‘play hard’, and I’m eternally grateful for my ping pong/sailing/skiing/fishing/real friend. Thanks to my little sister, Caroline, for always being available to chat and keep me grounded. And finally, a huge thanks to my parents who never stopped supporting me as a gradual student, I appreciate your love and encouragement.

DEDICATION

To the women of the world: let us lift each other up.

Chapter 1. Executive Summary And Specific Aims

Women are disproportionately affected by the HIV epidemic, especially in sub-Saharan Africa, where 70% of the world's HIV burden is located.[1] Development of technologies that allow for women to protect themselves from HIV is motivated by gender power disparity between men and women, which often leads to the inability for women to negotiate condom use and/or faithfulness, coupled with the greater risk of male-to-female than female-to-male transmission per sex act.[2] Preventative treatments, including male circumcision, treatment of other STIs and the development of an HIV vaccine, have been largely unsuccessful to-date. A microbicide is a product that can be applied either vaginally or rectally for the prevention of STIs, including HIV.[3] The current microbicide strategy is to incorporate one or more antiretroviral drugs into a delivery vehicle, including gels, intravaginal rings, tablets, films, or injectables, which are in varying stages of the development pipeline.

Recently, electrospun fibers have been explored in proof-of-concept studies as a novel microbicide delivery vehicle.[4, 5] Fibers offer a number of advantages including the possibility of discreet use by women, the potential for easy scale-up, the ability to incorporate multiple physicochemically diverse drugs, and the use of different polymers and microarchitecture to tailor release of active compounds. Electrospun fibers appear white, are silky, smooth and pliable to the touch, and can dissolve rapidly; attributes that may yield the microbicidal fibers acceptable to female users. Thus far, fibers have been shown to be a promising microbicide, but are still a naïve topical, vaginal dosage form, and have yet to undergo testing relevant nonhuman primate models. The goal of this dissertation is to characterize material and formulation properties of microbicidal electrospun fibers, probe the use of novel polyurethane polymers for sustained antiretroviral drug delivery, and test fibers in innovative yet relevant pre-clinical models to optimize electrospun fiber formulations that will be tested for safety and efficacy in a nonhuman primate challenge model.

1.1 AIM 1

Aim: Influence of microarchitecture, thickness and polymer chemistry on delivery of physicochemically diverse drugs from electrospun fibers.

Gap: Formulating multiple drugs with physicochemically diverse properties into electrospun fiber composites and controlling the release of encapsulated drugs is a challenge within the field of drug delivery. We investigated how microarchitecture and fabric thickness affect the release of drug combinations from electrospun fibers that were fabricated on a production-scale instrument with high drug loading. Furthermore, we sought to design PLGA-based polyurethane polymers that degraded on a physiologically relevant timescale, but maintained sustained drug release properties.

Impact: In order to translate drug-eluting fibers to clinical applications, it is imperative that electrospun fibers have the capacity to be loaded with relevant, potentially high doses of encapsulated drugs, and be produced efficiently in the quantities needed for larger trials. In addition, while hydrophobic polymers have been shown to sustain drug release, they often degrade on timescales that far exceed the completion of drug release, thus it is necessary to decouple the degradation and release properties of electrospun fibers.

Thesis Chapter(s): Chapter 3: Delivery of Multipurpose Prevention Drug Combinations from Electrospun Nanofibers Using Composite Microarchitectures, Chapter 4: Rapidly Biodegrading PLGA-Polyurethane Fibers for Sustained Release of Physicochemically Diverse Drugs

1.2 AIM 2

Aim: Evaluation of burst- and sustained-release electrospun fibers in a hydrogel tissue mimic and corresponding explant tissue.

Gap: Conventional *in vitro* release testing methods, such as an aqueous media sink, do not allow for anisotropic testing of complex fiber microarchitectures, wherein drug combinations with varying properties may affect the overall wetting and diffusion of co-encapsulated drugs from electrospun fibers.

Impact: An *in vitro* release platform that facilitates anisotropic evaluation of drug-eluting fiber composites intended for topical or transdermal drug delivery, and correlates the release profiles with release into the targeted tissue, allows for more rapid optimization of electrospun fibers formulations in the transition from *in vitro* testing to *in vivo* studies.

Thesis Chapter(s): Chapter 5: *In vitro-ex vivo* correlations between a cell-laden hydrogel and mucosal tissue for screening composite delivery systems

1.3 AIM 3

Aim 3: Safety, pharmacokinetics and efficacy of electrospun fibers for prevention of HIV in nonhuman primates

Gap: Electrospun fibers offer many advantages for vaginal, topical delivery of antiretrovirals, including high drug loading and co-encapsulation of diverse drugs, but have yet to been tested for safety or efficacy *in vivo*.

Impact: We have validated a method for detecting a triple combination of antiretrovirals in pigtail macaque vaginal secretions, tissue and plasma using a LC-MS/MS assay. The pharmacokinetic profiles will inform whether our dual layer and fiber-in-fiber formulations delivery adequate doses of a triple combination of antiretroviral drugs to vaginal tissue to prevent infection with RT-SHIV. Finally, the safety observations will provide insight into the acceptable dosing frequency of drug-eluting electrospun fibers to mucosal tissue.

Thesis Chapter(s): Chapter 6: Simultaneous Measurement of Etravirine, Maraviroc and Raltegravir in Pigtail Macaque Plasma, Vaginal Secretions and Vaginal Tissue using a LC-MS/MS Assay, Chapter 7: In Vivo Pharmacokinetics and Ex Vivo Protection of Pigtail Macaque Vaginal Mucosal Tissue from RT-SHIV by Drug-Eluting Fibers Containing a Triple Antiretroviral Combination

Chapter 2. Introduction

Adapted from: Electrospun fibers for vaginal anti-HIV drug delivery. Anna K. Blakney, Cameron Ball, Emily A. Krogstad, Kim A. Woodrow. Antiviral Research 100:S9-S16 (2013). In pursuit of functional electrospun materials for clinical applications in humans. Ryan J. Stoddard, Arielle L. Steger, Anna K. Blakney, Kim A. Woodrow. Therapeutic Delivery 7 (6): 387-409 (2016).

2.1 ABSTRACT

Diversity of microbicide delivery systems is essential for future success in the prevention and treatment of HIV in order to account for the varied populations of women all over the world that may benefit from use of these products. Recently, a novel dosage form for intravaginal drug delivery has been developed using drug-eluting fibers fabricated by electrospinning. There is a strong rationale to support the idea that drug-eluting fibers can be designed to realize multiple design constraints in a single product for topical HIV prevention: fibers are able to deliver a wide range of agents, incorporate multiple agents via composites, and facilitate controlled release over relevant time frames for pericoital and sustained (coitally-independent) use. It is also technologically feasible to scale-up production of fiber-based microbicides. Electrospun fibers may allow for prioritization of physical attributes that affect user perceptions without compromising the capacity for biological efficacy. Electrospinning is a simple, low-cost and versatile approach to fabricate multifunctional materials useful in drug delivery and tissue engineering applications. Despite its emergence into other manufacturing sectors, electrospinning has not yet made a transformative impact in the clinic with a pharmaceutical product for use in humans. Challenges in using fibers as a microbicide include issues related to vehicle deployment, spreading and retention in the vaginal vault. In addition, studies will need to address the interaction of the fibers with the mucosal environment, including unknown safety and toxicity. Sustained release fiber microbicides capable of delivering multiple antiretroviral drugs while simultaneously exhibiting tunable degradation or dissolution of the fibers is also a challenge. However, electrospun fibers are a promising new platform for vaginal delivery of anti-HIV agents and future research will inform their place in the field.

2.2 INTRODUCTION

Topical microbicides are a critical component of the prevention portfolio to combat sexual transmission of HIV. One of the priorities in the field is to confront the low levels of user adherence that have been documented in clinical trials of microbicides. The early termination of VOICE due to low user adherence compromised evaluation of efficacy.[6] Vaginal drug delivery systems (DDS) play a principle role in bridging biological efficacy and behavioral adherence, which collectively determine the overall impact of a topical microbicide product. It is unlikely that a single DDS technology will solve the prevention needs for all women, particularly for adolescent women in low-resource settings where the crises of women's reproductive health is complicated by issues of poverty, malnutrition, poor education, and gender inequality. For this reason, the portfolio of available microbicide DDS needs to be numerous and diverse.

The further advancement and development of any single microbicide DDS must now prioritize the capacity of the DDS to design for physical attributes that impact user perceptions without compromising the design for biological efficacy. The ultimate decision to use a microbicide product is influenced by a complex combination of product attributes (sensory perceptions, dosing frequency, coital association), user demographics (age, race, culture), and perceived risks for HIV as well as perceived benefits from product use. These user perceptions are the first barrier to designing effective microbicide products, but are often the last consideration in product development. In addition to being accepted by users, the product must deliver bioactive compounds, possibly in combination, over a relevant period of time (both coitally dependent and independent), be affordable, and have the ability to be produced on an industrial scale. Future development of products will likely incorporate design iterations informed by user perception as well as biological efficacy.

A number of microbicide products are in various stages of the development pipeline, but the lead technologies include gels, films, tablets and intravaginal rings (IVRs).[7-10] There are a number of advantages and disadvantages associated with the leading DDS. Vaginal gels are relevant for pericoital

or daily use but have limited ability to deliver physicochemically diverse agents, are not amenable to sustained protection and are messy and may leak out of the vaginal cavity after application. Tablets are easily formulated and manufactured but may leave a grainy residue in the vaginal cavity after dissolution.[11] IVRs are currently the only sustained release dosage method and have enhanced product stability as a solid dosage form, but are relatively complicated and expensive to fabricate[9]. Vaginal films are also relevant for pericoital use, have demonstrated capability for delivering physicochemically diverse agents, and exhibit enhanced product stability compared to semi-solid dosage forms such as gels. However, vaginal microbicide films have reported loadings of < ~1%, and their low overall mass may preclude delivery of sufficient doses of certain APIs.[8, 12, 13] It is also not clear if current films will be amenable for sustained drug delivery and coitally-independent applications. In addition, the bulk physical properties of films must be controlled to avoid sharp edges and corners that could induce abrasion upon application and use.

Recently, a novel dosage form for intravaginal drug delivery has been developed using drug-eluting fibers fabricated by electrospinning, a technique that applies electrostatic forces to form polymeric fibers. Electrospinning is an elegant and facile method for formulating a solid-dosage form microbicide product. The process of electrospinning fibers is well-established,[14] efficient and relatively inexpensive, and since most synthetic and many biological polymers can be electrospun, there is a wide array of possible formulations envisioned for diverse antiretroviral drugs. A number of physicochemically diverse drugs have been encapsulated into electrospun fibers,[15] typically with high encapsulation efficiency.[16] Fiber-based "fabrics" are typically soft and non-abrasive, highly flexible, lack sharp corners and can realize a number of geometries (sheets, tubes, coatings). In addition, there is no leakage or mess expected with delivery of fibers into the vaginal cavity. Therefore, there is a strong rationale to support that drug-eluting fibers can be designed to realize multiple design constraints in a single product for topical HIV prevention.

2.3 ELECTROSPUN FIBERS FOR DRUG DELIVERY

Two recent publications investigated electrospun fibers as a platform for vaginal delivery as a topical microbicide for HIV prevention.[4, 5] Huang *et al.* encapsulated the reverse transcriptase inhibitors etravirine or tenofovir disproxil fumarate (Viread) into fibers based on cellulose acetate phthalate (CAP).[5] CAP has documented anti-HIV activity, which is thought to be mediated by interactions of the polymer with HIV glycoproteins. In addition to its anti-HIV activity, CAP undergoes a solution-to-gel phase transition in response to pH due to the phthalate function group of CAP (pKa of ~5.5). In the low pH environment of the vagina (pH of ~4-5) CAP is a semi-solid, but dissolves upon a semen-induced pH change that increases the pH of the vagina. Thus, CAP fibers were designed to dissolve and release antiretrovirals within seconds to minutes after exposure to semen (Figure 2.1). CAP fibers were found to be safe *in vitro* at concentrations of up to 1.8 mg/mL, with minimal toxicity in both TZM-bl cells and vaginal epithelial cells. Exposure to only 0.05 mg/mL of CAP fibers resulted in 50% HIV neutralization and complete neutralization was achieved upon incorporation of 17.8% (wt. drug/wt. polymer) TDF, for a final concentration of TDF of ~0.1 μg/mL.

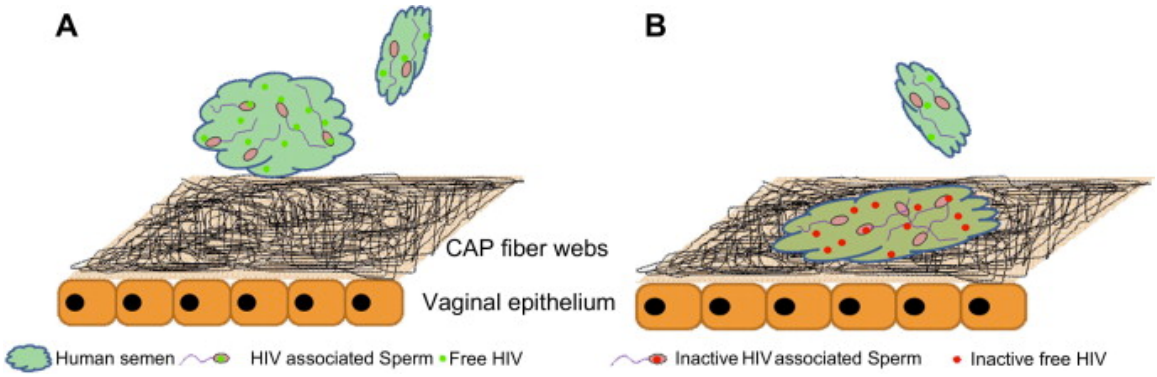

Figure 2.1: Schematic by Huang *et al.* depicting a layer of vaginal epithelial cells covered by a web of electrospun fibers containing antiretroviral drug before (left) and after (right) contacting human semen contaminated with HIV.[5]

Ball *et al.* fabricated nanofiber meshes from a polymer blend of poly-L-lactic acid (PLLA) and polyethylene oxide (PEO) with an assortment of antiretroviral and contraceptive agents for the dual prevention of HIV transmission and unintended pregnancy (Figure 2.2).[4] Fibers were loaded with

maraviroc (MVC), an inhibitor of CCR5-mediated HIV fusion, or 3'-azido-3'deoxythymidine (AZT). Both ARV drug-fibers were found to be non-toxic to TZM-bl cells and macaque ectocervical explants. ARV drug-loaded fibers also had comparable HIV inhibition to the free drugs and maintained IC50 levels at concentrations of 0.90 nM for MVC and 120 nM for AZT. Both MVC and AZT were found to exhibit burst-release from the fibers, but sustained release on the timescale of weeks was achieved by incorporation of poly-(D,L)-lactic acid into the fibers, although drug release was only monitored for 1 week. Glycerol monolaurate (GML) was also incorporated into the fibers and was found to inhibit sperm motility and viability at concentrations of 0.05-0.5 % wt./vol. With the inclusion of GML, the fibers formed both a chemical and physical barrier to sperm. Ball *et al.* electrospun fiber meshes in the geometry of a tampon applicator and observed release of a dye to assess coverage of the vaginal lumen and cervix in a mouse model.

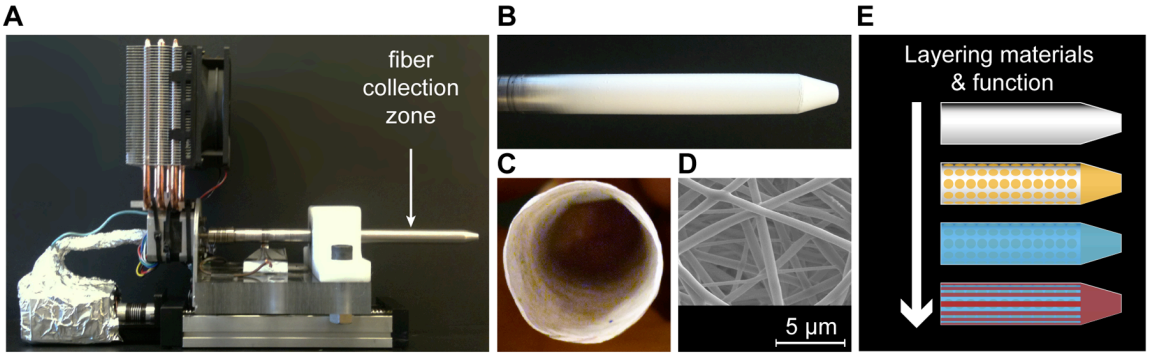

Figure 2.2: Potential manufacturing geometry as presented by Ball *et al.* A) a two-axis mandrel electrospinning rig for fiber collection, B) a mandrel in the shape of a tampon applicator that may be suitable for vaginal delivery, C) a fiber mesh removed from the mandrel with a hollow interior, D) a scanning electron micrograph of fibers with a porous microstructure, E) a schematic of a potential way to produce a layered mesh for a multifunctional material.[4]

These papers establish the potential for using electrospun fibers as a platform for vaginal drug delivery of antiretrovirals. In addition, the drug-eluting fiber platform may represent a discreet, female-controlled and reversible method of HIV prevention. The ability to combine antiretroviral therapy with other STI prevention or contraception offers an advantage that may increase user adherence and acceptance. For example, high-risk groups of women who have low perceived risk of HIV acquisition

may be more likely to employ a dual protection product that incorporates HIV prevention with a contraceptive.

Electrospun fibers offer a number of significant advantages that enable their potential for use as a vaginal microbicide platform. They have been used to deliver a wide range of agents,[17] and can be fabricated into composites for incorporation of multiple agents. Composites are created by spinning multiple solutions at one time,[18] layering different solutions,[19] coaxial spinning[20] or emulsion spinning.[21] It is also possible to formulate fibers with controlled release over time frames relevant for both pericoital and sustained (coitally-independent) use. Electrospun fibers have been successfully formulated for quick[22] and sustained[23] release of drugs. In addition, the ability to scale-up manufacturing of microbicide products for use in human clinical trials as well as widespread use is essential. The infrastructure for mass-production of electrospun fibers has already been established, as electrospinning is used widely in industrial applications.[24] Finally, the ability to design a fiber-based product to account for user preference could enhance performance regarding user adherence. Electrospun fibers offer a variety of possible geometries and mechanical properties that could enable user-centered design. In the following sections, we will discuss the delivery of diverse APIs using electrospun fibers, the ability to achieve quick and sustained release profiles, and current challenges with drug delivery from electrospun fibers.

2.3.1 *Breadth of API delivery using electrospun fibers*

Small molecules, peptides, nucleic acids, antibodies and nanocarriers all have potential for use in vaginal delivery systems for topical HIV prevention. The physico-chemical diversity of these agents alone and in combination demand that next generation microbicide dosage forms enable delivery of diverse agents. In addition, the vaginal environment consists of a low pH, degradative enzymes, microflora and other potential components that may inactive many microbicide agents before they can be effective.[25] Encapsulating drugs in electrospun fibers offers a way to protect the active compounds until they are released. The electrospinning process is carried out at room temperature and, because many

polymers can be electrospun using only water as the solvent, the fabrication process is gentle. The wide variety of polymers that can be electrospun allows for the specific formulation of a single agent, and multiple agents can then be combined by layering fibers, using a multi-jet configuration to produce interwoven fibers, or by combining multiple drugs in a single fiber.

Many studies have shown that electrospun fibers are capable of encapsulating drugs with a wide range of solubility.[26] Electrospun fibers can also be used as a way to increase the bioavailability of therapeutic agents through solid dispersion. When incorporated into a DDS, the drug may exist as an amorphous, polymorphous or crystalline solid. The ability of the drug to be released may depend on the solid state, with an inverse relationship between the degree of crystallinity, solubility and thus bioavailability. Verreck *et al.* incorporated itraconazole, a highly water insoluble drug, into electrospun fibers to produce dispersions of amorphous drug, which was confirmed by no evident melting endotherm for itraconazole as analyzed by differential scanning calorimetry.[27] Similarly, Yu *et al.* observed well-dispersed amorphous ketoprofen, a water-insoluble non-steroidal anti-inflammatory drug (NSAID), and hypothesized that the distribution was due to hydrogen bonding between the drug and polymer nanofibers[28]. Thus, due to their solid dosage form and wide range of applicable materials, electrospun fibers offer the potential for excellent bioavailability of drugs.

Biological agents such as peptides, antibodies, enzymes and nucleic acids have also been proposed for vaginal delivery, but current delivery vehicles limit usage. The challenge resides in delivering biologic agents to the vaginal mucosa without altering their activity. Loss of activity arises from instability in liquid based platforms or high temperature or abrasive solvents used in processing. A wide range of biologics have been encapsulated into electrospun fibers, including proteins,[29] viruses,[30] DNA,[31] siRNA,[32] bacteria[33] and cells.[34] Maretschek *et al.* were able to tune the release of a model hydrophilic protein, cytochrome C, from a fiber blend of PLLA and PEG.[35] Human β-nerve growth hormone and basic fibroblast growth factor have been encapsulated within[23] or deposited on the surface of nanofibers,[36] with intended use in tissue engineering. Liao *et al.* and Saraf *et al.* encapsulated adenovirus[30] and plasmid DNA,[31] respectively, using coaxial spinning for gene delivery purposes. Cao *et*

al. achieved controlled release of siRNA from PCL nanofibers for 28 days with a silencing efficiency comparable to conventional siRNA transfection.[32] Though many of the applications of electrospinning have been focused on cancer therapy or tissue engineering, the foundation of incorporation of biologics into electrospun fibers exposes the potential for their use as delivery systems for antibodies against HIV, antigens for vaginal mucosal vaccines, delivery of bacteria in the treatment of bacterial vaginosis, or gene delivery.

In addition to delivery of biologics, electrospun fibers may also offer potential to deliver drug-loaded nanoparticles. There is currently no well-established vehicle for vaginal delivery of nanoparticles, and the combination of nanofibers and nanoparticles could allow for enhanced precision control of drug release. As a solid dosage form, the fibers may overcome the issues associated with delivering nanoparticles in a vaginal gel, such as aqueous stability and long-term storage of the particles. Coumarin 6, a model drug, was released from PLGA nanoparticles encapsulated in PVA/PEO blend nanofibers over a period of 2-8 hours, depending on the ratio of PVA to PEO.[37] Beck-Broichsitter *et al.* were able to show an altered release profile, i.e. slower release, *in vitro* of coumarin 6 from the PVA nanofiber/nanoparticle composites compared to nanoparticles alone, but not for PEO meshes. FGF-2 was released from heparin-containing polyelectrolyte complex nanoparticles encapsulated in chitosan fiber networks over a period 30 days, with maintained bioactivity of the encapsulated drug.[38] Furthermore, Volpato *et al.* were able to show the preservation of nanoparticle structure when encapsulated in electrospun fibers using fluorescent dyes and confocal microscopy. The duo of nanofibers and nanoparticles may broaden the delivery capabilities of fibers as a vaginal microbicide.

2.3.2 *Rapid and sustained release from drug-eluting fibers*

Drug release from polymeric fibers depends on the erosion and degradation of the polymer used and the diffusive properties of the incorporated drugs. Release of drugs from gels is governed by both erosion and diffusion and depends on hydration, swelling and dissolution of the polymer.[39] The vaginal

film matrix also swells, but release largely depends on diffusion of the drug from the polymer matrix.[40] In contrast, intravaginal rings undergo very minimal swelling and erosion, but also rely on diffusion of the drug from the polymer matrix.[41] Electrospun fiber meshes similarly rely mostly on diffusion for drug delivery, although erosion of individual fibers has been observed.[42]

By utilizing a variety of polymers and blends of polymers, researchers have achieved both rapid (<15 minutes) and sustained (>7 days) release of various drugs from electrospun fibers (Table 2.1). This is a huge advantage in vaginal delivery of antiretroviral drugs, as there are a number of scenarios in which vaginal microbicides might require different timescales for delivery. Quickly dissolving fibers could be useful for a vaginal microbicide intended for pericoital use, in which rapid delivery of antiretroviral drugs would be imperative to act against immediate viral exposure. Although similar to vaginal microbicide films, electrospun fibers have the advantage of a silky texture as well as the ability to control micro-scale architecture for tuned release properties. Long-term release is coitally independent and would be preferable in a situation where a user could dose monthly and have sustained levels of drug in tissue for HIV prevention.

Several groups have demonstrated rapid drug release from electrospun fibers by using quickly dissolving polymers such as PVA, PEO, alginate and chitosan. The use of quickly dissolving polymer fibers allows for burst release of drug. Li *et al.* used PVA nanofibers to burst-release caffeine and riboflavin. They observed dissolution of fibers within 5 seconds and 100% release of caffeine and 40% release of riboflavin within 60 seconds.[43] Macri *et al.* used tyrosine-derived polycarbonate terpolymer fiber mats to deliver a hydrophilic peptide, P12, with complete release within 9 hours.[44]

Table 2.1: Reported in vitro release kinetics of small molecule drugs from polymeric fibers.

Time-frame of drug release	Released compound	Fiber and Mesh Properties	% Released at 24 h	Time to release:		Ref.
				50%	100%	
Rapid release (<60 min)	Azidothymidine (AZT), acyclovir (ACV), maraviroc (MVC)	Polymer: PLLA/PEO Solvent: Chloroform/Trifluoroethanol Fiber diameter: 200 - 700 nm Drug loading: 1 wt%	100%	<1h	<1 h	[4]
	Cefoxitin	Polymer: PLGA (75:25) Solvent: Dimethlyformamide Fiber diameter: 200 – 400 nm Drug loading: 1 - 5 wt%	100%	<1h	<1h	[45, 46]
Intermediate release (1-3 d)	bis-chloroethylnitrosourea (BCNU, Carmustine®)	Polymer: PEG-PLLA Solvent: Chloroform Fiber diameter: 700 – 1400 nm Drug loading: 5 – 30 wt%	60-80%	5-15 h	70 h	[47, 48]
	Ciprofloxacin	Polymer: PVA/PVAc Solvent: Water/Acetic acid Fiber diameter: 400 – 500 nm Drug loading: 10 wt%	40 - 50%	<50 h	>100 h	[49, 50]
Sustained release (>7 d)	Paclitaxel	Polymer: PLGA (50:50) Solvent: Dichloromethane Fiber diameter: 700 – 2500 nm Drug loading: 10 wt%	13-22%	>20 d	>60 d	[4, 51]
	SN-38	Polymer: PCL/PGC-C18 (90:10) Solvent: Chloroform/methanol Fiber diameter: ~7000 nm Drug loading: 0.1 – 1 wt%	~30%	~40 d	>70 d	[52]

Extended release kinetics of drugs from polymer fibers are also highly desirable for vaginal microbicides. A once-monthly dosage form, like vaginal rings, has potential to overcome challenges related to low user adherence. Long-term drug release from fibers has been demonstrated by a number of groups.[22, 52] Sustained release is achieved using a variety of polymers and techniques that have been optimized for slowing release, including coating the fibers to prevent burst release,[53] coaxial or emulsion spinning to create a shell around a core fiber of drug,[54] or crosslinking the polymer.[55] Jannesari *et al.* observed that by decreasing drug loading of ciprofloxacin HCl in PVA/PVAc nanofibers and increasing thickness, release could be extended to 80 days.[49] Xie *et al.* delivered paclitaxel, a chemotherapy agent for the treatment of C6 glioma, for up to 60 days from PLGA micro- and nanofibers.[51] Because many

sustained delivery fiber systems require the use of slowly degrading materials, the product might require removal, much like vaginal rings. By manipulating either polymer chemistry or physical attributes of the fibers, sustained delivery of therapeutics is achievable.

The composition of the fiber formulation has a significant impact on the electrospinning process as well as the final fiber solid-state properties, which will impact safety and efficacy. Table 2.2 lists the most commonly investigated carrier polymers used in electrospinning for drug delivery applications.[56] Careful consideration of the thermal and solid-state properties of polymers used in the formulation is also critically important for modulating drug release from electrospun fibers. Polymer crystallinity defines the ratio of ordered, aligned crystalline segments of polymer chains relative to the random, disorganized amorphous regions. The degree of crystallinity influences mechanical properties such as hardness, modulus, tensile strength and melting temperature but will also impact drug release kinetics. Ball et al. found that the ratio of semicrystalline poly-L-lactic acid (PLLA) to amorphous poly-D,L-lactic acid (PDLLA) could be used to modulate the release of a water soluble antiretroviral drug.[4] Although the polymers were chemically identical, incorporating more amorphous PDLLA likely enhanced the rate of water penetration into the polymer network and led to faster drug release from the fibers. The melt temperature (Tm) is used to measure the degree of crystallinity of both semi-crystalline polymers and crystalline drugs. Differential scanning calorimetry enables observation of melt peaks for both polymers and drugs, and can be used to characterize crystalline content in the solid dispersion. The absence of a polymer of drug melt peak can be an indicator of an amorphous dispersion and shifts in polymer Tm may be evidence of drug-polymer interactions.[57] As was observed by Verreck et al. upon reaching 40% loading of itraconazole and ketanserin in polyurethane fibers, high drug loading can result in crystalline drug formation.[58] Polymer glass transition temperature (Tg), which is the temperature at which the polymer transitions from a hard, rigid "glassy" state to a more compliant, pliable "rubbery" state due to increased chain mobility, is also an important factor influencing drug release from electrospun fibers. Peng et al. observed that incorporating a small molecule drug into PDLLA and poly(ethylene glycol-co-D,L-lactic acid) (PELA) electrospun fibers reduced the polymer glass transition, likely due to the drug

allowing for more facile movement of polymer chains.[59] The Tg of electrospun fibers was also decreased by higher percentage of PELA relative to PDLLA, and correlated with faster drug release. Drastic alterations in polymer Tg can directly influence the clinical relevance of electrospun materials. For example, if the Tg is below body temperature, fibers may transition into an undesired amorphous state and cause rapid drug release. Polymer crystallinity, Tg and Tm are not necessarily independent properties, but allow for strategic design of formulations with desired clinical performance.

Table 2.2: Common attributes of electrospun materials used for drug delivery *in vivo*.[60-78]

Composition				Structure or Form			Biomedical Application	
Electrospinning Polymer	[1]FDA Inactives List (UNII)	[2]Solvent(s)	Therapeutic	Electrode Configuration	[3]Fiber Diameter	Macroarchitecture (alignment, composites, etc)	In Vivo Study	Outcome Measures
Synthetic Polymers								
Poly(L-lactic acid)	F9S9FFU82N	$CHCl_3/C_2H_4Cl_2$/ EtOAc	small molecule drug (cyclosporin A)	free surface	10 nm- 10 µm	Single mesh	Mouse (topical, 0.1 mg/mouse, single dosage)	Expression of inflammatory genes
Poly(L-lactide-co-caprolactone) 70:30, poly(propylene glycol), sodium acetate	N/A, N/A, 4550K0SC9B	HFIP	N/A	single nozzle	N/A	Single mesh, two layers (one random, one aligned)	Rats (subcutaneous, N/A, single dosage)	Electrophysiology amplitude recoverage, fibrous layer thickness, myelinated axon diameter
Poly(caprolactone), Poly(styrene)	N/A, N/A	$CHCl_3$/DMF	small molecule drug (apigenin)	single nozzle	200-1200 nm	Single mesh	Rat (transdermal, NDS, single dosage)	Wound healing
Poly(lactic-co-glycolic) acid	WE369X5600	HFIP	small molecule drug (vancomycin)	single nozzle	50-267 nm	Single mesh	Rat (implanted, NDS, single dosage)	Local antibiotic delivery (brain), histological evaluation
Poly(L-lactic acid), poly(ethylene oxide)	F9S9FFU82N, 11628IH70O	DMF	peptide (nisin)	single nozzle	466 nm	Single mesh	Mouse (dermal, NDS, single dosage)	Wound healing, bacterial burden at wound site
Poly(lactic-co-glycolic) acid	WE369X5600	THF/DMF	smalle molecule drugs (fusidic acid, rifampicin)	single nozzle	285-656 nm	Single mesh	Rat (subcutaneous, NDS, single dosage)	Infection at implant site, histological evaluation
Poly(lactic-co-glycolic) acid	WE369X5600	HFIP	small molecule drug (bupivacaine HCL)	single nozzle	N/A	Single mesh	Rat (suture, NDS, single dosage)	Local analgesia, wound healing
Poly (vinyl alcohol)	532B59J990	water	small molecule drug (neostigmine)	single nozzle	500-1000 nm	Single mesh	Mouse (injection, 0.05 mg neostigmine, single dosage)	Tail-flick test, locomotor activity
Poly(lactic-co-glycolic) acid, poly(ester urethane urea)	WE369X5600, N/A	HFIP, HFIP	small molecule drug (tetracycline hydrochloride)	dual stream	102-390 nm	Single mesh (PLGA + PEUU fibers)	Rat (implanted, NDS, single dosage)	Wound dehiscene, abcess formation
Poly(lactic-co-glycolic) acid	WE369X5600	HFIP	biologic (insulin)	single nozzle	1360 nm	Composite (PLGA fibers with attached hyaluronic acid microneedles)	Mouse (topical, 0.2 IU insulin, single dose)	Blood glucose level
Poly(caprolactone), poly(glycerol monostearate-co-caprolactone)	N/A, N/A	$CHCl_3$/MeOH	small molecule drug (SN-38)	single nozzle	1-5 µm	Layered mesh (hydrophobic shield layers around core layer)	Rat (subcutaneous, NDS, single dosage)	Tissue integration, foreign body response
Natural Polymers								
Pullulan, dextran, fucoidan, gelatin, trisodium trimetaphosphate	N/A, K3R6ZDH4DU, N/A, 2G86QN327L, 3IH6169RL0	water/DMF	biologic (VEG-F)	single nozzle	500 nm	Single mesh	Mouse (subcutaneous, NDS, single dosage)	Migrated cells, formation of blood vessels
Hyaluronic acid	N/A	water	N/A	single nozzle	58-1016 nm	Single mesh	Pig (transdermal, N/A, single dosage)	Wound healing
Synthetic/Natural Polymers								
Gelatin, Polyvinyl alcohol (PVA)	2G86QN327L, 532B59J990	AcOH/water, water	small molecule drug (doxorubicin)	coaxial nozzle	211-339 nm	Single mesh	Mouse (implanted, 1mg/kg, single dosage)	Tumor volume, body weight, survival rate
Eudragit S 100, Zein	N/A	EtOH, MeOH	small molecule drugs (aceclofenac, pantoprazole)	single nozzle	50-200 nm	Single mesh	Mouse (oral, 20 mg/kg, single dosage)	Stomach ulceration, infiltration of inflammatory cells into gut mucosa
Poly(caprolactone), poly(ethylene oxide), collagen I	N/A, 11628IH70O, N/A	HFIP	N/A	single nozzle	N/A	Composite, with hydroxylapatite nanoparticles	Rat (bone implant, N/A, single dosage)	Endogenous cell infiltration
Gelatin, glyoxal, poly(caprolactone)	2G86QN327L, N/A, N/A	AcOH/EtOAc/ water	N/A	single nozzle	680 nm	Single mesh, gelatin/PCL/ gelatin layers	Pig (peridontal, N/A, single dosage)	Epithelial wound closure
Poly(lactic-co-glycolic) acid, collagen	WE369X5600, 58X445TH30, 7SVE964630; N/A	HFIP	small molecule drugs (vancomycin, gentamicin, lidocaine)	single nozzle	55-314 nm	Single mesh, three layers (PLGA/collagen, PLGA/ drugs, PLGA collagen)	Rat (transdermal, NDS, singal dosage)	Wound healing, histological evaluation
Poly(lactic-co-glycolic) acid, poly (ethylene glycol), 2-hydroxypropyl-beta-cyclodextrin	WE369X5600, 58X445TH30, 7SVE964630,; 30IQX730WE, 1I96OHX6EK	DCM (shell), DMSO (core)	small molecule drug (hydroxycamptothecin)	single nozzle, emulsion	540 nm	Single mesh (core/shell)	Mouse (subcutaneous, 4 mg/kg, single dosage)	Tumor volume, body weight, survival rate
Poly(caprolactone), gelatin	N/A, 2G86QN327L	TFE	small molecule drug (doxorubicin)	single nozzle	N/A	Single mesh	Mouse (subcutaneous, NDS, single dosage)	Tumor suppression

[1]Unique ingredient identifier (UNII) for specific material compositions and molecular weights as listed on the FDA inactive ingredient database (http://www.accessdata.fda.gov/scripts/cder/iig/index.cfm); may not correspond to actual material used in reference.
[2]Reported solvents that have been used to electrospin polymer class. Solvetns: $CHCl_3$ = chloroform; $C_2H_4Cl_2$ = 1,2 dichloroethane; AcOH = acetic acid; DMF = dimethylformamide; DMSO = dimethylsulfoxide; EtOH = ethanol; EtOAc = ethyl acetate; DCM = methylene chloride; HFIP = hexafluoro-2-propanol; MeOH = methanol; THF = tetrahydrofuran; TFE = tetrafluoroethylene
[3]Reported fiber diameters resulting from electrospinning specified polymer class.
[4]Reference is to specific biomedical application described.
N/A: nat applicable or not found; NDS: no dose specified.

Solid-state properties of the fiber-formulated drug or biologic also affects its solubility, bioavailability and stability. Amorphous solid dispersions (ASDs) occur when both the carrier polymer and drug co-exist within the fiber matrix in a molecularly dispersed state. ASDs are a useful category of drug delivery systems as they are able to achieve transient drug concentrations significantly higher than the equilibrium solubility of the drug due to the absence of crystalline lattice energy in amorphous solids Depending on polymer-drug compatibility, the high surface to volume ratio of electrospun fibers promotes rapid solvent evaporation and minimization of lattice energy between the polymer and drug. This may be particularly useful for pharmaceutical actives that are difficult to formulate or have poor solid state properties alone.[79] For example, electrospinning poorly water-soluble drugs in carrier polymers as ASDs can enhance drug dissolution compared to the crystalline form, which may be more hydrophobic as well as needing to overcome the crystalline lattice energy.[80] For example, Verreck et al. showed the release rate of two poorly water-soluble drugs was tunable by altering the drug to polymer ratio in hydrophobic polyurethane fibers.[58] Because both drugs were distributed in an amorphous form within the carrier polymer, the rate-limiting solubilization step was avoided and a supersaturated system was generated to provide the chemical potential for drug release. ASDs of biologic payloads in a carrier polymer can also enable long-term stability of proteins as well as preserve bioactivity. Kim et al. showed that lysozyme formulated in fiber blends of PCL and PEO maintained 90% of its catalytic activity from the dried mesh.[81] In summary, the mild electrospinning process and resulting ASDs enable the delivery and stability of challenging pharmaceutics, including poorly water-soluble drugs and fragile biologics.

2.3.3 *Challenges in electrospun fibers for vaginal delivery*

While electrospun fibers are a promising new platform for vaginal delivery of microbicides, there are a number of challenges that must be confronted. Co-delivery of multiple drugs from a single electrospun fiber mat with precisely controlled release profiles may be difficult. In addition, delivering multiple, physicochemically diverse agents may require a novel approach to design of the electrospun

fiber vehicle, such as manipulation of microarchitecture or use of polymer blends. Unlike drug-loaded nanoparticles, which are able to penetrate tissue and deliver their payload intracellularly, fibers are limited by the pharmacokinetics at the site of administration. The maximum achievable drug loading in fibers will likely be drug-dependent, as high loading into polymer solutions may negatively alter the ability to electrospin the solution. However, our lab has successfully electrospun fibers containing 60% tenofovir by mass with high encapsulation efficiency on a production-scale electrospinning instrument.[82] Future research into the area of the physics of electrospinning may offer more control over fiber sizes, drug distribution and release profiles.[83] A clear mode of administration, i.e. the way the fibers will be inserted into the vaginal cavity, has not been established. It is also unclear whether any residual polymer film will persist in the vaginal cavity, which may impact user acceptability.

In vivo testing of biocompatibility of fibers for vaginal drug delivery has not been conducted, and safety and toxicity studies will need to be performed before efficacy can be fully evaluated. Ball *et al*. did not conduct *in vivo* safety, toxicity or release kinetics but did observe release of dye and coverage of the cervicovaginal tract from ICG-loaded fibers in mice.[4] However, there are a number of examples of fiber materials used *in vivo* that would support their safety and ability for sustained drug delivery. Silva *et al.* are currently conducting a Phase III clinical trial to evaluate efficacy of an electrospun fiber-based patch that releases nitric oxide for the treatment of diabetic ulcers.[84] Ranganath *et al*. used an electrospun fiber patch to deliver paclitaxel in the treatment of malignant glioma in a mouse model and found increased tumor inhibition when compared to acute administration of Taxol.[85] Furthermore, Hong *et al*. observed therapeutic effects based on mechanical properties as well as sustained antibiotic release from an electrospun fiber patch used after laparotomy.[86] Though vaginal testing has yet to be completed, promising results from alternate routes of administration of drug-eluting electrospun fibers indicate the feasibility of their use *in vivo*.

2.4 SCALE-UP OF ELECTROSPUN FIBERS

To date, only academic research laboratories have pursued the investigation of electrospun fibers as a platform for vaginal microbicides. One of the main challenges in translation of this research to a clinical setting, in addition to thoughtful design of the ideal product, is developing a clear strategy for product development and implementation. Clinical translation will require establishing the design, usage, storage parameters and production cost. Currently, parallel investigation into product design, including rationale, form, and deployment of a fiber-based vaginal microbicide as well as rigorous testing of established pre-clinical models for microbicides[10] are acting to inform prototype development. Manufacturing requirements are a critical component to product realization, so we will discuss in the following sections the scalability and material requirements for a potential fiber-based microbicide product.

2.4.1 *3.1 Materials and capital investments*

The required materials for a fiber-based delivery system will be highly dependent on the intended use. A quick-dissolving fiber for pericoital use may have different requirements than a sustained-release fiber that is used monthly for HIV prevention. Composites containing multiple drugs, either combinations of antiretrovirals or antiretrovirals and contraception/STI prevention, may necessitate the use of different materials. While there is no consensus on the final form of a fiber delivery system at this point, the first fiber-based microbicide product to be realized may share a geometry similar to vaginal films, as this has been a relatively acceptable microbicide delivery mode. The International Partnership for Microbicides found that 85% of women in Burkina Faso, Tanzania and Zambia said they would use a vaginal film as an HIV prevention method.[87] In addition, the ease of producing a simple geometry that resembles a film will establish the proof-of-principle for manufacturing scale-up of a fiber-based microbicide product. Prioritizing materials that have already been FDA-approved for use in vaginal delivery, such as polyvinyl alcohol (PVA), hydroxyethyl

cellulose (HEC), hydroxypropryl methylcellulose (HPMC) and polyurethane (PU) may enable more rapid clinical translation of this new technology. However, a fiber-based microbicide should focus on addressing gaps not currently addressed by the lead dosage forms.

2.4.2 *3.2 Manufacturing capability*

A number of large-scale electrospinning instruments exist due to applications of electrospinning in industries such as air and water filtration, energy and construction. Because of the large demand for fiber-based technologies, which are expected to reach $2.2 billion by 2020,[88] the infrastructure for mass production is already established. However, there may be limitations to current large-scale instrumentation for production of electrospun fiber based dosage forms. Current production-scale instruments are not specifically made for pharmaceutical applications and may be challenging to adapt to FDA standards. Likewise, if coaxial fibers prove advantageous for sustained antiretroviral drug delivery, production-scale instruments capable of making this architecture are still in early development.

Production costs can be estimated by assuming that initial fiber-based products will be similar to a vaginal film or gel, as far as dosage requirements and size. Currently, vaginal films are dosed at around 300 mg and vaginal gels are dosed around 2 g (gel density ~0.6 g/mL).[10] Production yields for large scale instruments could theoretically reach up to 6.5 kg/h, which would correlate to production of 10-20 million doses annually.[88] Therefore, although production will depend on the specific formulation, scale-up for a fiber-based microbicide is theoretically achievable on a production level that is necessary for human clinical trials.[9] Additional constraints on manufacturing include initial capital investments, availability of raw materials, cost of APIs, utilities and infrastructure, and product reproducibility.

Table 2.3: Electrospinning platforms for scalable manufacturing.[47, 80, 82, 89-104]

Production-scale Electrospinning Instrumentation					[3]Configurable Attributes for Biomedical Applications			
Electrode Configuration (Ref.)	[1]Max. Production Rate, Basis Weight	Instrument Manufacturers	Commercialized Products	Pros/Cons	Fiber Dimater	Core-Shell Fibers?	Fiber Alignment?	Other
Multinozzle	≤0.2g/hr per nozzle	Linari Engineering, E-Spin Nanotech, Holmarc, NaBond, Inovenson (Nanospinner), Donaldson, Yflow, Kato-Tech, IME technologies	filtration products (HVAC, HEPA, etc.), textiles/apparel, acoustics	**Pros:** most versatile, compatibile with coaxial electrospinning **Cons:** lowest throughput, nozzle-nozzle interactions, needle clogging, waste from non-optimal flow rate	≥50 nm	Yes	Yes	3D volumes
Free Surface	≤60g/(hr•m) for wire electrodes; 0.1-10 gsm	Elmarco, Revolution Fibers , Nfiber	filtration products (HVAC, HEPA, etc.); skin care/ cosmetics; composite reinforcement, acoustics	**Pros:** higher throughput, self-optimized jet spacing and throughput, simple designs, many design options/versatile. **Cons:** coaxial electrospinning challenging	≥50 nm	emulsion; parallel slits	Yes	3D volumes
Melt	NR	NaBond, Electrospunra	NR	**Pros:** No solvent required **Cons:** limited polymers (only low melting point), products not thermally stable, no ultrathin fibers, not compatible with making composites or interesting architectures	typically ≥0.5 μm	NR	Yes	NR
Centrifugal	NR	Dienes	NR	**Pros:** highest throughput, aligned fibers. **Cons:** highest capital costs, least versatile with interesting architectures/composite materials	≥50 nm	NR	Yes	NR

[1]Values are highly dependent on materials and electrospinning conditions.
NR: not reported.

2.4.3 *Scale-up equipment*

As shown in Table 2.3, there are four classes of electrospinning equipment that are commercially available, and of these the multi-nozzle and free-surface classes (Figure 2.3) are the most mature. Free surface (or nozzle-less) electrospinning initiates charged fluid jets from a free surface entrained with a thin film of solution rather than from a solution pumped through a needle tip.[105] Free surface electrospinning is of particular interest for this review due to the high throughput achievable for these designs. Advantages of free surface technology emerge from avoiding needle clogging issues and avoiding nozzle-nozzle interactions since jets emanating from a free surface will achieve self-optimize spacing based on applied voltage and solution properties. Free surface designs may also allow for scale-up of nanofibers containing particles or fiber mats fabricated with distinct microarchitectures for drug delivery applications.[91, 106] Although both free surface and multi-nozzle designs have their advantages, it seems the industrial landscape has become more focused on free surface designs because of the increased compatibility with manufacturing. Many different free surface electrospinning designs have been developed, which can be evaluated by throughput capabilities for comparable electrode dimensions,

compatibility with technologies, and tunability of mass deposition profile (Table 2.3). Free surface designs widely used in academia include the rotating wire design, [47, 95, 107, 108] rotating coil design, [109] oscillating carriage design,[110] rotary cone design,[111] and rotating disc/cylinder.[112] The rotating cylinder, disc or wire designs are popular due to the simplicity of set-up and the detailed modeling efforts the Rutledge group has conducted focused on this design specifically.[47, 95, 107, 108] However, these electrode configurations have fewer design parameters available to tune mass deposition of nanofibers. Further, the open solution bath may cause issues with solution aging in continuous processing. Although other free surface designs are not as widely studied, other configurations with more factors to control mass deposition include the rotating coil design[113] (spiral distance, maximum coil diameter, relative coil diameters, and wire diameter) and oscillating carriage design[110] (carriage speed and orifice size). Although free surface configurations are evolving to meet challenges in clinical applications, more research and development is required in order to accommodate emerging designs and translation of multi-phase precursors to free surface instrumentations. Through understanding of the current industrial landscape as well as the research literature, we feel that the free surface class of equipment is best suited for production of pharmaceutical products and tissue engineering scaffolds through electrospinning. A major consideration is process throughput; the multi-nozzle configuration is far less productive than mature fiber and film production technologies making economics unfavorable. Further, free-surface electrospinning is well poised to confront the remaining scalability challenges in production of electrospun medical fabrics. The self optimized jet spacing and throughput and elimination of nozzle-nozzle interactions and jet clogging makes the free surface technologies more compatible with development of process and quality control mechanisms. Further, the relatively simplicity of the design and minimal contact components could also be beneficial for process approval as well as routine maintenance and cleaning requirements for pharmaceutical production. Finally, in lieu of coaxial spinning capabilities emulsion electrospinning from free surface electrodes is an emerging technique capable of producing the core-shell fiber architectures popular especially in controlled drug release applications. Although the commercially available electrospinning instruments have the desired capacity,

none are made specifically for pharmaceutical applications. Therein lie the challenges, and a potentially higher cost associated with scale-up of drug-eluting fibers to meet requirements for good manufacturing practices (GMP). Given the limited information available on the production cost of electrospun fibers, some reports show that the costs of fibers produced by an industrial-scale instrument is \$1-\$5 kg^{-1} [88]. These reported costs are likely to increase substantially based on the complexity of the GMP pharmaceutical manufacturing process required to produce an ARV-based microbicide, and we estimate that the cost for a 300 mg dose may be on the order of \$0.50-\$3.00 depending on the annual production volume. These estimates are based on incomplete information and rough assumptions for meeting stringent requirements for compliance with ISO and GMP. Based on these estimates, electrospun fibers would be a competitive with other ARV dosage vehicles, such as vaginal films and rings. Low-cost electrospun fibers would present another option for a globally accessible dosage form for ARVs.

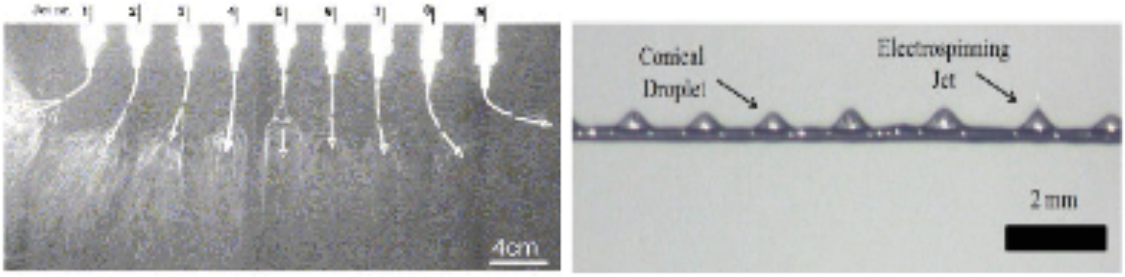

Figure 2.3: Comparison of multi-nozzle electrospinning and wire electrospinning. Images show multi-nozzle electrospinning, where multiple Taylor cones form from separate nozzles, (left) and wire electrospinning, where multiple Taylor cones form on the same electrode (wire or cylinder) (right).[18, 114]

2.5 CONCLUSION

Electrospun fibers are a promising new platform in the context of vaginal delivery of microbicides. Fibers are a solid dosage form that offers a silky texture as well as enhanced product stability. Fibers are capable of delivering a number of therapeutics that may be useful for microbicides, including biologics and nanoparticles, and can exhibit burst, sustained and asynchronous release profiles. Because electrospinning is a well-established technology, there are already commercial-scale

instruments available, which would ease the translation to clinical applications and possibly widespread use. At this point, it is unclear whether fibers will be used for a quick pericoital dosage or a sustained monthly dosage, but the potential for both applications offers an exciting outlook to create innovative new designs as challenges in the field arise.

Chapter 3. Delivery Of Multipurpose Prevention Drug Combinations From Electrospun Nanofibers Using Composite Microarchitectures

Adapted from: Delivery of Multipurpose Prevention Drug Combinations from Electrospun Nanofibers using Composite Microarchitectures. Anna K. Blakney, Emily A. Krogstad, Yonghou Jiang, Kim A. Woodrow. International Journal of Nanomedicine 9: 2967-2978 (2014).

3.1 ABSTRACT

Background: Electrospun drug-eluting fabrics have enormous potential for delivery of physicochemically diverse drugs in combination by controlling the underlying material chemistry and fabric microarchitecture. However, the rationale for formulating drugs at high drug loading in the same or separate fibers is unknown but has important implications for product development and clinical applications.

Methods: Using a production scale free-surface electrospinning instrument, we produced electrospun nanofibers with different microscale geometries for co-delivery of tenofovir (TFV) and levonorgestrel (LNG) – two lead drugs being considered for multipurpose prevention of HIV acquisition and unintended pregnancy. We investigated *in vitro* drug release of TFV and LNG combinations from composites that deliver the two drugs from the same fiber (combined fibers) or from separate fibers in a stacked or interwoven architecture. For stacked composites, we also examined the role that fabric thickness has on drug release kinetics. Using an engineered HeLa cell line that is susceptible to HIV-1 infection, we also measured the cytotoxicity and antiviral activity of the drugs delivered alone and in combination.

Results: We report on the solution and processing parameters for free-surface electrospinning of medical fabrics with controlled microarchitecture and high drug loading (up to 20 wt. %). We observed that *in vitro* release of the highly water-soluble TFV, but not the water-insoluble LNG, was affected by composite microarchitecture, fabric thickness and drug content. Finally, we show that the drug-loaded

nanofibers are non-cytotoxic and that the antiviral activity of TFV is preserved through the electrospinning process and when combined with LNG.

Conclusion: Electrospun fabrics with high drug loading content create multicomponent systems that benefits from independent control of the nanofibrous microarchitecture. Our findings are significant because they inform the design and production of composite electrospun fabrics for co-delivery of physicochemically diverse drugs that may be useful for multipurpose prevention.

3.2 INTRODUCTION

The clinical use of drug combinations in the treatment of cancer,[115] HIV/AIDS,[116] and multi-drug resistant bacterial infections[117] underscores their importance for realizing synergies that enhance treatment efficacy while reducing toxicity and addressing the emergence of drug resistance.[118] However, co-delivering drugs requires strategies for combining physicochemically diverse agents and delivery of these combinations to target tissues and cells at therapeutically relevant concentrations.[119, 120] To realize the full potential of drug combinations, advances in drug delivery systems must address these challenges. Electrospun fabrics are an ideal topical delivery system for co-delivery of multiple agents because of their proven capacity to encapsulate and deliver physicochemically diverse drugs and ability to modulate drug release kinetics over both short and long time frames.[26, 43, 121] A specific application of electrospun fabrics for topical delivery that demands these versatile product attributes is in the development of multipurpose prevention technologies (MPT). MPTs are combination drug delivery systems capable of simultaneous prevention of HIV, other STIs and unintended pregnancy.[122] Two leading drug candidates for MPTs that target prevention of unintended pregnancy and HIV acquisition are tenofovir (TFV), a hydrophilic nucleotide reverse transcriptase inhibitor (NRTI),[123] and levonorgestrel (LNG), a widely-used, hydrophobic hormonal contraceptive.[124] TFV and LNG have physicochemical properties that prevent their easy combination at the high drug loadings that are useful for sustained prevention.

Ball *et al.* and Huang *et al.* have used electrospun fabrics to deliver a variety of ARV drugs but never in combination.[4, 5] Combination drug delivery from electrospun fabrics can be achieved by co-delivery of multiple drugs encapsulated within the same fiber or into separate fibers. Okuda *et al.* used separate fibers that were combined in a multi-layer fiber mat for sustained delivery of two model drugs.[125] In contrast, Xu *et al.* encapsulated paclitaxel and doxorubicin hydrochloride in the same PEG-PLA fibers and observed asynchronous drug release.[126] However, in all of these studies to date, less than 1 wt.% of drug has been used alone or in combination, which makes these systems limited in scope to applications employing drugs with high potency. Even drugs with nanomolar potency are required at a minimum composition of ≥10 wt.% to be realistically useful as a medical fabric. Currently, no systematic study has been performed to assess the co-delivery of physicochemically diverse drugs at high drug loading composition in electrospun fabrics with different underlying microarchitectures. Here we demonstrate the feasibility of assembling electrospun fabrics, produced on a production-scale instrument, with different micro-scale geometries for co-delivery of a hydrophilic (TFV) and hydrophobic (LNG) drug. We show that medical fabrics with high drug loading content benefits from independent control of the nanofibrous microarchitecture to predict drug release kinetics.

3.3 MATERIALS AND METHODS

3.3.1 *Polymer Solution Preparation*

Polyvinyl alcohol (MW 85-124 kDa, 87-89% hydrolysis) and levonorgestrel were purchased from Sigma-Aldrich. Tenofovir was a generous gift from CONRAD. Alexa Fluor-488 and -555 hydrazide sodium salts were purchased from Life Technologies. For all polymer solutions, PVA was dissolved in deionized water at 10% wt./vol. Drugs were mixed with polymer solution at 20% wt. drug/wt. polymer (for equal loading fabrics) or 0.0067% (LNG) and 15.3% (TFV) wt. drug/wt. polymer (for relevant daily dosage fabrics) and stirred for ≥6 hours prior to electrospinning.

3.3.2 *Electrospinning*

Polymer solutions were electrospun on a NS 1WS500U (Elmarco, Inc.) free surface electrospinning instrument and using the following processing conditions unless otherwise specified: 160 mm wire electrode distance, -25 kV collecting electrode, 60 kV spinning electrode and 250 mm cartridge traveling distance. All microarchitectures were prepared using 15 mL batch volumes in the single 20 mL cartridge (Figure 3.2a), unless otherwise noted. For the stacked composite, we electrospun 7.5 mL of a LNG polymer solution followed by 7.5 mL of a TFV polymer solution. Interwoven composites were prepared similarly except the volumes were separated into different reservoirs of the 40 mL dual cartridge (Figure 3.2b). For the fluorescent fibers, LNG and TFV were combined with 0.025% wt./vol of either Alexa Fluor-488 or -555, respectively, and collected onto a glass slide. To prepare fabrics of different thicknesses, we decreased the travel distance of the cartridge.

3.3.3 *Solution, Fiber and Fabric Characterization*

Density, conductivity, surface tension, viscosity and pH were measured in triplicate for all solutions prior to electrospinning. Density was measured by taking the mass of a known volume of solution. Conductivity and pH were measured using an Orion Star A212 conductivity (Thermo Scientific) meter and Orion Star A111 pH meter. Surface tension was measured using an AquaPi surface tensiometer (Kibron). Viscosity was measured using a TA Instruments AR-G2 Series Rheometer at a constant strain of 4% with a cone (angle = 1° 58’ 48”, diameter=40 mm) and plate geometry.

For SEM images, fabrics were sputter coated with a mixture of gold and palladium for 90 s and imaged at magnifications of 500X and 5,000X using a Sirion scanning electron microscope at the University of Washington (UW) Nanotechnology User Facility. Cross-sectional SEMs were acquired by freezing the fabrics in liquid nitrogen for ~30 seconds and then abruptly fracturing the fabrics to provide a clean break. ImageJ (NIH) was used to determine fiber diameter by measuring 45 random fibers.

Thermograms were generated using an Auto Q20 Differential Scanning Calorimeter (TA Instruments) for the purpose of calculating relative crystallinity of drugs in the electrospun fabrics at the UW

Materials Science Engineering User Facility. 5 mg samples were prepared in an aluminum pan (Tzero) and heated at a constant ramp from 10 to 350 °C with a sampling interval of 1 s/point. Heat flow was normalized to sample weight. TA Universal Analysis software was used for both rheometry and DSC data collection and analysis. The mechanical properties of electrospun fabrics were measured using an Instron 5543 series with a 10N load cell, a strain rate of 0.01/second, a single-column, screw-driven apparatus at 20 °C and relative humidity of 40%. The mechanical testing was performed according to method ASTM D5034-95, with a dog bone sample shape (ASTM D-1708-96) with length = 22 mm, width = 5 mm and variable thickness. The Young's Modulus was calculated by analyzing the linear region of the resulting stress vs. strain curve, and the tensile strength was calculated by analyzing the peak stress that the sample was able to endure. The encapsulation efficiency (EE), percent yield, productivity and relative crystallinity[127] were calculated using the following equations:

$$EE = 100 * \frac{Actual\ mass\ drug\ in\ fibers}{Expected\ mass\ drug\ in\ fibers}$$

$$\%\ Yield = 100 * \frac{Actual\ total\ mass\ fibers}{Calculated\ mass\ solids\ in\ volume\ of\ solution\ added\ to\ cartridge}$$

$$Productivity = \frac{Actual\ total\ mass\ fibers}{Total\ area\ fibers * Spinning\ time}$$

$$\%\ Relative\ Crystallinity = 100 * \frac{Area\ Under\ Curve_{\ sample\ peak} * Mass_{\ sample}}{Area\ Under\ Curve_{\ standard} * Mass_{\ standard}}$$

Fabric thickness was measured using digital calipers and averaging three measurements from different locations at the center of the fabric. Fluorescent fabrics were imaged using a Zeiss Leica TCS NT/SP DMIRBE inverted confocal microscope located in the UW Keck Imaging Facility.

3.3.4 *Drug Loading and Release*

Drug loading was analyzed by dissolving approximately 5 mg of fabrics in 20 mL of a mixture of 1:1 isopropanol:water in a glass vial. *In vitro* release was analyzed at sink conditions (2.6 mg/mL) in a 1:1 solution of isopropanol:water due to the limited solubility of LNG in water.[122] Samples were incubated at 37 °C on a rotational shaker and replenished with fresh media upon sampling. Triplicate samples were quantified using a Shimadzu Prominence LC20AD UV-HPLC system. A Phenomenex Luna C18 column (5 μm, 250x4.6 mm) and LC Solutions software were used to analyze samples. A method for dual analysis of TFV and LNG was developed using the following gradient method using mobile phase A (0.1% formic acid in water) and mobile phase B (acetonitrile). The run consisted of 5 minutes 72% A, 5 minutes ramp to 15% A, 10 minutes 15% A, 5 minutes ramp to 72% A, 5 minutes 72% A. The total method time was 30 minutes, with an oven temperature of 30 °C, flow rate of 1 mL/min, and injection volume of 20 μL. LNG and TFV were detected at 238 nm and 259 nm, respectively, and at retention times of 18.5 minutes and 2.3 minutes, respectively. LNG had a linear standard range from 0.05 μg/mL to 100 μg/mL and TFV had a linear standard range from 0.01 μg/mL to 200 μg/mL.The HPLC method was also validated for >95% recovery of a known concentration of both TFV and LNG, consistent retention time between standards and samples, and >95% recovery in a spiked sample containing dissolved fibers and a known concentration of TFV and LNG.

3.3.5 *Cytotoxicity and HIV Inhibition Assays*

TZM-bl cells and HIV-1 BaL isolate were obtained from the NIH AIDS Research and Reference Reagent Program, NIAID. TZM-bl cells are a HeLa-derived cell line that express CD4, CCR5 and CXCR4.[128-131] Cells were plated in a black 96-well plate at a density of 5,000 cells/well (Corning, Corning, NY) and maintained with Dulbecco's Modified Eagle Medium (DMEM) (Gibco Life Technologies) with 10% fetal bovine serum (Hyclone), 1% 100X penicillin/streptomycin (Invitrogen) and 1% 200 mM L-glutamine. Cells were incubated in 5% CO_2 and 37 °C for 24 h prior to exposure to

drugs. Fabrics were sterilized by UV irradiation for one hour per side prior to use. Treatments were added at a volume of 50 μL. Cytotoxicity was analyzed using the CellTiter Blue assay (Promega) to assess TZM-bl cell viability after 48 h of exposure to drug eluates from fabric release in cDMEM (24 h release, in triplicate). Percent viability was calculated by normalizing to the average of media control wells (n=9). For composite fabrics, the drug concentration shown applies to both the amount of LNG and of TFV (1:1 ratio). Positive control (12.5% DMSO) resulted in 4.6% viability (not shown).

For the HIV-infectious inhibition assay, 100 μL of HIV-1 BaL (240 TCID50/well) was added to wells 1 h after drug treatment (24h release eluates). Media was removed from wells after 48 h and 100 μL of phosphate buffered saline (Gibco Life Technologies) and 100 μL of Bright-Glo Luciferase reagent (Promega) were added to wells. Inhibition of infectious activity was quantified by measuring luminescence on a plate reader (Tecan). IC_{50} values of drug compounds were estimated using sigmoidal regression in Graphpad Prism, version 5.0.

3.3.6 *Statistical Analysis*

Drug release is reported as mean ± standard deviation, and values at each timepoint were compared using a two-way ANOVA to compare all microarchitectures and a Bonferonni post-test to directly compare values for two individual microarchitectures. Two-sided tests were used at a significance level of $\alpha=0.05$ for all hypothesis testing. Statistical analyses were done in Graphpad Prism, version 5.0.

3.4 RESULTS

3.4.1 *Properties of Electrospun Fabrics*

Free-surface electrospinning was used to prepare fabrics of different microarchitectures for combination delivery of TFV and LNG (Figure 3.1). We observed that the addition of LNG and TFV, either alone or in combination, to the PVA polymer solution led to minimal differences in solution

properties (Table 3.1). The fabrics were macroscopically indistinguishable from each other irrespective of the drugs loaded or composite microarchitecture (stacked, interwoven, or combined). Fabrics appeared white, were silky to the touch, flexible and easily folded. SEM microscopy revealed fibers of ~250 nm diameter with a smooth and rounded morphology (Table 3.2). All fabrics were also free of physical defects.

Table 3.1: Composition and solution properties of fiber formulations.[a]

Fabrics	Density (g/mL)	Conductivity (µS/cm)	pH	Viscosity[b] (Pa*s)	Surface Tension (mN/m)
PVA Only	1.10	573	5.58	0.45	59.0
LNG Only (20 wt.%)	1.12	649	5.58	0.46	58.0
TFV Only (20 wt.%)	1.08	527	3.85	0.53	59.4
Combined TFV/LNG (20 wt.% each)	1.05	438	4.01	0.45	55.3

[a] n=1 for all measurements.
[b] Viscosity is reported at 10 s^{-1}.

We achieved high encapsulation efficiencies of >80% for all fabric formulations except for interwoven fabrics of TFV and LNG, where an artifact of the processing led to TFV encapsulation efficiencies <50% and LNG encapsulation efficiency >150% (Table 3.2). In this case, an extra valve and length of tubing present in the dual cartridge used to fabricate interwoven fabrics resulted in impeded flow of TFV solution onto the wire electrode (Figure 3.2b). Therefore, this particular cartridge design limited the amount of TFV polymer solution that was deposited on the electrode and ultimately incorporated into the finished fibers. The differences in polymer solution deposition could not be accounted for in the predicted drug loading since the values assume equal flow, and is hence manifested as an artifact in the calculated %EE.

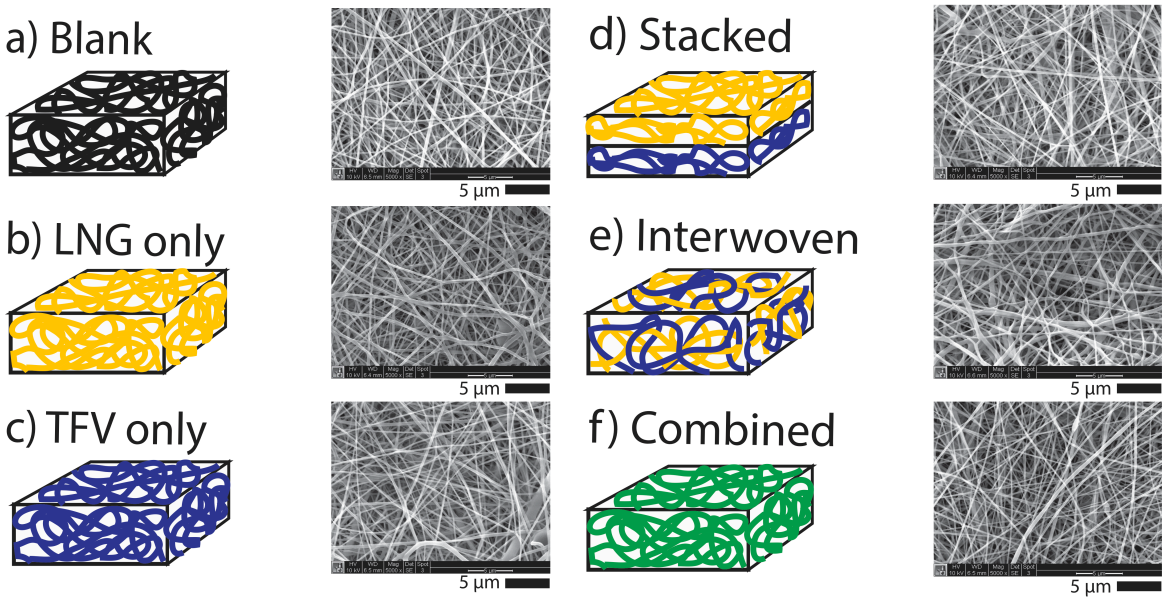

Figure 3.1: Electrospun fabric microarchitectures for topical delivery of single and combination drugs. Levonorgestrel (LNG) and tenofovir (TFV) were delivered alone (b,c) or together using different composite microarchitectures (d,e,f). Vehicle control fabrics (blank) were prepared with only the PVA polymer (a). Schematic shows micro-scale rendering of idealized dispersions of LNF and TFV in fibers (left), and actual scanning electron micrographs (right) of representative fabrics that were produced.

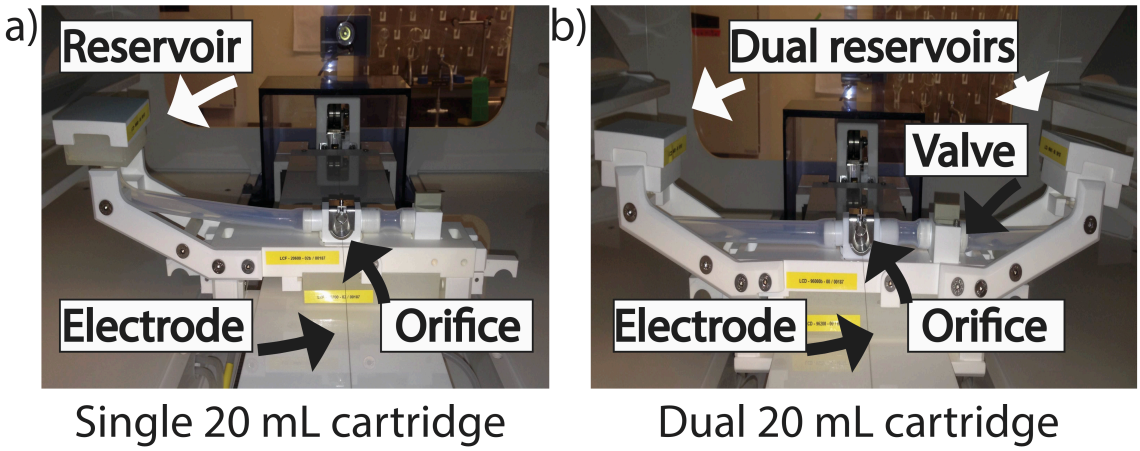

Figure 3.2: Photographs of NS 1WS500U cartridges used to fabricate TFV and LNG medical fabrics. a) A single 20 mL reservoir was used to electrospin blank, LNG only, TFV only, stacked and combined fibers. b) A dual 20 mL reservoir was used to electrospin interwoven fibers. Images depict the reservoir housing for the electrospinning polymer solution, which drains via the clear tubing toward the metal orifice where the solution is deposited onto the wire electrode.

Table 3.2: Properties of drug-loaded electrospun fibers.[a]

Fabrics	EE (%), Loading (wt%)		Fiber Diameter (nm)	Fiber Yield (%)	Productivity ($g/m^2/hr$)	Drug (%)	Crystallinity
	LNG	TFV				LNG	TFV
PVA Only	-	-	208±106	39.4	12.9	-	-
Single Drug Fabrics							
LNG Only	100±1.1 (16.7%)	-	260±105	33.8	18.0	1.2%	-
TFV Only	-	85±1.3 (14.3%)	267±176	49.9	18.0	-	0.2%
Multidrug Composite Fabrics							
Stacked	114±9.4 (9.6%)	83±1.1 (6.9%)	251±107	67.9	26.6	n.d.	0.2%
Interwoven	[d]166±9.6 (13.9%)	[d]44±2.4 (3.7%)	303±123	31.9	16.8	n.d.	n.d.
Combined	82±1.5 (11.6%)	93±1.9 (14.3%)	251±83	39.7	18.7	n.d.	2.3%

[a] n=3 for drug encapsulation efficiency, n=45 for average fiber diameter, values represent mean ± s.d.
[b] n=1 for yield, productivity, drug crystallinity.
[c] Drug loading (shown in parentheses) is expressed as wt. drug/wt. fiber.
[d] Values do not account for differences in theoretical loadings that arose due to cartridge asymmetry.
n.d. = not detected.

3.4.2 *Differential Scanning Calorimetry Analysis of Electrospun Fibers*

We used differential scanning calorimetry (DSC) to characterize the solid dispersion of LNG and TFV in the final fabric products. The T_m measured for PVA, LNG and TFV in all of our formulations was 195 °C, 234 °C and 270 °C respectively (Figure 3.3), which is consistent with measured values reported elsewhere.[132-134]

PVA is a semi-crystalline polymer and our PVA fabrics had a measured T_g of ~95 °C. Incorporation of LNG did not significantly change the T_g of PVA fabrics. However, upon incorporation of TFV, the T_g of PVA fabrics increased by >15 °C to ~110 °C. Only the LNG-only fabric had detectable amounts of crystalline LNG of ~1%, but also higher LNG loading (~17 wt.%) compared to the other LNG fabric formulations (Table 3.2). Crystalline TFV was detected in TFV-only, stacked and combined fabrics, but not interwoven fabrics, likely due to their nominally lower loading of ~4% (Table 3.2). In summary, electrospun drug-loaded fabrics were prepared with minimal TFV and LNG crystallinity. Incorporation of TFV but not LNG increased the T_g, of PVA and suggests an interaction between the polymer and TFV.

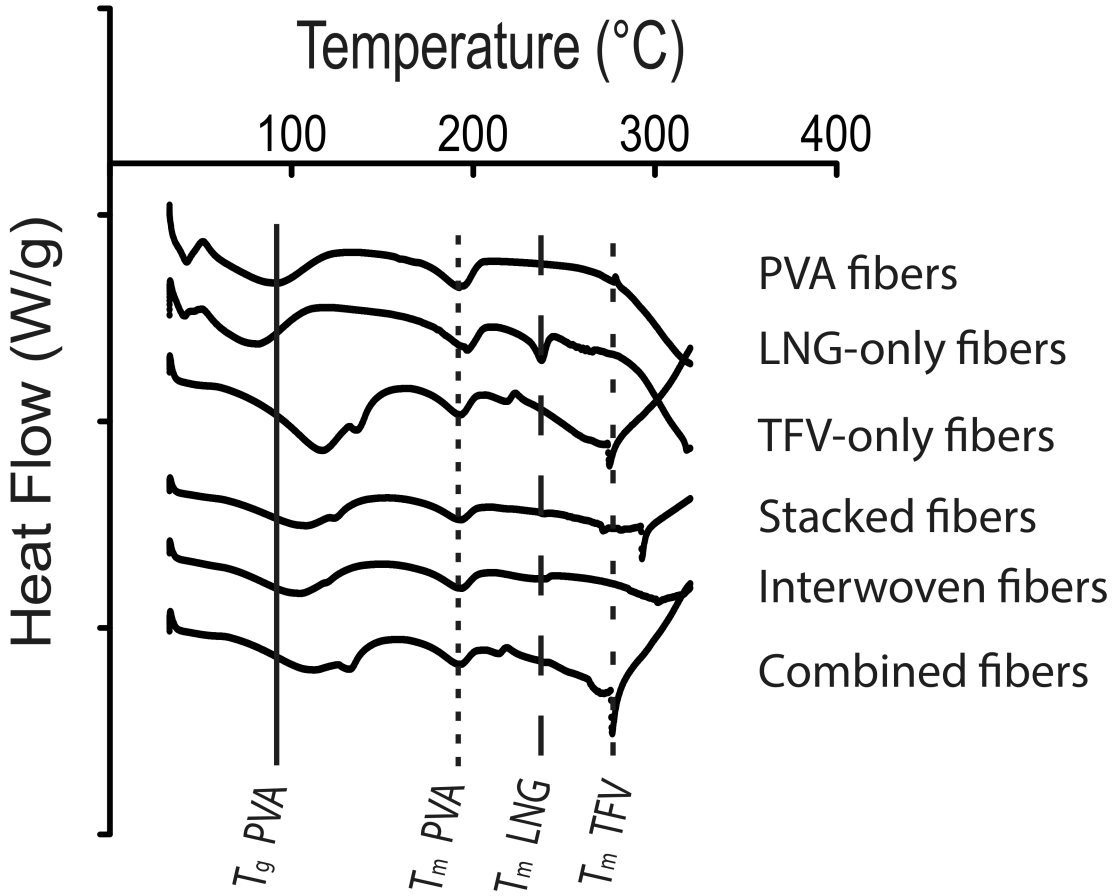

Figure 3.3: Thermograms of electrospun fibers of varying microarchitectures as determined by differential scanning calorimetry. The T_g and T_m peaks of the pure components are indicated with vertical lines.

3.4.3 *Mechanical Testing of Electrospun Fibers*

All fibers were tested to assess whether incorporation of drugs into PVA fibers or composite microarchitecture altered the mechanical properties of the resulting fabric. While incorporating TFV (Figure 3.4) did not affect the Young's Modulus or tensile strength compared to blank PVA fibers, incorporating LNG lowered the Young's Modulus and tensile strength by approximately 3-fold (Figure 3.4). The three composite microarchitectures had lower Young's Modulus and tensile strength than PVA

alone, as expected based on the presence of both LNG and TFV in these samples. The Young's Modulus and tensile strength does not appear to vary based on microarchitecture for this system.

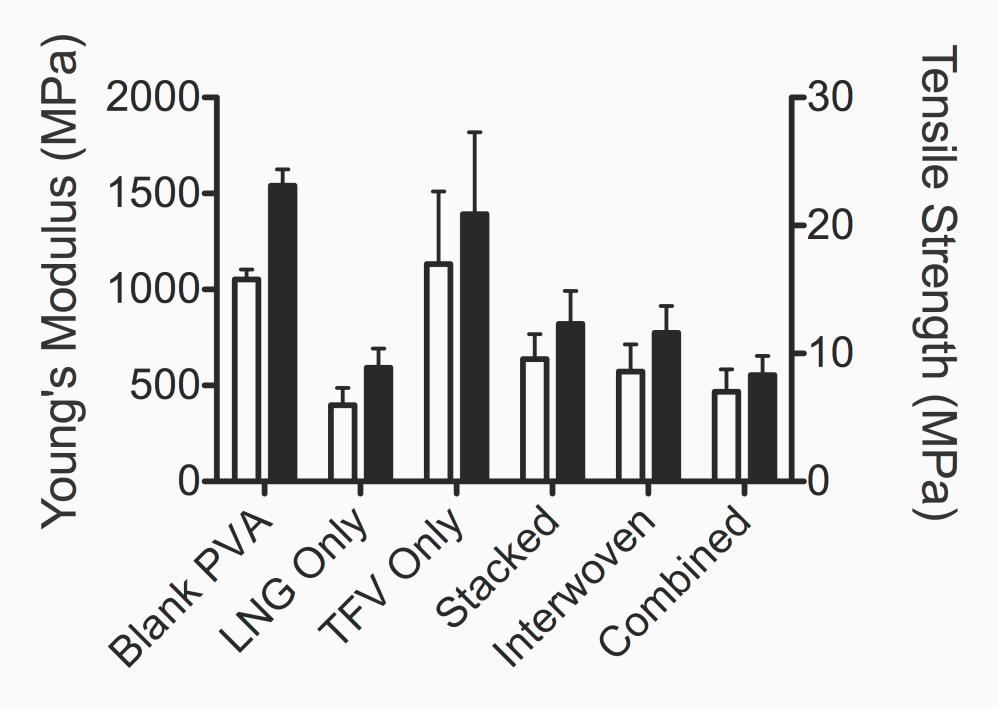

Figure 3.4: Mechanical properties, including Young's Modulus and tensile strength, for electrospun fabrics. White bars represent Young's Modulus data and black bars represent tensile strength. Values are reported as mean ± standard deviation for n=5 samples.

3.4.4 *Visualization of Composite Microarchitectures*

Confocal microscopy was used to visualize the stacked, interwoven, and combined composite microarchitectures by co-loading the fibers with drugs and different fluorophores. AlexaFluor 488 was co-loaded with LNG whereas AlexaFluor 555 was co-loaded with TFV. LNG-only fibers were observed only in the green channel (Figure 3.5a) while TFV-only fibers were observed only in the red channel (Figure 3.5b), while co-localization of the fluorophores (and drugs) was visualized as an orange color in the merge channel. The stacked composites were imaged at the interface of the LNG/TFV layers, where we observed distinct red and green fibers and no fluorescence co-localization (Figure 3.5c). In contrast to the stacked composites, the interwoven fabrics showed intermingling LNG-only and TFV-only fibers, as

well as orange fibers in the merged fluorescent images (Figure 3.5d). This assortment of fiber compositions may be due to the ability of solutions to mix at the orifice before fiber formation. The interwoven fabrics showed less red fibers compared to the number of green fibers, which supports our earlier observation of low TFV loading in this fabric composition (Table 3.2). Visualization of orange fluorescence in the combined microarchitectures confirmed the co-localization of both fluorophores (Figure 3.5e). For the fluorescent microscopy, fabrics were collected onto a glass slide that altered the electric field and caused polymer droplets to collect.

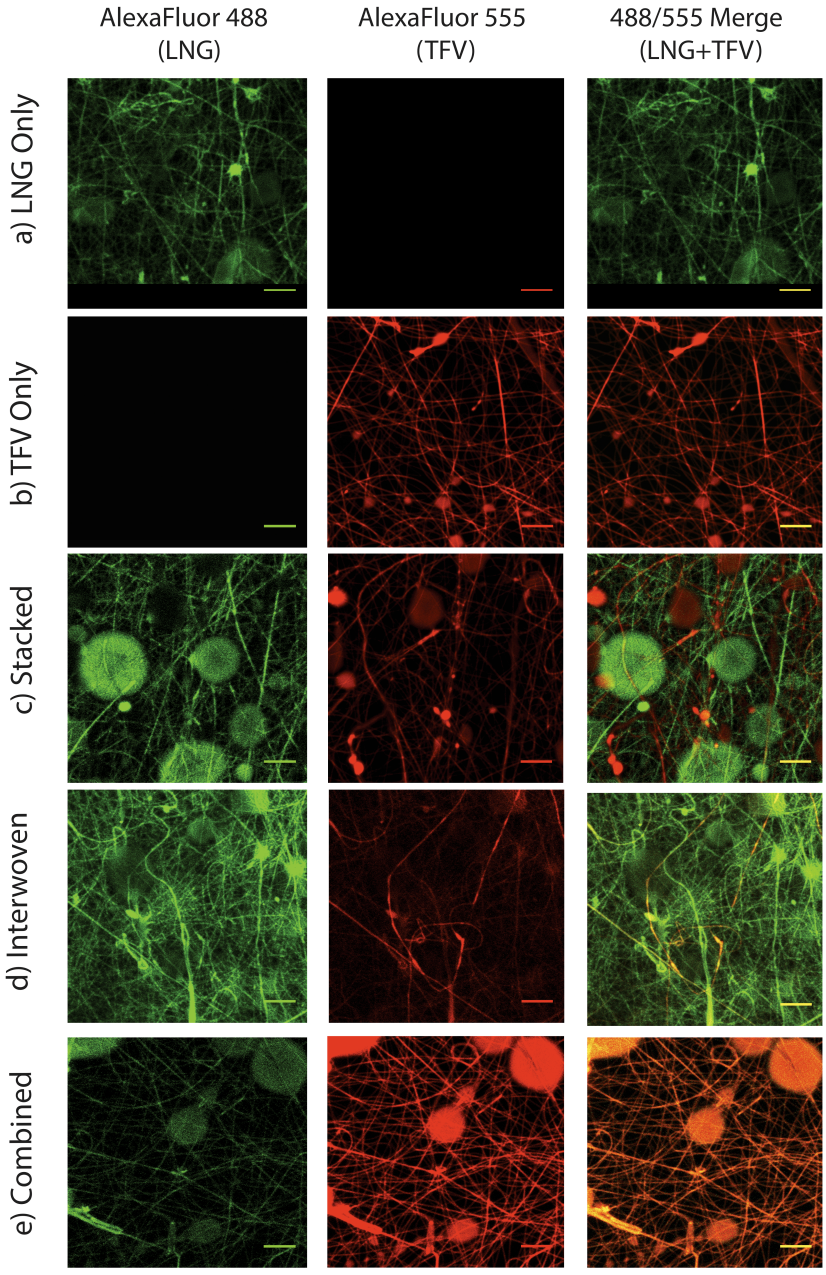

Figure 3.5: Confocal images of fabric microarchitectures. LNG and TFV were fabricated alone (a and b, respectively) or combined in different composites (c-e). To visualize the underlying fabric microarchitectures, LNG solutions were co-loaded with AlexaFluor 488 and TFV solutions were co-loaded with AlexaFluor 555. Fluorescently labeled fibers were analyzed with a confocal laser scanning microscope (Leica TCS NT/SP, Zeiss). Samples were scanned for AlexaFluor 488 (green channel, left), AlexaFluor 555 (red channel, center) and the two channels were merged (right) using NIH Image J to detect fluorescence co-localization. Equal exposure time was used for all images. Scale bar = 10 μm.

Cross-sectional SEM imaging did not reveal any differences in the composite microarchitecture as far as distinct layering based on fiber size or morphology alone. Images of control fabrics (Figure 3.6a-c) show a single layer of fibers with similar size and morphology. Though the stacked composite (Figure 3.6d) is comprised of distinct layers of TFV- and LNG-loaded fibers, this microarchitecture is not visible by SEM as the TFV- and LNG-only fibers have very similar morphology. Furthermore, no distinct layering or varying fiber morphologies was visible in the cross-section of the interwoven or combined composites (Figure 3.6e, f).

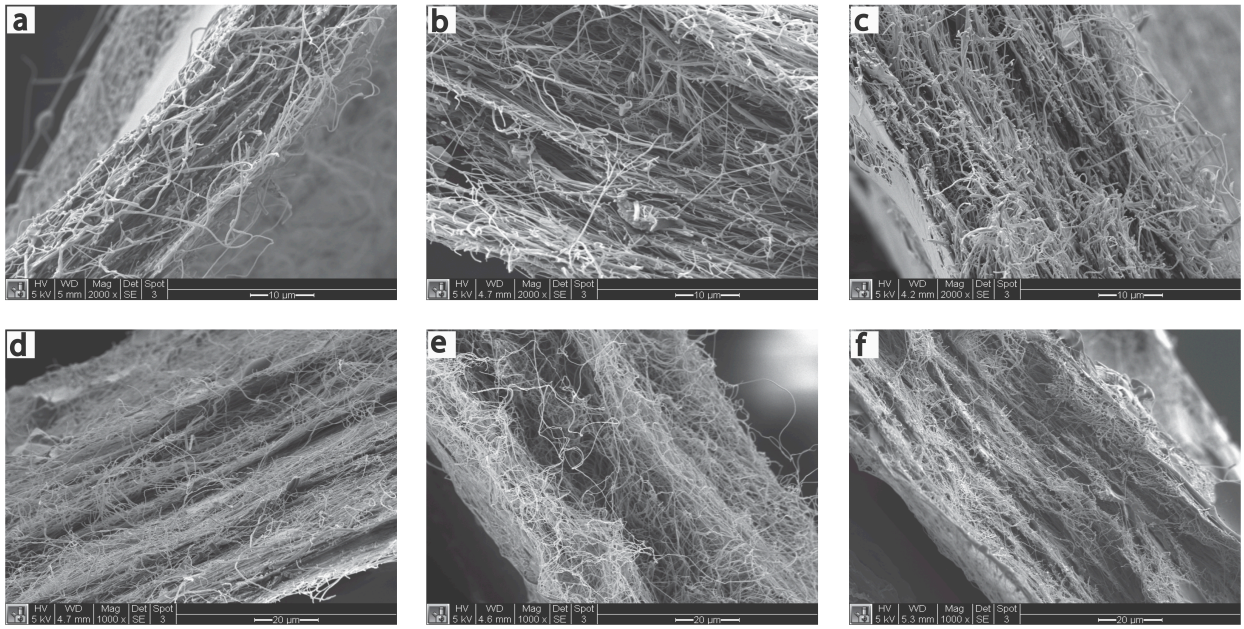

Figure 3.6: Cross-sectional scanning electron micrographs of electrospun fabrics. Samples were cryo-fractured using liquid nitrogen to achieve a clean break, and then imaged in order to observe microarchitectural differences in the z-plane. PVA only (a), LNG only (b), and TFV only (c) images have a scale bar of 10 μm. Stacked (d), interwoven (e) and combined (f) imaged of composite fabrics have a scale bar of 20 μm.

3.4.5 *In Vitro Release of TFV and LNG*

We assessed the role of composite microarchitecture, drug loading and fabric thickness on release of TFV and LNG *in vitro*. Despite the similar actual drug loading of TFV and LNG in PVA

fibers, LNG displayed much slower release kinetics. TFV reached 100% release within 30 minutes whereas LNG did not reach 100% release until 4 hours (Figure 3.7a, b). The significant difference in release is attributed to the highly hydrophobic nature of fabrics containing LNG, which appeared to take hours as opposed to minutes to wet and dissolve in the release media compared to TFV-only fabrics (data not shown).

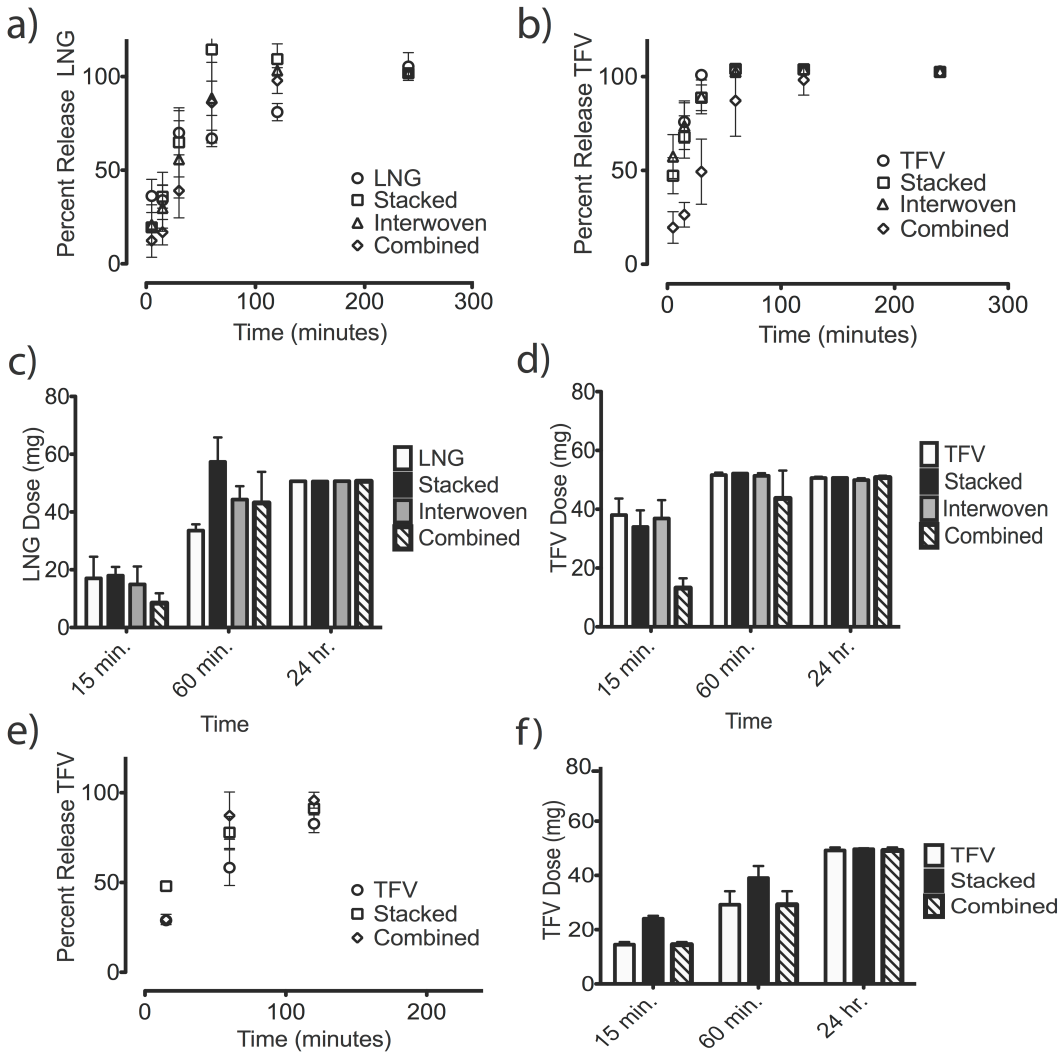

Figure 3.7: *In vitro* release profiles (a,b,e) and dosage profiles (c,d,f) of LNG and TFV delivered from different composite fibers. Fabrics were prepared at 1:1 equal TFV:LNG mass loading (a-d) or at 2000:1 TFV:LNG mass loading (e-f). The delivered dose was calculated at each time point using the percent release at that time and an assumed delivery of 500 mg of total fabric. Values are reported as mean and standard deviation for n=3.

We next compared co-release of TFV and LNG from the three distinct composite microarchitectures to the release kinetics of TFV- or LNG-only fabrics. TFV release was similar between the control, stacked and interwoven microarchitectures, where we observed ~50% TFV release after 5 minutes and 100% release after 30 minutes. In contrast, TFV release from the combined microarchitecture was much slower, with ~50% TFV release after 30 minutes and 100% release after 60 minutes (Figure 3.7b, d). Percentage TFV release measured at 5, 15 and 30 minutes was significantly ($p<0.05$) less from the combined microarchitecture compared to the stacked and interwoven microarchitectures. LNG release was similar for all microarchitectures, and showed complete release within 4 hours (Figure 3.7a, c). We observed that TFV release was two-fold slower from the combined fabrics compared to the TFV-only fabrics despite similar TFV loading (14.3 wt.%) (Figure 3.7b). In contrast, percent TFV release from interwoven fabrics was similar to TFV-only fabrics despite the high LNG loading. Therefore, combination of both drugs in a single fiber (combined microarchitecture), but not the stacked or interwoven microarchitectures, had an impact on TFV release.

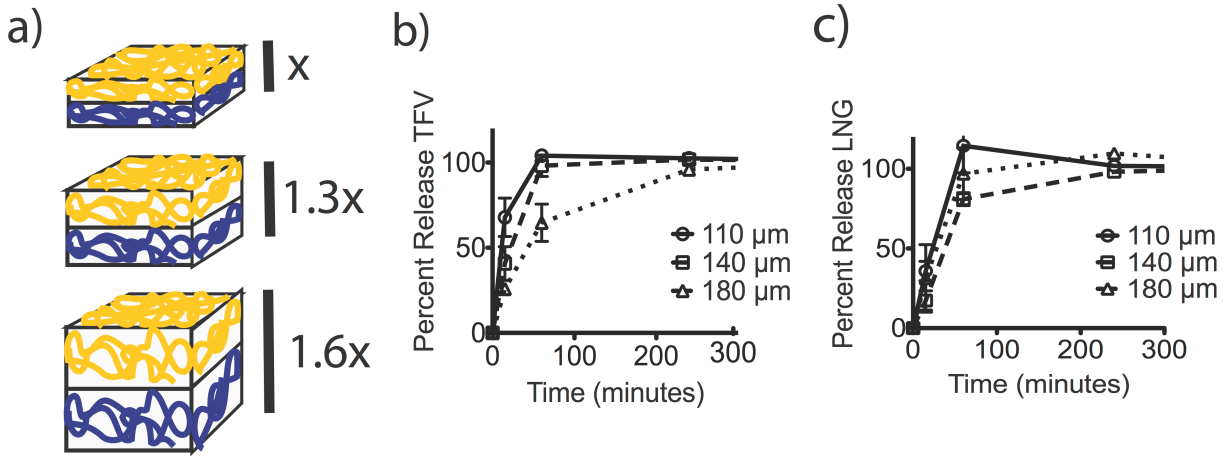

Figure 3.8: Effect of LNG and TFV release from stacked composites of different thickness. a) Schematic of stacked composite fibers with increasing thicknesses, b-c) in vitro release profiles of TFV and LNG, respectively, from stacked composite fibers of varying thickness.

We also prepared PVA fabrics containing relative loadings of TFV to LNG of 2000 to 1, a ratio that is better representative of the daily dosing requirements of these two drugs,[135, 136] and allowed us to test the hypothesis that decreasing the LNG loading would reduce the hindered release of TFV. Indeed, the combined microarchitecture with this ratio had similar TFV release to the TFV-only or stacked microarchitecture, with all three achieving 100% release after 2 hours (Figure 3.7e, f). We did not measure LNG release from these fabrics because the low LNG loading was below the detection limit of our HPLC method.

As previously reported by Jannesari *et al.*, increasing the thickness of electrospun fabrics can slow the release of a single agent.[49] Using the stacked microarchitecture, we prepared three different thicknesses ranging from 110 μm to 180 μm (Figure 3.8a). TFV release was slowest from the thickest fabric (Figure 8b), like due to increased diffusion distance and wetting time for the thicker fabrics. In contrast we did not observe a difference in LNG release with changes in mat thickness (Figure 3.8c).

3.4.6 *In Vitro Cytotoxicity and Inhibition of HIV-1 BaL Infection*

The activity and toxicity of PVA, LNG only, TFV only, stacked and combined fabrics were evaluated using *in vitro* assays for cytoxicity and HIV infection. PVA and TFV only fabrics were found to be non-toxic to TZM-bl cells at all concentrations tested (Figure 3.9a). Fabrics containing LNG were toxic at concentrations of 5 μM LNG and higher (Figure 3.9a). Based on these results and the more clinically relevant dosing, antiviral HIV activity was assessed using fabrics with the lower loading of LNG (0.0067 wt.%). TFV only, stacked and combined fabrics had IC_{50} values of 2.2, 1.7 and 2.9 μM TFV, respectively (Figure 3.9b). There were no statistically significant differences in antiviral activity between the fabrics of varying microarchitectures, or between the free drug, which has a measured IC_{50} of 1.8 μM and is similar to previously reported values.[4] Therefore, activity of TFV was preserved through the electrospinning process and did not depend on composite geometry.

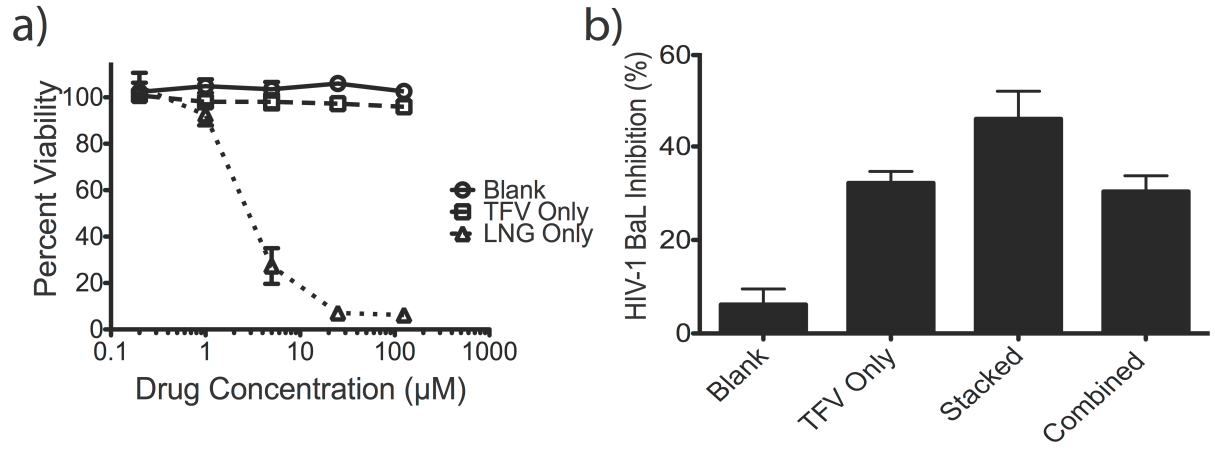

Figure 3.9: *C*ytotoxicity and HIV antiviral activity of drug-loaded fabrics of varying microarchitecture. a) Cytotoxicity of blank, TFV-only and LNG-only fabrics in TZM-bl cells. b) Inhibition of HIV-1 BaL infection of TZM-bl cells by blank, TFV-only, stacked and combined fibers at a delivered TFV concentration of 1 μM (IC_{50} of free TFV was 1.8 μM). Due to toxicity observed for LNG, fabrics with TFV:LNG ratio of 2000:1 were used for testing antiviral activity. Blank fibers were tested based on equivalent polymer concentrations used for TFV only fabrics. Values are reported as mean ± standard deviation for n=3.

3.5 DISCUSSION

We present the first report of combination drug-eluting fabrics with high drug loading and varying microarchitectures that have been fabricated using a free-surface, production-scale electrospinning instrument. Electrospinning allows for the formation of nanofibers from a drug-loaded polymer solution by subjecting the solution to an applied voltage, which charges the fluid and causes the eruption of a jet. The charged fluid jet is accelerated in an electric field towards the region of lower potential and polymer entanglement prevents break up of the stream while the solvent evaporates and results in fiber formation. While the differences in the release properties varied with microarchitecture, the macroscopic appearance and mechanical properties were unaltered. The ability to realize different microarchitectures without changing the visual or tactile properties of the materials may support better

designs of topical delivery systems for both biological efficacy and user acceptability.[137] The ability to vary the microstructure on a production scale instrument may also prove to be useful in a number of drug delivery applications, including wound healing and tissue engineering.[138-140]

We observed differences in the release of TFV from fabrics of varied loading and microarchitecture (Figure 3.7b, e) but not in the release of the more hydrophobic LNG (Figure 3.7a). The slower release of TFV seen with increasing fabric thickness likely correlates to hindered release due to slower wetting and increased distance for drug diffusion through the fiber matrix. The release of LNG was largely unchanged by the microarchitecture and fabric thickness, where the hydrophobicity and dissolution of the fabric may be the limiting factor in release. We suspect that the slowed release of TFV in the combined fabrics was due to depletion of TFV in the interfacial layer between the dissolving front and the solvent, leading to the creation of a surface layer rich in LNG through which the TFV and PVA must dissolve.[141] However, the versatile nature of electrospinning may allow for the decoupling of complex, multicomponent systems into single component systems via stacked or interwoven architectures that may be easier to control drug release.

The composite microarchitectures utilized in these experiments could be used to tailor release for different types of vaginal topical delivery. In concept, the fabrics would be inserted vaginally and then release drugs into the local tissue at appropriate doses of TFV and LNG to prevent both HIV-1 acquisition and unintended pregnancy. The fibers would then dissolve and be eliminated, or be cleared by the flow of vaginal mucus. For example the stacked composite could potentially be used to asynchronously deliver drugs in the vaginal mucosal environment by incorporating a layer that provides rapid drug release towards the mucosal tissue and a layer for sustained drug delivery towards the vaginal lumen. The combined microarchitecture has the advantage of manufacturing ease since only one solution is prepared and electrospun, but may not allow for decoupling of co-delivery release profiles. Pending improved drug loading efficiency, the interwoven microarchitecture may allow for independent release profiles of physicochemically diverse drugs. The highly loaded fabrics developed in this study could potentially be used as a fast-acting pericoital product for prevention of both HIV-1 transmission and

unwanted pregnancy. However, extensive testing regarding safety, toxicity, effectiveness and user perception need to be performed to clearly establish the potential of these fabrics.

3.6 CONCLUSIONS

We prepared composite fabrics containing high loading of TFV and LNG in three distinct microarchitectures by free-surface electrospinning using a production-scale instrument. We observed that the release of LNG from composite fabrics is largely unaffected by geometry, thickness and drug loading. However, TFV release was slower when combined in the in the same fiber with LNG as well as with increasing fabric thickness. The antiviral activity of TFV against HIV-BaL infection in TZM-bl cells was similar to the unformulated drug, and was not affected by the architecture of the composite fabrics. Our findings are significant because they are the first to inform the design and production of composite electrospun fabrics with high drug loading for co-delivery of physicochemically diverse drugs that may be useful in topical delivery systems for multipurpose prevention.

Chapter 4. Rapidly Biodegrading PLGA-Polyurethane Fibers for Sustained Release of Physicochemically Diverse Drugs

Adapted from: Rapidly Biodegrading PLGA-Polyurethane Fibers for Sustained Release of Physicochemically Diverse Drugs. Anna K. Blakney, Felix I. Simonovsky, Ian T. Suydam, Buddy D. Ratner, Kim A. Woodrow. ACS Biomaterials Science and Engineering: In Press (2016).

4.1 ABSTRACT

Sustained release of physicochemically diverse drugs from electrospun fibers remains a challenge and precludes the use of fibers in many medical applications. Here we synthesize a new class of polyurethanes with PLGA moieties that degrade faster than polyurethanes based on polycaprolactone. The new polymers, with varying hard to soft segment ratios and fluorobenzene pendant group content, were electrospun into nanofibers and loaded with four topically relevant but physicochemically diverse small molecule drugs. Polymers were characterized using GPC, XPS and ^{19}F NMR. The size and morphology of electrospun fibers were visualized using SEM, and drug/polymer compatibility and drug crystallinity were evaluated using DSC. We measured the *in vitro* release of physicochemically diverse drugs, and polymer degradation and cytotoxicity of biodegradation products were evaluated in cell culture. We show that these newly synthesized PLGA-based polyurethanes degrade up to 65-80% within four weeks, and are cytocompatible *in vitro*. The resulting drug-loaded electrospun fibers were amorphous solid dispersions. We found that increasing the hard to soft segment ratio of the polymer enhances the sustained release of positively charged drugs, while increasing the fluorobenzene pendant content caused more rapid release of some drugs. Increasing the hard segment or fluorobenzene pendant content of segmented polyurethanes containing PLGA moieties allows for modulation of physicochemically diverse drug release from electrospun fibers, while maintaining a biologically relevant biodegradation rate.

4.2 INTRODUCTION

Electrospun fibers have been widely explored as drug delivery systems (DDS).[142] Sustained release remains a formidable challenge from these materials, which have large surface areas conducive to rapid diffusive transport. Hydrophobic polymers can sustain drug release from fibers, but are typically slow or non-biodegradable. [143] The ability to tune the degradation while maintaining sustained release of small molecule drugs will be important for many medical applications. A number of factors are important to consider when designing a delivery formulation that include drug crystallinity,[144] polymer degradation rate,[145] polymer swelling,[146] and polymer-drug interactions.[147] Understanding the degradation and mechanisms of release are most important for formulation design[148] and, in the context of electrospun fibers, the release mechanism may be directly impacted by the electrospinning solution characteristics, polymer chemistry, and polymer-drug compatibility.

Segmented, linear polyurethanes (PUs) allow for design of nontoxic and biocompatible polymers with tunable degradation rate and mechanical properties.[149, 150] Commercially available PUs are synthesized using oligoethers or oligoesters, which are typically based on aromatic diisocyanates that are slow degrading and generate toxic degradation products.[151] A subclass of segmented, linear, biodegradable PUs elastomers incorporate hard and soft segments in which backbone chain bonds can be hydrolyzed to biocompatible degradation products.[152] Various strategies have been employed to alter the degradation profiles and mechanical properties of biodegradable polyurethanes, including varying the soft [153-156] or hard[157] segment, incorporation of acid-cleavable hydrazone[158, 159] or collagenase-labile [160] linkers and varying the hard to soft segment ratio[161-164]. Synthesis of segmented biodegradable PUs allows for engineering polymer structure, such as the hard to soft segment ratio, or incorporation of pendant groups in order to exert control of the release mechanisms of physicochemically diverse drugs. Topical drug delivery applications, such as antibiotic-loaded wound dressings[165] or vaginal delivery of contraceptives and/or antiretrovirals for the prevention of unintended pregnancy and/or HIV,[166] require

dosage forms with both mechanical integrity during application and tunable drug release in which biodegradable PUs are particularly well suited.

Biodegradable PUs have been previously synthesized using polycaprolactone (PCL)-based soft segments and electrospun for applications such as soft [167-169] or hard[156] tissue engineering scaffolds, drug-eluting stents[170], vascular grafts[171] and antibiotic wound dressings.[170] The chemical tunability that has been employed for rational design of tissue engineering scaffolds can also be used to modulate the release of physicochemically diverse drugs from electrospun fibers. For example, Hong et al. observed that grafting aminated phosphorylcholine onto the PLC-based poly (ester urethane) urea backbone slightly enhanced the release of paclitaxel from electrospun fibers.[170] Changing polymer chemistry may also increase the overall hydrophobicity of the bulk polymer and swelling ratio of the polymer matrix, with generally predictable effects on how the polymer interacts with hydrophilic and/or hydrophobic drugs encapsulated within the fibers. Similarly, Galperin et al. observed more prolonged release of norfloxacin (NFL) from porous polyHEMA hydrogels with increasing fluorostyrene content in the bulk hydrogel.[172] In contrast to the hydrogels explored by Galperin et al., it is unclear as to whether minor alterations in polymer chemistry may likewise affect the release of physicochemically diverse drugs from electrospun fibers.

We investigated the release of physicochemically diverse drugs from fibers electrospun with a new class of biodegradable PLGA-based polyurethanes (PLGA-PUs) that incorporate PLGA-b-tetraethylene glycol (TEG)-b-PLGA copolymers. We hypothesized that a polyurethane urea based on PLGA as opposed to PCL would degrade more quickly given the relative degradation rates of these two polymers.[173] We also opted to use a PLGA-TEG-PLGA copolymer as the soft segment for increased hydrophilicity. Four small molecule drugs with varying aqueous solubilities and ionization states, but similar molecular weights, were chosen to probe the drug-polymer interactions. Levonorgestrel (LNG) is a hydrophobic hormonal contraceptive approved for use in vaginal, mucosal contraception. Maraviroc (MVC) is a hydrophilic antiretroviral currently being tested as a topical, intravaginal ring microbicide as part of a combination dosage form.[174] Norfloxacin (NFL) is a slightly-hydrophobic antibiotic used in

ophthalmic antibacterial eye drops. Tenofovir (TFV) is a hydrophilic antiretroviral being investigated for use as a topical microbicide gel for prevention of HIV.[175] We synthesized sixteen PLGA-based PUs and selected four that showed relatively higher molecular weight and fiber stability at room temperature for further investigation; two with varying hard to soft segment ratios and two with varying molecular content of a fluorobenzene pendant group. The four polymers were characterized for their composition and thermal properties, independently electrospun into fiber mats loaded with each of the four drugs, and then utilized for *in vitro* release and cytotoxicity experiments. We report on the use of drug-loaded electrospun PLGA-PU fibers to probe drug-polymer interactions and to determine the effects of alterations in PLGA-PU chemistry on the release of physicochemically diverse drugs.

4.3 MATERIALS AND METHODS

4.3.1 *PLGA-based poly(urethane urea) (PUUr) synthesis*

PLGA-b-TEG-b-PLGA diol (MW =1260 Da, LA:GA=50:50), PLGA-b-PEG-b-PLGA diol (M_w=4706 Da, LA:GA=50:50) and PLGA-BD-PLGDA diol (M_w = 1633 Da, LA:GA=50:50) were obtained from PolySciTech (West Lafayette, Indiana). Lysine diisocyanate (LDI) was purchased from Kyowa Hakko USA (New York, NY). N,N-dimethylacetamide (DMAc), tin(II) 2-ethylhexanoate (SnOc), 1,4-butanediamine (BDA), 1,3-diamino-2-hydroxypropane (DAHP) and 4-fluorophenylisocyanate (FPI) were obtained from Sigma-Aldrich (St. Louis, MO). DMAc was dried using 10 wt.% of 4 Å molecular sieves. 1 mole of PLGA-TEG-PLGA diol was dried at 105 °C and ~30 in Hg for 3 hours, decompressed with nitrogen, and then placed in a 50 mL round bottom flask and purged with N_2. 8.77 mL of DMAc was added and the macrodiol was completely dissolved before adding 2.08 moles of LDI. The mixture was stirred for 3.5 hours at 80 °C. The resulting prepolymer solution was cooled to room temperature while stirring. For PU polymers without fluorobenzene pendant groups, 1.08 mole of BDA was added to a 100 mL 3-neck round bottom flask with 16.27 mL of DMAc, which was preliminarily purged with nitrogen. The prepolymer solution was then added to the flask, dropwise, over 10 minutes, while stirring at room temperature. For the PLGA-PU containing the

fluorobenzene pendant groups, 0.96 mole of BDA and 0.12 mole of DAHP were added to a 100 mL 3-neck round bottom flask with 16.27 mL of DMAc at room temperature, until completely dissolved. The prepolymer solution was then added dropwise over 10 minutes, while stirring at room temperature. 0.1 wt.% of SnOc was added to the PUUr solution, and then heated to 80 °C, and stirred for ~5 minutes. Then, 0.12 mole of FPI was added dropwise to the OH-modified PUUr solution while stirring, and was mixed for 30 minutes at 80 °C. The final polymers were poured into Teflon trays and dried at 80 °C at atmospheric pressure for 4 hours, and then at 80 °C under 30 in Hg for 2 hours.

4.3.2 *Bulk polymer characterization*

The values of average molecular weights (Mw, Mn) and the polydispersity (PDI) of the polymers were determined by gel permeation chromatography (GPC) (SEC Tosoh TSK-GEL R-3000 and R-4000 columns, Tosoh Bioscience, Montgomeryville, PA) connected in series to a Viscotek GPMmax VE2001 and refractometer VE3580 (Viscotek, Houstin, TX). Samples were run at a concentration of 5 mg mL^{-1} in N-N-dimethylformamide (DMF). The mobile phase consisted of DMF containing 0.1 wt.% LiBr at a flow rate of 1 ml min^{-1}.

The fluorine content of each polymer was evaluated by quantitative ^{19}F NMR spectroscopy.[176, 177] Polymers were dissolved in DMSO-d_6 containing 2.0 mM fluorobenzene to a final polymer concentration of 10.0 mg/mL. NMR spectra were acquired at 25 °C using a Bruker Avance III spectrometer operating at 376.46 MHz for ^{19}F with broadband ^{1}H decoupling. Spectral parameters were as follows: 4096 scans; acquisition time 0.73 sec; spectral width 89.286 kHz; spectral size 131,072 points. Spectra were phased and baseline corrected from −110 to −125 ppm using a Whittaker smoothing routine, then referenced to fluorobenzene as an internal standard (−113.15 ppm, normalized area = 1.0). All ^{19}F resonances arising from polymer incorporated fluorobenzene pendant groups were observed at frequencies spanning −121 ppm to −123 ppm. The combined integrated area for all ^{19}F resonances

arising from polymer incorporated fluorobenzene pendant groups was referenced against the internal standard to quantitate fluorine content in each polymer.

X-ray photoelectron spectroscopy (XPS) was performed using a Surface Science Instruments S-Probe (Al $K_{\alpha 1,2}$ x-ray source) at the University of Washington NESAC/BIO surface analysis center. Survey scans and high-resolution scans of carbon, nitrogen and fluorine were taken for all polymer samples. Peak assignment and integration were performed using XPS analysis software (Casa XPS). Theoretical atomic percentages for C, N, O and F were calculated assuming a uniform elemental distribution across materials.

Polymers were dissolved in either dichloromethane (DCM) (PLGA-PU, PLGA-PU-FB, PLGA-PU-2FB) or 1,1,1,3,3,3-hexafluoro-2-propanol (HFIP) (PLGA-2PU) at 50% w/v and 1 mL aliquots of the resulting polymers solutions were cast into thin films on glass slides by drying overnight at 40 °C and atmospheric pressure. Thin films were analyzed using a contact angle goniometer (Ramè-Hart, Model 100, Mountain Lakes, NJ) with 10 µL of deionized water, with n=3 for each sample. Thin film polymer degradation in phosphate buffered saline (PBS) at a concentration of 1 mg mL^{-1} was monitored over 4 weeks at 37 °C on a rotational shaker. Polymers were cast into thin films and initial masses were recorded. At each timepoint (every 7 days), the remaining solid polymer was removed, lyophilized overnight, weighed, and then added to fresh PBS at a concentration of 1 mg mL^{-1}. Spent PBS was stored at -20 °C and utilized for the cytotoxicity assay. Thin films were analyzed for water uptake and were equilibrated in DI H_2O for 72 hours. They were then removed from the liquid, lightly blotted to remove extraneous water, and then the swollen film was weighed. Water uptake was calculated using the following equation:

$$\%\, Water\ Weight\ Increase = 100 * \frac{(Wt.film_{wet} - Wt.film_{dry})}{Wt.film_{dry}}$$

4.3.3 *Electrospinning and fabric characterization*

Synthesized polymers were dissolved in DCM (PLGA-PU, PLGA-PU-FB, PLGA-PU-2FB) or HFIP (PLGA-2PU) at 50% (w/v) and allowed to mix for one hour prior to electrospinning. LNG, MVC, NFL and TFV (Supplementary Figure 4.1) were micronized and added at 15% (wt. drug/wt. polymer). Polymer solutions were then electrospun at 18 kV over an 8-cm gap, using a flow rate of 20-40 μL min^{-1}. A total volume of 1 mL was dispensed from a glass syringe with a blunt 18-gauge stainless steel nee dle. Fibers were collected onto a flat, grounded aluminum surface covered by a single sheet of wax paper. After electrospinning, fiber samples were immediately stored in a lyophilizer until further use.

For scanning electron microscopy (SEM), fiber samples were sputter-coated with a mixture of Au and Pd for 90s and then imaged using a Sirion SEM (NanoTech User Facility, University of Washington). A voltage of 5 kV, spot size of 3 and working distance of 5 mm were used to obtain images at a magnification of 500X and 5,000X. Fiber sizes were measured using NIH ImageJ software for n=30 per sample. Fiber degradation was observed by submerging fiber samples still attached to wax paper in PBS and incubating at 37 °C for 4 weeks. At each timepoint, samples were removed from solution, dried at room temperature for 2 hours, and sputtercoated and imaged using SEM as described above.

Fiber samples of ~5 mg were sealed in T_{zero} aluminum pans and analyzed for drug crystallinity, polymer melting temperature and glass transition temperature using an Auto Q20 differential scanning calorimeter (TA Instruments, UW Materials Science Engineering User Facility). Samples were heated at a constant ramp from 30 °C to 300 °C with a sampling interval of 1 s $point^{-1}$, and heat flow was normalized to sample weight. Data collection and analysis was performed using TA Universal Analysis 2000 software.

4.3.4 *In vitro release*

Temporal release of drugs from electrospun fibers (~5 mg, n=3) was carried out in 2% Kolliphor HS 15 (a non-ionic solubilizer and emulsifying agent, Sigma) in deionized water. Prior to release experiments, drug saturation concentrations were calculated by adding excess drug to release media,

equilibrating over 24 hours, and then analyzing using HPLC with quantification of each drug using a standard curve prepared in DMSO (in which all of the drugs are soluble). Release samples were kept at sink conditions at 37 °C on a rotational shaker, and at each timepoint, a 100 μL aliquot was removed for HPLC analysis and replenished with fresh release media. HPLC analysis was carried out on a Shimadzu Prominence LC20AD UH-HPLC system equipped with a Phenomenex Luna C18 column (250 x 4.6 mm, 5 μm) using previously described HPLC methods.[178-181]

4.3.5 *Cytotoxicity of biodegradation products and cytocompatibility of electrospun fibers*

To evaluate cytotoxicity of biodegradation products of the synthesized polyurethane polymers, TZM-bl cells, an adherent HeLa cell line, were seeded on a 96-well tissue culture polystyrene plate at a concentration of 15,000 cells well^{-1}. Cells were allowed to culture for 24 hours, and then media was aspirated and replaced with 100 μL of cDMEM and 100 μL of either PBS (negative control) or spent PBS from 4 week biodegradation study. Cells were then allowed to culture for an additional 72 hours, and then analyzed for viability using a CellTiter-Blue assay (Promega). Briefly, 20 μL of CellTiter-Blue Reagent was added to each well, and allowed to incubate for 3 hours. The plate was then analyzed for fluorescence using a Tecan plate reader at an excitation wavelength of 560 nm and an emission of 590 nm. Percent viability was calculated by normalizing the sample wells to the fluorescence values of the negative control wells.

In order to assess the ability of electrospun PLGA-PU fibers (n=3) to support cellular adhesion, fiber samples were cut and placed at the bottom of a clear-bottomed black 96-well plate. TZM-bl cells were seeded at a concentration of 30,000 cells well^{-1}, and allowed to adhere for 24 hours, and then analyzed for cellular adhesion relative to a tissue-culture polystyrene (TCPS) control using the same CellTiter-Blue protocol as stated above. Cellular adhesion was expressed as percentage of TCPS control. PLGA-PU fibers (n=3) were similarly assessed for cell growth: cells were seeded on PLGA-PU fibers at the same concentration, and then analyzed after two, three, four and five days of culture using the CellTiter-Blue protocol. Fluorescence signal from each well was normalized to a standard curve of fluorescence

signal for a known number of cells. Images of cells were obtained by staining TZM-bl cells with CellTracker Red CMPTX dye (Molecular Probes by Life Technologies, Waltham, ME, USA) according to manufacturer protocol. Briefly, cells were incubated in a solution of 20 μm CMPTX dye in serum-free DMEM for 30 minutes, centrifuged and washed with PBS. Cells were then plated at a concentration of 30,000 cells well^{-1} in cDMEM on PLGA-PU fibers in a black 96-well plate with clear bottom, and incubated for 48 or 96 hours. At each timepoint, media was removed from the well, cells were washed 2X with PBS, and imaged on a Nikon ECLIPSE Ti microscope at 10X magnification in the brightfield, FITC and TRITC channels, and merged using Nikon Elements AR software (Version 3.0). PLGA-PU fibers exhibited auto-fluorescence in both the fluorescein isothiocyanate (FITC) channel (519 nm) and TRITC channels. Thus, when imaging cells on PLGA-PU fibers, fibers were imaged in the FITC channel while cells were imaged in the TRITC channel, and then the two images were merged.

4.4 RESULTS

4.4.1 *Characteristics of synthesized PLGA-PUs*

PLGA-based poly(urethane ureas) were synthesized as illustrated in Figure 4.1. We chose PLGA-b-TEG-b-PLGA (Mw=1190 Da) for our polyurethane polymers based on the hypothesis that the bulk polymer would be more hydrophilic than PLGA alone by incorporating TEG into the middle of the two PLGA blocks. The increased hydrophilicity is desirable to promote more rapid hydration of the polymer, which we predicted could result in faster hydrolysis of ester bonds and polymer degradation.[182] Furthermore, incorporating a fluorobenzene pendant has previously been shown to sustain drug release in hydrogels and we hypothesized that this phenomena could be translated to electrospun fibers.[172] Finally, we investigated if increasing the relative amount of hard segment to that of the soft segment would both limit the equilibrium water content of the polymer and sustain drug release.[183] Polymers were synthesized using standard polyurethane synthesis procedures[184] with a yield of >95%.

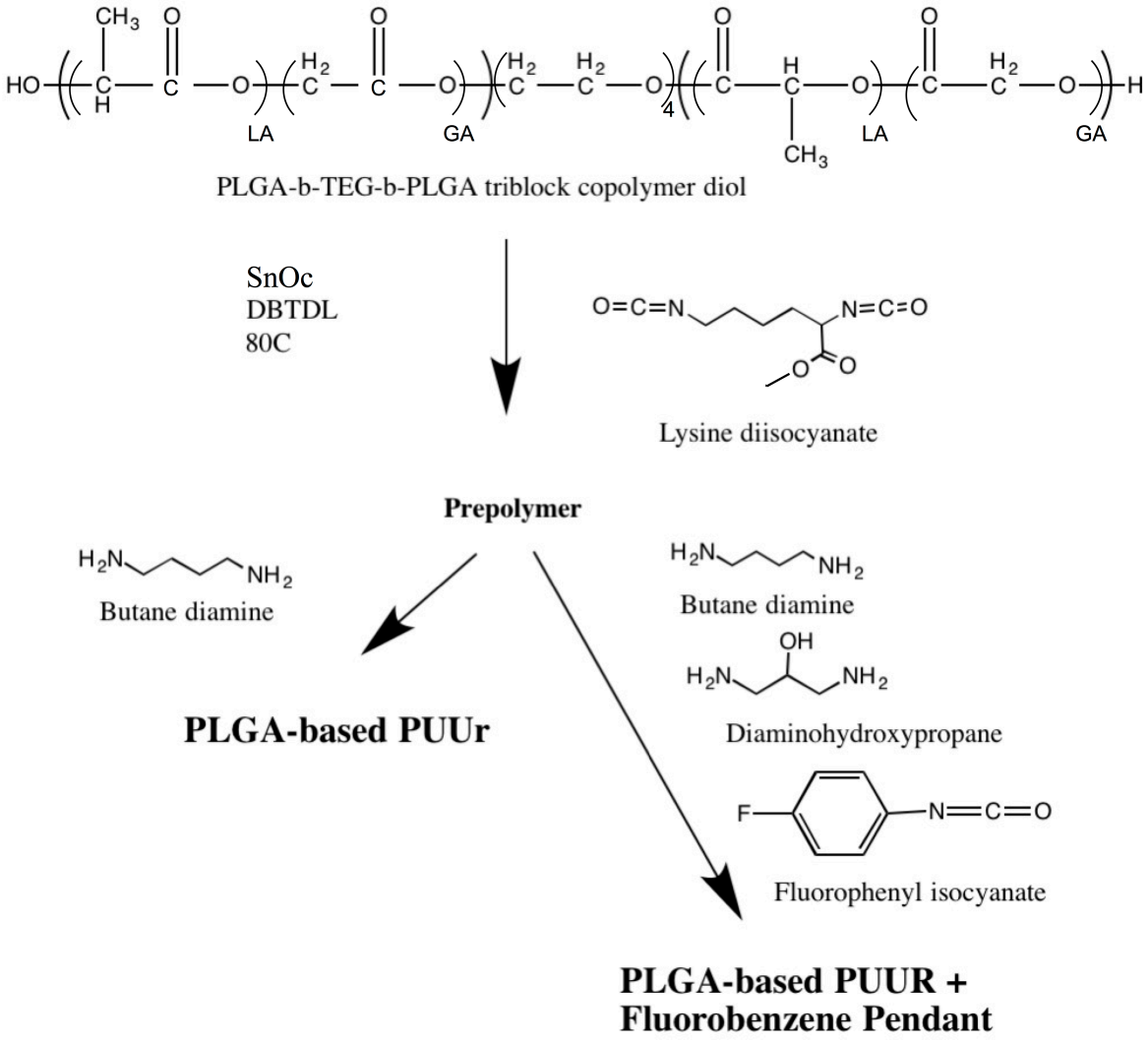

Figure 4.1: PLGA-based polyurethane urea synthesis.

Sixteen total polymers were synthesized, initially using PLGA-PEG-PLGA (1000:1000:1000) and PLGA-BD-PLGA (500:58:500) (Supplementary Table 4.1). However, these initial polymers were relatively low in molecular weight, and did not exhibit structural fiber integrity at room temperature. Polymers with similar compositions but based on PLGA-TEG-PLGA (500:190:500) were higher in molecular weight and maintained fiber morphology, and were used for further experimentation. The final polymers include a linear PLGA-based polyurethane urea (PLGA-PU), a linear PLGA-based

polyurethane with twice the original hard to soft segment ratio (PLGA-2PU), a PLGA-based polyurethane

with an added fluorobenzene pendant group (PLGA-PU-FB), and a PLGA-based polyurethane with twice the original fluorobenzene pendant group content (PLGA-PU-2FB). The molecular weight and PDI for each polymer are reported in Table 4.1. Prior to electrospinning, all polymers appeared as slightly yellow, semi-elastic solids at room temperature. All polymers were analyzed by ^{19}F NMR in order to measure the fluorine content of the bulk polymer (Supplementary Figure 4.2), and by XPS to measure the fluorine content at the surface of the polymer cast into thin films. As expected, fluorine was not detected in the PLGA-PU and PLGA-2PU by either technique. Quantitative ^{19}F NMR analysis of PLGA-PU-FB and PLGA-PU-2FB indicated that PLGA-PU-2FB has ~2.4 times the molar fluorobenzene content of PLGA-PU-FB (Table 4.2), consistent with complete incorporation of the added pendant group at the target molar ratio. Surprisingly, XPS analysis of PLGA-PU-FB or the PLGA-PU-2FB thin films did not detect any fluorine at the surface (<10 nm sampling depth) (Table 4.3).

Table 4.1: Polymer molecular weights and polydispersity index (PDI) as determined by gel permeation chromatography.*

Polymer ID	**Composition**					**M_w (g/mol)**	**M_n (g/mol)**	**PDI (Mw/Mn)**	**Hard Segment**	**Soft Segment**
	PLGA-TEG-PLGA	LDI	BDA	DAHP	FPI					
PLGA-PU	1.00	2.00	1.00	0	0	27,140	20,960	1.295	22%	78%
PLGA-2PU	1.00	3.00	2.00	0	0	7,805	3,226	2.419	31%	69%
PLGA-PU-FB	1.00	2.00	0.92	0.08	0.08	8,189	5,099	1.606	22%	78%
PLGA-PU-2FB	1.00	2.00	0.84	0.16	0.16	10,790	6,325	1.706	23%	77%

*A value of 0.07 was used for the dn/dc of all tested polymers.

Table 4.2: Fluorine content of PLGA-PU polymers containing a fluorobenzene pendant group.

Polymer ID	Polymer[a] (moles)	^{19}F Content[b] (moles)	^{19}F Mole Ratio (moles ^{19}F/moles polymer)
PLGA-PU-FB	6.39×10^{-7}	7.60×10^{-7}	1.19
PLGA-PU-2FB	4.63×10^{-7}	1.31×10^{-6}	2.83

[a] Mole quantity calculated based on the average M_w of PLGA-PU-FB of 8,189 g/mole and PLGA-PU-2FB of 10,790 g/mole.
[b] Measured based on quantitative ^{19}F NMR.

XPS was also used to confirm the composition of polymers synthesized with different hard (urethane urea) to soft (PLGA) segment ratios. We observed that polymers with equivalent hard to soft segment ratio (PLGA-PU, PLGA-PU-FB, PLGA-PU-2FB) had a carbon content of 74-81% (atomic %), oxygen content of 16-22%, and nitrogen content of 2.4-3.5% (Table 4.3). The carbon content for these polymers is higher than expected whereas the oxygen content is lower than expected. This result may be due to more efficient incorporation of BDA into the polymer chain, or molecular positioning of the hard segment towards the surface of the polymer. Doubling the hard to soft segment ratio (PLGA-2PU) resulted in a measured elemental composition of 59% carbon, 34% oxygen and 0.1% nitrogen. These values of carbon and oxygen content are more reflective of the predicted values, but the nitrogen content is much lower, possibly indicating less incorporation of the nitrogen-rich lysine block or positioning of the lysine block away from the surface of the polymer. Polymer compositions as revealed by ^{19}F NMR and XPS were as expected with only minor deviations.

Table 4.3: Composition of polymers as determined by x-ray photoelectron spectroscopy.

Polymer ID	Theoretical Atomic %				Measured Atomic % Average ± Standard Deviation			
	C	O	N	F	C 1s	O 1s	N 1s	F 1s
PLGA-PU	58.4	38.7	2.9	0	75.7 ± 0.006	20.8 ± 0.005	3.5 ± 0.002	n.d.
PLGA-2PU	59.6	36.5	3.8	0	58.5 ± 0.009	34.3 ± 0.01	0.07 ± 0.003	n.d.
PLGA-PU-FB	58.3	38.5	3.1	0.0006	73.9 ± 0.06	22.7 ± 0.06	3.3 ± 0.0009	n.d.
PLGA-PU-2FB	58.3	38.4	3.2	0.001	81.2 ± 0.03	16.3 ± 0.02	2.4 ± 0.006	n.d.

In order to determine how polymer composition may affect their behavior in aqueous release media, we measured polymer wettability and swelling using contact angle goniometry and equilibrium water content, respectively. All polymers were found to have intermediate wettability (both hydrophilic and hydrophobic characteristics, $0°<\theta<90°$) based on the measured contact angles. The contact angle increased by 15° and 28° when either the hard to soft segment ratio or fluorobenzene pendent content was increased, respectively (Table 4.4). However, addition of the fluorobenzene alone resulted in a reduced contact angle relative to the PLGA-PU polymer. In general, the contact angle measurements were supported by the equilibrium water content data. For example, the larger contact angle measured for PLGA-PU compared to PLGA-2PU and PLGA-PU-FB compared to PLGA-PU-2FB also resulted in an observed decrease in equilibrium water content of approximately 40% and 10%, respectively. Similarly, a 20° lower contact angle observed for PLGA-PU-FB compared to PLGA-PU showed almost a 60% increase in water content. In summary, although the polymers had varied hard to soft segment ratios and fluorobenzene pendant content, they showed similar wettability and swelling based on the resolution of the analysis methods, which suggest that they would behave similarly in release media.

Table 4.4: Wettability and equilibrium water content of polymers.

Polymer ID	Contact angle	Water Mass Uptake (72 hours)
PLGA-PU	67° ± 2°	34% ± 6%
PLGA-2PU	82° ± 3°	19% ± 1%
PLGA-PU-FB	47° ± 1°	54% ± 8%
PLGA-PU-2FB	75° ± 3°	49% ± 2%

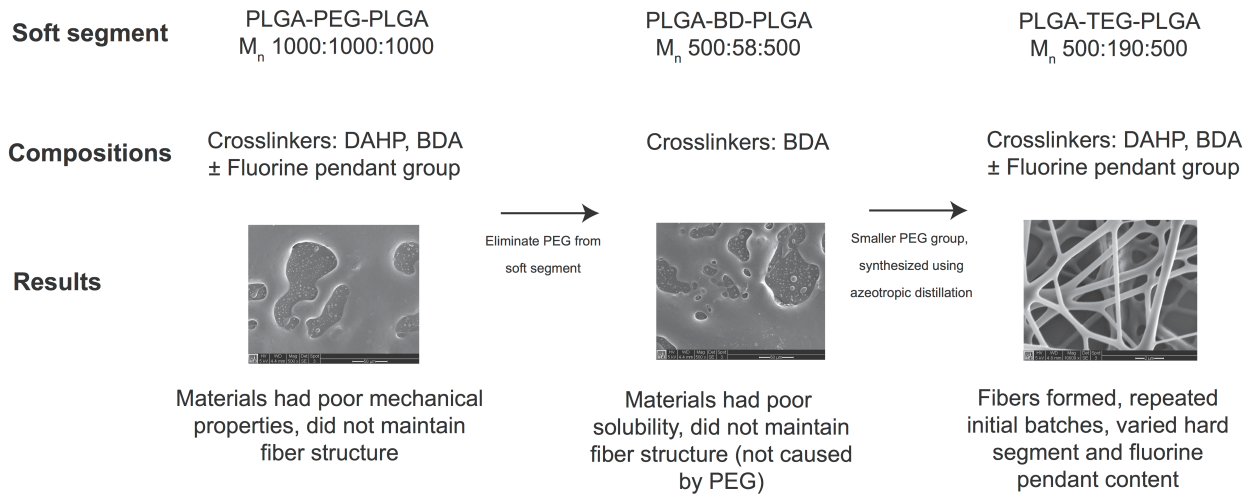

Figure 4.2: Evolution of PLGA-PU compositions.

4.4.2 *Drug and polymer compatibility in electrospun fibers*

Polymers were electrospun from DCM (PLGA-PU, PLGA-PU-FB, PLGA-PU-2FB) or HFIP (PLGA-2PU), and produced meshes of fibers diameters of ≤1 μm with a semi-melded fiber morphology as well as the presence of some non-fiber regions (Figure 4.3). Non-fiber regions were likely due to the relatively low molecular weights and inherently low melting temperature (T_m) of these polymers. Likewise, fibers were lyophilized immediately after electrospinning in order to remove residual solvent and prevent meshes from coalescing into films.

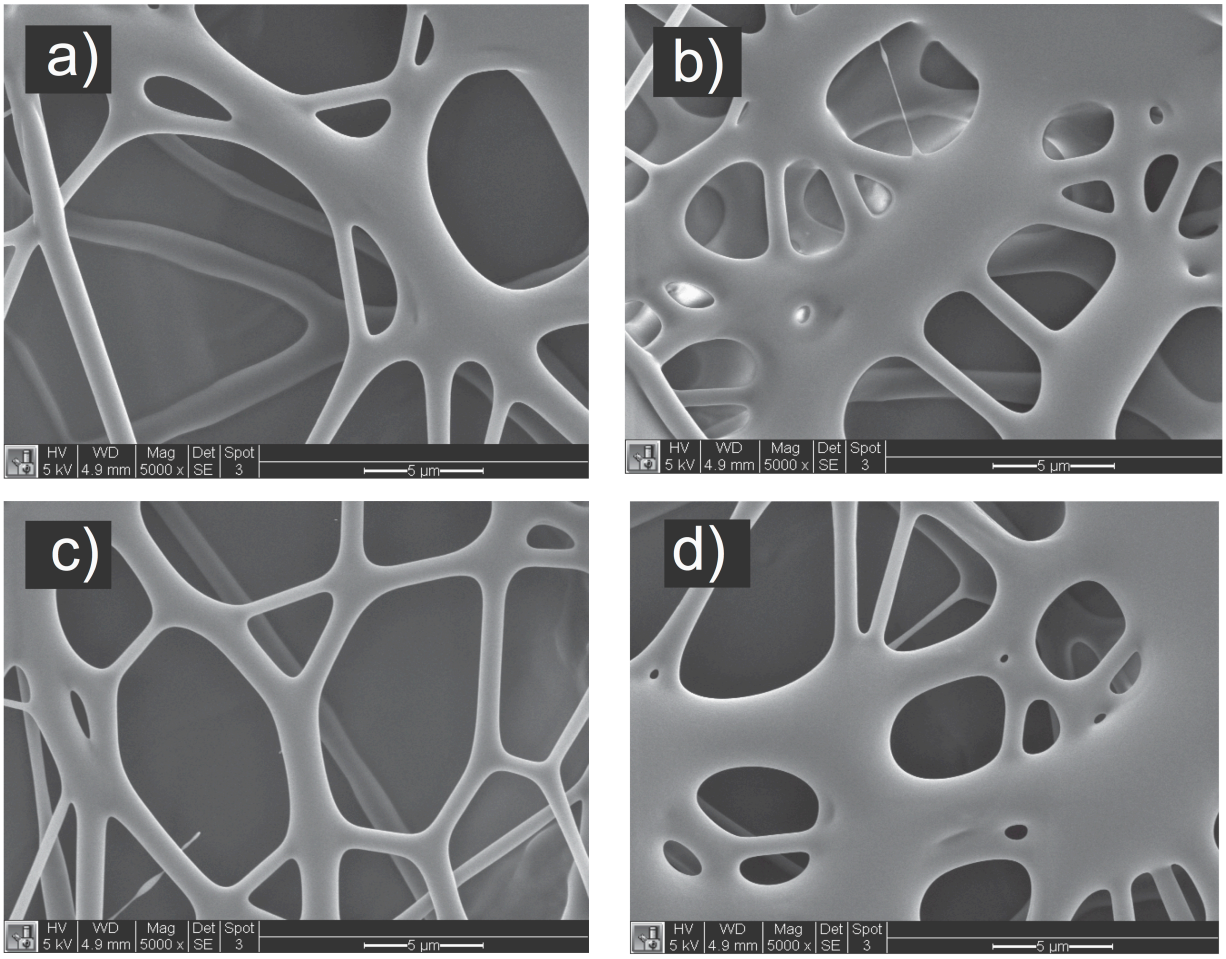

Figure 4.3: Scanning electron micrographs of electrospun polyurethane polymers. a) PLGA-PU, b) PLGA-2PU, c) PLGA-PU-FB and d) PLGA-PU-2FB. Magnification = 5000X and scale bar = 5 µm.

Drug solubility in a polymer-solvent system may affect electrospinning as well as the resulting drug crystallinity in the finished fibers. Only MVC was soluble in all the polymer solutions, whereas LNG, NFL and TFV were either partially soluble or insoluble as assessed by qualitative visual inspection. However, analysis of drug-loaded electrospun fibers, which all had >90% loading efficiency, using differential scanning calorimetry (DSC) showed no crystalline drug present in any of the samples. A representative thermogram of LNG and PLGA-PU-FB polymer shows a broad polymer melting peak present in samples both with and without drug, and a lack of any crystalline drug (Figure 4.4a). PLGA-

PU, PLGA-PU-FB and PLGA-PU-2FB had a polymer melting temperature of approximately 260 °C, and increasing the hard to soft segment ratio of the polymer (PLGA-2PU) decreased the T_m by ~20°C (Figure 4.4b). Unchanged or increased polymer T_m indicates good drug/polymer compatibility, or physicochemical interactions between components of the formulation that facilitate drug dissolution and dispersion within the solid matrix.[185] Based on this criterion, PLGA-PU and PLGA-2PU showed good compatibility with all four drugs despite physicochemical differences in the compounds. In contrast, PLGA-PU-FB had poor compatibility with MVC and NFL but was compatible with LNG and TFV. PLGA-PU-2FB had poor compatibility with LNG and MVC but was compatible with NFL and TFV. Glass transition temperature (T_g) is also an indicator of drug/polymer compatibility where a decrease in T_g upon incorporation of a small molecule drug is evidence of more mobile polymer chains due to the plasticizing effect of the drug. [186] All drugs caused a decrease in T_g for PLGA-2PU but had little effect on the T_g of PLGA-PU, PLGA-PU-FB and PLGA-PU-2FB. We observed an increase of ~5 °C in the T_g when MVC was incorporated into PLGA-PU and PLGA-PU-FB and when TFV was incorporated into PLGA-PU-2FB (Figure 4.4c). Overall, PLGA-2PU showed good compatibility with all drugs, while PLGA-PU, PLGA-PU-FB and PLGA-PU-2FB showed minor deviations in T_m and T_g upon incorporation of LNG/MVC, MVC/NFL and LNG/MVC, respectively.

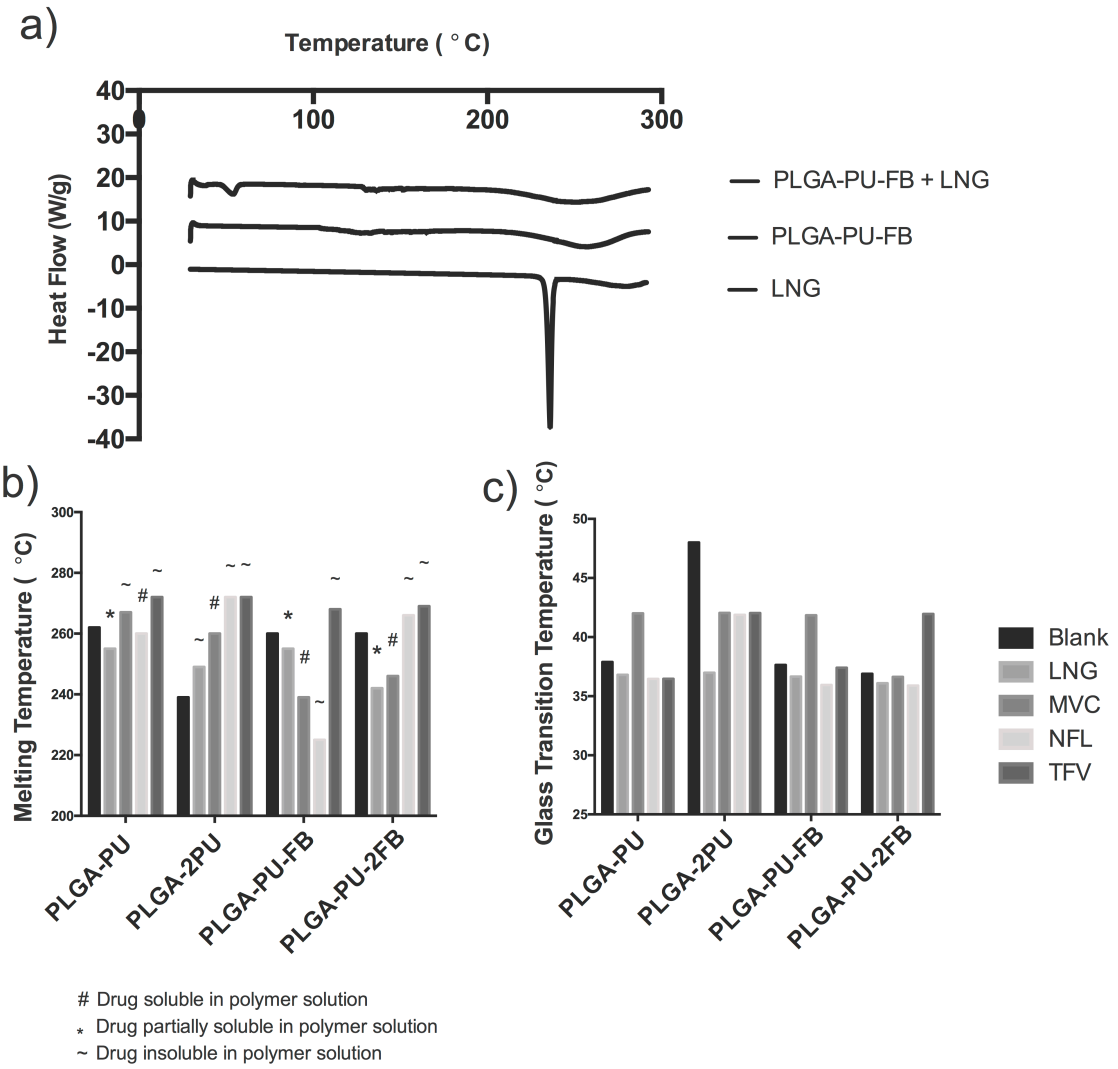

Figure 4.4: Thermal properties of polymers in blank and drug-loaded electrospun fibers as determined by differential scanning calorimetry. a) Representative differential scanning calorimetry thermograms of crystalline LNG, electrospun PLGA-PU-FB polymer, and electrospun PLGA-PU-FB polymer loaded with LNG, b) melting temperatures, and c) glass transition temperatures of PLGA-PUs.

4.4.3 *Release of physicochemically diverse drugs from PLGA-PUs with higher hard to soft segment ratio*

We measured the effect of polymer hard to soft segment composition on the release of physicochemically diverse drugs. We observed that increasing the hard to soft segment ratio (PLGA-PU

and PLGA-2PU) had a significant effect on the *in vitro* release rate of all the drugs except for LNG (Figure 4.5). We observed that MVC and NFL had a 20-30% reduction in the burst release phase with PLGA-2PU compared to PLGA-PU, but similar pseudo-linear release rates resulting in a lower cumulative percent release after 72 hours. In contrast, increasing the hard to soft segment ratio had the opposite effect on TFV release, where the amount of burst release almost tripled whereas the pseudo-linear phase was similar or slightly higher. The burst and pseudo-linear phases were almost identical between PLGA-PU and PLGA-2PU for release of LNG.

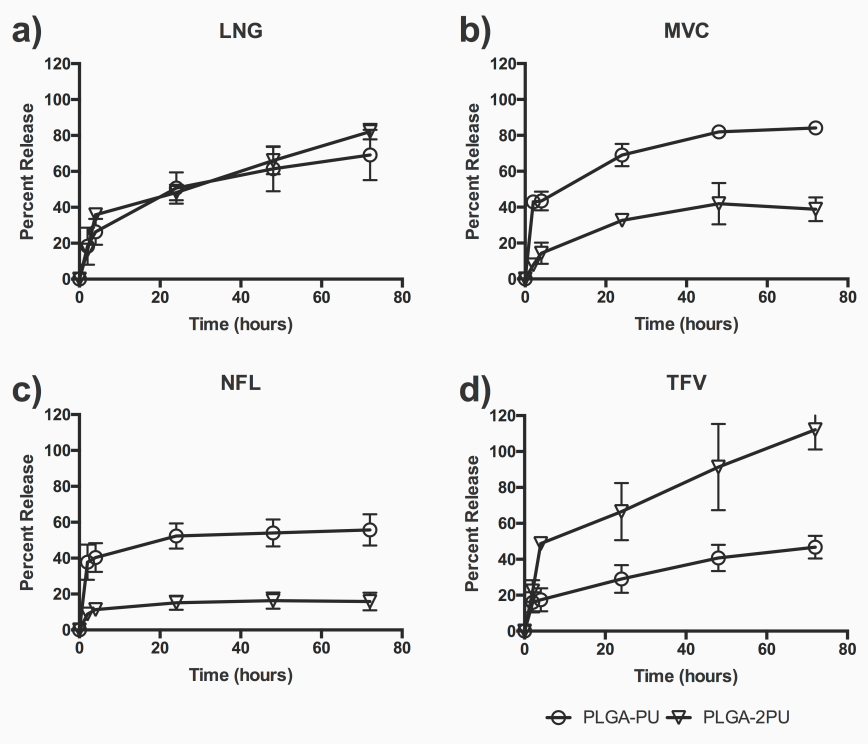

Figure 4.5: Release of LNG (a), MVC (b), NFL (c), and TFV (d) from electrospun fibers from polyurethanes PLGA-PU and PLGA-2PU (both sans fluorobenzene pendant) into 2% solutol in deionized water at sink conditions over 72 hours. Each point represents the mean ± standard deviation for n=3.

4.4.4 *Release of physicochemically diverse drugs from PLGA-PUs with higher fluorobenzene pendant group content*

We measured the effect that increased fluorobenzene pendant content of the polymer has on the release of these physicochemically diverse drugs. We observed that doubling the fluorobenzene pendant content of the PLGA-PU enhanced sustained *in vitro* release of LNG and NFL, but not MVC nor TFV (Figure 4.6). MVC and TFV showed an initial burst of ~40% followed by similar pseudo-linear release rates between PLGA-PU-FB and PLGA-PU-2FB. LNG and NFL showed a similar trend of reduced burst release with PLGA-PU-FB compared to PLGA-PU-2FB but comparable pseudo-linear release rates. However, a 20% reduction in burst release was measured for LNG whereas the reduction in NFL burst release was ~60%. Overall, increasing fluorobenzene pendant content did not affect MVC or TFV release, but resulted in a greater burst release for both LNG and NFL.

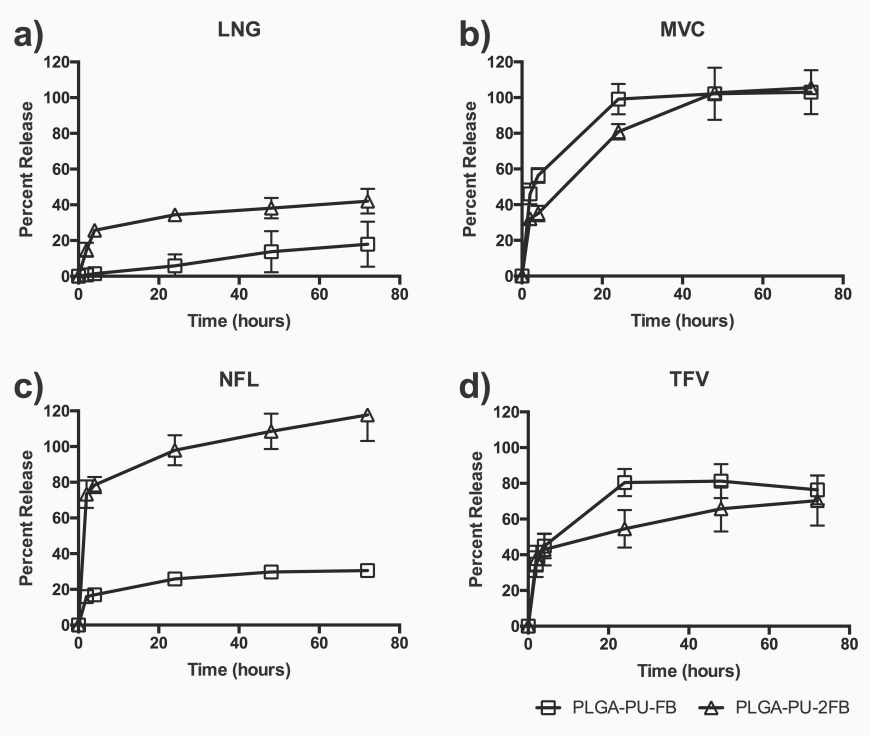

Figure 4.6: Release of LNG (a), MVC (b), NFL (c), and TFV (d) from electrospun fibers from polyurethanes PLGA-PU-FB and PLGA-PU-2FB (2 and 4 mol% fluorobenzene pendant, respectively) into 2% solutol in deionized water at sink conditions over 72 hours. Each point represents the mean ± standard deviation for n=3.

4.4.5 *Biodegradation and cytocompatibility of PLGA-PU fibers and degradation products*

Biodegradability and cytocompatibility are essential considerations for polymers intended for use in topical drug delivery. We measured biodegradation in PBS of all polymers cast as thin films over the course of four weeks. Thin films were used in the place of fibers in order to ensure that all samples had equivalent thickness and surface area. We observed that thin films of the four polymers showed similar linear degradation profiles (Figure 4.7a). PLGA-PU and PLGA-2PU degraded at similar rates of -21.3% ± 1.4% and -19.3% ± 2.4% per week, respectively. Incorporation of the fluorobenzene pendant group enhanced degradation by <1% to 4% and yielded rates of -22.1% ± 3.4% and -23.5% ± 1.8% per week for PLGA-PU-FB and PLGA-PU-2FB, respectively. The degradation products of each polymer were subsequently analyzed for cytotoxicity in the presence of TZM-bl cells (Figure 4.7b). To complement the PLGA-PU thin film biodegradation studies, we also measured biodegradation of electrospun PLGA-PU fibers in PBS (Figure 4.7c). Fibers were predicted to show faster degradation rates than the films due to their comparatively higher porosity and surface area and indeed this was confirmed. After 24 hours, all fibers had almost completely lost the fibrous structure, and had started to relax into films. The fibers then appeared to be meld into a thin, smooth layer of polymer film, which was present after one and two weeks. After four weeks, only small droplet-like structures of polymer were present on the wax paper.

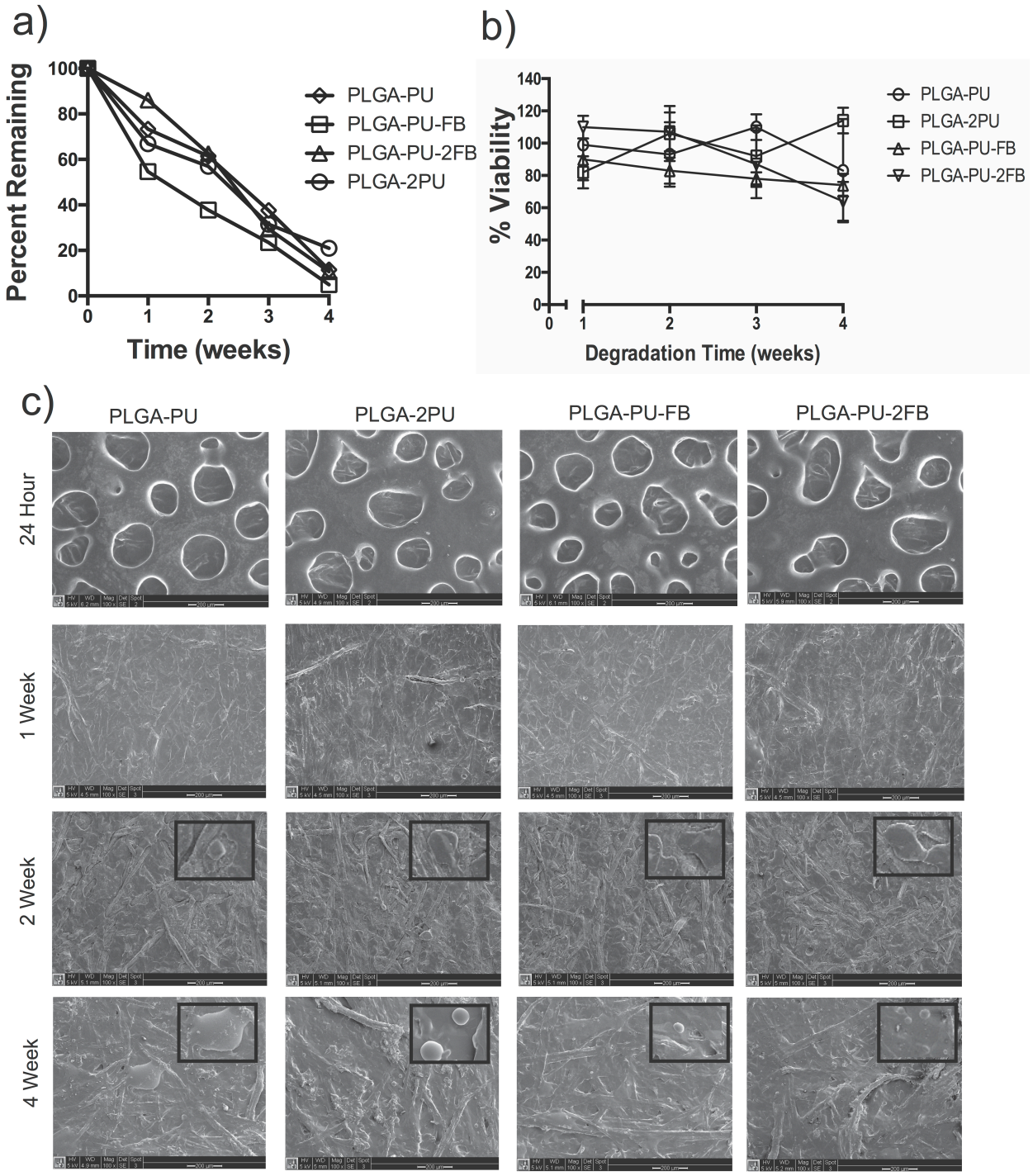

Figure 4.7: Degradation characteristics of PLGA-PUs over 4 weeks. a) Mass loss degradation profile, b) the cytotoxicity of corresponding biodegradation products in TZM-bl cells, and c) scanning electron micrographs of degrading electrospun PLGA-PU fibers in PBS at 37 °C (c). Scale bar = 200 μm. Inset shows a higher-resolution view of the formation of polymer droplets.

The cytocompatibility of PLGA-PUs was evaluated using viability as an indicator of metabolic activity and cellular adhesion and growth as indicators of cellular function. Polymer degradation products were cytocompatible with measured cellular viability of >80% for all time points. PLGA-PU, PLGA-PU-FB and PLGA-PU-2FB degradation products showed increased cytotoxicity over time. However, PLGA-2PU degradation products were cytocompatible over the entire four-week time course. All PLGA-PU fiber had similar cellular adhesion to TCPS (Figure 4.8a) and cell growth over five days (Figure 4.8b), indicating that these materials are cytocompatible. In order to visualize the cytocompatibility of PLGA-PU fibers, TZM-bl were stained with CellTracker™Red CMPTX dye and cultured on PLGA-PU fibers for four days. CMPTX-stained TZM-bl cells exhibit fluorescence in the tetramethylrhodamine (TRITC) channel (532 nm) (Figure 4.8c). Cells appeared to be attached to and surround the fibers after both 48 and 96 hours, further confirming the cytocompatible nature of PLGA-PUs. For imaging purposes, the PLGA-PU fibers used in this experiment were very thin, and as observed in the fiber degradation experiments, the fibers had begun to meld into films after 48 hours, and appear as polymer droplets.

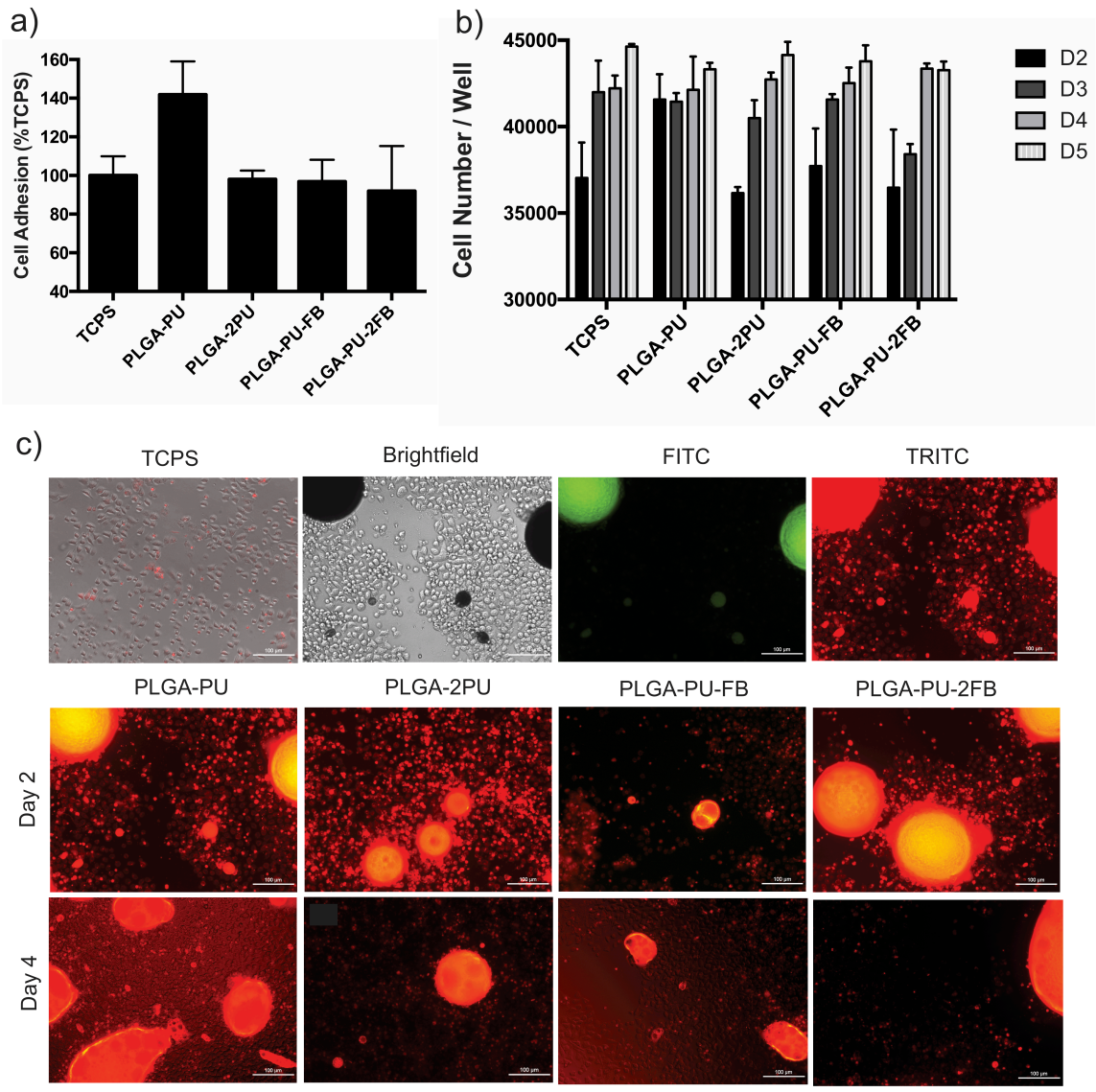

Figure 4.8: TZM-bl cell cytocompatibility with electrospun PLGA-PU fibers. a) Cellular adhesion after 24 hours, normalized to tissue culture polystyrene (TCPS), b) cell growth on TCPS and electrospun PLGA-PU fibers over the course of 2-5 days, fluorescence normalized to a standard curve of known number of cells, and c) CellTracker™ Red CMPTX stained TZM-bl cells on PLGA-PU fibers after 2 and 4 days of culture. TCPS= merge of FITC, TRITC and brightfield channels of cells on TCPS only, Brightfield= brightfield channel of cells of PLGA-PU fibers, FITC= FITC channel of cells on PLGA-PU fibers, and TRITC= TRITC channel of cells on PLGA-PU fibers. Day 2 and 4 images are a merge of the FITC and TRITC channels. PLGA-PU fibers exhibit auto-fluorescence in both the FITC and TRITC channels, while cells stained with CMPTX exhibit fluorescence in TRITC channel only. Scale bar = 100 µm.

4.5 DISCUSSION

PLGA-based polyurethanes exhibit biologically relevant degradation profiles, are non-cytotoxic, produce amorphous solid dispersions when electrospun into drug-loaded nanofibers, and can be tuned to sustain release of a variety of physicochemically diverse drugs. While all synthesized polymers had relatively low molecular weight ranging from 7-27 kDa, this did not preclude their ability to be electrospun into fibers. Repeated batches of the synthesized PLGA-PU polymers yielded similar molecular weights, indicating that it may not be possible to achieve higher molecular weights with these commercially sourced oligo-PLGA molecules that might not have the required functionality of 2.0 for achieving high polymer molecular weights (Figure 4.2, Supplementary Table 4.1). At room temperature, the polymers and electrospun meshes were soft and pliable, likely due to the relatively low molecular weight. In order to maintain the structural integrity of the fibers and remove any residual solvent, the fabrics were immediately lyophilized after electrospinning to preserve the fiber morphology. However, the materials were generally easy to handle and could feasibly be used as a topical dosage form for drug delivery.

NMR was used to measure bulk fluorine content and XPS measured the fluorine content in the outermost <10 nm of surface.[187] Although ^{19}F NMR indicated that the PLGA-PU-2FB bulk polymer had approximately two-fold higher fluorine content compared to PLGA-PU-FB, XPS was unable to detect fluorine at the surface of either of these polymers cast as thin films. XPS is highly sensitive to fluorine so it can be concluded that the fluorobenzene pendant group is present at < 0.1 atomic percent at the surface of the polymer when the polymer is cast as a thin film. The low surface energy of fluorine typically causes it to surface-localize in polymer thin films,[188-190] and we predicted that XPS would measure it at the stoichiometric atomic ratio or concentrated at the surface. In another study, phase separation forced lower surface energy soft segment to the surface, which decreased the XPS signal from fluorine-containing hard segment.[191] However, our XPS data of carbon enrichment and oxygen depletion suggests surface enrichment of the hard segment in which the fluorobenzene pendant group is attached. This

phenomenon could potentially alter the release of certain drugs that partition within the polymer matrix and preferentially localize within the hard segment. XPS analysis also revealed unexpected ratios of carbon and oxygen in the PLGA-PUs containing the lower hard to soft segment ratio (PLGA-PU, PLGA-PU-FB and PLGA-PU-2FB). The carbon to oxygen ratio for these polymers is much closer to that of butane and lysine, components of the hard segment, and further indicates enrichment of the hard segment at the surface of the polymer thin film. Hydrocarbon contamination, indicated by higher than expected carbon content and lower than expected nitrogen content,[192] was not apparent for any samples. On a bulk polymer level, there were no major differences in wettability and all polymers exhibited a mixed hydrophobic and hydrophilic nature.[193] This is consistent with XPS and polymer degradation results, as enrichment of fluorine on the film or fiber surface would likely cause an observable increase in hydrophobicity and slower degradation, however, the polymers did not exhibit differences in wettability nor degradation. In particular, our PLGA-based biodegradable PU all degraded more quickly than previously synthesized PCL-based polyurethanes[167, 194, 195] and showed <20% mass remaining after 4 weeks. Given the observed mass loss profiles (Figure 4.7a) and visually observed fiber degradation (Figure 4.7c), these polymers likely undergo bulk matrix degradation, as opposed to surface erosion, which is expected for PLGA-based polymers.[22, 196]

Despite the physicochemically diverse drugs having variable solubility within the polymer solution prior to electrospinning, all electrospun fibers were found to have undetectable drug crystallinity. This is likely due to the nature of the electrospinning process where solvent evaporation takes place rapidly and limits the amount of time for the formation of crystalline pockets of drug. Thus, the PLGA-PU drug-loaded electrospun fibers are considered amorphous solid dispersions, which allows for enhanced control over release properties via polymer engineering, as the release of drug from fibers does not depend on solubilizing crystalline drug.[197] The melt temperature of the polymer, as determined by DSC, can be used as an indicator of drug/polymer compatibility.[185] Unchanged or increased T_m of the polymer upon incorporation of the drug indicates good compatibility owing to the superior ordering of drug and polymer molecules within the solid matrix. Despite varying solubility, all drugs had good

compatibility with PLGA-PU and PLGA-2PU. However, only TFV had good compatibility with PLGA-PU-FB, while both NFL and TFV had good compatibility with PLGA-PU-2FB. This difference may be due to the higher number of hydrogen bonding groups on TFV and NFL compared to LNG and MVC, which may facilitate interaction with the added fluorobenzene pendant group.

The differences in bulk polymer properties and drug/polymer compatibility manifest themselves in varying levels of sustained release of the physicochemically diverse drugs into aqueous media. Increasing the hard to soft segment ratio had no effect on the release of LNG, which has no ionizable groups, suggesting the release is not controlled by charge-based interaction with the polymer. The release of both MVC and NFL was prolonged by increasing the hard to soft segment ratio, while the opposite is true for TFV. Increasing the hard to soft segment ratio caused TFV to essentially burst release over 48 hours. The enhancement of sustained release of MVC and NFL upon the augmentation of the hard segment may be due to the positive ionization state of MVC and NFL interacting with the more electronegative hard segment, while TFV has a negative charge when ionized, facilitating more rapid release.[198] Increasing the fluorobenzene pendant group content had a minimal effect on the sustained release of MVC and TFV, while it caused more rapid release of LNG and NFL. This could be because LNG and NFL have incompatible interactions with the pendant group, and when it is increased, the drugs may be forced to the surface, as we know the pendant is internalized within the bulk polymer matrix. The greater presence of drug at the surface may allow for more rapid diffusion and dissolution from the fibers. These release profiles may also be observed for similar small molecule drugs, depending on hydrogen bonding and degree of ionization, demonstrating the wide overall applicability of this promising new class of polymers, which degrade on a biologically relevant timescale, and can sustain release of a variety of small molecule drugs relevant to topical drug delivery applications.

4.6 CONCLUSIONS

A novel class of faster biodegrading polyurethanes with PLGA-moieties was synthesized with varying hard to soft segment ratios and fluorobenzene pendant group content. Though increasing the

fluorobenzene pendant group content increased the total fluorine content of the bulk polymer, the fluorine was not present at the surface. Resulting polymers had both hydrophilic and hydrophobic surface properties, were non-cytotoxic and biodegrade *in vitro* within one month. PLGA-PUs were successfully electrospun and loaded with LNG, MVC, NFL and TFV to produce amorphous solid dispersions. Increasing the hard to soft segment ratio augmented the sustained release of positively charged drugs (NFL, MVC), while increasing the fluorobenzene pendant group content caused the drugs repelled by the fluorobenzene pendant (LNG, NFL) to be released more quickly. Increasing the hard to soft segment ratio or fluorobenzene content of PLGA-PUs allows for modulation of drug release of both hydrophobic and hydrophilic drugs from electrospun fibers while maintaining a biologically relevant biodegradation rate.

Chapter 5. In vitro-ex vivo correlations between a cell-laden hydrogel and mucosal tissue for screening composite delivery systems

Adapted from: In vitro-ex vivo correlations between a cell-laden hydrogel and mucosal tissue for screening composite delivery systems. Anna K. Blakney, Adam B. Little, Yonghou Jiang, Kim A. Woodrow. Under Review (2016).

5.1 ABSTRACT

Composite delivery systems where drugs are electrospun in different layers and vary the drug stacking-order are posited to affect bioavailability. We evaluated how the formulation characteristics of both burst- and sustained-release electrospun fibers containing three physicochemically diverse drugs: dapivirine (DPV), maraviroc (MVC) and tenofovir (TFV) affect *in vitro* and *ex vivo* release. We developed a poly(hydroxyethyl methacrylate) (pHEMA) hydrogel release platform for the rapid, inexpensive in vitro evaluation of burst- and sustained-release topical or dermal drug delivery systems with varying microarchitecture. We investigated properties of the hydrogel that could recapitulate ex vivo release into nonhuman primate vaginal tissue. Using a DMSO extraction protocol and HPLC analysis, we achieved >93% recovery from the hydrogels and >88% recovery from tissue explants for all three drugs. We found that DPV loading, but not stacking order (layers of fiber containing a single drug) or microarchitecture (layers with isolated drug compared to all drugs in the same layer) impacted the burst release in vitro and ex vivo. Our burst-release formulations showed a correlation for DPV accumulation between the hydrogel and tissue (R^2=0.80), but the correlation was not significant for MVC or TFV. For the sustained release formulations, the PLGA/PCL content did not affect TFV release in vitro or ex vivo. Incorporation of cells into the hydrogel matrix improved the correlation between hydrogel and tissue explant release for TFV. We expect that this hydrogel tissue mimic maybe a promising preclinical model to evaluate topical or transdermal drug delivery systems with complex microarchitectures.

5.2 INTRODUCTION

Drug-eluting fibers fabricated by electrospinning are a versatile platform for encapsulation and delivery of physicochemically diverse drugs. The ability of this platform to fabricate complex microarchitectures [106, 125] as well as control of macroscopic geometry[199] is relevant to various prophylaxis and therapeutic applications. For example, Yuan et al. found that initial release of an anti-inflammatory agent coupled with sustained release of a chemotherapeutic from pH-responsive electrospun fibers resulted in higher life expectancy in a mouse model of hepatocellular carcinoma.[200] Drug combinations are often more challenging to formulate and deliver but necessary to some applications such as cancer treatment [201] and HIV prevention,[174] where the drugs are physicochemically different (e.g. solubility, pKa, etc.). While electrospun fibers allow fabrication of composites of diverse drugs with different release profiles, how drug-specific release kinetics observed *in vitro* are recapitulated *in vivo* for various routes of administration are more challenging to predict. In particular, dosage forms for transdermal or topical delivery where release is unidirectional and not isotropic may exhibit release profiles *in vitro* that are not recapitulated in tissues and cells. For example, Chen et al. observed much lower *in vivo* release of vancomycin, gentamicin and lidocaine compared to *in vitro* release profiles from poly(lactic-co-glycolic acid) (PLGA)/collagen sandwich-structured nanofibers for topical delivery of wound healing agents.[61]

Conventional methods for measuring drug release or dissolution fail to recapitulate the anisotropic release that is typical of specific *in vivo* administration routes. For example, parenteral and oral delivery routes are suited for vial- or SOTAX-based *in vitro* release experiments because release from the drug delivery system is isotropic. On the other hand, sophisticated and expensive *in vitro* release setups such as Franz cells are needed for evaluation of transdermal and topical dosage forms, which release anisotropically. While Franz cells account for the directionality of different drug delivery systems, they can be costly and the number of available devices limits the number of experiments. Explant tissue from either humans or non-human primates have been used to test safety and pharmacokinetics for a variety of dosages including vaginal delivery of microbicides,[202, 203] oral delivery

of nanoparticle chemopreventative drugs, [204] and chemoembolization of doxorubicin-eluting beads for treatment of hepatocellular carcinoma.[205] However, explant tissue is expensive, difficult to obtain, limited in quantity and precludes testing of drug delivery systems over long time periods due to inability to maintain the viability and integrity of tissue in culture.

Poly(2-hydroxyethyl methacrylate) (pHEMA) hydrogels have been widely used in drug delivery and tissue engineering, and are useful for their high water content, porosity, easy fabrication and formulation flexibility. Formulation parameters of pHEMA hydrogels have been well-defined, including altering cross-linking density to control drug diffusion,[206] incorporating specific monomers to enhance drug loading and release properties,[207] and varying cross-linker concentration to increase kinetic solubility of amorphous solid dispersions.[208] Due to the tunability of pHEMA hydrogels, as well as their high water content and inexpensive and rapid fabrication, we hypothesized that these biomaterials could be used as a three-dimensional non-sink testing medium for electrospun fibers with intricate microarchitecture that are designed for transdermal or topical drug delivery applications. A three-dimensional platform more realistically capitulates the *in vivo* environment, while evaluating drug delivery systems in non-sink conditions provides the best discriminating dissolution profiles between formulations.[209]

In this study, we evaluated how microarchitecture, stacking order and drug loading affect burst-release kinetics and how polymer composition affects sustained-release kinetics. We developed a pHEMA hydrogel *in vitro* release platform for rapid, high-throughput evaluation of electrospun fiber formulations and compared the release profiles between the *in vitro* hydrogel release and the corresponding *ex vivo* mucosal tissue explant release. Finally, we investigated the correlations between release into hydrogels and tissue, and whether incorporation of cells into the hydrogel matrix could improve the *in vivo-ex vivo* prediction of drug concentrations in tissue.

5.3 MATERIALS AND METHODS

5.3.1 *Burst- and sustained-release fiber preparation*

Polyvinyl alcohol (M_w=84-124 kDa, 87-89% hydrolysis) and polycaprolactone (M_n=80 kDA) purchased from Sigma-Aldrich (St. Louis, MO, USA). Poly (lactic-co-glycolic acid) (50:50 DL:PLG, acid terminated, 0.15-0.25 dL/g) was purchased from Lactel (Birmingham, AL, USA). Tenofovir (TFV) and dapivirine (DPV) were generous gifts from CONRAD (Arlington, VA, USA). Maraviroc was purchased from the UW pharmacy and purified in house.

PVA fibers ("burst release fibers") were electrospun using a 10% (w/v) solution of PVA in water on a NS 1WS500U (Elmarco, Inc.) free surface electrospinning instrument, using the following parameters: 160 mm wire electrode distance, -25 kV collecting electrode, 60 kV spinning electrode and 250 mm cartridge travel distance. Single-drug fibers, used for stacking experiments, were prepared using 20% (wt. drug/wt. polymer) of DPV, MVC or TFV, or 60% (wt. drug/wt. polymer) DPV. Equal loading combination fibers were prepared using 6.67% (wt. drug/wt. polymer) of DPV, MVC and TFV, for a total drug loading of 20% (wt. drug/wt. polymer). Higher DPV loaded fibers were prepared using 6.67% (wt. drug/wt. polymer) of MVC and TFV, and 20% (wt. drug/wt. polymer). The drug to polymer ratio was kept constant between the stacked and combined fibers.

PLGA/PCL fibers ("sustained release fibers") were electrospun, as previously described [210], using a 15% (w/v) solution of PLGA/PCL in HFIP using a needle electrospinning setup. PLGA:PCL content was varied to create four blends: 100:0, 80:20, 80:20 and 0:100, and TFV was added to each polymer solution at 15% (wt. drug/wt. polymer). The solutions were then extruded from a glass 5mL syringe with a 22-gauge stainless steel needle at 30-50 μL/min using a NE-1000 syringe pump (Farmingdale, NY, USA), exposed to a voltage of 11.2 kV, and collected on a grounded metal plate at a distance of 10 cm.

All fibers were stored in a vacuum desiccator until further analysis. For scanning electron microscopy (SEM) imaging, fibers were sputter coated for 90 seconds with Au/Pd and imaged at a magnification of

5000X using a Sirion scanning electron microscope at the University of Washington Nanotechnology User Facility.

5.3.2 *Hydrogel formulation and characterization*

Hydroxyethyl methacrylate (HEMA), ethylene glycol dimethacrylate (EGDMA) and benzoin isobutyl ether (BIE) were purchased from Sigma-Aldrich (St. Louis, MO, USA). The pre-polymer solution was prepared with 50% (v/v) deionized water, 49% (v/v) HEMA, 0.05% (v/v) EGDMA and 0.05% BIE. For cell-loaded hydrogels, HeLa cells (NIH AIDS Research Reagent Program, Division of AIDS, NIH, Bethesda, MD, USA) were suspended in PBS at a concentration of 1.514×10^5 cells/mL were used in the pre-polymer solution in the place of water. 500 µL of pre-polymer solution was added each well of a 48-well plate (11 mm in diameter), and placed under UV light for 10 minutes. After polymerization, hydrogels were gently removed from the plate, and placed in deionized water at 37°C. Water was exchanged 3X to rid the hydrogels of any impurities leftover from polymerization. Water content was measured by completely dehydrating hydrogels in a 110°C oven, measuring the dry weight, then allowing to equilibrate in water at 37°C, measuring the wet weight, and calculated using the following equation:

$$\%\ \text{Water} = 100 * \frac{\text{Wet weight} - \text{Dry weight}}{\text{Wet weight}}$$

5.3.3 *Hydrogel extraction validation*

Drugs were extracted from the hydrogels by incubating overnight on a rotational shaker at 37 °C. Samples were then vortexed well and filtered through a 0.22 µm PVDF filter (Millipore, Darmstadt, Germany) to remove any remaining debris. Drug concentration was analyzed in triplicate using a Shimadzu Prominence LC20AD UV-HPLC system, with a Phenomenex Luna C18 Column (5 µm, 250x4.6 mm) and LC Solutions software. The HPLC methods for DPV, MVC and TFV can be found in Supplementary Table 5.1.

Hydrogel extraction was validated by polymerizing known amounts of each drug into separate hydrogels, extracting, analyzing using HPLC and calculating % recovery using the following equation:

$$\% \, Recovery = 100 * \frac{Mass \, drug \, recovered}{Initial \, mass \, drug}$$

HPLC methods were validated using a standard curve of drug in DMSO, samples with known amounts of each drug spiked individually and in combination to ensure complete recovery and no peak overlap. Extracted samples were either analyzed within 24 hours or store at -20 °C until further analysis.

5.3.4 *In vitro hydrogel release*

Fibers were cut into circles with a diameter of 9.525 mm. Stacked fibers were prepared by cutting the single-drug fibers individually, orienting the samples in the correct stacking order, and firmly indenting the center of all three layers using forceps in order to keep the layers together. Stacked and combined fibers had approximately the same total mass (~6 mg) and thickness. At the initiation of a release study, prepared hydrogels were placed in a 48-well plate, 200 μL of PBS was added to the top, and then fiber discs were added to the well. Samples were kept in a 37 °C incubator until the appropriate timepoint. At each timepoint, the hydrogel was removed from the plate, any remaining fibers were scraped from the top of the hydrogel, and the hydrogel was immediately submerged in 4 mL of DMSO for extraction.

5.3.5 *Tissue extraction validation*

Drugs were extracted from tissue by adding 1 mL of DMSO to sample and incubating for 2 hours at 37° C to allow DMSO to permeate tissue. After incubation, samples were further homogenized using a Precellys tissue homogenizer (Bertin Technologies) at 5000 RPM for 2 X 20s cycles. Samples were then centrifuged at 5000 RPM for 7 minutes. Supernatant was removed and filtered using a 0.45 μm filter to remove any remaining debris. Samples were analyzed using identical HPLC methods as the hydrogel extraction. To validate the methods for the tissue extraction protocol, each batch included a sample of blank DMSO, blank DMSO and tissue eluate, standards prepared in DMSO and tissue eluate,

two spiked samples with known amount of drug, and a sample containing all three drugs to confirm that the peaks did not overlap. Retention times and wavelengths for detection were identical to the hydrogel methods for all drugs. Recovery for drugs spiked into untreated tissue samples can be found in Table 5.1.

5.3.6 *Ex vivo tissue explant release*

Whole reproductive tracts of pigtail macaques (*M. nemesetrina*) was purchased from the Washington National Primate Research Center (WaNPRC). Tissue from the vaginal tract only was cut into ~500 mg sections within 2 hours of euthanasia, and placed in a 48-well plate, lumen side up, with 200 μL of DMEM in the bottom of each well. Fiber samples were then placed on top of the tissues, and kept in a 37 °C incubator until the appropriate timepoint. At each timepoint, any remaining visible fibers were removed from the top of the tissue using forceps, and then each tissue was rinsed in 5 mL of sterile PBS to remove remaining fiber debris. Samples were stored at -80° C until further processing.

5.3.7 *Statistical analysis*

Release data is represented as the average ± standard deviation. For each hydrogel and tissue correlation, a linear regression was carried out between the hydrogel dose (μg drug/g hydrogel/mg fiber) and tissue dose (μg drug/g tissue/mg fiber). A significant correlation was defined as a non-zero slope with $p<0.01$. Statistical analyses were done in GraphPad Prism, version 6.0.

5.4 RESULTS

5.4.1 *Burst- and sustained-release fibers exhibit uniform fiber morphology and fiber mat properties*

We verified that all fiber formulations exhibited similar fiber density, thickness and fiber diameter since these properties can impact drug release profiles and confound comparisons. SEM showed that PVA fibers containing DPV, MVC and TFV have a round and smooth morphology with a

fiber diameter of ~200 nm (Figure 5.1). Sustained release fiber formulations of PLGA/PCL blends containing 15 wt.% TFV were also found to have a round and smooth morphology (Figure 5.2). For the sustained-release formulations, the average fiber diameter of PLGA-dominant fibers was ~1 μm while PCL-dominant fibers were ~1.6 μm in diameter. Fibers containing 60 wt.% DPV revealed some non-fiber regions (Figure 5.1b), and PCL-dominant fibers also appeared to exhibit a dimpled a morphology (Figure 5.2).

DPV, MVC and TFV are physicochemically diverse drugs, and were fabricated as a triple drug combination by either independently isolating them in their own layer or blending them together into a single layer. These two variations in formulation allowed us to test whether stacking order and microarchitecture (three drugs in three distinct layers or three drugs in one distinct layer) would impact release kinetics. Single-drug fibers were combined into a composite mat by pressing three layers together to maintain a mat thickness of ~0.5 mm, which resulted in an equivalent thickness to the fiber formulations containing all three drugs in one layer. Sustained-release fibers showed a consistent thickness of ~0.7 mm among different blends of PLGA/PCL. Fiber characteristics, including diameter, density and thickness were consistent within burst- and sustained-release fiber groups.

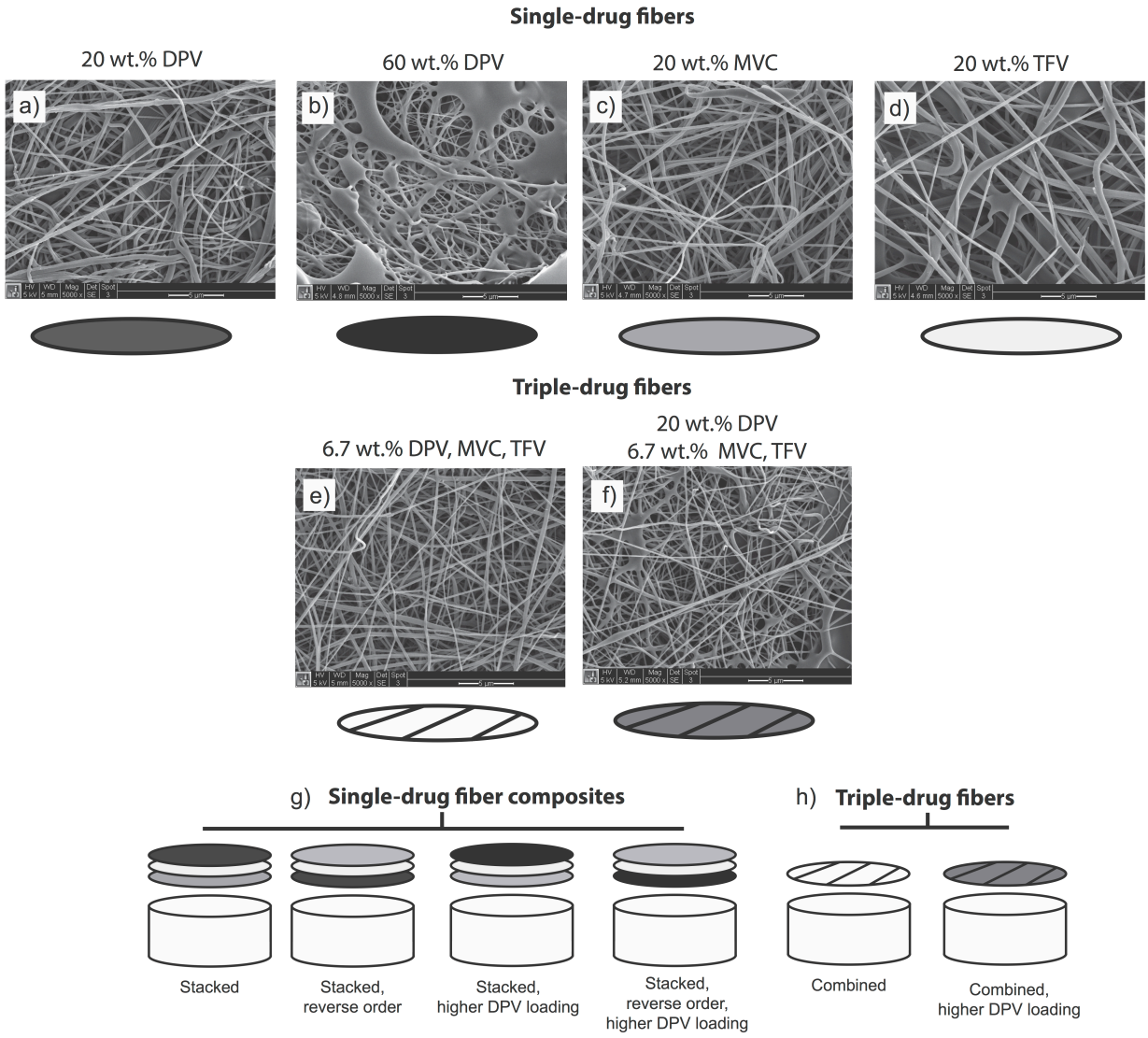

Figure 5.1: Scanning electron micrographs of electrospun PVA fibers containing either a single drug (DPV, MVC or TFV) (a-d) or the triple-drug combination (DPV + MVC + TFV) (e-f), and treatment arms of triple-drug combinations (g-h). Scale bars = 5 μm.

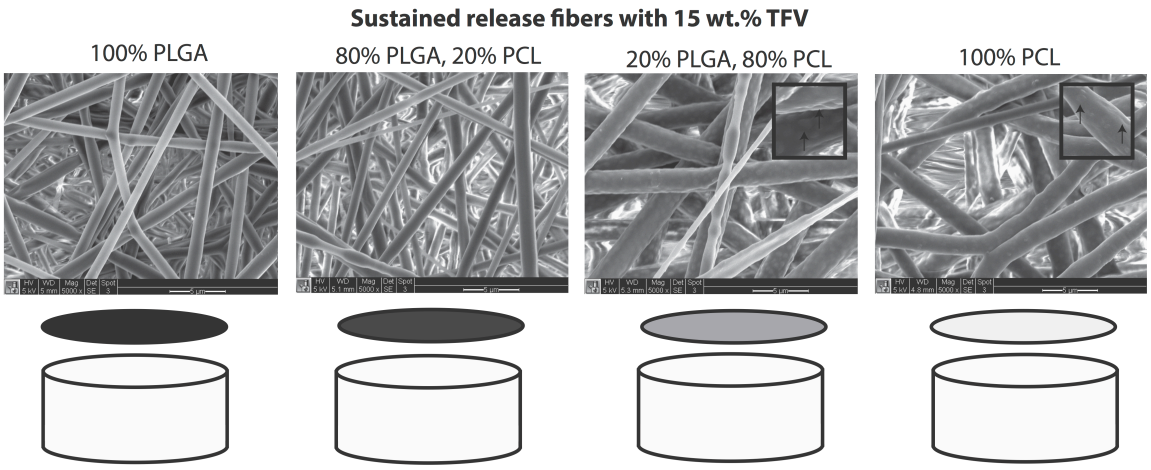

Figure 5.2: Scanning electron micrographs of electrospun sustained release fibers containing 15 wt.% TFV, and schematic of single-drug sustained release microarchitecture. Inset shows dimpled fibers in majority PCL samples. Scale bars = 5 μm.

5.4.2 *Validation of hydrogel and tissue extraction methods*

We validated a method for efficient extraction of DPV, MVC and TFV from both hydrogel and tissue explant samples to quantify drug concentrations and establish correlations between the *in vitro* and *ex vivo* release profiles. First, we identified conditions that maintained >95% of hydrogel water mass over the course of 72 hours as water evaporation over time could confound release kinetics between formulations groups. Hydrogels lost ~35% water mass due to convective evaporation when placed in a rotational shaker but not when kept in a static incubator with remaining wells filled with water as a source for humidity. Hydrogels and tissue explants were sized to fit exactly into a 48 well plate, with approximate dimensions of 11 mm in diameter and 5 mm in height, and a wet mass of ~500 mg. For our hydrogels, total drug recovery and extraction efficiency were evaluated using a known amount of each drug spiked directly into the hydrogel precursor solution (Table 5.1). The extraction protocol involved soaking pHEMA hydrogels or tissue in DMSO for 24 hours, and then analyzing an aliquot of the extraction media for drug content using HPLC. For the tissue explants, known amounts of drug were combined with tissue prior to homogenization to ensure that exposure to viable tissue and ceramic beads

did not absorb or degrade drugs (Table 5.1). The extraction procedure was considered valid and acceptable if the drug recovery fell within the range of 100% ± 15%. We measured a hydrogel extraction recovery of 93-108% and a tissue recovery between 88-100% for all three drugs. Finally, all three drugs were spiked into a neat sample of DMSO to test whether drug peaks were adequately separated on HPLC for individual detection (Table 5.1). Each drug showed a separation resolution of at least 0.5 minutes, including the sample spiked with all three drugs. The triple drug spike resulted in 96-101% recovery for all three drugs. Given these results, our DMSO extraction protocol and HPLC methods are suitable for extraction of DPV, MVC and TFV from both hydrogels and tissue.

Table 5.1: Validation of extraction of DPV, MVC and TFV from hydrogels and tissue explants alone and in the presence of the triple drug formulation.

Drug	% Recovery, Hydrogel Spike	% Recovery, Tissue Spike	% Recovery, Triple Drug Spike	Range of Quantification (μg/mL)	Limit of Detection (μg/mL)
DPV	92.9 ± 16.7	100.4 ± 6.1	99.8%	0.1-100	0.01
MVC	108.0 ± 9.75	98.6 ± 4.2	96.4%	5-500	0.5
TFV	100 ± 14.5	88.0 ± 3.3	101.0%	5-500	0.5

5.4.3 *DPV loading, but not stacking order or microarchitecture, enhances burst drug release in vitro and ex vivo*

We compared the effects of stacking order, microarchitecture and DPV drug loading in burst-release PVA fibers on drug release into both hydrogel and tissue. We found that, despite the widely varying physicochemical properties of these drugs, stacking order and microarchitecture (drugs in separate fiber layers versus the same fibers) do not affect DPV, MVC or TFV release into either hydrogel or tissue. For example, the stacked, reverse stacked and combined fibers released a similar amount of DPV in the hydrogel of ~50μg/g/mg (Figure 5.3a) and ~15 μg/g/mg for the parallel doses in tissue (Figure 5.3d). However, increasing DPV loading enhanced burst release of DPV, MVC and TFV

into hydrogels but only led to enhanced release of DPV into tissue. We found that increasing DPV loading resulted in ~3-fold higher release rate from the combined fibers after 2 hours into both hydrogel and tissue (Figure 5.3a,d). At 0.5 hours in both hydrogel and tissue, DPV also showed a trend of super-saturation as indicated by a sudden increase in drug concentration and subsequent decline. The combined fiber with higher DPV loading showed ~2-fold higher release of MVC after 2 hour in hydrogel but not tissue (Figure 5.3b,e). Combined fibers with higher DPV loading also had a 2-fold higher release of TFV after 2 hours in hydrogel, but not in tissue (Figure 5.3c,f). Overall, increasing the DPV loading in fibers increased the DPV release rate and total DPV dose delivered after 2 hours to both hydrogel and tissue.

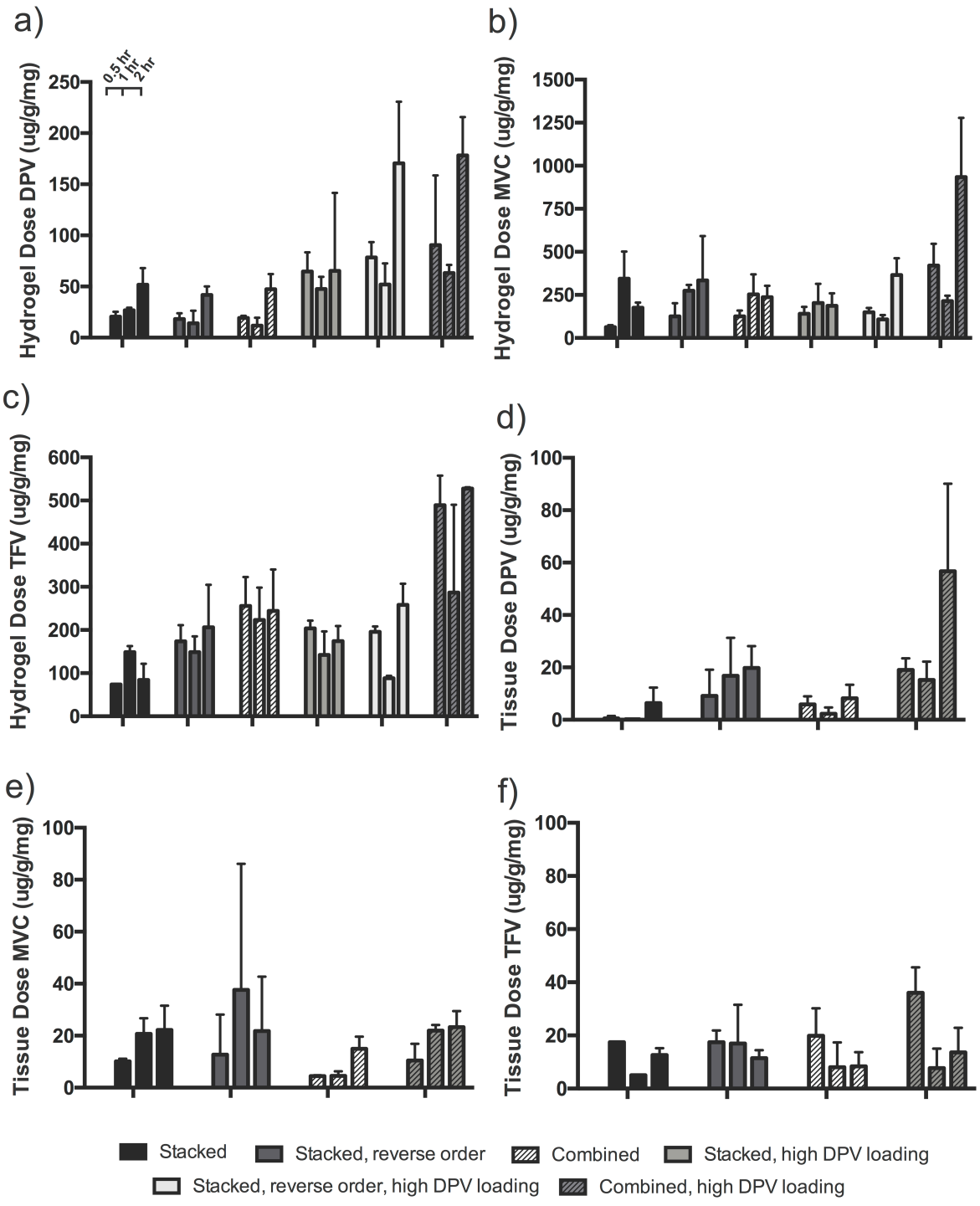

Figure 5.3. Release profiles of burst fiber formulations of DPV (a,d), MVC (b,e) and TFV (c,f) in hydrogels (a-c) and tissue explants (d-f). Each bar represents the mean of n=3 for hydrogel release and n=4 for tissue explant release, with error bars representing standard deviation.

We used linear regression to correlate the dose of drug delivered to the hydrogel and the dose delivered to tissue in order to evaluate whether the *in vitro* hydrogel system could be predictive of *ex vivo* dosing (Figure 5.4). We found that DPV had a statistically significant correlation ($p<0.0001$) and non-zero slope, while the correlations for MVC and TFV were not statistically significant ($p=0.33$ and 0.18, respectively). These results indicate that this pHEMA formulation may be useful for assessment of DPV burst release, but not MVC or TFV.

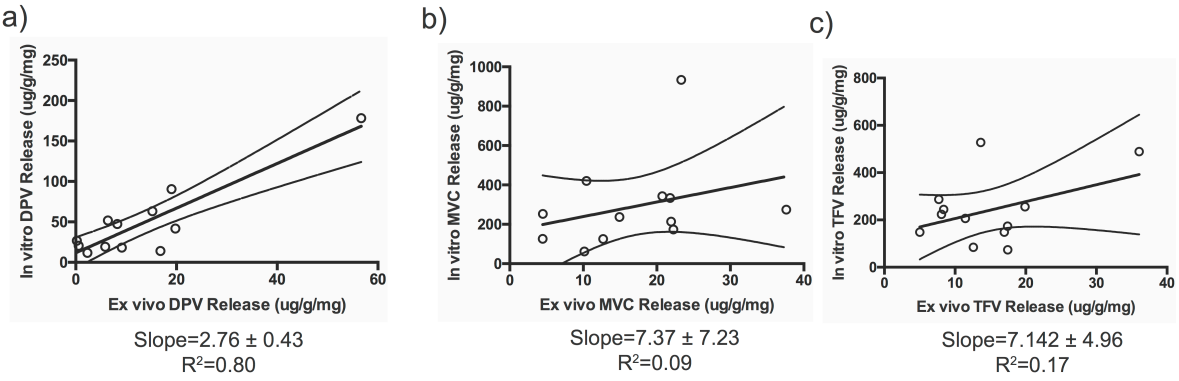

Figure 5.4: Correlation between hydrogel and tissue explant release profiles for burst release fiber formulations of a) DPV, b) MVC and c) TFV.

5.4.4 *PLGA/PCL content does not alter release rate of TFV in vitro or ex vivo but incorporating cells into hydrogel improves hydrogel/tissue release correlation*

In order to evaluate the hydrogels for informing release from sustained formulations and to compare to previously observed sink *in vitro* release profiles,[210] we assessed how the ratio of PLGA to PCL affects release of TFV into hydrogels and tissue. We observed a slight trend for PLGA-dominant fibers to enhance sustained release of TFV compared to PCL-dominant fibers (Figure 5.5). For example, ~0.5 μg/g/mg TFV was released into the hydrogel for the PLGA-only formulation after 72 hours compared to ~1.0 μg/g/mg for the PCL-only formulation (Figure 5.5a).

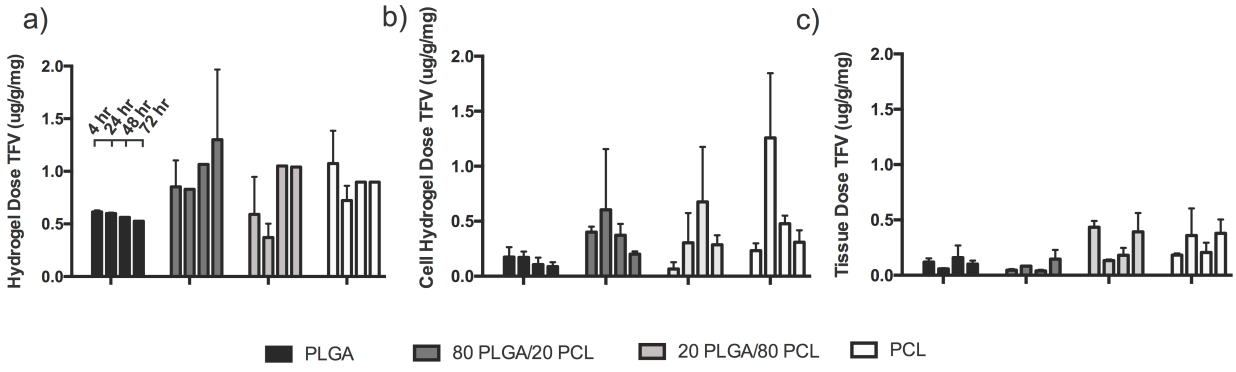

Figure 5.5: Release profiles of sustained release fiber formulations loaded with 15 wt.% TFV in a) hydrogel, b) hydrogels with encapsulated cells, and c) tissue explants. Each point represent n=3 for hydrogel samples and n=4 for tissue samples, with error bars representing standard deviation.

We hypothesized that encapsulating mammalian cervical epithelial cells into pHEMA hydrogels could improve the bulk composition of the hydrogel matrix to have more tissue-like properties and improve the correlation between drug release with tissue. We entrapped approximately 75,000 HeLa cells into each hydrogel and since these hydrogels undergo UV polymerization, it is unlikely that any of the cells remained viable post-polymerization. However, cell viability is unimportant for our purpose since our aim was only to impart physicochemical properties of cells into the bulk hydrogel matrix rather than recreating a metabolically active tissue-mimic. We measured TFV released into cell-laden hydrogels compared to release into hydrogels-only and tissue explants (Figure 5.5). After 72 hours, TFV release was ~1.0 μg into hydrogels, ~0.5 μg into cell-laden hydrogels, and ~0.4 μg into tissue explants. There were no significant differences between any of the sustained-release formulations in hydrogel-only, cell-laden hydrogel, or tissue. We next evaluated the correlation between released TFV content into the hydrogel compared to tissue, and also between cell-laden hydrogel and tissue (Figure 5.6). A slope of unity would predict the same dosage being released into both the hydrogel and tissue. Linear regression between drug content measured in hydrogel-only and tissue had a measured slope of 2.20 ± 0.53 (R^2=0.55), indicating that ~2.2 mg TFV are released into the hydrogel for every 1 mg released into tissue. In contrast, the drug content correlation between tissue and cell-laden hydrogel had a slope of

1.43 ± 0.33 (R^2 of 0.71), indicating that ~1.4 mg are released into cell-hydrogel for every 1 mg released into tissue. Thus, incorporation of cells improved fit and linearity of the correlation between hydrogel and tissue release of TFV.

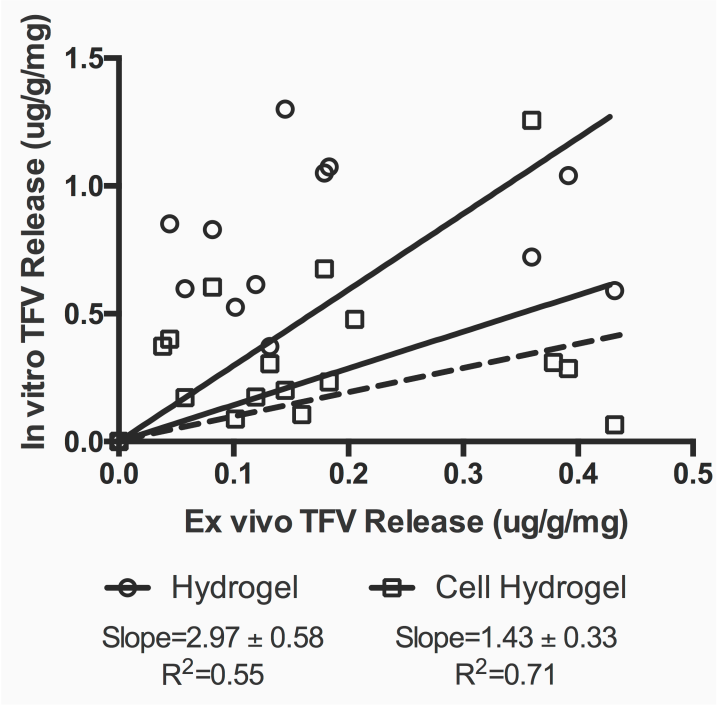

Figure 5.6: Correlation between hydrogel and tissue explant release profiles for burst release fiber formulations.

5.5 DISCUSSION

We investigated hydrogels as a non-sink release platform that could discern differences in release from fiber meshes with varying microarchitecture and drug loading. We found that pHEMA hydrogels could recapitulate *ex vivo* release of DPV from burst release formulations and release of TFV from sustained release formulations. However, the correlations between hydrogel and tissue release were not significant for burst-release formulations of MVC and TFV. In addition, incorporating cells into pHEMA hydrogels improved the correlation between TFV release in hydrogel and tissue.

For our burst release formulations, we found that there was a significant correlation between DPV release into hydrogel and tissue, which is likely due to the greater solubility of DPV in the hydrogel matrix compared to either MVC or TFV, which are more water-soluble. The large error observed for some of the fiber formulations is likely a result of inherent variation in the hydrogels, tissue, and extraction efficiency. We expect that minimizing variation in these experimental conditions could improve hydrogel-tissue correlations for MVC and TFV. One strategy to formulate the hydrogel to improve correlation for MVC and TFV release is to lower the cross-linking density, which has previously been shown to accelerate release kinetics of a water soluble drug (pilocarpine) out of the hydrogel matrix.[206] Alternatively, a more hydrophilic, longer cross-linking group, such as tetraethylene glycol diacrylate (TEGDA) or polyethylene glycol diacrylate (PEGDA) could be used to create a more porous, hydrophilic hydrogel that could also increase diffusion of hydrophilic drugs.[211] We expect that pHEMA hydrogels may also be used to evaluate DPV release from other solid dosage forms that are placed proximal to tissue and release profiles can be manipulated by the formulation, such as films or rings.[212, 213]

Overall, we observed that DPV and TFV show a trend towards a higher amount of released drug at the 0.5 hour timepoint compared to the 1 hour timepoint. A release profile wherein the drug amount peaks and then sharply declines is a hallmark of supersaturation,[148] and suggests that the drug reaches a critical saturation point and then crashes out of solution. The observed trends for DPV and TFV could be due to supersaturation of drugs in the hydrogel, which has previously been observed to occur from medium-soluble carrier films in non-sink conditions.[148] PVA is water-soluble but likely less soluble in pHEMA hydrogel and tissue, which would lead to a dissolution-controlled mechanism and then potential to supersaturate both the hydrogel and tissue with amorphously dispersed drugs. TFV and MVC were previously shown to create amorphous solid dispersions in electrospun fibers,[106, 214] and while we did not test the crystallinity of these drugs in our fibers, we expect that these drugs rapidly dissolve from PVA fibers into the hydrogel matrix. This outcome would results in initial super-saturation but eventually nucleation and crystallization, leading to a decrease in concentration at the 1 hour time point.[215]

Carson et al. previously observed that increasing PLGA content in PLGA/PCL blend fibers sustains TFV release *in vitro* under sink conditions.[210] We also observed that increasing PLGA content showed a trend for sustaining TFV release in both hydrogels and explant tissue, but the sustained release phase was more modest. It is possible that the hydrogel and explant release systems are not solely dissolution controlled as with sink conditions for *in vitro* release, and thus drug release profiles in the two conditions would be inherently different. Experimental error due to variation in hydrogel and tissue samples and extraction efficiency could also mask trends in sustained TFV release. With an *in vitro* hydrogel and *ex vivo* tissue release system, the fibers are not completely surrounded by fluid and there is only minimal fluid convection, so the release kinetics may be limited by wetting of the fibers and the dissolution of TFV. Thus, the previously observed release profiles of TFV from PLGA/PCL blends in sink conditions *in vitro* may be entirely different in non-sink conditions, as expected. In parallel, we had previously observed that fiber microarchitecture does impact hydrophilic drug release *in vitro*, which was not observed for the triple-drug combination fibers in these experiments.[106]

We incorporated HeLa cells into our pHEMA hydrogels to assess whether imparting a cellular makeup to the hydrogel matrix could improve the correlation between the hydrogel and tissue sustained TFV release kinetics. Although live cells have been incorporated into hydrogels,[216, 217] our aim was only to recapitulate the overall bulk material properties of tissue using a simple hydrogel system. In order to avoid defining and attempting to formulate the exact composition of tissue, such as the percentage proteins, lipids, sugars, etc., the cell itself presented the most obvious reagent. While a cell-laden hydrogel is similar to tissue on a bulk matrix level, one downfall is that this system cannot recapitulate metabolism since we did not attempt to maintain cell viabilty. Thus, hydrogels and cell-laden hydrogels differ strictly in the composition of the bulk hydrogel matrix, and it is likely that TFV solubility in the cell-laden hydrogel more closely matches the solubility of TFV in the tissue matrix. It is possible that by further increasing the number of cells in each hydrogel, the correlation between the dosage of drug into the hydrogel and tissue could be improved. Given the broad formulation potential of pHEMA hydrogels,

we expect that this *in vitro* release platform could be extended to other topical routes such as oral, nasal or dermal delivery.

5.6 CONCLUSION

We evaluated how electrospun fiber formulation affects the *in vitro* and *ex vivo* release profiles for three physicochemically diverse drugs. A novel cell-laden hydrogel platform was developed for the rapid, inexpensive *in vitro* evaluation of burst- and sustained-release electrospun fiber formulations of varying microarchitecture. The hydrogel tissue mimic was used to establish *in vitro-ex vivo* correlations with release into vaginal mucosal tissue explants. To establish the correlations, we first validated the extraction and analysis using HPLC from both the hydrogel and tissue for DPV, MVC and TFV. We show that the stacking order and microarchitecture did not affect burst release kinetics, whereas increasing DPV loading enhanced release of all three drugs from the composites. For our rapid-release PVA formulations, drug release into the hydrogel correlated to release into tissue for DPV but not MVC or TFV. For our sustained-release polyester formulations, the ratio of PLGA to PCL did not affect the sustained release of TFV in either the hydrogel or tissue. Incorporating a model cell type into the hydrogel improved the correlation between the *in vitro* and *ex vivo* release of sustained TFV formulations. Overall, the versatility of the pHEMA hydrogel system may offer a new approach for rapid evaluation and optimization of topical and transdermal drug delivery dosages *in vitro* to predict *in vivo* performance.

Chapter 6. Simultaneous Measurement of Etravirine, Maraviroc and Raltegravir in Pigtail Macaque Plasma, Vaginal Secretions and Vaginal Tissue using a LC-MS/MS Assay

Adapted from: Simultaneous measurement of etravirine, maraviroc and raltegravir in pigtail macaque plasma, vaginal secretions and vaginal tissue using a LC-MS/MS assay. Anna K. Blakney, Yonghou Jiang, Dale Whittington, Kim A. Woodrow. Journal of Chromatography B 1025: 110-118 (2016).

6.1 ABSTRACT

Etravirine (ETR), maraviroc (MVC) and raltegravir (RAL) are promising antiretroviral drugs being used in HIV treatment and may be interesting for prevention applications such as oral or topical pre-exposure prophylaxis. Here we describe a sensitive and accurate method for the simultaneous detection of ETR, MVC and RAL from pigtail macaque plasma, vaginal secretions, and vaginal tissue. This method is characterized by a straightforward precipitation extraction method, a limit of quantification <0.5 ng mL^{-1} for all three antiretrovirals bolstered by a corresponding internal standard for each drug analyte, and short run time. Quantification is performed using positive ion electrospray triple quadrupole mass spectrometry. This method was validated over clinically relevant ranges for the three ARV drugs in all three matrices: 0.1-100 ng mL^{-1} for ETR, 0.05-100 ng mL^{-1} for MVC and 1-100 ng mL^{-1} for RAL. Our method is accurate and precise, with measured mean inter-assay precision (%CV) and accuracy (% bias) of 5.08% and 1.96%, respectively, while the mean intra-assay precision and accuracy were 3.44% and 1.08 %. The overall post-extraction recovery for ETR, MVC and RAL was >94% in all cases. We also show that extracted biological samples are stable after storage at room temperature or 4 °C and after three freeze/thaw cycles. This is the first analytical method capable of quantifying ETR, MVC and RAL in biological matrices relevant for pre-clinical testing of oral or topical HIV prevention methods in pigtailed macaques.

6.2 INTRODUCTION

Disparate rates of HIV acquisition between men and women have motivated development of oral and topical prevention methods intended as discreet, woman-initiated dosage forms. Poor performance of the 1% tenofovir gel in recent clinical trials has spurred the inclusion of new, more potent antiretrovirals into microbicides.[218] Furthermore, much like formulations for treatment of HIV, cocktails of multiple antiretrovirals with varied mechanisms of action may prove to have synergistic capacity and lower required drug dosage, with a lower risk for development of resistant HIV strains.[219] The majority of HIV prevention dosage forms in development, including pills,[218] gels,[175] rings,[213] films[220] and fibers,[166] aim to prevent acquisition of HIV in the genital tract.[221] HIV prevention formulations are typically tested first in non-human primate models for safety and efficacy, motivating development of quick, highly sensitive bioanalytical methods for the detection of antiretroviral cocktails in affected tissues, including vaginal tissue and secretions, as well as plasma.

Etravirine (TMC125, Intelence®) is non-nucleoside reverse transcriptase inhibitor (NNRTI) that is highly active against both wild-type and NNRTI-resistant HIV strains,[222] has a higher genetic barrier to the development of resistance than currently available NNRTIs,[223] and has been shown to be safe, tolerable and effective in the treatment-experienced patients.[224] Maraviroc (UK-427,857, Celsentri®, Selzentry®) is a selective CCR-5 antagonist with potent anti-HIV activity,[225] that has been investigated for microbicide use alone in gel form[226] and in combination with dapivirine as a vaginal ring.[174] Raltegravir (MK-0518, Isentress®) is a novel HIV-1 integrase inhibitor that prevent proviral DNA-strand transfer,[227] which has been shown to protect macaques from SHIV challenge when applied post-exposure in a topical gel.[228]

To date, several methods have been published for the quantification of ETR, MVC and/or RAL in a variety of tissue matrices. Fayet et al. validated a LC-MS/MS assay for ETR, MVC and RAL, in addition to darunavir, in human plasma.[229] Other LC-MS/MS assays have been published for quantification of each drug alone, including ETR in human plasma and peripheral blood mononuclear

cells and rat plasma,[230, 231] MVC in human plasma, urine and cerebrospinal fluid,[232] and RAL in human plasma and peripheral blood mononuclear cells.[233, 234] The combination of ETR, MVC and RAL has also been quantified using LC-MS/MS in human plasma in addition to a combination of eight other relevant antiretroviral drugs.[235] Currently, no LC-MS/MS assay has been validated to quantify ETR, MVC and RAL combinations in vaginal tissue and secretions, or plasma.

Here we present a validated analytical method for the simultaneous quantification of etravirine, maraviroc and raltegravir in pigtail macaque vaginal tissue, vaginal secretions and plasma using liquid chromatography coupled with tandem triple quadrupole mass spectrometry detection. A single step extraction is performed using acetonitrile precipitation of plasma, vaginal secretions and homogenized vaginal tissue, after the addition of ETR-$^{13}C_6$, MVC-d_6 and RAL-d_6 as internal standards. The mixture is vortexed vigorously, centrifuged for 10 minutes at 10,000 RPM and filtered before a 2 µL injection into an EMD Chromolith® Performance RP-18e 100-3mm analytical column. Analytes are separated using a gradient method of water with 10 mM formic acid and 1:1 acetonitrile:methanol with 10mM formic acid. Our method enables the simultaneous quantification of these three antiretroviral drugs for pharmacokinetic and pharmacodynamic preclinical studies in pigtail macaque studies.

6.3 MATERIALS & METHODS

6.3.1 *Reagents and tissues*

Etravirine (ETR) and maraviroc (MVC) drug standards were obtained from the NIH AIDS Reagent Program (Division of AIDS, NIAID, NIH, Bethesda, MD, USA). Raltegravir (RAL) drug standard and maraviroc-d_6 (MVC-d_6), raltegravir-d_6 (RAL-d_6), and etravirine-$^{13}C_6$ (ETR-$^{13}C_6$) internal standards were purchased from Alsachim, Inc. (Illkirch-Graffenstaden, France). Acetonitrile (ACN), methanol (MeOH) and formic acid, all Optima-LC/MS grade, were purchased from Thermo Fisher Scientific (Waltham, MA, USA). Ultrapure water was obtained using a Milli-Q UF-Plus apparatus

(Millipore, Burlington, MA, USA). Naïve pigtail macaque (macaca nemestrina) plasma, vaginal secretions and vaginal tissue were purchased from the Washington National Primate Research Center (WaNPRC) Tissue Distribution Program (Seattle, WA, USA).

6.3.2 *Instrumentation and equipment*

The liquid chromatography system was composed of an I-Class Acquity UPLC (Waters Corporation, Milford, MA, USA) with a direct infusion syringe pump and temperature-controlled 96 vial autosampler maintained at 4 °C. Samples were separated on a Chromolith Performance RP-18e 100-3mm analytical column (Merck, Darmstadt, Germany) at ambient conditions. The chromatographic system was coupled to a Waters Xevo TQ-S tandem quadrupole mass spectrometer (Waters Corporation, Milford, MA, USA) with a Micromass Zspray™ Atmospheric Pressure Ioniation (API) Source. The LC-MS/MS system and data analysis was carried out using MassLynx® software (version 4.1) (Waters Corporation, Milford, MA, USA).

Processing of plasma, secretions and tissue was performed using a Precellys® 24 tissue homogenizer (Bertin Corporation, Rockville, MD, USA) (tissue only) and a Sorvall Legend 14 centrifuge (Thermo Scientific, Waltham, MA, USA).

6.3.3 *Calibration standard, internal standard and quality control (QCs) solutions*

Stock solutions of ETR, MVC and RAL (Figure 6.1) were prepared at a concentration of 1 mg mL^{-1} in DMSO, and then were combined and diluted with ACN to make working solutions at concentrations of 10,000 ng mL^{-1}, 200 ng mL^{-1} and 2 ng mL^{-1} (Table 6.1). Calibration standards were then diluted with appropriate amounts of ACN (neat standards), or plasma, vaginal secretions, or tissue to achieve a working calibration range from 0.01-100 ng mL^{-1}. Internal standards (ETR-$^{13}C_6$, MVC-d_6, RAL-d_6) were likewise diluted as stock solutions in DMSO at 1 mg mL-1. A working solution of all three internal standards was prepared at a concentration of 10 ng mL^{-1} in ACN. Internal standards were added to all samples at a ratio of 1:10 (vol:vol) resulting in a final internal standard concentration of 1 ng

mL^{-1}. Three separate quality control stock and working solutions were weighed and prepared separately from the calibration standards. QCs were prepared at concentrations of 0.5 ng mL^{-1} (low), 5 ng mL^{-1} (medium) and 50 ng mL^{-1} (high). All solutions were prepared according to recommendations on bioanalytical method validation stating that the total added volume must be ≤10% of the biological sample[236]. Samples were prepared fresh for intraday experiments, and then aliquoted and stored at -80°C until analysis.

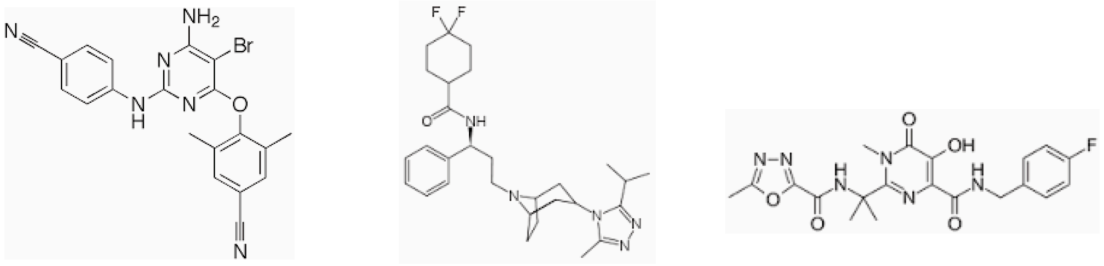

Figure 6.1: Chemical structures of antiretroviral drugs.

Table 6.1: Concentrations of stock solutions, working solutions and QC controls.

Solution	Stock Solution Solvent	Stock Solution Concentration	Working Solution Concentration*	Calibration Range	QC Controls
Drug (ETR, MVC, RAL)	DMSO	1 mg mL^{-1}	10,000; 200; 2 ng mL^{-1}	0.01-100 ng mL^{-1}	0.5; 5; 50 ng mL^{-1}
Internal Standard (ETR-$^{13}C_6$, MVC-d_6, RAL-d_6)	DMSO	1 mg mL^{-1}	10,000 ng mL^{-1}; 10 ng mL^{-1}	N/A	N/A

*Obtained by dilution of stock solution with ACN

6.3.4 *LC-MS/MS conditions*

Mobile phase A was composed of 10 mM formic acid in ultrapure water and mobile phase B was composed of 10mM formic acid in 50:50 ACN:MeOH. Solvents were prepared before each set of analysis. The mobile phase gradient was delivered over 8.5 minutes and consisted of 98% A: 2% B for 1

minute, ramping to 100% B by 6 minutes, holding for one minute, and then transitioning back to 98% A: 2% B over 1.5 minutes. The flow rate was 0.5 mL min^{-1} with an injection volume of 2 µL.

The mass spectrometer was operated in positive ion mode. The selected *m/z* transitions and typical retention time for each analyte are reported in Table 6.2. The ionization parameters were as follows: capillary voltage of 3 kV, source temperature of 150°C, cone gas flow of 150 L hr^{-1}, desolvation gas flow of 1000 L hr^{-1} and collision gas flow of 0.15 mL min^{-1}. The spectrometer was engaged during minutes 2-7 of each run. All species were analyzed at a cone voltage of 50 kV and a collision energy of 28 V (ETR, MVC, ETR-$^{13}C_6$, MVC-d6) or 40 V (RAL, RAL-d_6).

Table 6.2: Instrument method for the LC-MS/MS analysis for ETR, MVC and RAL with ETR-$^{13}C_6$, MVC-d_6, and RAL-d_6 as internal controls.

Drug/Internal Standard	Precursor Ion (m/z)	Fragment Ion (m/z)	Dwell Time (s)	Cone Voltage (kV)	Collision Energy (V)	Retention Time (minutes)
ETR	435.22	162.98	0.079	50	28.0	6.74
ETR-$^{13}C_6$	441.20	162.98	0.079	50	28.0	6.74
MVC	514.48	280.22	0.079	50	28.0	4.33
MVC-d_6	520.48	280.22	0.079	50	28.0	4.33
RAL	445.35	109.10	0.079	50	30.0	5.56
RAL-d_6	451.35	115.10	0.079	50	30.0	5.56

6.3.5 *Sample preparation*

6.3.5.1 Plasma

Plasma samples were precipitated with cold ACN (with or without analytes depending on the sample), vortexed thoroughly, centrifuged for 10 minutes at 10,000 RPM, filtered using a 0.22 µm PVDF syringe filter (Millipore, Burlington, MA, USA) and added to a 200 µL HPLC vial.

6.3.5.2 Vaginal secretions

Secretion samples were collected with a Merocel ophthalmic sponge (Medtronix, Jacksonville, FL, USA), diluted with 300 µL of phosphate buffered saline (PBS) to thin the mucus, and then incubated

for 1 hour at 4°C. Sponge and extraction buffer were then transferred to Spin-X centrifuge tubes with 0.22 µm cellulose acetate filters (Corning Inc., Corning, NY, USA). Secretion eluate was then precipitated with cold ACN (with or without analytes depending on the sample), vortexed thoroughly, centrifuged for 10 minutes at 10,000 RPM, filtered using a 0.22 µm PVDF syringe filter (Millipore, Burlington, MA, USA) and added to a 200 µL HPLC vial.

6.3.5.3 Vaginal tissue

Tissue biopsies were collected with a 5 mm biopsy punch and added to an eppendorf tube with 640 mg of 1.4 mm and six 2.8 mm zirconium oxide ceramic beads (Precellys, Bertin Corporation, Rockville, MD, USA). The samples were homogenized on the Precellys at 6,500 RPM for three cycles of 20 seconds. Homogenized samples were then centrifuged for 10 minutes at 10,000 RPM, and filtered using a 0.22 µm PVDF syringe filter (Millipore, Burlington, MA, USA) and added to a 200 µL HPLC vial.

6.3.6 *Quantification*

Quantitative analysis of the three antiretroviral drugs was performed using the internal standard method, relative to deuterated internal standard (e.g. ETR and ETR-$^{13}C_6$). Each level of the calibration curve was analyzed in triplicate at the beginning of the run, and one high and low standard was analyzed at the end of each run. An eight-point calibration curve was calculated and fit using linear regression of peak area ratios (drug peak area/internal standard peak area) versus concentration. The calibration was established over the range of 0.1-100 ng mL^{-1} for ETR, 0.05-100 ng mL^{-1} for MVC and 0.5 ng mL^{-1} for RAL in all tissue matrices so as to cover the clinically relevant expected concentrations for microbicide application. Separate calibration curves were made for the bottom four and top four points of each curve. Chromatographic data acquisition, peak integration and quantification were performed in MassLynx® software (version 4.1) (Waters Corporation, Milford, MA, USA).

6.3.7 *Accuracy and precision*

The method validation procedure was based on recommendations published from the Conference on Analytical Methods Validation.[236] Replicate analysis (n=3) of QC samples at the low, medium and high concentrations were used for the intra-assay precision and accuracy determination in pigtail macaque plasma, vaginal secretions and vaginal tissue. Inter-assay accuracy and precision were determined by repeated analysis performed on three different occasions (Table 6.3). The concentration in each sample was determined using calibration standards prepared on the same day. The precision was calculated as the coefficient of variation (%CV) within a single run (intra-assay) and between three different assays (inter-assay), and the accuracy as the percentage of deviation between nominal and measured concentrations. The analytical series were considered valid and accepted only if the precision %CV between nominal and back-calculated concentrations of each calibration level and QC were less than ±15%, and less than ±20% at the lowest QC level.

Table 6.3: Precision and accuracy of the assay for the three antiretroviral drugs in pigtail macaque plasma, vaginal secretions and vaginal tissue at low, medium and high concentrations.

Drug/Matrix		Nominal Concentration (ng mL^{-1})	Inter-assay (n=3)				Intra-assay (n=3)			
			Conc. Found (ng mL^{-1})	±SD	Precision %CV	Accuracy Bias %	Conc. Found (ng mL-1)	±SD	Precision %CV	Accuracy Bias %
Plasma	ETR	0.5	0.52	0.03	5.80	3.93	0.55	0.05	9.88	10.89
		5	4.93	0.12	2.36	-1.42	4.91	0.18	3.63	-1.80
		50	49.94	2.02	4.11	-0.12	47.58	1.26	2.66	-4.84
	MVC	0.5	0.51	0.01	1.66	1.07	0.50	0.02	3.17	-0.68
		5	5.29	0.15	2.81	5.73	5.18	0.14	2.73	3.52
		50	52.95	1.24	2.34	5.90	51.79	0.58	1.12	3.58
	RAL	0.5	0.50	0.09	17.54	0.47	0.44	0.02	4.42	-12.90
		5	5.39	0.07	1.36	7.77	5.46	0.20	3.65	9.28
		50	55.29	0.95	1.73	10.59	56.15	0.81	1.45	12.29
Vaginal Secretions	ETR	0.5	0.52	0.04	6.79	4.30	0.56	0.05	9.67	11.22
		5	5.11	0.05	1.03	2.10	5.07	0.33	6.50	1.38
		50	51.39	1.96	3.82	2.78	49.70	0.26	0.52	-0.60
	MVC	0.5	0.43	0.02	5.49	-13.47	0.43	0.00	0.68	-13.37
		5	4.60	0.41	8.99	-8.09	5.00	0.07	1.35	0.08
		50	42.57	2.52	5.92	-14.87	40.46	0.62	1.53	-19.08
	RAL	0.5	0.53	0.12	21.61	6.90	0.47	0.01	2.66	-6.62
		5	5.74	0.24	4.15	14.72	5.78	0.20	3.46	15.53
		50	58.34	3.49	5.99	16.68	58.36	2.46	4.21	16.72
Vaginal Tissue	ETR	0.5	0.51	0.00	0.69	2.60	0.51	0.02	3.80	1.82
		5	4.92	0.08	1.61	-1.56	4.89	0.19	3.98	-2.13
		50	48.90	1.94	3.98	-2.21	47.44	0.69	1.46	-5.11
	MVC	0.5	0.56	0.02	3.23	11.81	0.56	0.05	9.03	12.52
		5	5.08	0.17	3.42	1.65	4.90	0.08	1.64	-1.98
		50	50.33	0.87	1.73	0.66	49.56	0.50	1.01	-0.88
	RAL	0.5	0.50	0.08	16.18	0.60	0.52	0.03	4.83	3.65
		5	4.70	0.04	0.76	-5.92	4.72	0.06	1.31	-5.54
		50	50.21	1.06	2.12	0.42	51.13	1.33	2.59	2.27

6.3.8 *Limit of quantification and limit of detection*

The limit of quantification (LOQ) for each drug analyzed was defined as the lowest calibration standard for which the standard curve returned accurate and precise results within the given limits. The limit of detection (LOD) was defined as the lowest calibration level for which a drug peak above the noise level was visible on the chromatogram, with a signal to noise of 3:1. LOQ and LOD for each drug can be found in Table 6.4.

Table 6.4: Limit of detection and limit of quantification of antiretroviral drugs.

	LOD ($ng\ mL^{-1}$)	**LOQ**		**Accuracy at LOQ** (bias %)	**Precision at LOQ** (%CV)
		($ng\ mL^{-1}$)	(pg)		
Etravirine (ETR)	0.01	0.1	0.2	-1.22	18.28
Maraviroc (MVC)	0.01	0.05	0.1	-7.99	10.36
Raltegravir (RAL)	0.05	0.5	1	-4.62	5.33

6.3.9 *Stability of antiretroviral drugs in plasma, vaginal secretions and vaginal tissue*

Stability studies of ETR, MVC and RAL were performed to determine sample storage procedures should samples be prepared but the instrument unusable due to unforeseen circumstances. The stability studies were carried out as follows:

a) Stability of samples at room temperature and 4°C: separate QC samples at low, medium and high concentrations of antiretrovirals in plasma, secretions and tissue were kept at room temperature or 4°C for 48 hours. Samples were analyzed immediately after preparation and after 48 hours at respective conditions, and antiretroviral drug concentrations were expressed as % deviation from the initial concentration.

b) Stability of samples after three freeze/thaw cycles: QC samples at low, medium and high concentrations of antiretrovirals in plasma, secretions and tissue frozen at -80°C and then allowed to thaw at room temperature three times. Samples were analyzed immediately after preparation and after three freeze/thaw cycles, and antiretroviral drug concentrations were expressed as % deviation from the initial concentration.

6.3.10 *Matrix effect and recovery*

In the initial method validation steps, the matrix effect on chromatography for plasma, vaginal secretions and vaginal tissue was examined by observing whether blank matrix samples had any visible peaks at the expected retention times for each analyte, and whether matrix eluates spiked with analytes caused any shift or perturbation of the retention time for each analyte. Subsequently, the matrix effect for each analyte in each matrix was assessed. Three series of QC samples at low, medium and high concentrations in triplicate were prepared as follows:

a) Neat standards of antiretroviral drugs subjected to the same extraction process, sans matrix;
b) Plasma, vaginal secretion and vaginal tissue samples spiked with antiretroviral drugs and internal standards **after** extraction;
c) Plasma, vaginal secretion and vaginal tissue samples spiked with antiretroviral drugs and internal standards **before** precipitation.

The recovery and ion suppression/enhancement of the MS/MS signal of drugs and internal standards in the presence of plasma, vaginal secretion and tissue matrices (i.e. the matrix effect) was assessed by comparing the absolute peak areas of analytes either solubilized in extraction buffer (A), or added after (B) or before (C) the extraction process, based on the recommendations by Matuszewski et al.[237, 238] Mean peak area ratios (B_2, C_2) were calculated as the ratio of drug to appropriate internal standard (e.g. ETR to ETR-$^{13}C_6$) within the same sample. The matrix effect (ME) is expressed as the ratio of peak areas of the analytes added to blank matrix after extraction to the neat standard (B/A), expressed as a percentage. The extraction yield (EY) is expressed as the ratio of peak areas of blank matrix samples

spiked before and after extraction (C/B), expressed as a percentage. The overall recovery (OR) was expressed as the ratio of mean peak area ratios for each antiretroviral for samples spiked before extraction to those spiked after extraction (C_2/B_2). The process efficiency (PE) is expressed as the ratio of the peak area of analytes spiked before extraction to the peak area of analytes spiked into neat extraction buffer (C/A).

6.4 Results and Discussion

6.4.1 *Chromatograms*

We present a single method for simultaneous detection of ETR, MVC, RAL by liquid chromatography coupled with tandem mass spectrometry. Typical chromatographs of ETR, MVC and RAL at the lowest calibration level (Figure 6.2, a-c) and highest calibration level (Figure 6.2, d-f) of the neat standards reveal that peak retention time and shape are consistent across the calibration range. Typical retention times for each analyte can be found in Table 6.2. The internal standards were spiked at a single concentration for all samples (1 ng mL^{-1}) and resulting chromatograms can be found in Figure 6.2 (g-i). The chromatograms for the internal standards (ETR-$^{13}C_6$, MVC-d_6 and RAL-d_6) (Figure 6.2, g-i) reveal identical retention to the corresponding analyte (ETR, MVC and RAL). The separation occurs between 4-7 minutes of the 8.5-minute run, and is satisfactory for obtaining sufficient peak resolution for all analytes.

Figure 6.3 shows chromatograms for ETR, MVC and RAL at the medium level QC concentration (5 ng mL^{-1}) in each of the tested matrices (plasma, vaginal secretions and vaginal tissue). None of the matrices caused a shift in retention time or peak shape for any of the drug analytes, or internal standards (not shown). Changes in peak intensity due to the presence of matrix (matrix effects) are discussed in section 6.3.5.

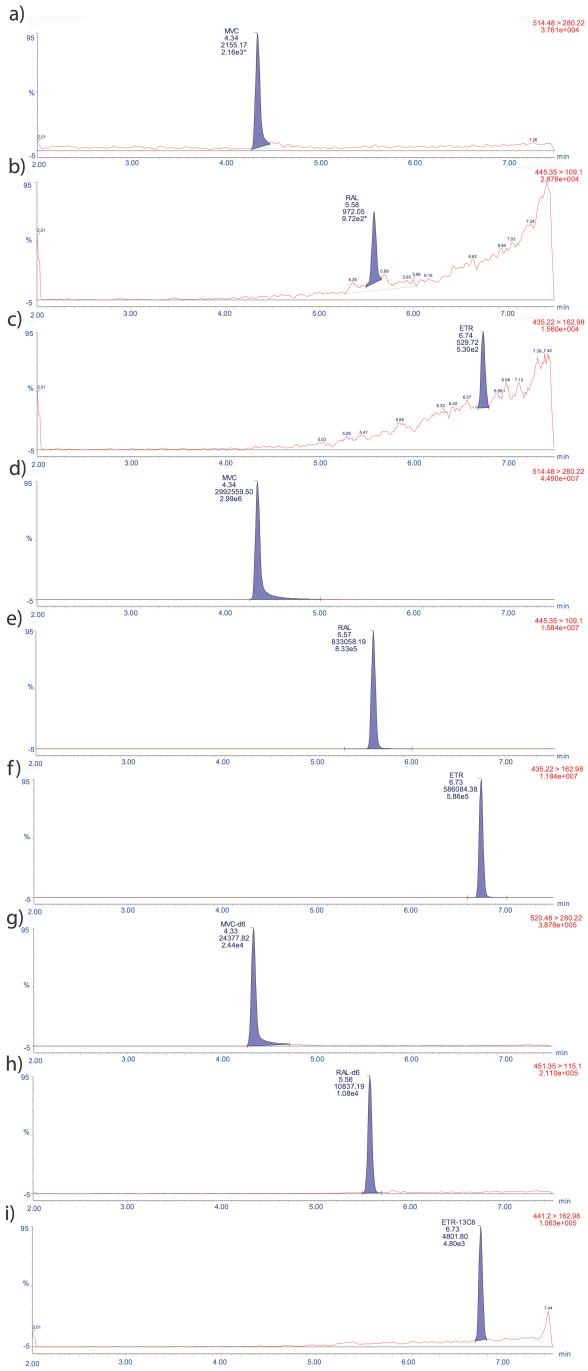

Figure 6.2: Chromatograms for drugs (MVC, RAL, ETR) and internal standards (MVC-d_6, RAL-d_6, ETR-$^{13}C_6$) at high and low concentrations. Neat chromatograms for 0.1 ng mL^{-1} standards (a-c), 100 ng mL^{-1} standards (d-f) and 1 ng mL^{-1} internal standards (g-i).

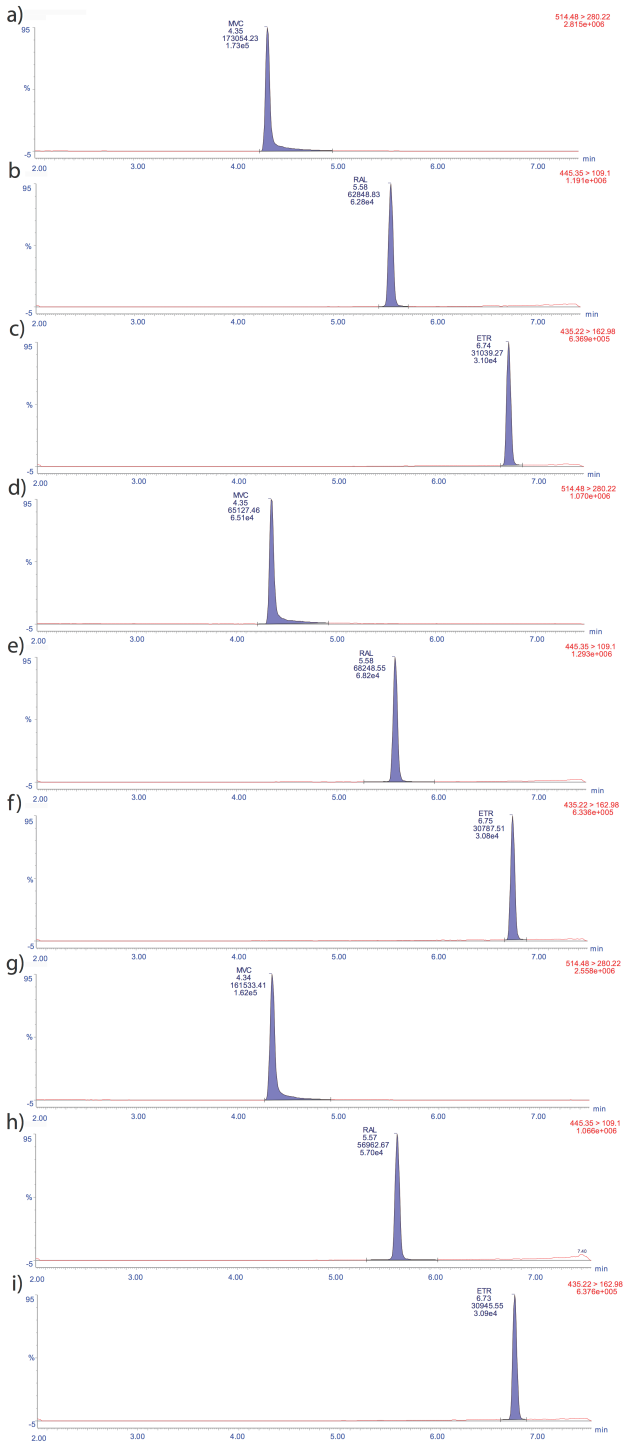

Figure 6.3: Chromatograms for (ETR, MVC, RAL) in each matrix. Each drug was at a concentration of 5 ng mL^{-1} in plasma (a-c), vaginal secretions (d-f) and vaginal tissue (g-i).

6.4.2 *Calibration curve and internal standard*

Calibration curves for each antiretroviral drug (Table 6.1) were described by a split linear regression. Samples at a concentration of 1 ng mL^{-1} or above were analyzed using a calibration curve that included all eight calibration levels (regardless of LOQ), while samples at lower concentrations were analyzed using a calibration curve that included the four calibration levels from 0.01-1 ng mL^{-1}. This method allowed for the widest, reproducible range of quantification for each drug. Over the considered calibration range, the regression coefficient (r^2) was >0.99 for each curve. The back-calculated calibration standards were within ±15% (or ±20% at LOQ) of the nominal concentration.

Stable, isotopically labeled analogues were used as internal standards for each antiretroviral drug. Studies in analyte detection using LC-MS/MS have revealed that labeling compounds with three to eight ^{2}H or ^{13}C is the most common strategy to achieve co-elution of drug and internal standard, while minimizing cross-talk on the mass analyzer and compensating for small errors that may arise during processing and samples analysis.[239, 240] Based on availability and suitability, ETR-$^{13}C_6$, MVC-d_6 and RAL-d_6 were chosen and produced a corresponding internal standard for each antiretroviral drug that was shifted by +6 mass units. The individual internal standard for each ARV drug allows for precise observation of matrix-induced change retention time for each drug/internal standard combination and are appropriate for use across species.

6.4.3 *Precision, accuracy, LOQ and LOD*

Precision and accuracy as determined by the low, medium and high QC samples in plasma, vaginal secretions and vaginal tissue (Table 6.3). The levels of QC samples were chosen to reflect low, medium and high concentrations of the linear calibration range as determined with preliminary experiments, as well as anticipated clinically relevant drug concentrations. The mean inter-assay precision (%CV) and accuracy (% bias) were 5.08% and 1.96%, respectively. Intra-assay precision and accuracy were 3.44% and 1.08 %, respectively. The inter-assay and intra-assay deviations (bias) from nominal concentrations ranged from -14.87% to 16.68% and -19.08% to 16.72%, respectively. Overall,

the quantification of ETR and MVC were more accurate and precise than RAL in all matrices. The lowest QC for RAL (0.5 ng mL^{-1}) had a large deviation in %CV in plasma (17.54%), vaginal secretions (21.61%), and vaginal tissue (16.18%), which is likely due to effects from the matrix on the ionization efficiency of RAL. Heine et al. also observed an increased recovered concentration compared to nominal concentration for RAL in peripheral blood mononuclear cells (PBMCs).[230] Increasing the organic precipitation volume to matrix ratio may decrease matrix effects, thereby increasing the range of quantification for RAL. For more conservative analyses, it may be appropriate to consider only concentrations of 1 ng mL^{-1} of RAL in matrix, while neat standards are viable down to 0.5 ng mL^{-1}.

Based on standard pharmacokinetics and pharmacodynamics for topical delivery we expect that secretion concentrations > tissue concentrations >> plasma concentrations, in comparison to oral delivery, wherein the order is reversed.[241] Thus, topical delivery will likely dictate the maximum concentration for vaginal secretions and tissue but minimum concentration for plasma, whereas oral delivery will define the maximum plasma concentration but minimum vaginal secretion and tissue concentrations. Topical gel and ring microbicide formulations of MVC have yielded concentrations of 10^0-10^1 ng mL^{-1} in plasma, 10^4-10^7 ng mL^{-1} in vaginal fluid and 10^2-10^4 ng mL^{-1} in vaginal tissue.[226, 242, 243] Though ETR has not yet been tested as a microbicide, dapivirine, a chemically similar antiretroviral has been extensively tested as a microbicide, yielding concentrations of 10-10^3 ng mL^{-1} in vaginal tissue, 10^0-10^2 ng mL^{-1} in plasma and ng mL^{-1} in vaginal fluid.[213, 244-246] RAL concentration after administration as a topical, vaginal microbicide has not yet been reported in the literature. Orally delivery yields plasma concentrations of 10^2-10^3 ng mL^{-1} ETR,[230] 10^2-10^3 ng mL^{-1} MVC,[247] and 10^2-10^3 ng mL^{-1} RAL,[248] but have not yet been quantified in the vaginal compartment. Given these reported values, we anticipate that this quantitative method for simultaneous detection of ETR, MVC and RAL will adequately span the clinically relevant range for all three drugs.

6.4.4 *Stability of extracted antiretrovirals*

The stability of ETR, MVC and RAL in plasma, vaginal secretions and vaginal tissue samples were evaluated under room temperature and 4°C storage conditions for 48 hours (Table 6.5.) The deviation after storage at room temperature ranged from -11.76% to 15.66% of the original concentration measured for ETR, MVC and RAL. For the samples stored at 4°C, deviations ranged from -9.66% to 12.74%. Given the analytical variation, these results indicate that ETR, MVC and RAL are stable in all matrices for at least 48 hours at either room temperature or 4°C. The stability of the three antiretrovirals was also evaluated after three freeze/thaw cycles, wherein samples were allowed to completely freeze at -80°C, before completely thawing at room temperature. Compared to previously measured concentrations for these samples, the deviations ranged from -9.58% to 15.48% for all three drugs. Thus, we expect that standards and samples may be frozen and thawed up to three times before analysis without risking skewed results due to drug degradation.

Table 6.5: Stability of ETR, MVC, RAL in plasma, vaginal secretions and vaginal tissue after storage at room temperature, 4°C and three freeze(-80°C)/thaw cycles.

Matrix	**Drug**	**(ng mL^{-1})**	**Room Temperature (48 hours)**, %	**4°C (48 hours)**, %	**3X Freeze-thaw**, %
Plasma	ETR	0.5	-4.43	1.82	3.78
		5	-6.07	-4.94	0.29
		50	-1.43	-1.46	-1.49
	MVC	0.5	7.60	-3.25	-9.58
		5	-3.76	-1.70	4.21
		50	-5.46	-0.78	-3.74
	RAL	0.5	-12.78	-0.51	-7.91
		5	0.14	3.51	-3.45
		50	0.41	0.84	-2.20
Vaginal Secretions	ETR	0.5	14.36	1.40	-0.09
		5	2.18	-7.37	-5.67
		50	1.80	-4.83	5.92
	MVC	0.5	15.66	-9.66	13.33
		5	10.69	7.36	15.48
		50	9.70	5.59	4.98
	RAL	0.5	-4.49	-0.38	9.17
		5	-2.87	7.03	-5.27
		50	-1.04	5.67	-4.97
Vaginal Tissue	ETR	0.5	3.78	3.57	-2.26
		5	0.79	-8.27	-5.38
		50	-7.71	-4.31	-4.31
	MVC	0.5	-5.03	-1.93	-6.10
		5	0.84	-4.65	-5.87
		50	-2.45	0.74	0.62
	RAL	0.5	-11.76	12.74	1.80
		5	1.57	1.97	1.02
		50	-1.24	3.11	2.13

6.4.5 *Matrix effect and recovery*

The matrix effect, extraction yield, overall recovery, and process efficiency were analyzed for ETR, MVC and RAL in plasma, vaginal secretions and vaginal tissue (Table 6.6). The assessment of matrix effect was quantified as the ratio of mean peak area of analytes spiked before extraction to that of the neat standard (ratio B/A, Table 6.6). A value above or below 100% indicates enhancement or suppression of ionization, respectively, by the given matrix.[249] Our results indicate that ETR and MVC are minimally affected by plasma (100-119% recovery) and vaginal secretions (98-120% recovery), while RAL undergoes significant ionization enhancement (185%-377% recovery) in these matrices. ETR is minimally affected (99%-106% recovery) in the vaginal secretions whereas MVC undergoes ionization suppression (45-52%), and RAL undergoes ionization enhancement (189%-384%). These differences may be due to inherent variations in pH and protein content in these matrices that alter the solubility and ionization efficiency for these physicochemically diverse drugs.[250-252]

Extraction yield (EY) was evaluated by normalizing the samples spiked after extraction to those spiked before extraction (ratio C/B) for each matrix (Table 6.6). As expected, there was a loss of each drug and internal standard through the extraction process, although this was remarkably consistent across concentrations. Extraction in plasma and vaginal tissue yielded the greatest recovery of MVC, followed by ETR and RAL whereas vaginal secretions yielded highest recovery of ETR, followed by MVC and then RAL. Process efficiency (PE) as evaluated by normalizing peak areas of samples spiked before extraction to the corresponding neat standards, and echo the trends observed with the extraction yield for plasma samples. However, for vaginal secretions, MVC has a very low (~28%) but consistent PE, while RAL is high (94-190%). In vaginal tissue, the PE of ETR is similar to plasma and secretions, while the PE for MVC and RAL are both higher than expected, with increasing PE with decreasing concentration. These differences reflect how the different matrices and varied extraction protocols affect the drug ionization, and are attenuated by carefully timing the spiking of internal standard.

Most importantly, the overall recovery (OY) was assessed using peak adjusted ratios for each drug and corresponding internal standard (ratio C_2/B_2) in order to ensure that unknown concentrations from future study samples are quantified accurately. All drugs were within ±15% of the neat standard, indicating that samples in all matrices may be normalized to a neat standard with this assay, and that internal standards must be spiked before extraction to overcome the matrix effects and extraction inefficiencies associated with this assay.

Table 6.6: Matrix effect, extraction yield, process efficiency, and overall recovery of antiretroviral drugs.

Matrix	Compound	Nominal Conc. (ng mL^{-1})	Mean Peak Areas			Mean Peak Area Ratios		ME (%)	EY (%)	PE (%)	OR (%)
			A (n=3)	B (n=3)	C (n=3)	B_2	C_2	B/A	C/B	C/A	C_2/B_2
Plasma	ETR	50	309365	308815	216646	52.68	53.98	100%	70%	70%	102%
		5	30904	32003	21663	5.23	5.09	104%	68%	68%	97%
		0.5	3168	3426	2222	0.56	0.52	108%	65%	65%	94%
	MVC	50	1495418	1665409	1369574	53.78	53.45	111%	82%	82%	99%
		5	148516	169360	140618	5.42	5.34	114%	83%	83%	99%
		0.5	13762	16419	15054	0.52	0.56	119%	92%	92%	108%
	RAL	50	343857	635792	334203	40.48	41.84	185%	53%	53%	103%
		5	23781	63743	33353	4.06	4.06	268%	52%	52%	100%
		0.5	1759	6623	3403	0.42	0.42	377%	51%	51%	100%
	ETR-$^{13}C_6$	50	5801	5862	4013	-	-	101%	68%	-	-
		5	5868	6120	4256	-	-	104%	70%	-	-
		0.5	5813	6173	4254	-	-	106%	69%	-	-
	MVC-d_6	50	27979	30969	25625	-	-	111%	83%	-	-
		5	28021	31255	26325	-	-	112%	84%	-	-
		0.5	23674	31438	26730	-	-	133%	85%	-	-
	RAL-d_6	50	8492	15708	7988	-	-	185%	51%	-	-
		5	5473	15702	8208	-	-	287%	52%	-	-
		0.5	3207	15595	8014	-	-	486%	51%	-	-
Vaginal Secretions	ETR	50	309365	307674	210309	55.00	53.97	99%	68%	68%	98%
		5	30904	31249	21237	5.34	5.36	101%	68%	69%	100%
		0.5	3168	3348	2207	0.54	0.54	106%	66%	70%	101%
	MVC	50	1495418	678174	399876	41.51	45.94	45%	59%	27%	111%
		5	148516	65043	39438	4.15	4.71	44%	61%	27%	113%
		0.5	13762	7210	3935	0.47	0.46	52%	55%	29%	100%
	RAL	50	343857	651437	321720	40.90	46.61	189%	49%	94%	114%
		5	23781	65916	32024	4.18	4.49	277%	49%	135%	107%
		0.5	1759	6747	3346	0.42	0.47	384%	50%	190%	112%
	ETR-$^{13}C_6$	50	5801	5594	3897	-	-	96%	70%	-	-
		5	5868	5853	3959	-	-	100%	68%	-	-
		0.5	5813	6242	4067	-	-	107%	65%	-	-
	MVC-d_6	50	27979	16338	8705	-	-	58%	53%	-	-
		5	28021	15658	8380	-	-	56%	54%	-	-
		0.5	23674	15487	8476	-	-	65%	55%	-	-
	RAL-d_6	50	8492	15926	6902	-	-	188%	43%	-	-
		5	5473	15763	7130	-	-	288%	45%	-	-
		0.5	3207	15902	7061	-	-	496%	44%	-	-
Vaginal Tissue	ETR	50	309365	304446	208348	52.50	51.00	98%	68%	67%	97%
		5	30904	31048	21526	5.18	5.13	100%	69%	70%	99%
		0.5	3168	3177	2209	0.57	0.54	100%	70%	70%	95%
	MVC	50	1495418	1575348	1255628	50.82	50.78	105%	80%	84%	100%
		5	148516	160173	133328	5.21	5.21	108%	83%	90%	100%
		0.5	13762	16464	16186	0.55	0.63	120%	98%	118%	116%
	RAL	50	343857	561681	299121	36.60	38.05	163%	53%	87%	104%
		5	23781	56126	29092	3.57	3.57	236%	52%	122%	100%
		0.5	1759	5906	3149	0.39	0.40	336%	53%	179%	105%
	ETR-$^{13}C_6$	50	5801	5799	4085	-	-	100%	70%	-	-
		5	5868	5990	4195	-	-	102%	70%	-	-
		0.5	5813	5613	4125	-	-	97%	73%	-	-
	MVC-d_6	50	27979	30996	24727	-	-	111%	80%	-	-
		5	28021	30722	25593	-	-	110%	83%	-	-
		0.5	23674	30018	25514	-	-	127%	85%	-	-
	RAL-d_6	50	8492	15346	7862	-	-	181%	51%	-	-
		5	5473	15701	8157	-	-	287%	52%	-	-
		0.5	3207	15303	7784	-	-	477%	51%	-	-

6.5 CONCLUSIONS

We report a validated LC-MS/MS method for the simultaneous detection of ETR, MVC and RAL in pigtail macaque plasma, vaginal secretions and vaginal tissue. This analytical method should enable the pharmacokinetic study of these antiretrovirals applied through a topical, vaginal microbicide or oral treatment/prophylaxis. The high sensitivity and specificity attained allows for the quantification of as little as 0.2 pg for ETR, 0.1 pg for MVC, and 1 pg for RAL from a 2 μL injection volume. These outcomes will allow for accurate quantification of these antiretroviral drugs in non-human primate, as well as human, pharmacokinetics studies. The combination of a corresponding internal standard for each drug analyte and quantification using a neat standard curve highlight the usability and robust nature of this analytical method. To our knowledge, this is the first LC-MS/MS method to quantify these three antiretroviral drugs simultaneously in matrices appropriate for detection in reproductive tract tissues (vaginal secretions, vaginal tissue and plasma).

Chapter 7. In Vivo Pharmacokinetics and Ex Vivo Protection of Pigtail Macaque Vaginal Mucosal Tissue from RT-SHIV by Drug-Eluting Fibers Containing a Triple Antiretroviral Combination

Adapted from: In Vivo Pharmacokinetics and Ex Vivo Protection of Pigtail Macaque Vaginal Mucosal Tissue from RT-SHIV by Drug-Eluting Fibers Containing a Triple Antiretroviral Combination. Anna K. Blakney, Yonghou Jiang, Christina Nhan, Yvonne Cosgrove Sweeney, Ryan Stoddard, Edward Roberts, Joseph Phan, Rick Edmark, Dorothy L. Patton, Kim A. Woodrow. Manuscript in preparation.

7.1 ABSTRACT

Recent microbicide clinical trials have motivated the development of alternative dosage forms to meet the varying preferences of women worldwide that are affected by the ongoing HIV epidemic. Here, we have developed two rapidly dissolving fiber formulations containing a triple combination of antiretroviral drugs, for on-demand prevention of sexual transmission of HIV. The combination of etravirine (ETR), maraviroc (MVC) and raltegravir (RAL) was chosen for the variety of mechanisms of actions, physicochemical diversity and a potency known to be 10-fold greater than tenofovir disproxil fumarate (TDF) alone.[253] We quantified the concentrations of each drug in vaginal secretions and plasma after a single dose of the fiber formulation, and assessed the safety profile of repeated dosing of the dual layer fibers. The concentration of all three drugs was quantified in tissue after a single dose of the dual layer fibers, and the corresponding tissue biopsies were challenged *ex vivo* with RT-SHIV. We observed that the dual layer fibers resulted in a quick, high concentration (~10^6 ng/mL) of MVC and RAL, while the fiber-in-fiber formulation provided a more constant concentration (~10^3 ng/mL) of these drugs over 14 days. The pharmacokinetic profile of ETR in vaginal secretions, and all three drugs in plasma, was similar between the two formulations. There was a significant, positive correlation between the secretion and plasma concentrations for all three drugs after 24 hours, indicating effective tissue penetration. A single dose of the dual layer fibers resulted in high tissue concentrations of all three drugs (~10^6 ng/g) after 1 hour, which prevented infection with RT-SHIV in these tissues for up to 24 hours. These results support the potential of electrospun fibers as an on-demand dosage form for the prevention of HIV.

7.2 INTRODUCTION

In 2015, 2.1 million people were infected with HIV.[254] While new HIV infections in children have fallen 50% since 2010, new infections in adults have only decreased by 6%.[254] The primary driver for the epidemic is sexual transmission, thus motivating the development of HIV prevention strategies including microbicides, oral pre-exposure prophylaxis, and vaccines.

Recent clinical trials have demonstrated the potential for vaginal, topical microbicides to prevent HIV. In the CAPRISA 004 trial, a 1% tenofovir (TFV) gel reduced HIV acquisition by 39%,[255] with a strong relationship between local TFV exposure in the genital tract and HIV prevention.[256] In the VOICE trial, a 1% TFV gel was found to reduce the risk of HIV acquisition in adherent users by 50%; however, less than 40% of users were found to adhere to the specified dosing regimen.[257] Similarly, the FACTS 001 trial found that TFV gel was highest in effectiveness in women who reported proper product use, but this subgroup was only 20% of the study population.[258] A user preference study of HIV prevention dosage forms conducted by IPSOS in South Africa, Uganda, and Nigeria found that there was not a single preference amongst women between a vaginal film, intravaginal ring, implant, or injectable, but that women desired both an on-demand and a long-acting option.[259] The indications from these studies are twofold for the microbicide community. First, it is imperative to develop alternative dosage forms to meet the variety of preferences of women who may use the products in order to increase adherence. Second, there must be adequate concentrations of antiretrovirals in vulnerable tissues, thus motivating expanding the repertoire of vaginally administered antiretrovirals to drugs with high capacity to penetrate tissue.

Drug-eluting electrospun fibers have been widely investigated for delivery of antiretrovirals *in vitro* including encapsulating drugs with varying physiochemical properties,[4, 106] tunable drug release using polyester polymers,[210] scale-up of fibers with remarkably high drug loading,[82] amorphous solid dispersions,[260] and fibers that release a bolus of drug in response to a change from vaginal pH (~4) to that

of semen (~7),[5] but have yet to be tested *in vivo*. Depending on the polymer and drug composition, electrospun fibers can be engineered to dissolve in a wide range of timescales, from a few seconds[260] to a few months.[261] For application as a practical vaginal, topical microbicide, solid dosage forms must either dissolve quickly or be sub-micron in size in order to remain imperceptible to the user or the user's partner during coitus. We developed two formulations to probe the potential of electrospun fibers for pericoital HIV prevention *in vivo*. First, we developed a dual layer fabric composed of water-soluble polymers (polyvinyl alcohol (PVA) and polyethylene oxide (PEO)) as a quick-dissolving delivery system. Then, we augmented the dual layer fabric with fibers composed of water-insoluble but biodegrading polymers (poly(lactic-co-glycolic acid) (PLGA) and polycaprolactone (PCL)), that had been reduced to a sub-micron size ("micronized") using a novel blending and sieving process, yielding a fiber-in-fiber (FIF) system.

Here, we investigated the safety and pharmacokinetics of a triple combination of antiretrovirals with mechanisms of action targeted to early, middle, and late stages of the HIV replication cycle including maraviroc (MVC), an entry inhibitor, etravirine (ETR), a non-nucleoside reverse transcriptase inhibitor, and raltegravir (RAL), an integrase inhibitor. We aimed to quantify concentrations of ETR, MVC, and RAL in vaginal secretions and plasma to inform the optimal dosing strategy for both the dual layer and fiber-in-fiber fabrics. We observed the correlation between concentration in vaginal secretions and plasma as an indicator of drug tissue penetration. Finally, we evaluated the potential of the dual layer formulation to protect tissue biopsies from SHIV challenge *ex vivo*, and observed the correlation between tissue drug concentration and SHIV infectivity.

7.3 MATERIALS & METHODS

7.3.1 *Preparation of electrospun fiber dosage forms*

7.3.1.1 Dual layer fiber dosage form

Polyvinyl alcohol (MW=30-70 kDa, 87-90% hydrolysis, Sigma Aldrich, St. Louis, MO, USA) and polyethylene oxide (MW= 400 kDa, Scientific Polymer Products Inc., Ontario, NY, USA) were dissolved in deionized H_2O (DI H_2O) at 20.4 % (w/v) at a ratio of 86% PVA and 14% PEO with 0.02% (w/v) NaCl and allowed to dissolved overnight at 35 °C. Etravirine (ETR), maraviroc (MVC) and raltegravir (RAL) (purified by the Suydam laboratory, Seattle University, Seattle, WA, USA) were micronized using a mortar and pestle prior to addition to polymer solution. RAL was added to the polymer solution at 4.06 % (wt. drug/wt. solution) with 1.5 molar equivalent of NaOH (Sigma Aldrich) in order to fully solubilize drug. RAL polymer solution was then electrospun on a Nanospider™ Production Line NS 1WS500U (Elmarco Inc., Morrisville, NC, USA) using the following conditions: 250 mm wire electrode distance, -40 kV collecting electrode, 60 kV spinning electrode, 250 carriage traveling distance. Brown wax paper was used as a collection substrate, and was passed back and forth through the collection zone every 20 minutes while spinning. ETR and MVC were then added to a single polymer solution (as previously described) at 1.86 and 2.20 wt.% (wt. drug/wt. solution), respectively, homogenized for 5-10 minutes using a Ultra-Turrax® homogenizer (Ika Works Inc., Wilmington, NC, USA), and then spun directly onto the RAL fiber layer (Figure 7.1), using the same electrospinning conditions. Dual layer fibers were then cut into a 4x4 cm square and stored in a vacuum desiccator until use.

7.3.1.2 Polyester fiber electrospinning and micronization

Poly(lactic-co-glycolic acid) (50:50, acid end group, 0.15-0.25 dL/g, Lactel Absorbable Polymers, Birmingham, AL, USA) and polycaprolactone (MW= 80 kDa, Sigma Aldrich, St. Louis, MO, USA) were dissolved in 1,1,1,3,3,3-hexafluoro-2-propanol (HFIP) at 15% (w/v) at a mass ratio of 9:1 PLGA:PCL. ETR, MVC, and RAL were dissolved in polyester polymer solution at 50% (wt. total

drug/wt. polymer) at an equimolar ratio, and then spun on the Nanospider™ instrument at the following conditions: 200 mm wire electrode distance, -25 kV collecting electrode, 60 kV spinning electrode, and 250 mm carriage traveling distance, using brown wax paper as a collection substrate. Fibers were dried overnight at ambient conditions. Approximately 6g of fibers were then added to a blender (Blendtec, Orem, UT, USA) with 500 mL of DI H_2O, and blended using the following regimen: 1X ice crush, 1X ice cream. Micronized fibers <250 μm were then separated by flowing the blended solution through a 250 μm stainless steel sieve (VWR, Radnor, PA, USA). Larger fiber fragments were returned to the blender and processed until size conformity was achieved. Micronized fibers were then dried using a 1.2 μm nylon filter paper (Merck Millipore Ltd., Tulagreen, Ireland) and house vacuum. Dried micronized fibers were then stored at 4 °C.

7.3.1.3 Fiber-in-fiber dosage form

Fiber-in-fiber dosages were fabricated using the same process as the dual layer fibers and incorporating the micronized drug-loaded polyester fibers into each layer. RAL polymer solution was prepared as stated above, and then 28.6 wt.% (wt. micronized fibers/wt. solids) micronized fibers were added to solution, homogenized, and electrospun using aforementioned conditions. Then, the ETR and MVC polymer solution was prepared, and 28.6 wt.% (wt. micronized fibers/wt. solids) micronized fibers were added to the solution, homogenized, and electrospun on top of RAL fiber layer loaded with micronized polyester fibers, using aforementioned conditions. Fiber-in-fiber doses were then cut into a 4x4 cm square, and stored in a vacuum desiccator.

7.3.1.4 Placebo dosages

Placebo fibers were prepared for both the dual layer and FIF dosage forms, using identical processing conditions, sans drugs. Placebo fibers were cut into 4x4 cm squares, and stored in a vacuum desiccator.

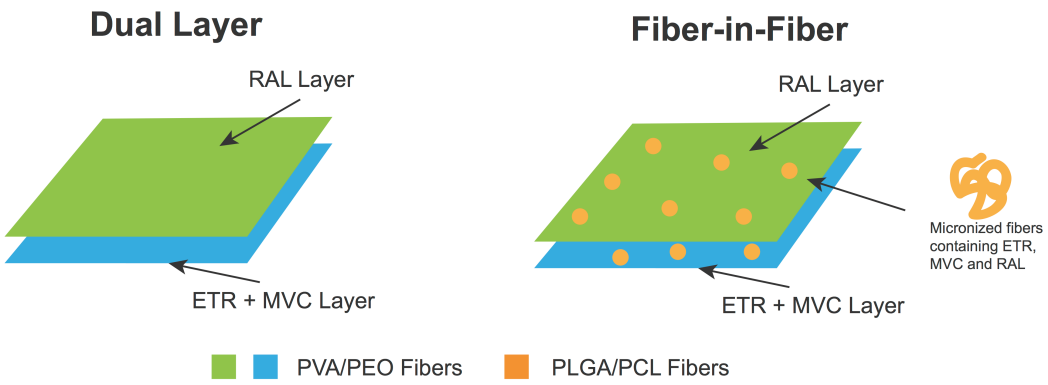

Figure 7.1: Schematic of drug-eluting electrospun fiber formulations loaded with ETR, MVC and RAL.

7.3.2 *Nonhuman primate dosing schedule*

Eight sexually matured pigtail macaques (*Macaca nemestrina*) were tested in this study. Animals were housed at the Washington National Primate Research Center (WaNPRC). All studies were carried out according to approved University of Washington IACUC protocols. The dual layer and FIF dosages were administered according to two different dosing regimens in order to assess the pharmacokinetic decay of ETR, MVC, and RAL in vaginal secretions, tissue, and plasma after a single dose, and the safety of daily dosing (Figure 7.2). For PK studies, both the dual layer and FIF formulations were administered vaginally a single time in pigtail macaques (n=8), who were under ketamine sedation, without the use of a speculum. For the dual layer safety study, anesthetized animals were dosed intravaginally every 24h for 5 days using a speculum. For the FIF safety study, anesthetized animals were dosed intravaginally a single time using a speculum. Regardless of formulation, the RAL layer was placed proximal to tissue upon administration. For both safety studies, n=4 animals were dosed with the drug-loaded fibers and n=4 animals were dosed with placebos initially. The study was carried out, animals were given a two week recovery period, and then crossed over to the other arm of the study, e,g, animals that received placebo first then received drug-loaded fibers, for a total of n=8 for each condition.

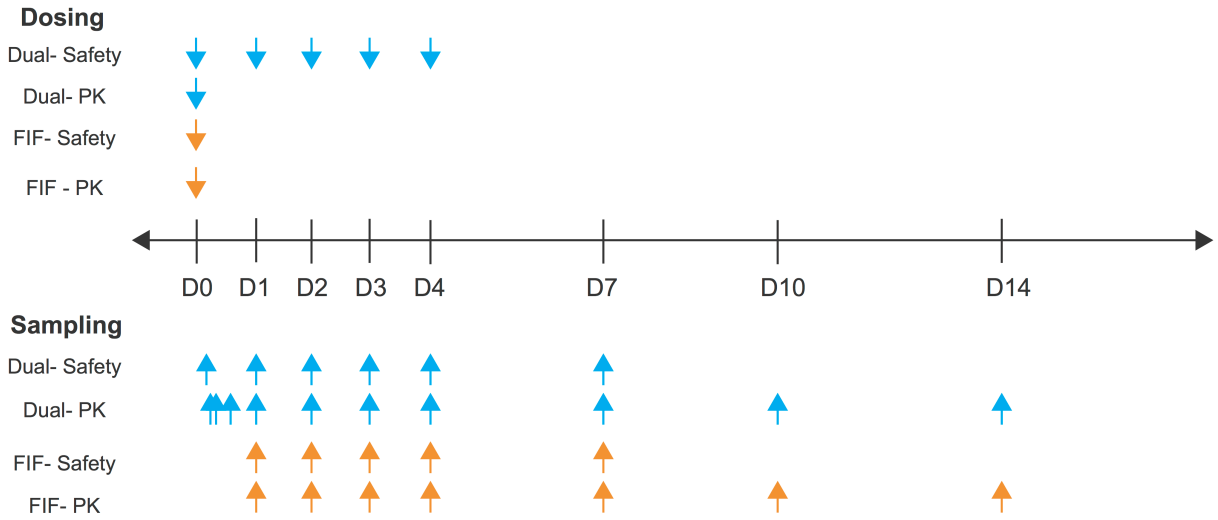

Figure 7.2: Dosing and sampling schedule for safety and pharmacokinetic studies of dual layer and fiber-in-fiber formulations.

7.3.3 *Safety observation*

Colposcopy was used to observe changes in the vaginal and cervical tissue and secretions in response to both placebo and drug-loaded fiber dosages. For the dual layer safety study, animals were observed at 0.5 h and 1, 2, 3, 4, and 7 days (Figure 7.2). For the FIF safety study, animals were observed at 1, 2, 3, 4, 7, 10 and 14 days (Figure 7.2).

7.3.4 *Pharmacokinetic sample collection*

Vaginal secretion samples were collected using a Merocel opthalmic swab (Medtronix, Jacksonville, FL, USA), placed in a cryovial, and immediately frozen at -80°C. Swabs were then diluted using 300 µL of phosphate buffered saline (PBS) to thin the mucus, and incubated for 1h at 4°C. The swab and extraction buffer were then transferred to Spin-X centrifuge tubes with a 0.22 µm cellulose acetate filter (Corning Inc., Corning, NY, USA) and centrifuged at 10,000 RPM for 10 min. Secretion eluate was then frozen at -80 °C. Blood was taken in an EDTA-coated 5 mL tube, centrifuged at 3000

RPM, and then the plasma layer was separated and frozen at -80 °C. Vaginal and cervical tissue biopsies were taken using tissue biopsy forceps and immediately frozen at -80 °C.

In the dual layer PK study, vaginal secretion and plasma samples were collected at 1h, 2h, 4h, and 1, 2, 3, 4, 7, 10, and 14 days (n=8). For the FIF PK study, vaginal secretion and plasma samples were collected at 1, 2, 3, 4, 7, 10 and 14 days. After both the dual layer and FIF studies to assess pharmacokinetics of ETR, MVC, and RAL in secretions and plasma were completed, a single study using the dual layer fibers was carried out to assess the concentration of each drug in vaginal and cervical tissue. Tissue biopsies were taken 1h (n=2), 2h (n=2), 1 day (n=2), 2 days (n=2), 3 days (n=3), 4 days (n=3), 7 days (n=4), 10 days (n=4), and 14 days (n=8).

7.3.5 *Pharmacokinetic sample processing and analysis*

Vaginal secretions, tissue, and blood plasma samples were analyzed for ETR, MVC, and RAL concentration using a previously published LC-MS/MS assay.[262] Briefly, 50 µL of cold acetonitrile (ACN) was added to 50 µL of processed vaginal secretions or plasma. For tissue samples, 200 µL of cold ACN was added to each biopsy, along with 640 mg of 1.4 mm and six 2.8 mm zirconium oxide ceramic beads (Precellys, Bertin Coporation, Rockville, MD, USA), which was then homogenized using a Precellys® 24 tissue homogenizer (Bertin Corporation, Rockville, MD, USA) for three cycles of 20 s at 6500 RPM. 10 µL of a 10 ng/mL internal standard solution of ETR-$^{13}C_6$, MVC-d_6, and RAL-d_6 (Alsachim Inc., Illkirch-Grafefenstaden, France) was added. Samples were vortexed for ~1 min., and then centrifuged at 10,000 RPM for 10 min. using a Sorvall Legend 14 centrifuge (Thermo Scientific, Waltham, MA, USA). Eluate was filtered using a 0.22 µm PVDF syringe tip filter (Millipore, Burlington, MA, USA) and added to an 200 µL Qsert vial (Waters Corporation, Milford, MA, USA). Analytes were separated on an EMD Chromolith® Performance RP-183 100-3mm analytical column (Merck, Darmstadt, Germany) using a gradient method of water with 10 mM formic acid and 1:1 acetonitrile : methanol with 10 mm formic acid on a I-Class Acquity UPLC (Waters Corporation, Milford, MA, USA). The chromatography system was coupled to a Waters Xevo TQ-S tandem

quadrupole mass spectrometer (Waters Corporation, Milford, MA, USA) with a Micromass Zspray™ Atmospheric Pressure Ionization (API) Source. The following ion transitions (m/z) were used: 435.22→162.98 (ETR), 441.20→162.98 (ETR-$^{13}C_6$), 514.48→290.22 (MVC), 520.38→280.22 (MVC-d_6), 445.35→109.10 (RAL), and 451.35→115.10 (RAL-d_6). The LC-MS/MS system and data analysis was carried out using MassLynx® software (version 4.1, Waters Corporation, Milford, MA, USA). The limit of quantification was 0.1, 0.05 and 0.5 ng/mL for ETR, MVC, and RAL respectively.

7.3.6 *Ex vivo tissue biopsy challenge assay*

Immediately after excision and being weighed, fresh cervical and vaginal tissue biopsies (n=1) were used for virus challenge assay. Briefly, biopsy tissues were exposed to $5x10^4$ RT-SHIV at 37 °C for 2 hours. Tissues were then washed and placed in fresh medium. Culture supernatant was collected after 3, 6 and 9 days and was frozen at -80°C. Infection was monitored by viral p27 using SIV p27 Antigen ELISA (ZeptoMetrix Corporation, Buffalo, NY, USA) according to manufacturer protocol.

7.3.7 *Data analysis*

Secretion, plasma, and tissue concentrations are reported as mean ± standard deviation. Pharmacokinetic parameters, including C_{max}, T_{max}, and AUC were calculated using GraphPad Prism (version 6.0). AUC was calculated using the trapezoidal rule. Comparison of the concentrations and AUC values for the dual layer vs. FIF dosage forms was performed using a paired Student's t-test using a two-tailed distribution. For correlations between vaginal secretion and blood plasma drug concentrations, data was log-transformed and fit using linear regression using GraphPad Prism. Tissue penetration ratio (TPR) was calculated using the following equation:

$$\text{TPR} = \frac{Conc._{Plasma}}{Conc._{Secretion}}$$

7.4 RESULTS

7.4.1 *Dual layer and FIF formulations are safe despite high ARV concentrations in secretions*

We assessed whether daily administration of the dual layer formulation and a single administration of the FIF formulation were safe, as defined by a lack of genital irritation, inflammation, or mucosal breakdown. In addition, we measured the concentration of ETR, MVC, and RAL in vaginal secretions and plasma to observe the pharmacokinetics of the dosing regimen for the safety study. For the dual layer fibers, the concentrations in secretions for all three drugs were remarkably high, reaching levels of ~10^9 ng/mL for MVC and RAL and ~10^5 ng/mL for ETR (Figure 7.3a). These concentrations remained high over the 5 days that the animals were dosed, and then falling by ~4 orders of magnitude 3 days after the final dose. Despite the high drug concentrations in the vaginal secretions, no adverse events, such as cervical friability, epithelial disruption, blister or ulceration, were observed by colposcopy for any of the animals. There were no changes in the vaginal pH of any of the animals after repeated dual layer fiber dosing.

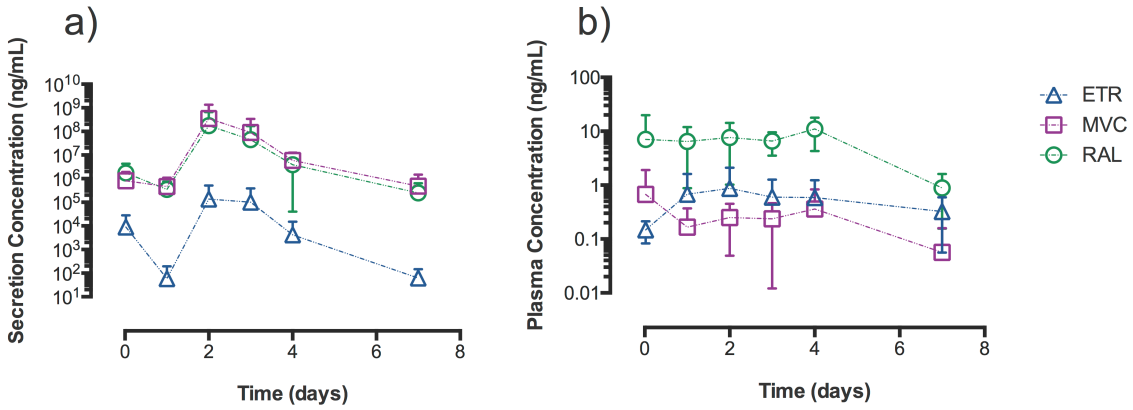

Figure 7.3: Concentrations of ETR, MVC and RAL in vaginal secretions (a) and blood plasma (b) after daily dosing for dual layer formulation. Dual layer fibers were dosed daily for five days, beginning at t=0. Shapes represent mean concentrations for ETR (blue), MVC (purple) and RAL (green) and error bars represent standard deviation.

The safety profile of the FIF formulation was evaluated after a single administration, since they would not be used daily. The drug concentrations in secretions and plasma were quantified (not shown), and mirrored the results from the PK study (Figure 7.4). After 4 days, one of the animals was observed to have ecchymosis. No other adverse events or changes in vaginal pH were observed over the course of the study.

7.4.2 *Dual layer formulation resulst in rapid and high ARV concentrations while FIF formulation results in more constant concentrations in secretions and plasma*

Despite wide variations of drug solubility in polymer solution, ETR, MVC, and RAL were encapsulated in the dual layer fibers at 4.1, 3.7 and 6.7 % (wt. drug/wt. fiber). Each administered dosage was ~160 mg, resulting in a delivered dose of 6.6 mg ETR, 5.9 mg MVC, and 10.7 mg RAL, and 23.2 mg of total drug. We aimed to quantify the amount of all three ARVs in pigtail macaque vaginal secretions and blood plasma over the course of 14 days after a single dose. ETR, MVC and RAL all reached their individual maximum concentrations in the secretions after 1 hour, at values of $1.5x10^5$, $6.3x10^6$ and $6.7x10^6$ ng/mL, respectively (Table 7.1), indicating a ~40-fold greater concentration of MVC and RAL than ETR. All three drugs exhibited pseudo-linear decay from 0-72 hours, and then exponentially decreased (Figure 7.4, a-c). Remarkably, after two weeks all three of the drugs were still present in the secretions at levels of $\sim10^2$ ng/mL for MVC and RAL, and ~10 ng/mL for ETR. This is particularly significant as all of the fiber doses were completely dissolved within 24 hours as observed by colposcopy.

Table 7.1: Pharmacokinetic parameters of ETR, MVC and RAL in blood plasma and vaginal secretions for dual layer and fiber-in-fiber formulations.

Drug	Formulation	Secretions			Plasma		
		T_{max} (h)	C_{max} (ng/mL)	AUC (ng*h/mL)	T_{max} (h)	C_{max} (ng/mL)	AUC (ng*h/mL)
ETR	Dual	1	145,923	703,798	96	10.77	1425
	FIF	24	1,490	47,235	24	0.99	98.62
MVC	Dual	1	6,314,096	6,867,000	4	7.20	111.4
	FIF	48	4,370	470,471	24	2.70	490.8
RAL	Dual	1	6,712,524	65,740,000	2	10.70	733
	FIF	48	8,796	996,698	24	16.70	613

As expected, drug concentrations in plasma had lower C_{max} and delayed T_{max} compared to secretion concentrations. RAL, MVC, and ETR reached maximum concentrations of 10.7, 7.2, and 10.8 ng/mL after 2, 4, and 96 hours (Figure 7.4, d-f). However, while concentrations in the secretions varied as much as 5-fold in 14 days, the concentrations in plasma were much more consistent. As such, MVC and ETR were present in plasma after 14 days at concentrations of ~0.5 and ~10 ng/mL, while RAL was not detectable after 72 hours.

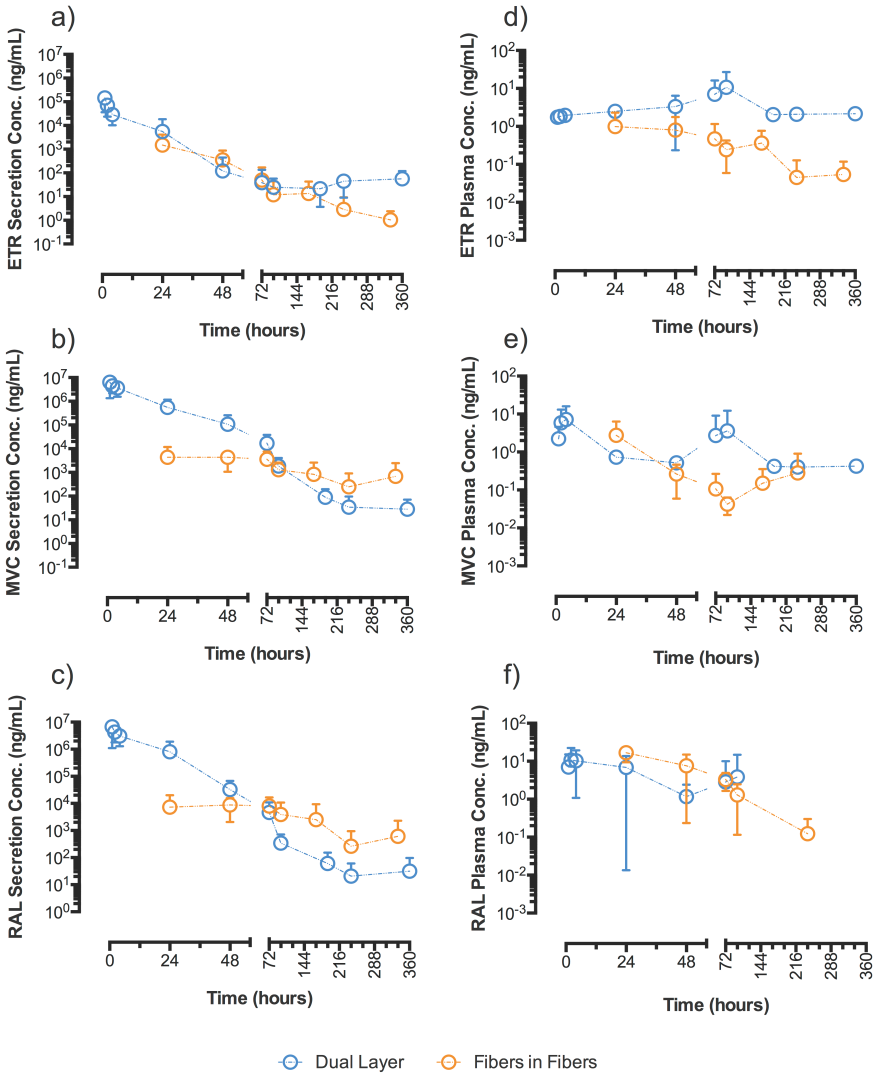

Figure 7.4: Concentrations of ETR, MVC and RAL in vaginal secretions (a-c) and blood plasma (d-f) for 14 days after a single dose of dual layer or fiber-in-fiber formulations. Circles represent mean concentration for dual layer (blue) or FIF (orange) and error bars represent standard deviation.

We hypothesized that using electrospun fibers composed of PLGA and PCL, two hydrophobic but biodegradable polymers, to deliver ETR, MVC, and RAL would dampen the burst release of drugs from the fibers, and provide a more sustained dose over time. We anticipated that rapid dissolution of the fibers and imperceptibility to the user would be important physical attributes for any microbicide product. Instead of applying a single layer of PLGA/PCL, that would takes on the order of months to

degrade,[263, 264] we micronized the fibers using a novel blending and sieving process, and electrospun them directly into the dual layer fiber dosage form. ETR, MVC, and RAL were encapsulated in the fiber-in-fiber dosages at 2.45, 1.96, and 3.56 % (wt. drug/wt. fiber). Each administered dosage was ~240 mg, resulting in a delivered dose of 5.9 mg ETR, 4.7 mg MVC, 8.5 mg RAL, and 19.1 mg of total drug.

Compared to the dual layer dosages, all three drugs had delayed T_{max} and lower C_{max} for the FIF formulation; ETR, MVC, and RAL achieved maximum concentrations of $1.5x10^3$, $4.4x10^3$, and $8.8x10^3$ ng/mL in vaginal secretions at 24, 48, and 48 hours, respectively (Table 7.1). Over the course of two weeks, ETR decreased in a pseudolinear fashion to a final concentration of ~10 ng/mL, while MVC and RAL remained at a more constant concentration of ~10^3 ng/mL (Figure 7.4, a-c). This is significant because similar to the dual layer fabrics, the FIF formulation dissolved within 24 hours, and were not visible thereafter during the colposcopy examinations. Interestingly, the concentration of ETR, MVC, and RAL peaked in plasma after 24 hours, at concentrations of 16.7, 2.7, and 0.99 ng/mL, respectively. All three drugs were detected in plasma at a concentration of ~0.1 ng/mL after 14 days.

Concentrations of MVC and RAL were higher in vaginal secretions for the dual layer fibers than the FIF formulation after 24 hours ($p<0.001$), but ETR were equivalent. We then compared the concentrations in secretions and plasma after 3, 7, and 14 days and the AUC_{3-14} for ETR, MVC, and RAL for the dual layer and FIF formulations (Table 7.2) to elucidate if there was a significant difference in the sustained release properties between the two formulations. While the average MVC and RAL concentration at 7 and 14 days, and the AUC_{3-14} was higher for FIF formulation, the trends were not statistically significant. The concentrations of ETR and MVC were statistically significantly higher in plasma for the dual layer formulation after both 7 and 14 days.

Table 7.2: Pharmacokinetic parameters comparing capacity of dual layer and fiber-in-fiber electrospun fiber formulations to sustain release of ETR, MVC and RAL.

		Concentration $_{\text{Day 3}}$ (ng/mL)			**Concentration** $_{\text{Day 7}}$ (ng/mL)			**Concentration** $_{\text{Day 14}}$ (ng/mL)			**AUC** $_{\text{Day 3-14}}$ (ng*h/mL)		
Matrix	Drug	Dual	FIF	p	Dual	FIF	p	Dual	FIF	p	Dual	FIF	p
Secretions	ETR	43.1 ± 102	49.94 ± 118	0.91	23.3 ± 18.3	2.87 ± 6.47	0.47	60.9 ± 64.3	1.04 ± 1.37	**0.033**	547 ± 236	176. ± 385	0.071
	MVC	18,800 ± 22,300	3,590 ± 4,010	0.11	99.9 ± 107	823 ± 1,770	0.28	29.4 ± 45.7	685 ± 1,770	0.32	43,400 ± 47,100	14,500± 14,300	0.14
	RAL	5,200 ± 6,490	7,940 ± 8,680	0.53	67.7 ± 94.1	2,520 ± 6,840	0.34	33.4 ± 70.2	609 ± 1,670	0.36	12,800 ± 12,800	334,500 ± 40,000	0.19
Plasma	ETR	7.05 ± 9.20	0.47 ± 0.69	0.085	2.03 ± 0.26	0.36 ± 0.40	**<0.001**	2.15 ± 0.23	0.05 ± 0.06	**<0.001**	59.7 ± 41.9	2.78 ± 2.31	**0.0064**
	MVC	2.73 ± 6.30	0.11 ± 0.16	0.27	0.42 ± 0.02	0.15 ± 0.21	**0.0070**	0.43 ± 0.06	n.d.	**<0.001**	18.1 ± 23.6	1.74 ± 2.76	0.096
	RAL	2.86 ± 7.22	3.29 ± 1.63	0.85	n.d.	n.d.	N/A	n.d.	n.d.	N/A	15.3 ± 28.7	9.60 ± 5.59	0.53

7.4.3 *ARV concentrations in secretions and plasma are positively correlated after 24h*

Correlations between vaginal fluid and plasma concentrations may be a qualitative proxy for antiretroviral penetration into tissue.[265] We aimed to analyze whether increased ARV concentrations in vaginal secretions were positively correlated with concentrations in plasma, indicating that the drugs were penetrating through the tissue. First, we observed how the tissue penetration ratio (TPR) (plasma concentration/secretion concentration) changed over time, after a single dose of the dual layer fibers (Figure 7.5). All three drugs had a drastic increase in the TPR in the first 24 hours, but then reached a pseudo steady-state ratio of ~10^{-2} for ETR and ~10^{-3} for MVC and RAL. Log-transform of all the secretion and corresponding plasma concentrations for all timepoints between 24h and 14 days for both formulations (Figure 7.6) showed a positive correlation between ETR, MVC and RAL secretion and plasma concentrations (p=0.023, 0.029, and 0.0007, respectively).

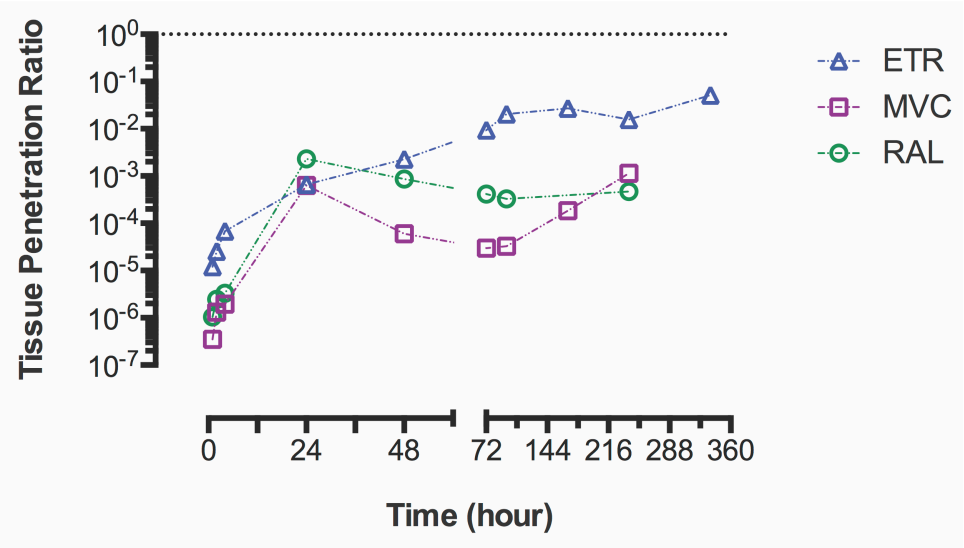

Figure 7.5: Tissue penetration ratio (TPR) of plasma concentration to vaginal secretion concentration for ETR, MVC and RAL after a single application of dual layer fibers. Dotted line at unity indicates equal concentrations in plasma and secretions, thus a higher (TPR) show better penetration from the secretion, through tissue, to plasma for a given drug.

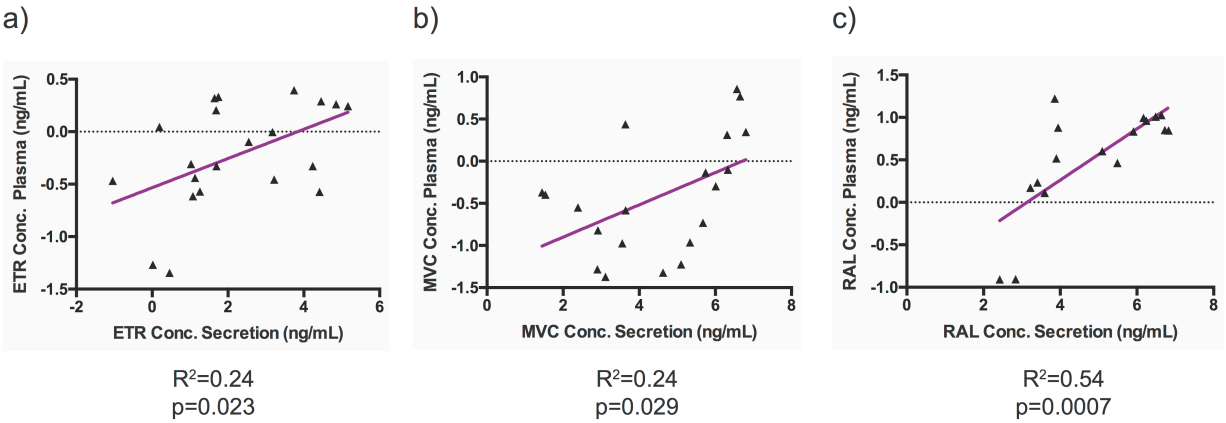

Figure 7.6: Correlations between vaginal secretion and blood plasma concentrations for ETR (a), MVC (b) and RAL (c). Data for timepoints between day 1 and day 14 for both dual layer and FIF formulations were $\log_{10}$ transformed and fit using linear regression. R^2 value indicates goodness of fit and p value indicates significance of a non-zero slope.

7.4.4 *A single dose of dual layer fibers results in high vaginal and cervical tissue concentrations of all three ARVs after just 1 hour and for up to 14 days*

We measured the concentration of ETR, MVC and RAL in cervical and vaginal tissues over the course of 14 days after a single dose of dual layer fibers to assess whether the fibers were capable of providing high enough concentrations of drug in the tissue to prevent RT-SHIV infection at the effector site. Despite much higher initial MVC and RAL concentrations compared to ETR concentration in vaginal secretions, the concentration of all three ARVs was ~10^6 ng/g after 1 hour (Figure 7.7). The maximum concentration for ETR and RAL in cervical tissue occurred after 2 hours, while MVC reached maximum concentration after 24 hours (Table 7.3). All three drugs reached maximum concentration in vaginal tissue after 24 hours. The maximum concentration in cervical tissue for all three drugs was equivalent (~10^6 ng/g) while in vaginal tissue, MVC and RAL reached a concentration of 3x10^6 ng/g compared to a 4-fold lower concentration of 7x10^5 ng/g for ETR. While the concentration of all three drugs peaked within 24 hours, they diminished to a concentration of ~10^3 ng/g by 48 hours. Between the 3 day and 24 day timepoints, ETR was maintained at a concentration of ~10^3 ng/g (Figure 7.7a), while

MVC and RAL experienced slight peaks again after 4 days, but falling to ~10^2 ng/g by day 14 (Figure 7.7, b-c). The AUC for MVC and RAL was ~2-fold the AUC for ETR in both cervical and vaginal tissue.

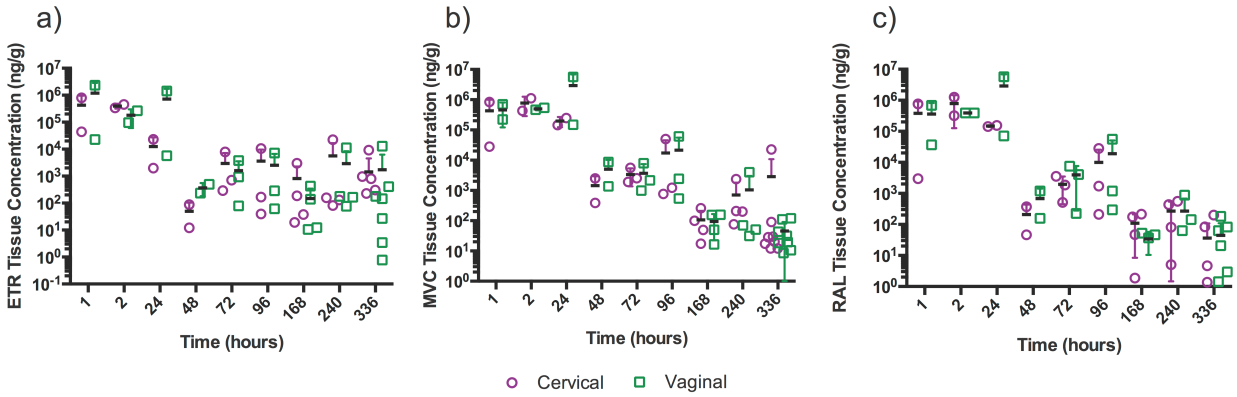

Figure 7.7: Concentration of ETR (a), MVC (b) and RAL (c) in cervical and vaginal tissue over 7 days after a single dose of dual layer fibers.

Table 7.3: Pharmacokinetic parameters of ETR, MVC and RAL in vaginal and cervical tissue after a single dose of the dual layer formulation.

	Cervical			Vaginal		
Drug	**T_{max}** (h)	**C_{max}** (ng/g)	**AUC_{1-14}** (ng*h/g)	**T_{max}** (h)	**C_{max}** (ng/g)	**AUC_{1-14}** (ng*h/g)
ETR	2	398,039	635,988	24	716,675	1,501,000
MVC	24	195,437	1,208,000	24	2,908,050	3,670,000
RAL	2	786,261	1,137,000	24	2,880,322	3,473,000

7.4.5 *A single dose of dual layer fibers prevents RT-SHIV infection in tissue biopsies for 24 hours*

We challenged vaginal and cervical biopsies of tissue that been treated with a single dose of dual layer fibers with RT-SHIV to assess the functional protective capabilities of the fibers over 7 days (Figure 7.8). We measured p27 SIV antigen in the culture media after 6 days for tissue that had been untreated (control) and tissue at various timepoints from 1 to 168 hours after a single dose of the dual

layer fiber formulation (Figure 7.8a). All of the untreated tissue biopsies were infected after 3 days, with an average of 1000 ng p27/g tissue after 6 days. The tissue biopsies that were excised one hour after fiber administration did not produce p27 after 6 days in culture. p27 production increased with time elapsed since fiber administration. For all samples that were challenged 72 hours or more after fiber administration, all biopsies became infected. These results are reflected in the survival curve (Figure 7.8b), which shows that 100% of the control becomes infected, while a single administration offers 100% protection after 1 hour and 75% protection after 2 hours. We then log transformed the p27 production and total drug concentration, and observed the correlation, to establish whether higher drug concentration in tissue correlated with a decrease in infectivity (Figure 7.8c). We found that an increase of each drug individually correlated with a decrease in p27 production ($p<0.0001$ for ETR, MVC and RAL) (data not shown). Similarly, we found that an increase in the total drug concentration (ETR + MVC + RAL) correlated inversely with p27 production ($R^2=0.61$ and $p<0.0001$). Overall, these results show that an increased concentration of drug in tissue correlates with less RT-SHIV infectivity in cervical and vaginal tissue, and that a single administration of dual layer fibers may be protective for 24 hours against challenge with RT-SHIV with a high viral load.

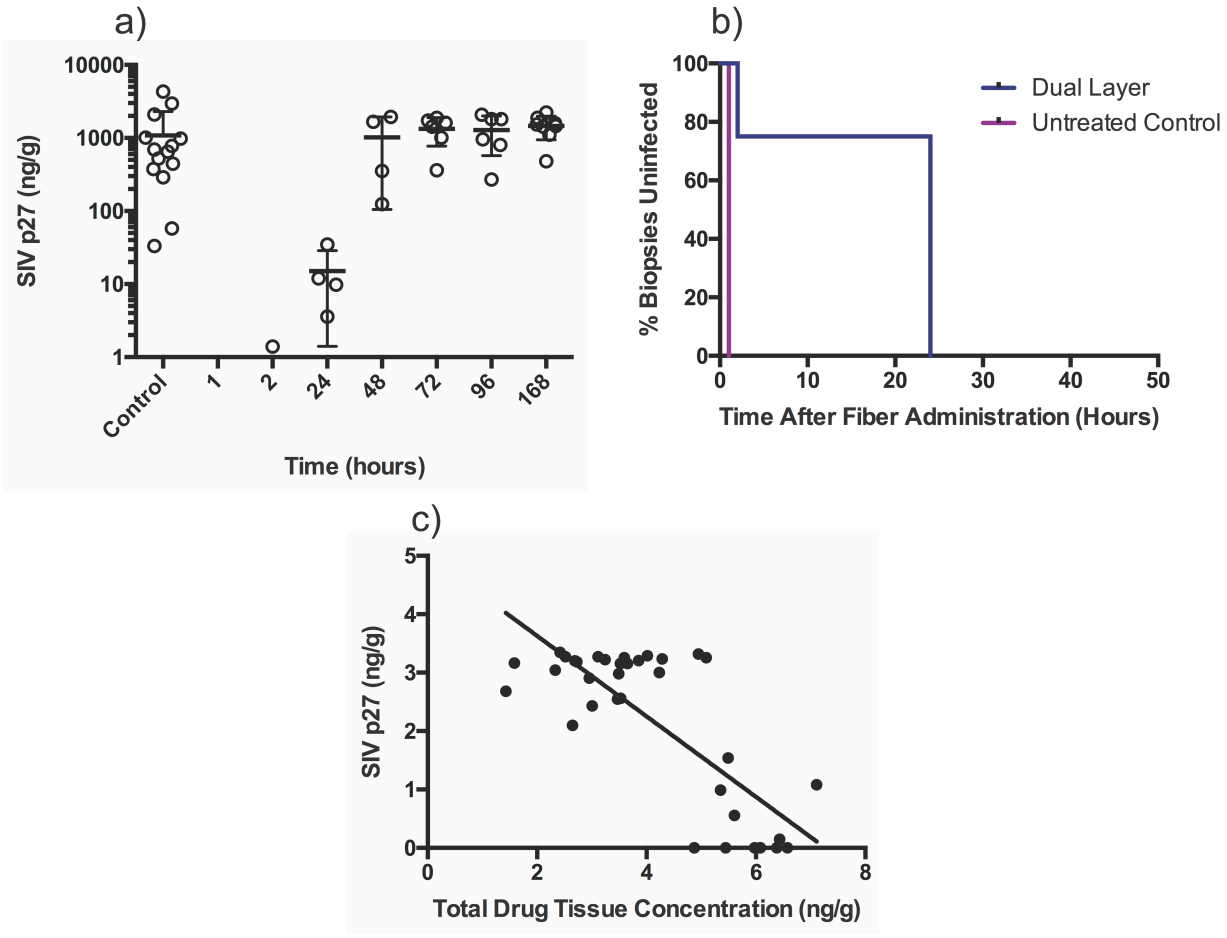

Figure 7.8: Infectivity of pigtail macaque cervical and vaginal biopsies after a single dose of dual layer fibers and subsequent challenge with RT-SHIV. a) SIV p27 production by cervical and vaginal tissue biopsies. Control represents cervical and vaginal tissue biopsies that were not exposed to fibers nor drugs. Line and error bars represents mean and standard deviation. b) Kaplan-Meier survival curves for untreated control (pink) and a single treatment of dual layer fibers (blue). Percent of biopsies uninfected was calculated by the total number of tissue samples that produced a measurable level of p27 compared to the total number of tissue samples at each timepoint. c) Correlation between log-transformed total drug tissue concentration (sum of ETR, MVC and RAL concentration in ng/g) and log p27 production by the corresponding biopsy.

7.5 DISCUSSION

Here, we studied the safety and pharmacokinetics of ETR, MVC, and RAL in vaginal secretions, tissue, and blood plasma over the course of two weeks after delivery by drug-eluting nanofibers. We

studied two novel microbicide formulations: dual-layer fibers containing ETR and MVC in one layer and RAL in the other, and the dual-layer fibers with encapsulated, drug-loaded, micronized fibers, deemed fibers-in-fibers. We observed that both formulations resulted in similar concentrations of ETR in vaginal secretions over time, but the dual layer fibers produced higher, more rapid concentrations of MVC and RAL, compared to more continuous, consistent concentrations with the FIF dosage. We found that a single dose of the dual layer fibers prevents RT-SHIV infection *ex vivo* for 24 hours.

The effective concentration of ETR, MVC, and RAL in vaginal tissue for prevention of HIV acquisition has not been previously defined for each individual drug, let alone the combination of all three. ETR, MVC, and RAL are potent antiretrovirals, with EC_{50} values of 1.4 nM,[266] 3.3 nM,[267] and 15 nM,[250] which make them ideal candidates for use in vaginal microbicides. A 30 mg dose of RAL alone, formulated in a vaginal gel, was found to protect macaques from SHIV infection when applied 3 hours after vaginal gel, although corresponding secretion and tissue concentrations were not quantified.[228] A gel formulation of 132 mg of MVC prevented SHIV infection with 100% efficacy when challenged 30 minutes after gel application, reaching tissue concentrations of ~1200 ng/g 24h after application.[242] In this study, we achieved a concentration of ETR, MVC *and* RAL that was ~800-fold higher in cervical and vaginal tissue after 24 hours, and maintain tissue concentrations similar to the reported protective concentration of MVC out to 14 days. A similar study, with a much lower dose of MVC (12 mg), prevented SHIV acquisition in 6/7 macaques when challenged 30 minutes after gel application.[268] ETR has not yet been investigated as a vaginal microbicide by itself. The combination of these drugs is of particular interest, as MVC was shown to have pre-exposure efficacy,[242, 268] while RAL has been shown to have post-exposure efficacy,[228] presenting for the potential of a product that could be used before or after coitus. However, formulating these three drugs into a single dosage form, whether liquid or solid, presents quite a challenge given that MVC and RAL are relatively water soluble, but ETR is highly water insoluble. Electrospun fibers have been shown to encapsulate, and co-encapsulate, antiretroviral drugs with a wide variety of water solubility,[4, 82, 106, 210, 260] allowing for formulation of multiple drugs into a single dose. In this study, we achieved high encapsulation efficiency (>90%) and drug distribution in

the scale-up of both the dual-layer and FIF formulations, further warranting the investigation of fibers as a vaginal microbicide.

There is increasing precedent for alternative dosage forms to those currently in the pipeline, including on-demand and long-acting prevention methods.[259] We found that both the dual layer and FIF formulations dissolved within 24 hours, upon colposcopy inspection. Despite the quick dissolution, all three drugs persisted in vaginal secretions for 14 days (Figure 7.4). This is a particularly powerful attribute of the fiber dosage form; it dissolves quickly but provides a local, imperceptible depot of drug for up to 14 days. However, this is only useful if the concentrations at the effector site, i.e. in vaginal secretions and tissue, are high enough to prevent HIV acquisition. We found that a tissue concentration of ~10^3 ng/g was present until 14 days. Using an *ex vivo* challenge assay with RT-SHIV, we found that cervical and vaginal biopsies were completely protected for 24 hours after a single administration of the dual layers fibers. The discrepancy between high concentrations of drug in tissue for 14 days and protection from RT-SHIV challenge may be due to exposure to a relatively high titer of virus ($5x10^4$ copies) for a small tissue biopsy (~5 mg). Dobard *et al*. used $1.5x10^6$ RNA copies of $SHIV_{SF162P3}$, a SIVmac239 backbone virus known to be less potent than RT-SHIV,[269] for *in vivo* challenge of the entire vaginal tract.[270] Because we measured tissue concentration of each drug, it is not possible to discern whether the drugs are located at the appropriate effector sites, either intracellularly (ETR, RAL) or extracellularly (MVC), although an inverse correlation with each drug and p27 production indicates that it is possible that each drug is protecting the tissue to some extent. It may also be possible to use secretion drug concentrations to inform protection windows and dosing strategies for vaginal microbicides. A post-hoc analysis of the CAPRISA 004 trial found that tenofovir (TFV) concentrations of >1000 ng/mL were correlated strongly with decreased HIV incidence.[241] While our drugs have different half-lives, partitioning properties, etc., than TFV, if we use 1000 ng/mL of drug as a benchmark, the dual layer formulation may protect from RT-SHIV/HIV infection up to 6 days, and the FIF formulation up to 9 days (Figure 7.4). The prolonged presence of drugs past the point of fiber

dissolution may be due to a functional, local depot wherein the fibers shift towards a mucoadhesive,[271, 272] gel-like state, and continue to release drugs.

There are many limitations associated with this study. Due to a limited number of animals, we did not evaluate the FIF formulation for tissue concentration, or the corresponding *ex vivo* challenge with RT-SHIV. Thus, it is still unknown if, and for how long, the FIF formulation may be effective against RT-SHIV. Furthermore, we did not use formulations of ETR, MVC, and RAL by themselves as controls. Therefore, we cannot claim which of the drugs are acting effectively, nor that there are synergistic benefits to using this combination. Finally, there are noted differences in the vaginal tissue of pigtail macaques and humans,[273] which may result in different pharmacokinetics and efficacy in human trials.

Our study offers new insight into the use of electrospun fibers for HIV prevention. This is the first time fiber formulations have been used as a quick-dissolving vaginal dosage form that is shown to protect against *ex vivo* RT-SHIV challenge for up to 14 days. Electrospun fibers are an elegant strategy to co-deliver antiretroviral drugs with varying solubility, and have the capacity to efficiently encapsulate a high drug loading. This study warrants further investigation into the use of fibers formulations, which completely dissolve within hours, to deliver high concentrations of antiretrovirals to tissue for days after a single dose.

7.6 Conclusion

We encapsulated ETR, MVC, and RAL, a potent combination of antiretrovirals with varying mechanisms of action, in two novel electrospun fibers, including dual layer and FIF formulations. After a single dose of either the dual layer fibers or FIF, all three drugs were detectable in the vaginal secretions of pigtail macaques after 14 days, although the dual layer formulation resulted in a higher, more rapid concentration of MVC and RAL, while the FIF formulation yielded a more consistent concentration of these drugs. The pharmacokinetics of ETR in secretions was similar for the two formulations, as were all three drugs in plasma. The dual layer and FIF dosages were observed to be safe, even given the high secretion concentrations observed after repeated dosing of the dual layer fibers.

There was a positive, significant correlation between the plasma and secretion concentrations after 24h, indicating good tissue penetration. Similarly, all drugs were detected in tissue out to 14 days, and *ex vivo* challenge of tissue biopsies with RT-SHIV showed that a single dose of dual layer fibers protected tissue from infection for 14 days. These results show the promise of drug-eluting fibers for local delivery of antiretroviral drug combinations for on-demand prevention of HIV.

7.7 FUTURE WORK

Given the promising results from the *in vivo* pharmacokinetic study of a single dose of the dual layer fibers, we plan to test the efficacy of this dosage form in a pigtail macaque challenge model. Similar vaginal, topical microbicides have identified a tissue concentration of MVC[242] or TFV[241] of ~10^3 ng/g to be protective against SHIV challenge. We observed tissue concentrations of ETR, MVC *and* RAL of ~10^3 ng/g for up to 14 days after a single administration of the dual layer fibers. If a fiber dosage containing this triple drug combination could prevent RT-SHIV infection for 14 days, this would highly impact the microbicide field and could potentially establish a useful new HIV prevention method for women. Our goal for the challenge study is to rigorously test the efficacy of the fibers against RT-SHIV infection, and to answer the following questions:

- Does a single administration of the dual layer fibers containing ETR, MVC and RAL prevent RT-SHIV infection when applied before or after viral challenge?
- Is there any protective effect from blank fibers?

We propose the following groups to probe the functional efficacy of the fibers against RT-SHIV infection:

Table 7.4: Proposed challenge schedule for efficacy study of dual layer fibers.

Group	Description	Challenge Timing	Number of NHPs
Positive control	No fibers	N/A	3
Blank fiber control	Single administration of fibers containing no drugs	1 hour after administration	3
Post-exposure	Single administration of fibers containing ETR, MVC and RAL	1 hour after administration	6
Pre-exposure	Single administration of fibers containing ETR, MVC and RAL	1 hour before administration	6
Late pre-exposure	Single administration of fibers containing ETR, MVC and RAL	72 hours after administration	6
		Total animals	**24**

Because we will challenge each animal a single time, we will use a high dose of RT-SHIV, as opposed to repeating, low doses. We propose to use a similar challenge model as Malcolm et al., which consisted of a dose of 500 $TCID_{50}$ of RT-SHIV,[242] which is an order of magnitude higher than the doses used by Dobard et al. and Smith et al.[228, 274] The primary outcome of this study is RT-SHIV infection as monitored by RT-PCR in blood samples taken for up to 60 days after challenge.

REFERENCES

1. UNAIDS *Global Report on the AIDS Epidemic*; 2013.
2. Boily, M. C.; Baggaley, R. F.; Wang, L.; Masse, B.; White, R. G.; Hayes, R.; Alary, M. Heterosexual risk of HIV-1 infection per sexual act: systematic review and meta-analysis of observational studies. *The Lancet infectious diseases* **2009,** *9*, 118-129.
3. Charlotte, W.; Peter, V. The impact of microbicides on HIV and STD transmission: model projections. *AIDS* **2001**.
4. Ball, C.; Krogstad, E.; Chaowanachan, T.; Woodrow, K. Drug-Eluting Fibers for HIV-1 Inhibition and Contraception. *PloS one* **2012,** *7*, (11).
5. Huang, C.; Soenen, S.; van Gulck, E.; Vanham, G.; Rejman, J.; Van Calenbergh, S.; Vervaet, C.; Coenye, T.; Verstraelen, H.; Temmerman, M.; Demeester, J.; De Smedt, S. Electrospun cellulose acetate phthalate fibers for semen induced anti-HIV vaginal drug delivery. *Biomaterials* **2012,** *33*, (3), 962-969.
6. Marrazzo, J.; Ramjee, G.; Nair, G. In *Pre-exposure prophylaxis for HIV in women: daily oral tenofovir, oral tenofovir/emtricitabine or vaginal tenofovir gel in the VOICE study (MTN 003)*, 20th Conference on Retroviruses and Opportunistic Infections, Atlanta, GA, March 3-6, 2013, 2013; Atlanta, GA.
7. Abdool Karim, Q.; Abdool Karim, S.; Frohlich, J.; Grobler, A.; Baxter, C.; Mansoor, L.; Kharsany, A.; Sibeko, S.; Mlisana, K.; Omar, Z.; Gengiah, T.; Maarschalk, S.; Arulappan, N.; Mlotshwa, M.; Morris, L.; Taylor, D.; Group, C. T. Effectiveness and safety of tenofovir gel, an antiretroviral microbicide, for the prevention of HIV infection in women. *Science (New York, N.Y.)* **2010,** *329*, (5996), 1168-1174.
8. Akil, A.; Parniak, M.; Dezzuitti, C.; Moncla, B.; Cost, M.; Li, M.; Rohan, L. Development and Characterization of a Vaginal Film Containing Dapivirine, a Non- nucleoside Reverse Transcriptase Inhibitor (NNRTI), for prevention of HIV-1 sexual transmission. *Drug Delivery and Translational Research* **2011,** *1*, (3), 209-222.
9. Malcolm, R.; Edwards, K.-L.; Kiser, P.; Romano, J.; Smith, T. Advances in microbicide vaginal rings. *Antiviral research* **2010,** *88 Suppl 1*, 9.
10. Garg, S.; Goldman, D.; Krumme, M.; Rohan, L.; Smoot, S.; Friend, D. Advances in development, scale-up and manufacturing of microbicide gels, films, and tablets. *Antiviral research* **2010,** *88 Suppl 1*, 29.
11. Garg, S.; Kandarapu, R.; Vermani, K.; Tambwekar, K.; Garg, A.; Waller, D.; Zaneveld, L. Development pharmaceutics of microbicide formulations. Part I: preformulation considerations and challenges. *AIDS patient care and STDs* **2003,** *17*, (1), 17-32.
12. Sassi, A.; Cost, M.; Cole, A.; Patton, D.; Gupta, P.; Rohan, L. Formulation development of retrocyclin 1 analog RC-101 as an anti-HIV vaginal microbicide product. *Antimicrobial agents and chemotherapy* **2011,** *55*, (5), 2282-2289.
13. Mahalingam, A.; Simmons, A.; Ugaonkar, S.; Watson, K.; Dezzutti, C.; Rohan, L.; Buckheit, R.; Kiser, P. Vaginal microbicide gel for delivery of IQP-0528, a pyrimidinedione analog with a dual mechanism of action against HIV-1. *Antimicrobial agents and chemotherapy* **2011,** *55*, (4), 1650-1660.
14. Schiffman, J. D.; Schauer, C. L. A Review: Electrospinning of Biopolymer Nanofibers and their Applications. *Polymer Reviews* **2008,** *48*.
15. Taepaiboon, P.; Rungsardthong, U.; Supaphol, P. Drug-loaded electrospun mats of poly (vinyl alcohol) fibres and their release characteristics of four model drugs. *Nanotechnology* **2006,** *17*, (9), 2317.
16. Agarwal, S.; Wendorff, J. H.; Greiner, A. Use of electrospinning technique for biomedical applications. *Polymer* **2008,** *49*, (26), 5603-5621.

17. Zeng, J.; Xu, X.; Chen, X.; Liang, Q.; Bian, X.; Yang, L.; Jing, X. Biodegradable electrospun fibers for drug delivery. *Journal of controlled release : official journal of the Controlled Release Society* **2003,** *92*, (3), 227-231.
18. Theron, S. A.; Yarin, A. L.; Zussman, E.; Kroll, E. Multiple jets in electrospinning: experiment and modeling. *Polymer* **2005,** *46*.
19. Vaz, C.; van Tuijl, S.; Bouten, C.; Baaijens, F. Design of scaffolds for blood vessel tissue engineering using a multi-layering electrospinning technique. *Acta Biomaterialia* **2005,** *1*, (5), 575-582.
20. Jiang, H.; Hu, Y.; Li, Y.; Zhao, P.; Zhu, K.; Chen, W. A facile technique to prepare biodegradable coaxial electrospun nanofibers for controlled release of bioactive agents. *Journal of controlled release : official journal of the Controlled Release Society* **2005,** *108*, (2-3), 237-243.
21. Xu, X.; Zhuang, X.; Chen, X.; Wang, X.; Yang, L.; Jing, X. Preparation of Core-Sheath Composite Nanofibers by Emulsion Electrospinning. *Macromolecular Rapid Communications* **2006,** *27*.
22. Cui, W.; Li, X.; Zhu, X.; Yu, G.; Zhou, S.; Weng, J. Investigation of drug release and matrix degradation of electrospun poly(DL-lactide) fibers with paracetanol inoculation. *Biomacromolecules* **2006,** *7*, (5), 1623-1629.
23. Chew, S.; Wen, J.; Yim, E.; Leong, K. Sustained release of proteins from electrospun biodegradable fibers. *Biomacromolecules* **2005,** *6*, (4), 2017-2024.
24. Frenot, R.; Ioannis, S. C. Polymer nanofibers assembled by electrospinning. *Current Opinion in Colloid & Interface Science* **2003,** *8*.
25. Richardson, J. L.; Illum, L. (D) Routes of delivery: Case studies. *Advanced drug delivery reviews* **1992,** *8*.
26. Prabaharan, M.; Jayakumar, R.; Nair, S. Electrospun nanofibrous scaffolds-current status and prospects in drug delivery. *Springer* **2012**, 241-262.
27. Verreck, G.; Chun, I.; Peeters, J.; Rosenblatt, J.; Brewster, M. Preparation and characterization of nanofibers containing amorphous drug dispersions generated by electrostatic spinning. *Pharmaceutical research* **2003,** *20*, (5), 810-817.
28. Yu, D.-G.; Branford-White, C.; Shen, X.-X.; Zhang, X.-F.; ZhuZhu, L.-M. Solid Dispersions of Ketoprofen in Drug-Loaded Electrospun Nanofibers. *Journal of Dispersion Science and Technology* **2010,** *31*.
29. Wang, Y.; Hsieh, Y. Immobilization of lipase enzyme in polyvinyl alcohol (PVA) nanofibrous membranes. *Journal of Membrane Science* **2008,** *309*, (1), 73-81.
30. Liao, I.; Chen, S.; Liu, J. B.; Leong, K. W. Sustained viral gene delivery through core-shell fibers. *Journal of Controlled Release* **2009,** *139*, (1), 48-55.
31. Saraf, A.; Baggett, L.; Raphael, R.; Kasper, F.; Mikos, A. Regulated non-viral gene delivery from coaxial electrospun fiber mesh scaffolds. *Journal of controlled release : official journal of the Controlled Release Society* **2010,** *143*, (1), 95-103.
32. Cao, H.; Jiang, X.; Chai, C.; Chew, S. RNA interference by nanofiber-based siRNA delivery system. *Journal of controlled release : official journal of the Controlled Release Society* **2010,** *144*, (2), 203-212.
33. Lopez-Rubio, A.; Sanchez, E.; Sanz, Y.; Lagaron, J. Encapsulation of living bifidobacteria in ultrathin PVOH electrospun fibers. *Biomacromolecules* **2009,** *10*, (10), 2823-2829.
34. Townsend-Nicholson, A.; Jayasinghe, S. Cell electrospinning: a unique biotechnique for encapsulating living organisms for generating active biological microthreads/scaffolds. *Biomacromolecules* **2006,** *7*, (12), 3364-3369.
35. Maretschek, S.; Greiner, A.; Kissel, T. Electrospun biodegradable nanofiber nonwovens for controlled release of proteins. *Journal of controlled release : official journal of the Controlled Release Society* **2008,** *127*, (2), 180-187.
36. Patel, S.; Kurpinski, K.; Quigley, R.; Gao, H.; Hsiao, B.; Poo, M.-M.; Li, S. Bioactive nanofibers: synergistic effects of nanotopography and chemical signaling on cell guidance. *Nano letters* **2007,** *7*, (7), 2122-2128.

37. Beck-Broichsitter, M.; Thieme, M.; Nguyen, J.; Schmehl, T.; Gessler, T.; Seeger, W.; Agarwal, S.; Greiner, A.; Kissel, T. Novel 'nano in nano' composites for sustained drug delivery: biodegradable nanoparticles encapsulated into nanofiber non-wovens. *Macromolecular bioscience* **2010,** *10*, (12), 1527-1535.
38. Volpato, Z. F.; Almodovar, J.; Erickson, K.; Popat, K.; Migliaresi, C.; Kipper, M. Preservation of FGF-2 bioactivity using heparin-based nanoparticles, and their delivery from electrospun chitosan fibers. *Acta Biomaterialia* **2012,** *8*, (4), 1551-1559.
39. Sinha Roy, D.; Rohera, B. Comparative evaluation of rate of hydration and matrix erosion of HEC and HPC and study of drug release from their matrices. *European journal of pharmaceutical sciences : official journal of the European Federation for Pharmaceutical Sciences* **2002,** *16*, (3), 193-199.
40. Donbrow, M.; Friedman, M. Timed release from polymeric films containing drugs and kinetics of drug release. *Journal of pharmaceutical sciences* **1975,** *64*, (1), 76-80.
41. Woolfson, A.; Malcolm, R.; Morrow, R.; Toner, C.; McCullagh, S. Intravaginal ring delivery of the reverse transcriptase inhibitor TMC 120 as an HIV microbicide. *International journal of pharmaceutics* **2006,** *325*, (1-2), 82-89.
42. Luong-Van, E.; Grondahl, L.; Chua, K.; Leong, K.; Nurcombe, V.; Cool, S. Controlled release of heparin from poly(epsilon-caprolactone) electrospun fibers. *Biomaterials* **2006,** *27*, (9), 2042-2050.
43. Li, X.; Kanjwal, M.; Lin, L.; Chronakis, I. Electrospun polyvinyl-alcohol nanofibers as oral fast-dissolving delivery system of caffeine and riboflavin. *Colloids and surfaces. B, Biointerfaces* **2013,** *103*, 182-188.
44. Macri, L.; Sheihet, L.; Singer, A.; Kohn, J.; Clark, R. Ultrafast and fast bioerodible electrospun fiber mats for topical delivery of a hydrophilic peptide. *Journal of controlled release : official journal of the Controlled Release Society* **2012,** *161*, (3), 813-820.
45. Feng-Lei, Z.; Rong-Hua, G.; Isaac, P. Mass production of nanofibre assemblies by electrostatic spinning. *Polymer International* **2009,** *58*.
46. Kim, K.; Luu, Y.; Chang, C.; Fang, D.; Hsiao, B.; Chu, B.; Hadjiargyrou, M. Incorporation and controlled release of a hydrophilic antibiotic using poly(lactide-co-glycolide)-based electrospun nanofibrous scaffolds. *Journal of controlled release : official journal of the Controlled Release Society* **2004,** *98*, (1), 47-56.
47. Forward, K. M.; Rutledge, G. C. Free surface electrospinning from a wire electrode. *Chemical Engineering Journal* **2012,** *183*, 492-503.
48. Xu, X.; Chen, X.; Xu, X.; Lu, T.; Wang, X.; Yang, L.; Jing, X. BCNU-loaded PEG¬ñPLLA ultrafine fibers and their in vitro antitumor activity against glioma C6 cells. *Journal of Controlled Release* **2006,** *114*, (3), 307-316.
49. Jannesari, M.; Varshosaz, J.; Morshed, M.; Zamani, M. Composite poly(vinyl alcohol)/poly(vinyl acetate) electrospun nanofibrous mats as a novel wound dressing matrix for controlled release of drugs. *International journal of nanomedicine* **2011,** *6*, 993-1003.
50. Persano, L.; Camposeo, A.; Tekmen, C.; Pisignano, D. Industrial Upscaling of Electrospinning and Applications of Polymer Nanofibers: A Review. *Macromolecular Materials and Engineering* **2013,** *298*.
51. Xie, J.; Wang, C.-H. Electrospun micro- and nanofibers for sustained delivery of paclitaxel to treat C6 glioma in vitro. *Pharmaceutical research* **2006,** *23*, (8), 1817-1826.
52. Yohe, S.; Colson, Y.; Grinstaff, M. Superhydrophobic materials for tunable drug release: using displacement of air to control delivery rates. *Journal of the American Chemical Society* **2012,** *134*, (4), 2016-2019.
53. Chunder, A.; Sarkar, S.; Yu, Y.; Zhai, L. Fabrication of ultrathin polyelectrolyte fibers and their controlled release properties. *Colloids and surfaces. B, Biointerfaces* **2007,** *58*, (2), 172-179.
54. Li, J.; Feng, H.; He, J.; Li, C.; Mao, X.; Xie, D.; Ao, N.; Chu, B. Coaxial electrospun zein nanofibrous membrane for sustained release. *Journal of biomaterials science. Polymer edition* **2013**.

55. El-Refaie, K.; Fouad, I. A.-H.; Mohamed, H. E.-N.; Gary, E. W. Controlled release of ketoprofen from electrospun poly(vinyl alcohol) nanofibers. *Materials Science and Engineering: A* **2007,** *459*.
56. Center for Drug Evaluation and Research: Inactive Ingredient Database. **2015**.
57. Qian, F.; Huang, J.; Hussain, M. A. Drug–polymer solubility and miscibility: stability consideration and practical challenges in amorphous solid dispersion development. *Journal of pharmaceutical sciences* **2010,** *99*, (7), 2941.
58. Verreck, G.; Chun, I.; Rosenblatt, J.; Peeters, J.; Dijck, A.; Mensch, J.; Noppe, M.; Brewster, M. E. Incorporation of drugs in an amorphous state into electrospun nanofibers composed of a water-insoluble, nonbiodegradable polymer. *Journal of Controlled Release* **2003,** *92*, (3), 349360.
59. Peng, H.; Zhou, S.; Guo, T.; Li, Y.; Li, X.; Wang, J.; Weng, J. In vitro degradation and release profiles for electrospun polymeric fibers containing paracetanol. *Colloids and Surfaces B: Biointerfaces* **2008,** *66*, (2), 206-212.
60. Holan, V.; Chudickova, M.; Trosan, P.; Svobodova, E.; Krulova, M.; Kubinova, S.; Sykova, E.; Sirc, J.; Michalek, J.; Juklickova, M.; Munzarova, M.; Zajicova, A. Cyclosporine A-loaded and stem cell-seeded electrospun nanofibers for cell-based therapy and local immunosuppression. *Journal of Controlled Release* **2011,** *156*, 406-412.
61. Chen, D. W.; Liao, J.-Y. Y.; Liu, S.-J. J.; Chan, E.-C. C. Novel biodegradable sandwich-structured nanofibrous drug-eluting membranes for repair of infected wounds: an in vitro and in vivo study. *International journal of nanomedicine* **2012,** *7*, 763-771.
62. Falde, E. J.; Freedman, J. D.; Herrera, V. L.; Yohe, S. T.; Colson, Y. L.; Grinstaff, M. W. Layered superhydrophobic meshes for controlled drug release. *Journal of controlled release : official journal of the Controlled Release Society* **2015,** *214*, 23-29.
63. Gilchrist, S. E.; Lange, D.; Letchford, K.; Bach, H. Fusidic acid and rifampicin co-loaded PLGA nanofibers for the prevention of orthopedic implant associated infections. *Journal of Controlled Release* **2013,** *170*, 64-73.
64. Heunis, T. D. J.; Smith, C.; Dicks, L. M. T. Evaluation of a nisin-eluting nanofiber scaffold to treat Staphylococcus aureus-induced skin infections in mice. *Antimicrobial agents and chemotherapy* **2013,** *57*, (8), 3298-3935.
65. Hong, Y.; Fujimoto, K.; Hashizume, R.; Guan, J.; Stankus, J. J.; Tobita, K.; Wagner, W. R. Generating elastic, biodegradable polyurethane/poly(lactide-co-glycolide) fibrous sheets with controlled antibiotic release via two-stream electrospinning. *Biomacromolecules* **2008,** *9*, (4), 1200-1207.
66. Karthikeyan, K.; Guhathakarta, S.; Rajaram, R.; Korrapati, P. S. Electrospun zein/eudragit nanofibers based dual drug delivery system for the simultaneous delivery of aceclofenac and pantoprazole. *International journal of pharmaceutics* **2012,** *438*, 117-122.
67. Luo, X.; Xie, C.; Wang, H.; Liu, C.; Yan, S.; Li, X. Antitumor activities of emulsion electrospun fibers with core loading of hydroxycamptothecin via intratumoral implantation. *International journal of pharmaceutics* **2012,** *425*, 19-28.
68. Motealleh, B.; Zahedi, P.; Rezaeian, I.; Moghimi, M.; Abdolghaffari, A. H.; Zarandi, M. A. Morphology, drug release, antibacterial, cell proliferation, and histology studies of chamomile-loaded wound dressing mats based on electrospun nanofibrous poly (ε-caprolactone)/polystyrene blends. *Journal of Biomedical Materials Research Part B: Applied Biomaterials* **2014,** *102B*, 977-987.
69. Phipps, M. C.; Clem, W. C.; Grunda, J. M.; Clines, G. A.; Bellis, S. L. Increasing the pore sizes of bone-mimetic electrospun scaffolds comprised of polycaprolactone, collagen I and hydroxyapatite to enhance cell infiltration. *Biomaterials* **2012,** *33*, (2), 524-534.
70. Rujitanaroj, P. O.; Aid-Launais, R.; Chew, S. Y.; Le Visage, C. Polysaccharide electrospun fibers with sulfated poly (fucose) promote endothelial cell migration and VEGF-mediated angiogenesis. *Biomaterials Science* **2014,** *2*, 843.
71. Schulz, S.; Angarano, M.; Fabritius, M.; Mülhaupt, R.; Dard, M.; Obrecht, M.; Tomakidi, P.; Steinberg, T. Nonwoven-based gelatin/polycaprolactone membrane proves suitability in a preclinical assessment for treatment of soft tissue defects. *Tissue engineering. Part A* **2014,** *20*, (13-14), 1935-1947.

72. Tseng, Y.-Y.; Kao, Y.-C.; Liao, J.-Y.; Chen, W.-A.; Liu, S.-J. Biodegradable Drug-Eluting Poly[lactic-co-glycol acid] Nanofibers for the Sustainable Delivery of Vancomycin to Brain Tissue: In Vitro and in Vivo Studies. *ACS Chemical Neuroscience* **2013,** *4*, (9), 1314-1321.
73. Uppal, R.; Ramaswamy, G. N.; Arnold, C.; Goodband, R.; Wang, Y. Hyaluronic acid nanofiber wound dressing—production, characterization, and in vivo behavior. *Journal of Biomedical Materials Research Part B: Applied Biomaterials* **2011,** *97B*, (1), 20-29.
74. Weldon, C. B.; Tsui, J. H.; Shankarappa, S. A.; Nguyen, V. T.; Ma, M.; Anderson, D. G.; Kohane, D. S. Electrospun drug-eluting sutures for local anesthesia. *Journal of Controlled Release* **2012,** *161*, (3), 903-909.
75. Yang, G.; Wang, J.; Wang, Y.; Li, L.; Guo, X.; Zhou, S. An implantable active-targeting micelle-in-nanofiber device for efficient and safe cancer therapy. *ACS nano* **2015,** *9*, (2), 1161-1174.
76. Yang, H.; Kim, S.; Huh, I.; Kim, S.; Lahiji, S. F.; Kim, M.; Jung, H. Rapid implantation of dissolving microneedles on an electrospun pillar array. *Biomaterials* **2015,** *64*, 70-77.
77. Yosefifard, M.; Hassanpour-Ezatti, M. Epidural administration of neostigmine-loaded nanofibers provides extended analgesia in rats. *DARU Journal of Pharmaceutical Sciences* **2014,** *22*, (1), 1.
78. Zhu, Y.; Wang, A.; Patel, S.; Kurpinski, K.; Diao, E.; Bao, X.; Kwong, G.; Young, W. L.; Li, S. Engineering bi-layer nanofibrous conduits for peripheral nerve regeneration. *Tissue engineering. Part C, Methods* **2011,** *17*, (7), 705-715.
79. Huang, L. F.; Tong, W. Q. T. Impact of solid state properties on developability assessment of drug candidates. *Advanced drug delivery reviews* **2004,** *56*, 321-334.
80. Nagy, Z. K.; Balogh, A.; Vajna, B.; Farkas, A.; Patyi, G.; Kramarics, A.; Marosi, G. Comparison of electrospun and extruded Soluplus®-based solid dosage forms of improved dissolution. *Journal of pharmaceutical sciences* **2012,** *101*, (1), 322-332.
81. Kim, T. G.; Lee, D. S.; Park, T. G. Controlled protein release from electrospun biodegradable fiber mesh composed of poly(epsilon-caprolactone) and poly(ethylene oxide). *International journal of pharmaceutics* **2007,** *338*, (1-2), 276-283.
82. Krogstad, E. A.; Woodrow, K. A. Manufacturing scale-up of electrospun poly(vinyl alcohol) fibers containing tenofovir for vaginal drug delivery. *International Journal of Pharmaceutics* **2014,** *475*, (1–2), 282-291.
83. Sill, T.; von Recum, H. Electrospinning: applications in drug delivery and tissue engineering. *Biomaterials* **2008,** *29*, (13), 1989-2006.
84. Silva, S.; Rueda, L.; Marquez, G.; Lopez, M.; Smith, D.; Calderon, C.; Castillo, J.; Matute, J.; Rueda-Clausen, C.; Orduz, A.; Silva, F.; Kampeerapappun, P.; Bhide, M.; Lopez-Jaramillo, P. Double blind, randomized, placebo controlled clinical trial for the treatment of diabetic foot ulcers, using a nitric oxide releasing patch: PATHON. *Trials* **2007,** *8*, 26.
85. Ranganath, S.; Wang, C.-H. Biodegradable microfiber implants delivering paclitaxel for post-surgical chemotherapy against malignant glioma. *Biomaterials* **2008,** *29*, (20), 2996-3003.
86. Hong, Y.; Fujimoto, K.; Hashizume, R.; Guan, J.; Stankus, J.; Tobita, K.; Wagner, W. Generating elastic, biodegradable polyurethane/poly(lactide-co-glycolide) fibrous sheets with controlled antibiotic release via two-stream electrospinning. *Biomacromolecules* **2008,** *9*, (4), 1200-1207.
87. Nel, A.; Mitchnick, L.; Risha, P.; Muungo, L.; Norick, P. Acceptability of vaginal film, soft-gel capsule, and tablet as potential microbicide delivery methods among African women. *Journal of women's health (2002)* **2011,** *20*, (8), 1207-1214.
88. Luo, C.; Stoyanov, S.; Stride, E.; Pelan, E.; Edirisinghe, M. Electrospinning versus fibre production methods: from specifics to technological convergence. *Chemical Society reviews* **2012,** *41*, (13), 4708-4735.
89. Blakeney, B. A.; Tambralli, A.; Anderson, J. M.; Andukuri, A.; Lim, D.-J.; Dean, D. R.; Jun, H.-W. Cell infiltration and growth in a low density, uncompressed three-dimensional electrospun nanofibrous scaffold. *Biomaterials* **2011,** *32*, (6), 1583-1590.

90. Brettmann, B. K.; Cheng, K.; Myerson, A. S.; Trout, B. L. Electrospun formulations containing crystalline active pharmaceutical ingredients. *Pharmaceutical research* **2013,** *30*, 238-246.
91. Brettmann, B. K.; Tsang, S.; Forward, K. M.; Rutledge, G. C.; Myerson, A. S.; Trout, B. L. Free surface electrospinning of fibers containing microparticles. *Langmuir* **2012,** *28*, (25), 9714-9721.
92. Edmondson, D.; Cooper, A.; Jana, S.; Wood, D.; Zhang, M. Centrifugal electrospinning of highly aligned polymer nanofibers over a large area. *Journal of Materials Chemistry* **2012,** *22*, (35), 18646-18652.
93. Erickson, A. E.; Edmondson, D.; Chang, F.-C.; Wood, D.; Gong, A.; Levengood, S. L.; Zhang, M. High-throughput and high-yield fabrication of uniaxially-aligned chitosan-based nanofibers by centrifugal electrospinning. *Carbohydrate polymers* **2015,** *134*, 467-474.
94. Fang, J.; Zhang, L.; Sutton, D.; Wang, X.; Lin, T. Needleless melt-electrospinning of polypropylene nanofibres. *J. Nanomaterials* **2012,** *2012*, 1-9.
95. Forward, K. M.; Flores, A.; Rutledge, G. C. Production of core/shell fibers by electrospinning from a free surface. *Chemical Engineering Science* **2013,** *104*, 250-259.
96. Hayes, T. R.; Hosie, I. C., Turning Nanofibres into Products: Electrospinning from a Manufacturer's Perspective. In *Electrospinning for High Performance Sensors*, Macagnano, A.; Zampetti, E.; Kny, E., Eds. Springer International Publishing: Cham, 2015; pp 305-329.
97. Jayasinghe, S. N. Cell electrospinning: a novel tool for functionalising fibres, scaffolds and membranes with living cells and other advanced materials for regenerative biology and medicine. *Analyst* **2013,** *138*, (8), 2215-2223.
98. Jiang, H.; Wang, L.; Zhu, K. Coaxial electrospinning for encapsulation and controlled release of fragile water-soluble bioactive agents. *Journal of controlled release : official journal of the Controlled Release Society* **2014,** *193*, 296-303.
99. Li, D.; Wu, T.; He, N.; Wang, J.; Chen, W.; He, L.; Huang, C.; Ei-Hamshary, H. A.; Al-Deyab, S. S.; Ke, Q.; Mo, X. Three-dimensional polycaprolactone scaffold via needleless electrospinning promotes cell proliferation and infiltration. *Colloids and Surfaces B: Biointerfaces* **2014,** *121*, 432-443.
100. Liu, S.-L.; Long, Y.-Z.; Zhang, Z.-H.; Zhang, H.-D.; Sun, B.; Zhang, J.-C.; Han, W.-P. Assembly of oriented ultrafine polymer fibers by centrifugal electrospinning. *Journal of Nanomaterials* **2013,** *2013*, (2514103), 8.
101. Luo, C. J.; Stoyanov, S. D.; Stride, E.; Pelan, E.; Edirisinghe, M. Electrospinning versus fibre production methods: from specifics to technological convergence. *Chemical Society reviews* **2012,** *41*, (13), 4708-4735.
102. Mary, L. A.; Senthilram, T.; Suganya, S.; Nagarajan, L.; Venugopal, J.; Ramakrishna, S.; Giri Dev, V. Centrifugal spun ultrafine fibrous web as a potential drug delivery vehicle. *eXPRESS Polym. Lett* **2013,** *7*, (3), 238-248.
103. Petrik, S.; Maly, M. In *Production Nozzle-Less Electrospinning Nanofiber Technology*, MRS Fall Meeting, 2009; Materials Research Society.
104. Qiu, Y.; Yu, J.; Rafique, J.; Yin, J.; Bai, X.; Wang, E. Large-scale production of aligned long boron nitride nanofibers by multijet/multicollector electrospinning. *The Journal of Physical Chemistry C* **2009,** *113*, (26), 11228-11234.
105. Yarin, A. L.; Zussman, E. Upward needleless electrospinning of multiple nanofibers. *Polymer* **2004,** *45*, (9), 2977-2980.
106. Blakney, A. K.; Krogstad, E. A.; Jiang, Y. H.; Woodrow, K. A. Delivery of multipurpose prevention drug combinations from electrospun nanofibers using composite microarchitectures. *International journal of nanomedicine* **2014,** *9*, 2967-2978.
107. Brettmann, B. K.; Cheng, K.; Myerson, A. S.; Trout, B. L. Electrospun formulations containing crystalline active pharmaceutical ingredients. *Pharmaceutical research* **2013,** *30*, (1), 238-46.
108. Brettmann, B. K.; Tsang, S.; Forward, K. M.; Rutledge, G. C.; Myerson, A. S.; Trout, B. L. Free surface electrospinning of fibers containing microparticles. *Langmuir : the ACS journal of surfaces and colloids* **2012,** *28*, (25), 9714-21.

109. Wang, X.; Wang, X.; Lin, T. Electric field analysis of spinneret design for needleless electrospinning of nanofibers. *Journal of Materials Research* **2012,** *27*, (23), 3013.
110. Krogstad, E. A.; Woodrow, K. A. Manufacturing scale-up of electrospun poly(vinyl alcohol) fibers containing tenofovir for vaginal drug delivery. *International journal of pharmaceutics* **2014,** *475*, (1-2), 282-91.
111. Lu, B.; Wang, Y.; Liu, Y.; Duan, H.; Zhou, J.; Zhang, Z.; Wang, Y.; Li, X.; Wang, W.; Lan, W.; Xie, E. Superhigh-throughput needleless electrospinning using a rotary cone as spinneret. *Small* **2010,** *6*, (15), 1612-6.
112. Fang, J.; Zhang, L.; Sutton, D.; Wang, X.; Lin, T. Needleless Melt-Electrospinning of Polypropylene Nanofibres. *Journal of Nanomaterials* **2012,** *2012*, 1-9.
113. Wang, X.; Niu, H.; Wang, X.; Lin, T. Needleless Electrospinning of Uniform Nanofibers Using Spiral Coil Spinnerets. *Journal of Nanomaterials* **2012,** *2012*, 1-9.
114. Forward, K. M.; Rutledge, G. C. Free surface electrospinning from a wire electrode. *Chemical Engineering Journal* **2012,** *183*.
115. Mayer, L.; Janoff, A. Optimizing combination chemotherapy by controlling drug ratios. *Molecular interventions* **2007,** *7*, (4), 216-223.
116. Sosnik, A.; Chiappetta, D.; Carcaboso, A. Drug delivery systems in HIV pharmacotherapy: what has been done and the challenges standing ahead. *Journal of controlled release : official journal of the Controlled Release Society* **2009,** *138*, (1), 2-15.
117. Wu, P.; Grainger, D. Drug/device combinations for local drug therapies and infection prophylaxis. *Biomaterials* **2006,** *27*, (11), 2450-2467.
118. Greco, F.; Vicent, M. a. Combination therapy: opportunities and challenges for polymer-drug conjugates as anticancer nanomedicines. *Advanced drug delivery reviews* **2009,** *61*, (13), 1203-1213.
119. Sengupta, S.; Eavarone, D.; Capila, I.; Zhao, G.; Watson, N.; Kiziltepe, T.; Sasisekharan, R. Temporal targeting of tumour cells and neovasculature with a nanoscale delivery system. *Nature* **2005,** *436*, (7050), 568-572.
120. Zhang, L.; Radovic-Moreno, A.; Alexis, F.; Gu, F.; Basto, P.; Bagalkot, V.; Jon, S.; Langer, R.; Farokhzad, O. Co-delivery of hydrophobic and hydrophilic drugs from nanoparticle-aptamer bioconjugates. *ChemMedChem* **2007,** *2*, (9), 1268-1271.
121. Zhang, Y.; Wang, X.; Feng, Y.; Li, J.; Lim, C.; Ramakrishna, S. Coaxial electrospinning of (fluorescein isothiocyanate-conjugated bovine serum albumin)-encapsulated poly(epsilon-caprolactone) nanofibers for sustained release. *Biomacromolecules* **2006,** *7*, (4), 1049-1057.
122. Friend, D.; Doncel, G. Combining prevention of HIV-1, other sexually transmitted infections and unintended pregnancies: Development of dual-protection technologies. *Antiviral research* **2010,** *88 Suppl 1*, 54.
123. De Clercq, E. Acyclic nucleoside phosphonates: past, present and future. Bridging chemistry to HIV, HBV, HCV, HPV, adeno-, herpes-, and poxvirus infections: the phosphonate bridge. *Biochemical pharmacology* **2007,** *73*, (7), 911-922.
124. Chrisman, C.; Curtis, K.; Mohllajee, A.; Gaffield, M.; Peterson, H. Effective use of hormonal contraceptives: Part II: Combined hormonal injectables, progestogen-only injectables and contraceptive implants. *Contraception* **2006,** *73*, (2), 125-133.
125. Okuda, T.; Tominaga, K.; Kidoaki, S. Time-programmed dual release formulation by multilayered drug-loaded nanofiber meshes. *Journal of controlled release : official journal of the Controlled Release Society* **2010,** *143*, (2), 258-264.
126. Xu, X.; Chen, X.; Wang, Z.; Jing, X. Ultrafine PEG-PLA fibers loaded with both paclitaxel and doxorubicin hydrochloride and their in vitro cytotoxicity. *European journal of pharmaceutics and biopharmaceutics.* **2009,** *72*, (1), 18-25.
127. Clare, F. R.; Adrian, C. W.; Peter, T.; Ian, G. Polymer-mediated disruption of drug crystallinity. *International journal of pharmaceutics* **2007**.

128. Takeuchi, Y.; McClure, M.; Pizzato, M. Identification of gammaretroviruses constitutively released from cell lines used for human immunodeficiency virus research. *Journal of virology* **2008,** *82*, (24), 12585-12588.
129. Derdeyn, C.; Decker, J.; Sfakianos, J.; Wu, X.; O'Brien, W.; Ratner, L.; Kappes, J.; Shaw, G.; Hunter, E. Sensitivity of human immunodeficiency virus type 1 to the fusion inhibitor T-20 is modulated by coreceptor specificity defined by the V3 loop of gp120. *Journal of virology* **2000,** *74*, (18), 8358-8367.
130. Platt, E.; Wehrly, K.; Kuhmann, S.; Chesebro, B.; Kabat, D. Effects of CCR5 and CD4 cell surface concentrations on infections by macrophagetropic isolates of human immunodeficiency virus type 1. *Journal of virology* **1998,** *72*, (4), 2855-2864.
131. Wei, X.; Decker, J.; Liu, H.; Zhang, Z.; Arani, R.; Kilby, J.; Saag, M.; Wu, X.; Shaw, G.; Kappes, J. Emergence of resistant human immunodeficiency virus type 1 in patients receiving fusion inhibitor (T-20) monotherapy. *Antimicrobial agents and chemotherapy* **2002,** *46*, (6), 1896-1905.
132. Changlu, S.; Hak-Yong, K.; Jian, G.; Bin, D.; Douk-Rae, L.; Soo-Jin, P. Fiber mats of poly(vinyl alcohol)/silica composite via electrospinning. *Materials Letters* **2003,** *57*.
133. Dasaratha Dhanaraju, M.; Vema, K.; Jayakumar, R.; Vamsadhara, C. Preparation and characterization of injectable microspheres of contraceptive hormones. *International journal of pharmaceutics* **2003,** *268*, (1-2), 23-29.
134. Johnson, T.; Gupta, K.; Fabian, J.; Albright, T.; Kiser, P. Segmented polyurethane intravaginal rings for the sustained combined delivery of antiretroviral agents dapivirine and tenofovir. *European journal of pharmaceutical sciences : official journal of the European Federation for Pharmaceutical Sciences* **2010,** *39*, (4), 203-212.
135. Gallo, M.; Nanda, K.; Grimes, D.; Schulz, K. Twenty micrograms vs. >20 microg estrogen oral contraceptives for contraception: systematic review of randomized controlled trials. *Contraception* **2005,** *71*, (3), 162-169.
136. Nicol, M.; Kashuba, A. Pharmacologic opportunities for HIV prevention. *Clinical pharmacology and therapeutics* **2010,** *88*, (5), 598-609.
137. Morrow, K.; Rosen, R.; Richter, L.; Emans, A.; Forbes, A.; Day, J.; Morar, N.; Maslankowski, L.; Profy, A.; Kelly, C.; Abdool Karim, S.; Mayer, K. The acceptability of an investigational vaginal microbicide, PRO 2000 Gel, among women in a phase I clinical trial. *Journal of women's health (2002)* **2003,** *12*, (7), 655-666.
138. Yue, E. M.; Hong, Z.; Dan, C.; Ruiyu, W.; Weng Weei, T.; Tianxi, L. Electrospun fibers of layered double hydroxide/biopolymer nanocomposites as effective drug delivery systems. *Materials Chemistry and Physics* **2012,** *134*.
139. Chen, D.; Liao, J.-Y.; Liu, S.-J.; Chan, E.-C. Novel biodegradable sandwich-structured nanofibrous drug-eluting membranes for repair of infected wounds: an in vitro and in vivo study. *International journal of nanomedicine* **2012,** *7*, 763-771.
140. Yi-Fan, G.; Imran, S.; Rafaqat, H. Electrospun fibers for tissue engineering, drug delivery, and wound dressing. *Journal of Materials Science* **2013,** *48*.
141. Craig, D. The mechanisms of drug release from solid dispersions in water-soluble polymers. *International journal of pharmaceutics* **2002,** *231*, (2), 131-144.
142. Sill, T. J.; von Recum, H. A. Electrospinning: applications in drug delivery and tissue engineering. *Biomaterials* **2008,** *29*, (13), 1989-2006.
143. Agarwal, S.; Wendorff, J. H.; Greiner, A. Use of electrospinning technique for biomedical applications. *Polymer* **2008,** *49*, 5603-5621.
144. Wang, F.; Saidel, G. M.; Gao, J. A mechanistic model of controlled drug release from polymer millirods: effects of excipients and complex binding. *Journal of controlled release* **2007,** *119*, 111-120.
145. Bishara, A.; Domb, A. J. PLA stereocomplexes for controlled release of somatostatin analogue. *Journal of controlled release* **2005,** *107*, 474-483.

146. Mochizuki, A.; Niikawa, T.; Omura, I.; Yamashita, S. Controlled release of argatroban from PLA film—Effect of hydroxylesters as additives on enhancement of drug release. *Journal of applied polymer science* **2008,** *108*, (5), 3353-3360.
147. Gaspar, M. M.; Blanco, D.; Cruz, M. E. M.; Alonso, M. J. Formulation of L-asparaginase-loaded poly (lactide-co-glycolide) nanoparticles: influence of polymer properties on enzyme loading, activity and in vitro release. *Journal of controlled release* **1998,** *52*, (1-2), 53-62.
148. Sun, D. D.; Lee, P. I. Probing the mechanisms of drug release from amorphous solid dispersions in medium-soluble and medium-insoluble carriers. *Journal of Controlled Release* **2015,** *211*, 85-93.
149. Heijkants, R.; van Calck, R. V.; van Tienen, T. G. Uncatalyzed synthesis, thermal and mechanical properties of polyurethanes based on poly (ε-caprolactone) and 1, 4-butane diisocyanate with uniform hard segment. *Biomaterials* **2005,** *26*, 4219-4228.
150. Santerre, J. P.; Woodhouse, K.; Laroche, G.; Labow, R. S. Understanding the biodegradation of polyurethanes: from classical implants to tissue engineering materials. *Biomaterials* **2005,** *26*, 7457-7470.
151. Xie, R.; Bhattacharjee, D.; Argyropoulos, J. Polyurethane elastomers based on 1, 3 and 1, 4-bis (isocyanatomethyl) cyclohexane. *Journal of applied polymer science* **2009,** *113*, (2), 839-848.
152. Rockwood, D. N.; Woodhouse, K. A.; Fromstein, J. D.; Chase, D. B.; Rabolt, J. F. Characterization of biodegradable polyurethane microfibers for tissue engineering. *Journal of Biomaterials Science-Polymer Edition* **2007,** *18*, (6), 743-758.
153. Ma, Z.; Hong, Y.; Nelson, D. M.; Pichamuthu, J. E.; Leeson, C. E.; Wagner, W. R. Biodegradable polyurethane ureas with variable polyester or polycarbonate soft segments: Effects of crystallinity, molecular weight, and composition on mechanical properties. *Biomacromolecules* **2011,** *12*, (3265-3274).
154. Hafeman, A. E.; Zienkiewicz, K. J.; Zachman, A. L.; Sung, H. J.; Nanney, L. B.; Davidson, J. M.; Guelcher, S. A. Characterization of the degradation mechanisms of lysine-derived aliphatic poly (ester urethane) scaffolds. *Biomaterials* **2011,** *32*, 419-429.
155. Guelcher, S. A.; Srinivasan, A.; Dumas, J. E.; Didier, J. E.; McBride, S.; Hollinger, J. O. Synthesis, mechanical properties, biocompatibility, and biodegradation of polyurethane networks from lysine polyisocyanates. *Biomaterials* **2008,** *29*, 1762-1775.
156. Kavlock, K. D.; Pechar, T. W.; Hollinger, J. O.; Guelcher, S. A.; Goldstein, A. S. Synthesis and characterization of segmented poly (esterurethane urea) elastomers for bone tissue engineering. *Acta biomaterialia* **2007,** *3*, 465-484.
157. Oniki, Y.; Suzuki, K.; Higaki, Y.; Ishige, R.; Ohta, N.; Takahara, A. Molecular design of environmentally benign segmented polyurethane (urea) s: effect of the hard segment component on the molecular aggregation states and biodegradation behavior. *Polymer Chemistry* **2013,** *4*, (13), 3735-3743.
158. Zhou, L.; Yu, L.; Ding, M.; Li, J.; Tan, H.; Wang, Z.; Fu, Q. Synthesis and characterization of pH-sensitive biodegradable polyurethane for potential drug delivery applications. *Macromolecules* **2011,** *44*, 857-864.
159. Zhou, L.; Liang, D.; He, X.; Li, J.; Tan, H.; Li, J.; Fu, Q.; Gu, Q. The degradation and biocompatibility of pH-sensitive biodegradable polyurethanes for intracellular multifunctional antitumor drug delivery. *Biomaterials* **2012,** *33*, 2734-2745.
160. Fu, H. L.; Hong, Y.; Little, S. R.; Wagner, W. R. Collagenase-Labile Polyurethane Urea Synthesis and Processing into Hollow Fiber Membranes. *Biomacromolecules* **2014,** *15*, 2924-2932.
161. Broekema, F. I.; Leeuwen, M. B. M.; Van Minnen, B.; Bos, R. R. M. In vivo degradation of polyurethane foam with 55 wt% polyethylene glycol. *J. Biomed. Mater. Res. Part A* **2015,** *103A*, 3666-3675.
162. Singhal, P.; Small, W.; Cosgriff-Hernandez, E.; Maitland, D. J.; Wilson, T. S. Low density biodegradable shape memory polyurethane foams for embolic biomedical applications. *Acta biomaterialia* **2014,** *10*, 67-76.

163. Davachi, S. M.; Kaffashi, B. Synthesis and characterization of a novel terpolymer based on L-lactide, glycolide, and trimethylene carbonate for specific medical applications. *Polymers for Advanced Technologies* **2012,** *23*, 565-573.
164. Alishiri, M.; Shojaei, A.; Abdekhodaie, M. J.; Yeganeh, H. Synthesis and characterization of biodegradable acrylated polyurethane based on poly (-caprolactone) and 1, 6-hexamethylene diisocyanate. *Materials Science and Engineering: C* **2014,** *42*, 763-773.
165. Unnithan, A. R.; Barakat, N. A. M.; Pichiah, P. B. T.; Gnanasekaran, G.; Nirmala, R.; Cha, Y.; Jung, C.; El-Newehy, M.; Kim, H. Y. Wound-dressing materials with antibacterial activity from electrospun polyurethane–dextran nanofiber mats containing ciprofloxacin HCl. *Carbohydrate polymers* **2012,** *90*, 1786-1793.
166. Blakney, A. K.; Ball, C.; Krogstad, E. A.; Woodrow, K. A. Electrospun fibers for vaginal anti-HIV drug delivery. *Antiviral research* **2013,** *100*.
167. Guan, J.; Fujimoto, K. L.; Sacks, M. S.; Wagner, W. R. Preparation and characterization of highly porous, biodegradable polyurethane scaffolds for soft tissue applications. *Biomaterials* **2005,** *26*, (18).
168. Karchin, A.; Simonovsky, F. I.; Ratner, B. D.; Sanders, J. E. Melt electrospinning of biodegradable polyurethane scaffolds. *Acta biomaterialia* **2011,** *7*, (9), 3277-3284.
169. Caracciolo, P. C.; Thomas, V.; Vohra, Y. K.; Buffa, F.; Abraham, G. A. Electrospinning of novel biodegradable poly (ester urethane) s and poly (ester urethane urea) s for soft tissue-engineering applications. *Journal of Materials Science* **2009,** *20*, 2129-2137.
170. Hong, Y.; Ye, S. H.; Pelinescu, A. L.; Wagner, W. R. Synthesis, characterization, and paclitaxel release from a biodegradable, elastomeric, poly (ester urethane) urea bearing phosphorylcholine groups for reduced thrombogenicity. *Biomacromolecules* **2012,** *13*, 3686-3694.
171. Punnakitikashem, P.; Truong, D.; Menon, J. U.; Nguyen, K. T. Electrospun biodegradable elastic polyurethane scaffolds with dipyridamole release for small diameter vascular grafts. *Acta biomaterialia* **2014,** *10*, 4618-4628.
172. Galperin, A.; Smith, K.; Geisler, N. S.; Bryers, J. D.; Ratner, B. D. Precision-Porous PolyHEMA-Based Scaffold as an Antibiotic-Releasing Insert for a Scleral Bandage. *ACS Biomaterials Science & Engineering* **2015,** *1*, (7), 593-600.
173. Hirenkumar, K. M.; Steven, J. S. Poly Lactic-co-Glycolic Acid (PLGA) as Biodegradable Controlled Drug Delivery Carrier. *Polymers* **2011,** *3*, (3).
174. Chen, B. A.; Panther, L.; Marzinke, M. A.; Hendrix, C. W.; Hoesley, C. J.; van der Straten, A.; Husnik, M. J.; Soto-Torres, L.; Nel, A.; Johnson, S.; Richardson-Harman, N.; Rabe, L. K.; Dezzutti, C. S. Phase 1 Safety, Pharmacokinetics, and Pharmacodynamics of Dapivirine and Maraviroc Vaginal Rings: A Double-Blind Randomized Trial. *Journal of acquired immune deficiency syndromes (1999)* **2015,** *70*, (3), 242-249.
175. Karim, Q.; Karim, S. S.; Frohlich, J. A.; Grobler, A. C.; Baxter, C.; Mansoor, L. E.; Kharsany, A. B. M.; Sibeko, S.; Mlisana, K. P.; Omar, Z.; Gengiah, T. N.; Maarschalk, S.; Arulappan, N.; Mlotshwa, M.; Morris, L.; Taylor, D. Effectiveness and Safety of Tenofovir Gel, an Antiretroviral Microbicide, for the Prevention of HIV Infection in Women. *Science* **2010,** *329*, 1168-1174.
176. Pauli, G. F.; Godecke, T.; Jaki, B. U.; Lankin, D. C. Quantitative 1H NMR. Development and potential of an analytical method: an update. *Journal of natural products* **2012,** *75*, (4), 834-851.
177. Pourcelle, V.; Duff, L. C. S.; Freichels, H.; Jérôme, C.; Marchand-Brynaert, J. Clickable PEG conjugate obtained by “clip” photochemistry: Synthesis and characterization by quantitative 19 F NMR. *Journal of Fluorine Chemistry* **2012,** *140*, 62-69.
178. Notari, S.; Tommasi, C.; Nicastri, E.; Bellagamba, R.; Tempestilli, M.; Pucillo, L. P.; Narciso, P.; Ascenzi, P. Simultaneous determination of maraviroc and raltegravir in human plasma by HPLC-UV. *IUBMB life* **2009,** *61*, (4), 470-475.
179. Samanidou, V. F.; Demetriou, C. E.; Papadoyannis, I. N. Direct determination of four fluoroquinolones, enoxacin, norfloxacin, ofloxacin, and ciprofloxacin, in pharmaceuticals and blood serum by HPLC. *Analytical and Bioanalytical Chemistry* **2003,** *375*, 623-629.

180. Kabra, V.; Agrahari, V.; Karthikeyan, C.; Trivedi, P. Simultaneous quantitative determination of zidovudine and nevirapine in human plasma using isocratic, reverse phase high performance liquid chromatography. *Tropical Journal of Pharmaceutical Research* **2009,** *8*, (1), 79-86.
181. Tao, T.; Pingliang, L.; Laixin, L.; Dazhao, S.; Jianqiang, L.; Yongsong, C. Development and validation of a HPLC method for determination of levonorgestrel and quinestrol in rat plasma. *Biomedical Chromatography* **2010,** *24*, (7).
182. Li, J.; Stayshich, R. M.; Meyer, T. Y. Exploiting sequence to control the hydrolysis behavior of biodegradable PLGA copolymers. *Journal of the American Chemical Society* **2011,** *133*, 6910-6913.
183. Tien, Y. I.; Wei, K. H. Hydrogen bonding and mechanical properties in segmented montmorillonite/polyurethane nanocomposites of different hard segment ratios. *Polymer* **2001,** *42*, (7), 32133221.
184. Krol, P. Synthesis methods, chemical structures and phase structures of linear polyurethanes. Properties and applications of linear polyurethanes in polyurethane elastomers, copolymers and ionomers. *Progress in materials science* **2007,** *52*, 915-1015.
185. Mura, P.; Faucci, M. T.; Manderioli, A.; Bramanti, G.; Ceccarelli, L. Compatibility study between ibuproxam and pharmaceutical excipients using differential scanning calorimetry, hot-stage microscopy and scanning electron microscopy. *Journal of pharmaceutical and biomedical analysis* **1998,** *18*, 151-163.
186. Xu, X.; Chen, X.; Xu, X.; Lu, T.; Wang, X.; Yang, L.; Jing, X. BCNU-loaded PEG-PLLA ultrafine fibers and their in vitro antitumor activity against Glioma C6 cells. *Journal of controlled release : official journal of the Controlled Release Society* **2006,** *114*, (3), 307-316.
187. Yih, R. S.; Ratner, B. D. A comparison of two angular dependent ESCA algorithms useful for constructing depth profiles of surfaces. *Journal of electron spectroscopy and relatedphenomena* **1987,** *43*, 61-82.
188. Kim, Y. S.; Lee, J. S.; Ji, Q.; McGrath, J. E. Surface properties of fluorinated oxetane polyol modified polyurethane block copolymers. *Polymer* **2002**.
189. Ming, W.; Laven, J.; van der Linde, R. Synthesis and surface properties of films based on solventless liquid fluorinated oligoester. *Macromolecules* **2000**.
190. Messori, M.; Bongiovanni, R.; Malucelli, G.; Priola, A. Poly (ϵ-caprolactone)-poly (fluoroalkylene oxide)-poly (ϵ-caprolactone) block copolymers. 2. Thermal and surface properties. *Polymer* **2001**.
191. Yoon, S. C.; Ratner, B. D. Surface structure of segmented poly (ether urethanes) and poly (ether urethane ureas) with various perfluoro chain extenders. An X-ray photoelectron spectroscopic investigation. *Macromolecules* **1986,** *19*, (4), 1068-1079.
192. Smith, G. C. Evaluation of a simple correction for the hydrocarbon contamination layer in quantitative surface analysis by XPS. *Journal of electron spectroscopy and related phenomena* **2005,** *148*, (21-28).
193. Zhang, D.; Gracias, D. H.; Ward, R.; Gauckler, M.; Tian, Y.; Shen, Y. R.; Somorjai, G. A. Surface studies of polymer blends by sum frequency vibrational spectroscopy, atomic force microscopy, and contact angle goniometry. *The Journal of Physical Chemistry B* **1998,** *102*, 6225-6230.
194. Skarja, G. A.; Woodhouse, K. A. Structure-property relationships of degradable polyurethane elastomers containing an amino acid-based chain extender. *Journal of Applied Polymer Science* **2000,** *75*, 1522-1534.
195. Chan-Chan, L. H.; Solis-Correa, R.; Vargas-Coronado, R. F. Degradation studies on segmented polyurethanes prepared with HMDI, PCL and different chain extenders. *Acta biomaterialia* **2010**.
196. Alexis, F. Factors affecting the degradation and drug-release mechanism of poly (lactic acid) and poly [(lactic acid)-co-(glycolic acid)]. *Polymer International* **2005,** *54*, 36-46.
197. Sun, D. D.; Lee, P. I. Probing the mechanisms of drug release from amorphous solid dispersions in medium-soluble and medium-insoluble carriers. *Journal of Controlled Release* **2015**.
198. Yoo, H. S.; Kim, T. G.; Park, T. G. Surface-functionalized electrospun nanofibers for tissue engineering and drug delivery. *Advanced drug delivery reviews* **2009**.

199. Ball, C.; Chou, S. F.; Jiang, Y.; Woodrow, K. A. Coaxially electrospun fiber-based microbicides facilitate broadly tunable release of maraviroc. *Materials Science and Engineering C* **2016,** *63*, 117-124.
200. Yuan, Z.; Zhao, X.; Zhao, J.; Pan, G.; Qiu, W.; Wang, X.; Zhu, Y.; Zheng, Q.; Cui, W. Synergistic mediation of tumor signaling pathways in hepatocellular carcinoma therapy via dual-drug-loaded pH-responsive electrospun fibrous scaffolds. *Journal of Materials Chemistry B* **2015,** *3*, (17), 3436-3446.
201. Wong, H. L.; Bendayan, R.; Rauth, A. M.; Wu, X. Y. Simultaneous delivery of doxorubicin and GG918 (Elacridar) by new polymer-lipid hybrid nanoparticles (PLN) for enhanced treatment of multidrug-resistant breast cancer. *Journal of controlled release* **2006,** *116*, 275-284.
202. Rohan, L. C.; Moncla, B. J.; Ayudhya, R.; Cost, M.; Huang, Y.; Gai, F.; Billitto, N.; Lynam, J. D.; Pryke, K.; Graebing, P.; Hopkins, N.; Rooney, J. F.; Friend, D.; Dezzutti, C. S. In Vitro and Ex Vivo Testing of Tenofovir Shows It Is Effective As an HIV-1 Microbicide. *PLoS ONE* **2010**.
203. Fletcher, P. S.; Wallace, G. S.; Mesquita, P. M. M.; Shattock, R. J. Candidate polyanion microbicides inhibit HIV-1 infection and dissemination pathways in human cervical explants. *Retrovirology* **2006,** *3*, 46.
204. Holpuch, A. S.; Hummel, G. J.; Tong, M.; Seghi, G. A.; Pei, P.; Ma, P.; Mumper, R. J.; Mallery, S. R. Nanoparticles for local drug delivery to the oral mucosa: proof of principle studies. *Pharmaceutical research* **2010,** *27*, 1224-1236.
205. Namur, J.; Citron, S. J.; Sellers, M. T.; Dupuis, M. H.; Wassef, M.; Manfait, M.; Laurent, A. Embolization of hepatocellular carcinoma with drug-eluting beads: doxorubicin tissue concentration and distribution in patient liver explants. *Journal of Hepatology* **2011,** *55*, 1332-1338.
206. Hsiue, G. H.; Guu, J. A.; Cheng, C. C. Poly(2-hydroxyethyl methacrylate) film as a drug delivery system for pilocarpine. *Biomaterials* **2001,** *22*, (13), 1763-1769.
207. Andrade-Vivero, P.; Fernandez-Gabriel, E.; Alvarez-Lorenzo, C.; Concheiro, A. Improving the loading and release of NSAIDs from pHEMA hydrogels by copolymerization with functionalized monomers. *Journal of pharmaceutical sciences* **2007,** *96*, (4), 802.
208. Sun, D. D.; Ju, T. R.; Lee, P. I. Enhanced kinetic solubility profiles of indomethacin amorphous solid dispersions in poly (2-hydroxyethyl methacrylate) hydrogels. *European Journal of Pharmaceutics and Biopharmaceutics* **2012,** *81*, 149-158.
209. Liu, P.; Wulf, D. O.; Laru, J.; Heikkilä, T.; van Veen, B.; Kiesvaara, J.; Hirvonen, J.; Peltonen, L.; Laaksonen, T. Dissolution studies of poorly soluble drug nanosuspensions in non-sink conditions. *AAPS Pharmaceutical Science and Technology* **2013,** *14*, (2), 748.
210. Carson, D.; Jiang, Y.; Woodrow, K. A. Tunable Release of Multiclass Anti-HIV Drugs that are Water-Soluble and Loaded at High Drug Content in Polyester Blended Electrospun Fibers. *Pharmaceutical research* **2015,** *33*, (1), 125-136.
211. Mabilleau, G.; Stancu, I. C.; Honore, T.; Legeay, G.; Cincu, C.; Basle, M. F.; Cahappard, D. Effects of the length of crosslink chain on poly (2-hydroxyethyl methacrylate)(pHEMA) swelling and biomechanical properties. *J. Biomed. Mater. Res. Part A* **2006,** *77*, (1), 35-42.
212. Devlin, B.; Nuttall, J.; Wilder, S.; Woodsong, C.; Rosenberg, Z. Development of dapivirine vaginal ring for HIV prevention. *Antiviral Research* **2013,** *100*.
213. Romano, J.; Variano, B.; Coplan, P.; Van Roey, J.; Douville, K.; Rosenberg, Z.; Temmerman, M.; Verstraelen, H.; Van Bortel, L.; Weyers, S.; Mitchnick, M. Safety and availability of dapivirine (TMC120) delivered from an intravaginal ring. *AIDS research and human retroviruses* **2009,** *25*, (5), 483-488.
214. Ball, C.; Woodrow, K. A. Electrospun solid dispersions of maraviroc for rapid intravaginal preexposure prophylaxis of HIV. *Antimicrobial agents and chemotherapy* **2014,** *58*, (8), 4855-4865.
215. Sun, D. D.; Lee, P. I. Evolution of Supersaturation of Amorphous Pharmaceuticals: Nonlinear Rate of Supersaturation Generation Regulated by Matrix Diffusion. *Molecular Pharmaceutics* **2015,** *12*, (4), 1203-1215.

216. Fu, Y.; Xu, K.; Zheng, X.; Giacomin, A. J.; Mix, A. W.; Kao, W. J. 3D cell entrapment in crosslinked thiolated gelatin-poly (ethylene glycol) diacrylate hydrogels. *Biomaterials* **2012,** *33*, 48-58.
217. Hwang, C. M.; Sant, S.; Masaeli, M.; Kachouie, N. N. Fabrication of three-dimensional porous cell-laden hydrogel for tissue engineering. *Biofabrication* **2010,** *2*, 1-12.
218. Celum, C.; Baeten, J. M. Tenofovir-based pre-exposure prophylaxis for HIV prevention: evolving evidence. *Current opinion in infectious diseases* **2012,** *25*, (1), 51-57.
219. Zolopa, A. R. The evolution of HIV treatment guidelines: current state-of-the-art of ART. *Antiviral research* **2010,** *85*, 241-244.
220. Patton, D. L.; Sweeney, Y.; Rohan, L. C.; Marzinke, M.; Hendrix, C. W.; Hillier, S. Dapivirine and Tenofovir Vaginal Films and Gels: Macaque Pharmacokinetics. *AIDS research and human retroviruses* **2014**, A157.
221. Mayer, K. H.; Maslankowski, L. A.; Gai, F.; El-Sadr, W. M.; Justman, J.; Kwiecien, A.; Mâsse, B.; Eshleman, S. H.; Hendrix, C.; Morrow, K.; Rooney, J. F.; Soto-Torres, L.; Team, H. Safety and tolerability of tenofovir vaginal gel in abstinent and sexually active HIV-infected and uninfected women. *AIDS (London, England)* **2006,** *20*, (4), 543-551.
222. Andries, K.; Azijn, H.; Thielemans, T.; Ludovici, D.; Kukla, M.; Heeres, J.; Janssen, P.; De Corte, B.; Vingerhoets, J.; Pauwels, R.; de Bethune, M. P. TMC125, a novel next-generation nonnucleoside reverse transcriptase inhibitor active against nonnucleoside reverse transcriptase inhibitor-resistant human immunodeficiency virus type I. *Antimicrobial agents and chemotherapy* **2004,** *48*, (12), 4680-4686.
223. Vingerhoets, J.; Azijn, H.; Fransen, E.; De Baere, I.; Smeulders, L.; Jochmans, D.; Andries, K.; Pauwels, R.; de Bethune, M. P. TMC125 displays a high genetic barrier to the development of resistance: evidence from in vitro selection experiments. *Journal of virology* **2005,** *79*, (20), 12773-12782.
224. Madruga, J. V.; Cahn, P.; Grinsztejn, B.; Haubrich, R.; Lalezari, J.; Mills, A.; Pialoux, G.; Wilkin, T.; Peeters, M.; Bingerhoets, J.; de Smedt, G.; Leopold, L.; Trefiglio, R.; Woodfall, B. Efficacy and safety of TMC125 (etravirine) in treatment-experienced HIV-1-infected patients in DUET-1: 24-week results from a randomised, double-blind, placebo-controlled trial. *The Lancet* **2007,** *370*, 29-38.
225. Dorr, P.; Westby, M.; Dobbs, S.; Griffin, P.; Irvine, B.; Macartney, M.; Mori, J.; Rickett, G.; Smith-Burchnell, C.; Napier, C.; Webster, R.; Armour, D.; Price, D.; Stammen, B.; Wood, A.; Perros, M. Maraviroc (UK-427,857), a potent, orally bioavailable, and selective small-molecule inhibitor of chemokine receptor CCR5 with broad-spectrum anti-human immunodeficiency virus type I activity. *Antimicrobial agents and chemotherapy* **2005,** *49*, (11), 4721-4732.
226. Forbes, C. J.; Lowry, D.; Geer, L.; Veazey, R. S.; Shattock, R. J.; Klasse, P. J.; Mitchnick, M.; Goldman, L.; Doyle, L. A.; Muldoon, B. C. O.; Woolfson, A. D.; Moore, J. P.; Malcolm, R. K. Non-aqueous silicone elastomer gels as a vaginal microbicide delivery system for the HIV-1 entry inhibitor maraviroc. *Journal of controlled release* **2011,** *156*, 161-169.
227. Lennox, J. L.; DeJesus, E.; Lazzarin, A.; Pollard, R. B.; Madruga, J. V.; Berger, D. S.; Zhao, J.; Xu, X.; Williams-Diaz, A.; Rodgers, A. J.; Barnard, R. J. O.; Miller, M. D.; DiNubile, M. J.; Nguyen, B.; Leavitt, R.; Sklar, P. Safety and efficacy of raltegravir-based versus efavirenz-based combination therapy in treatment-naive patients with HIV-1 infection: a multicentre, double-blind randomised controleld trial. *The Lancet* **2009,** *374*, 796-806.
228. Dobard, C.; Sharma, S.; Parikh, U. M.; West, R.; Taylor, A.; Martin, A.; Pau, C. P.; Hanson, D. L.; Lipscomb, J.; Smith, J.; Novembre, F.; Hazuda, D.; Garcia-Lerma, J. G.; Heneine, W. Postexposure protection of macaques from vaginal SHIV infection by topical integrase inhibitors. *Science translational medicine* **2014,** *6*, (227), 1-9.
229. Fayet, A.; Béguin, A.; Zanolari, B.; Cruchon, S.; Guignard, N.; Telenti, A.; Cavassini, M.; Günthard, H. F.; Buclin, T.; Biollaz, J.; Rochat, B.; Decosterd, L. A. A LC-tandem MS assay for the simultaneous measurement of new antiretroviral agents: Raltegravir, maraviroc, darunavir, and etravirine. *Journal of chromatography. B, Analytical technologies in the biomedical and life sciences* **2009,** *877*, (11-12), 1057-1069.

230. Heine, T. R.; Rosing, H.; Gorp, E. C. M.; Mulder, J. W.; Beijnen, J. H.; Huitema, A. D. R. Quantification of etravirine (TMC125) in plasma, dried blood spots and peripheral blood mononuclear cell lysate by liquid chromatography tandem mass spectrometry. *Journal of pharmaceutical and biomedical analysis* **2009,** *49*, 393-400.
231. Abobo, C. V.; Wu, L.; John, J.; Joseph, M. K.; Bates, T. R.; Liang, D. LC–MS/MS determination of etravirine in rat plasma and its application in pharmacokinetic studies. *Journal of Chromatography B* **2010,** *878*, 3181-3186.
232. Brewer, E.; Felix, T.; Clarke, P.; Edgington, A.; Muirhead, D. An LC-MS-MS method for quantitative determination of maraviroc (UK-427,857) in human plasma, urine and cerebrospinal fluid. *Biomedical Chromatography* **2010,** *12*, 1316-1323.
233. Long, M. C.; Bennetto-Hood, C.; Acosta, E. P. A sensitive HPLC-MS-MS method for the determination of raltegravir in human plasma. *Journal of chromatography. B, Analytical technologies in the biomedical and life sciences* **2008,** *867*, (2), 165-171.
234. Heine, T. R.; Hillebrand, M. J. X.; Rosing, H. Quantification of the HIV-integrase inhibitor raltegravir and detection of its main metabolite in human plasma, dried blood spots and peripheral blood mononuclear cell lysate by means of high-performance liquid chromatography tandem mass spectrometry. *Journal of pharmaceutical and biomedical analysis* **2009,** *49*, 451-458.
235. Else, L.; Watson, V.; Tjia, J.; Hughes, A.; Siccardi, M.; Khoo, S.; Back, D. Validation of a rapid and sensitive high-performance liquid chromatography–tandem mass spectrometry (HPLC–MS/MS) assay for the simultaneous determination of existing and new antiretroviral compounds. *Journal of Chromatography B* **2010,** *878*, (1455-1465).
236. Shah, V. P.; Midha, K. K.; Findlay, J. W. A.; Hill, H. M.; Hulse, J. D.; McGilveray, I. J.; McKay, G.; Miller, K. J.; Patnaik, R. N.; Powell, M. L. Bioanalytical method validation—a revisit with a decade of progress. *Pharmaceutical research* **2000,** *17*, (12), 1551-1557.
237. Matuszewski, B. K. Standard line slopes as a measure of a relative matrix effect in quantitative HPLC–MS bioanalysis. *Journal of Chromatography B* **2006**.
238. Matuszewski, B. K.; Constanzer, M. L.; Chavez-Eng, C. M. Strategies for the assessment of matrix effect in quantitative bioanalytical methods based on HPLC-MS/MS. *Analytical Chemistry* **2003,** *75*, 3019-3030.
239. Stokvis, E.; Rosing, H.; Beijnen, J. H. Stable isotopically labeled internal standards in quantitative bioanalysis using liquid chromatography/mass spectrometry: necessity or not? *Rapid Communications in Mass Spectrometry* **2005,** *19*, 401-407.
240. Avery, M. J. Quantitative characterization of differential ion suppression on liquid chromatography/atmospheric pressure ionization mass spectrometric bioanalytical methods. *Rapid communications in mass spectrometry* **2003,** *17*, 197-201.
241. Karim, S. S.; Kashuba, A. D. M.; Werner, L.; Karim, Q. Drug concentrations after topical and oral antiretroviral pre-exposure prophylaxis: implications for HIV prevention in women. *Lancet* **2011,** *378*, (9787), 279-281.
242. Malcolm, R. K.; Forbes, C. J.; Geer, L.; Veazey, R. S.; Goldman, L.; Klasse, P. J.; Moore, J. P. Pharmacokinetics and efficacy of a vaginally administered maraviroc gel in rhesus macaques. *Journal of antimicrobial chemotherapy* **2013,** *68*, 678-683.
243. Malcolm, R. K.; Lowry, D.; Boyd, P.; Geer, L.; Veazey, R. S.; Goldman, L.; Klasse, P. J.; Shattock, R. J.; Moore, J. P. Pharmacokinetics of a CCR5 inhibitor in rhesus macaques following vaginal, rectal and oral application. *Journal of antimicrobial chemotherapy* **2014,** *69*, 1325-1329.
244. Nuttall, J. P.; Thake, D. C.; Lewis, M. G.; Ferkany, J. W.; Romano, J. W.; Mitchnick, M. A. Concentrations of dapivirine in the rhesus macaque and rabbit following once daily intravaginal administration of a gel formulation of [14C] dapivirine for 7 days. *Antimicrobial agents and chemotherapy* **2008,** *52*, (3), 909-914.
245. Murphy, D. J.; Desjardins, D.; Dereuddre-Bosquet, N.; Brochard, P.; Perrot, L.; Pruvost, A.; Le Grand, R.; Lagatie, O.; Vanhooren, L.; Feyaerts, M.; van Roey, J.; Malcolm, K. Pre-clinical

development of a combination microbicide vaginal ring containing dapivirine and darunavir. *Journal of antimicrobial chemotherapy* **2014,** *69*, (9), 2477-2488.
246. Nel, A. M.; Coplan, P.; Smythe, S. C.; McCord, K.; Mitchnick, M.; Kaptur, P. E.; Romano, J. Pharmacokinetic assessment of dapivirine vaginal microbicide gel in healthy, HIV-negative women. *AIDS research and human retroviruses* **2010,** *26*, (11), 1181-1190.
247. Abel, S.; Ryst, V. E.; Rosario, M. C.; Ridgway, C. E.; Medhurst, C. G.; Taylor-Worth, R. J.; Muirhead, G. J. Assessment of the pharmacokinetics, safety and tolerability of maraviroc, a novel CCR5 antagonist, in healthy volunteers. *British journal of pharmacology* **2008,** *65*, 5-18.
248. Markowitz, M.; Morales-Ramirez, J. O.; Nguyen, B.; Kovacs, C. M.; Steigbigel, R. T.; Cooper, D. A.; Liporace, R.; Schwartz, R.; Isaacs, R.; Gilde, L. R.; Wenning, L.; Zhao, J.; Teppler, H. Antiretroviral activity, pharmacokinetics, and tolerability of MK-0518, a novel inhibitor of HIV-1 integrase, dosed as monotherapy for 10 days in treatment-naive HIV-1-Infected Individuals. *JAIDS Journal of Acquired Immune Deficiency Syndromes* **2006,** *43*, (5), 509-515.
249. Chambers, E.; Wagrowski-Diehl, D. M.; Lu, Z. Systematic and comprehensive strategy for reducing matrix effects in LC/MS/MS analyses. *Journal of Chromatography B* **2007,** *852*, 22-34.
250. Summa, V.; Petrocchi, A.; Bonelli, F.; Crescenzi, B.; Donghi, M.; Ferrara, M.; Fiore, F.; Gardelli, C.; Paz, O.; Hazuda, D. J.; Jones, P.; Kinzel, O.; Laufer, R.; Monteagudo, E.; Muraglia, E.; Nizi, E.; Orvieto, F.; Pace, P.; Pescatore, G.; Scarpelli, R.; Stillmock, K.; Witmer, M. V.; Rowley, M. Discovery of Raltegravir, a Potent, Selective Orally Bioavailable HIV-Integrase Inhibitor for the Treatment of HIV-AIDS Infection. *Journal of Medicinal Chemistry* **2008,** *51*, (18), 5843-5855.
251. Merschman, S. A.; Vallano, P. T.; Wenning, L. A.; Matuszewski, B. K.; Woolf, E. J. Determination of the HIV integrase inhibitor, MK-0518 (raltegravir), in human plasma using 96-well liquid–liquid extraction and HPLC-MS/MS. *Journal of Chromatography B* **2007,** *857*, 15-24.
252. Emory, J. F.; Seserko, L. A.; Marzinke, M. A. Development and bioanalytical validation of a liquid chromatographic-tandem mass spectrometric (LC-MS/MS) method for the quantification of the CCR5 antagonist maraviroc in human plasma. *Clinica Chimica Acta* **2014,** *431*, 198-205.
253. Jilek, B. L.; Zarr, M.; Sampah, M. E.; Rabi, S. A.; Bullen, C. K.; Lai, J.; Shen, L.; Siliciano, R. F. A quantitative basis for antiretroviral therapy for HIV-1 infection. *Nature medicine* **2012,** *18*, (3), 446-451.
254. UNAIDS. Global HIV Statistics. **2015**.
255. Quarraisha Abdool, K.; Salim, S. A. K.; Janet, A. F.; Anneke, C. G.; Cheryl, B.; Leila, E. M.; Ayesha, B. M. K.; Sengeziwe, S.; Koleka, P. M.; Zaheen, O.; Tanuja, N. G.; Silvia, M.; Natasha, A.; Mukelisiwe, M.; Lynn, M.; Douglas, T.; Group, C. T. Effectiveness and safety of tenofovir gel, an antiretroviral microbicide, for the prevention of HIV infection in women. *Science (New York, N.Y.)* **2010**.
256. Abdool Karim, S. S.; Kashuba, A. D. M.; Werner, L.; Karim, Q. A. Drug concentrations after topical and oral antiretroviral pre-exposure prophylaxis: implications for HIV prevention in women. *Lancet* **2011,** *378*, (9787), 279-281.
257. Marrazzo, J. M.; Ramjee, G.; Richardson, B. A.; Gomez, K.; Mgodi, N.; Nair, G.; Palanee, T.; Nakabiito, C.; van der Straten, A.; Noguchi, L.; Hendrix, C. W.; Dai, J. Y.; Ganesh, S.; Mkhize, B.; Taljaard, M.; Parikh, U. M.; Piper, J.; Mâsse, B.; Grossman, C.; Rooney, J.; Schwartz, J. L.; Watts, H.; Marzinke, M. A.; Hillier, S. L.; McGowan, I. M.; Chirenje, Z. M. Tenofovir-Based Preexposure Prophylaxis for HIV Infection among African Women. *New England Journal of Medicine* **2015,** *372*, (6), 509-518.
258. Rees, H.; Delaney-Moretlwe, S.; Lombard, C.; Baron, D.; Panchia, R.; Myer, L.; Schwartz, J. L.; Doncel, G. F.; Gray, G., FACTS 001: a muti-centred phase III randomised, double-blind, placebo controlled trial of pericoital tenofovir 1% fel for HIV prevention in women. In *Conference on Retroviruses and Opportunistic Infections*, Seattle, WA, USA, 2015.
259. El-Sahn, M.; Lucas, J.; Aikenhead, M.; Nemade, R.; Van Damme, L. Understanding the Potential for Multipurpose Prevention of Pregnancy and HIV: Results from surveys assessing four hypothetical concept profiles of MPTs in Uganda, Nigeria and South Africa. **2016**.

260. Ball, C.; Woodrow, K. A. Electrospun Solid Dispersions of Maraviroc for Rapid Intravaginal Preexposure Prophylaxis of HIV. *Antimicrobial Agents and Chemotherapy* **2014,** *58*, (8), 48554865.
261. Blakney, A. K.; Simonovsky, F.; Suydam, I. T.; Ratner, B. D.; Woodrow, K. A. Rapidly Biodegrading PLGA-Polyurethane Fibers for Sustained Release of Physicochemically Diverse Drugs. *ACS Biomaterials Science & Engineering* **2016**.
262. Blakney, A. K.; Jiang, Y.; Whittington, D.; Woodrow, K. A. Simultaneous measurement of etravirine, maraviroc and raltegravir in pigtail macaque plasma, vaginal secretions and vaginal tissue using a LC–MS/MS assay. *Journal of Chromatography B* **2016,** *1025*, 110-118.
263. Houchin, M. L.; Neuenswander, S. A.; Topp, E. M. Effect of excipients on PLGA film degradation and the stability of an incorporated peptide. *Journal of controlled release* **2007,** *117*, 413-420.
264. Lam, C. X. F.; Hutmacher, D. W.; Schantz, J. T.; Woodruff, M. A.; Teoh, S. H. Evaluation of polycaprolactone scaffold degradation for 6 months in vitro and in vivo. *J. Biomed. Mater. Res. Part A* **2009,** *90*, (3), 906-919.
265. Cottrell, M. L.; Prince, H.; Allmon, A.; Mollan, K. R.; Hudgens, M. G.; Sykes, C.; White, N.; Malone, S.; Dellon, E. S.; Madanick, R. D.; Shaheen, N. J.; Patterson, K. B.; Kashuba, A. Cervicovaginal and Rectal Fluid as a Surrogate Marker of Antiretroviral Tissue Concentration: Implications for Clinical Trial Design. *JAIDS Journal of Acquired Immune Deficiency Syndromes* **2016,** *Publish Ahead of Print*, (5), 498-506.
266. Grennan, T.; Walmsley, S. Etravirine for HIV-I: addressing the limitations of the nonnucleoside reverse transcriptase inhibitor class. *Journal of the International Association of Physicians in AIDS Care* **2009,** *8*, (6), 354-363.
267. Dorr, P.; Westby, M.; Dobbs, S.; Griffin, P.; Irvine, B.; Macartney, M.; Mori, J.; Rickett, G.; Smith-Burchnell, C.; Napier, C.; Webster, R.; Armour, D.; Price, D.; Stammen, B.; Wood, A.; Perros, M. Maraviroc (UK-427,857), a Potent, Orally Bioavailable, and Selective Small-Molecule Inhibitor of Chemokine Receptor CCR5 with Broad-Spectrum Anti-Human Immunodeficiency Virus Type 1 Activity. *Antimicrobial Agents and Chemotherapy* **2005,** *49*, (11), 4721-4732.
268. Veazey, R. S.; Ketas, T. J.; Dufour, J.; Moroney-Rasmussen, T.; Green, L. C.; Klasse, P. J.; Moore, J. P. Protection of rhesus macaques from vaginal infection by vaginally delivered maraviroc, an inhibitor of HIV-1 entry via the CCR5 co-receptor. *The Journal of infectious diseases* **2010,** *202*, (5), 739-744.
269. Jiang, Y.; Tian, B.; Saifuddin, M.; Agy, M. B.; Emau, P.; Cairns, J. S.; Tsai, C. RT-SHIV, an infectious CCR5-tropic chimeric virus suitable for evaluating HIV reverse transcriptase inhibitors in macaque models. *AIDS Research and Therapy* **2009,** *6*, (23), 1-11.
270. Dobard, C.; Sharma, S.; Parikh, U. M.; West, R. Postexposure protection of macaques from vaginal SHIV infection by topical integrase inhibitors. *Science translational ...* **2014**.
271. Peppas, N. A.; Mongia, N. K. Ultrapure poly (vinyl alcohol) hydrogels with mucoadhesive drug delivery characteristics. *European Journal of Pharmaceutics and Biopharmaceutics* **1997,** *43*, 51-58.
272. Serra, L.; Doménech, J.; Peppas, N. A. Design of poly (ethylene glycol)-tethered copolymers as novel mucoadhesive drug delivery systems. *European Journal of Pharmaceutics and Biopharmaceutics* **2006,** *63*, 11-18.
273. Zhou, T.; Hu, M.; Pearlman, A.; Patton, D. Expression and localization of p-glycoprotein, multidrug resistance protein 4, and breast cancer resistance protein in the female lower genital tract of human and pigtailed macaque. *AIDS research and human retroviruses* **2014,** *30*, (11), 1106.
274. Smith, J. M.; Rastogi, R.; Teller, R. S.; Srinivasan, P.; Mesquita, P. M. M.; Nagaraja, U.; McNicholl, J. M.; Hendry, R. M.; Chuong, T. D.; Martin, A.; Herold, B. C.; Kiser, P. F. Intravaginal ring eluting tenofovir disoproxil fumarate completely protects macaques from multiple vaginal simian-HIV challenges. *Proceedings of the National Academy of Sciences* **2013**, 1-6.

APPENDIX A: CHAPTER 4 SUPPLEMENTARY FILES

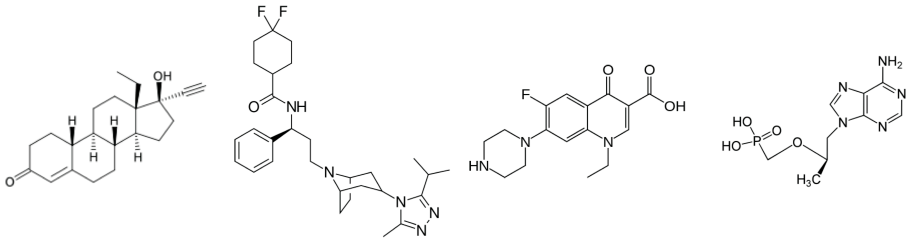

Drug Name	Levonorgestrel	Maraviroc	Norfloxacin	Tenofovir
Drug Class	Hormonal contraceptive	Antiretroviral (entry inhibitor)	Antibiotic	Antiretroviral (NRTI)
Molecular Weight	312.4 Da	513.7 Da	319.3 Da	287.2 Da
Solubility in Release Media	0.022 mg/mL	6.0 mg/mL	0.29 mg/mL	4.4 mg/mL
Hydrogen Acceptors/Donors	2/1	4/1	6/2	8/3

Supplementary Figure 4.1. Physicocehmically diverse drugs used in release experiments.

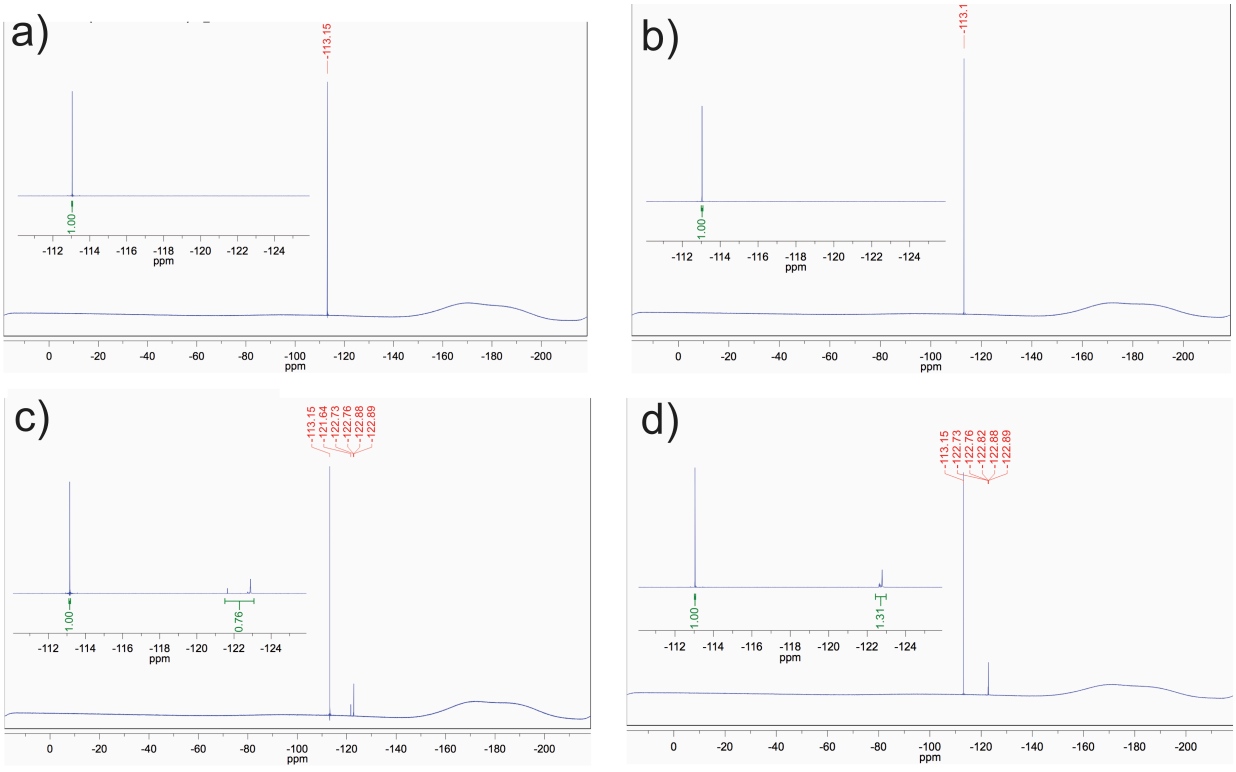

Supplementary Figure 4.2: ^{19}F NMR spectra of PLGA-PU polymers: a) PLGA-PU, b) PLGA-2PU, c) PLGA-PU-FB, d) PLGA-PU-2FB.

Supplementary Table 4.1. Evolution of PLGA-PU polymer compositions.

Polymer ID	Isocyanate	Soft segment	Chain Extender	Fluorine Pendant	Ratio	Solubility	Fibers?	Comments
634	LDI	PLGA-PEG-PLGA M_n 1000:1000:1000	DAHP	-	6/1/5	DMF HFIP	Yes	Low MW; loss of fiber morphology
635	LDI	PLGA-PEG-PLGA M_n 1000:1000:1000	DAHP	FPI	6/1/5/5	HFIP	Yes	Low MW; loss of fiber morphology
637	BDI	PLGA-PEG-PLGA M_n 1000:1000:1000	DAHP	-	6/1/5	HFIP	Yes	Low MW; loss of fiber morphology
638	BDI	PLGA-PEG-PLGA M_n 1000:1000:1000	DAHP	FPI	6/1/5/5	HFIP	Yes	Low MW; loss of fiber morphology
640	LDI	PLGA-PEG-PLGA M_n 1000:1000:1000	BDA	-	6/1/5	HFIP	Yes	Low MW; loss of fiber morphology; Poor solubility
642	BDI	PLGA-PEG-PLGA M_n 1000:1000:1000	BDA	-	6/1/5	HFIP	Yes	Low MW; loss of fiber morphology; Poor solubility
646	LDI	PLGA-BD-PLGA M_n 500:58:500	BDA	-	2/1/1	HFIP/DCM DMSO DMF	Yes	Low MW; loss of fiber morphology
668	LDI	PLGA-BD-PLGA M_n 500:58:500	BDA	-	2/1/1	Insoluble	NT	Low MW
670	MDI	PLGA-BD-PLGA M_n 500:58:500	BDA	-	2/1/1	Insoluble	NT	Low MW
648	LDI	PLGA-TEG-PLGA M_n 500:190:500	BDA	-	2/1/1	DCM	Yes	Fiber morphology maintained; M_w=27,000 Batch repeated (681)
676	LDI	PLGA-TEG-PLGA M_n 500:190:500	BDA/ DAHP	FPI	2/1/0.92 /0.08/0. 08	DCM	Yes	Fiber morphology maintained; M_w=10,000 Batch repeated (686)
681	LDI	PLGA-TEG-PLGA M_n 500:190:500	BDA	-	2/1/1	DCM	Yes	PLGA-PU Fiber morphology maintained; M_w=27,000

683	LDI	PLGA-TEG-PLGA M_n 500:190:500	BDA	-	3/1/2	HFIP	Yes	PLGA-2PU Fiber morphology maintained; M_w=8,000
686	LDI	PLGA-TEG-PLGA M_n 500:190:500	BDA/ DAHP	FPI	2/1/0.92 /0.08/0. 08	DCM	Yes	PLGA-PU-FB Fiber morphology maintained; M_w=8,000
689	LDI	PLGA-TEG-PLGA M_n 500:190:500	BDA/ DAHP	FPI	2/1/0.84 /0.16/0. 16	DCM	Yes	PLGA-PU-2FB Fiber morphology maintained; M_w=11,000
692	LDI	PLGA-TEG-PLGA M_n 500:190:500	BDA/ DAHP	FPI	3/1/1.88 /0.12/0. 12	HFIP	No	Low MW; loss of fiber morphology M_w=4,000

LDI lysine diisocyanate **BDI** butane diisocyanate **MDI** methane diisocyanate **PLGA-PEG-PLGA** PLGA co-block polymer with polyethylene glycol linker **PLGA-BD-PLGA** PLGA co-block polymer with butane linker **DAHP** diaminohydroxypropane **BDA** butane diamine **FPI** fluorophenylisocyanate **DMF** dimethyl formamide **HFIP** hexafluoroisopropanol **DCM** dichloromethane **DMSO** dimethylsulfoxide

APPENDIX B: CHAPTER 5 SUPPLEMENTARY FILES

Supplementary Table 5.1. HPLC method specifications for the detection of DPV, MVC and TFV from extracted hydrogel and tissue samples.

Drug	Mobile phase	Flow rate (mL/min)	Method time (min)	Column oven temperature (°C)	Injection volume (µL)	Detection wavelength (nm)	Retention time (min)
DPV	65% ACN + 35% 10 mM ammonium acetate in H_2O	1.0	10	30	10	310	6.4
MVC	26% ACN + 74% 50 mM KH_2PO_4 in H_2O, pH=3.2	1.0	15	44	20	193	8.9
TFV	28% ACN + 72% 0.045% TFA in H_2O	1.0	10	30	20	259	2.3

APPENDIX C: PROPERTIES AND STRUCTURES OF SELECTED APIS

Drug	Type	MW (Da)	Solubility in H_2O	pKa	logP	Structure
Levonorgestrel LNG	Hormonal contraceptive	312.45	$5.83x10^{-3}$ g/L	17.91	3.25	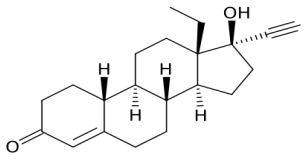
Tenofovir TFV	Antiretroviral NRTI	287.21	1.87 g/L	1.35	-1.5	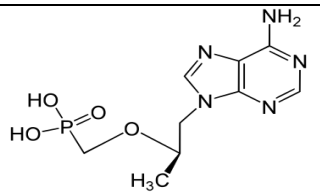
Maraviroc MVC	Antiretroviral Entry inhibitor	513.67	$1.06x10^{-2}$ g/L	14.5	4.3	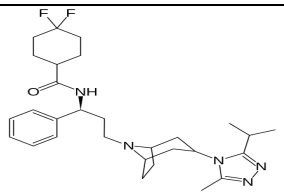
Norfloxacin NFL	Antibiotic	319.33	1.01 g/L	5.77	-0.47	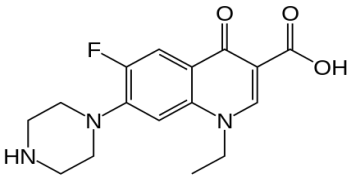
Dapivirine DPV	Antiretroviral NNRTI	329.41	$3.05x10^{-11}$ g/L	5.80	5.27	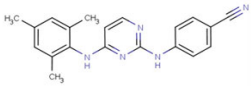
Raltegravir RAL	Antiretroviral Integrase Inhibitor	444.42	7.1 g/L	5.62	-0.39	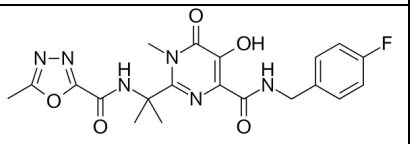
Etravirine ETR	Antiretroviral NNRTI	435.28	$1.69x10^{-2}$ g/L	12.49	3.67	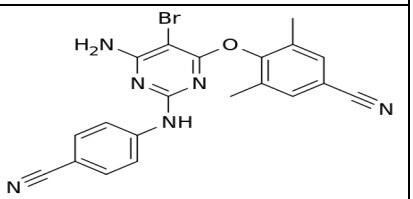

VITA

Anna K. Blakney is formally trained in Chemical and Biological Engineering, with specific expertise in polymeric biomaterials, tissue engineering, drug delivery, host response, electrospinning and global health applications of bioengineering. Anna received her B.S. in Chemical and Biological Engineering from University of Colorado at Boulder in 2012, where she worked in the laboratory of Dr. Stephanie Bryant. She completed her Ph.D. with Dr. Kim Woodrow at the University of Washington in the Department of Bioengineering in 2016. In her free time, Anna enjoys sailing, biking, backpacking, fly-fishing, skiing, tennis, rock climbing, riding horses, brewing beer and cooking.